# UNIVERSITY OF CAPE TOWN

## CENTRE FOR MINERALS RESEARCH

# MEASUREMENT OF IMPACT BREAKAGE PROPERTIES OF ORE PARTICLES USING A SERIES OF DEVICES

by

**BBOSA, Lawrence Sidney**

Thesis submitted in partial fulfillment of the requirements for the degree of Master of Science in Engineering

August 2007

## DECLARATION

1. I know that plagiarism is wrong. Plagiarism is to use another's work and pretend that it is one's own.

2. I have used the scientific convention for citation and referencing. Each significant contribution to, and quotation in this thesis from the work(s) of other people has been attributed, and has been cited and referenced.

3. This thesis is my own work.

4. I have not allowed, and will not allow anyone to copy my work with the intention of passing it off as his or her own work.

Signature: .....

Date: .....

# TABLE OF CONTENTS

# ACKNOWLEDGEMENTS

Gratitude must be expressed toward a number of people for their contribution to this project:

Dr. Aubrey Mainza for his erudite guidance and advice while overseeing this thesis.

Prof. Malcolm Powell for belief and support in my ability to carry out this work.

Prof. Robert Tait and Trevor Cloete for their thorough and immaculate instruction through the finer points of this study.

Dr Frank Shi, Dr. Toni Kojovic and Steve Larbi-Bram for their invaluable advice and encouragement during the RBT experiments.

Prof Gerald Nurick of BISRU, Doug Philips of ANGLO Research and both Adrian Hinde and Johnny Kalala of MINTEK for permitting me to conduct experimental work in their respective departments.

Dr. Liza Burdukova, Rueben Govender, Neville Jacobs and Megan Becker for eager and patient guidance through the stickier sections of this project.

Daniel Mnthambala and Amit Vara for inspiring me to break rocks as hard as you both rock.

Yvonne Chi for being an exquisite gem of a human being.

And, saving best for last, my inspiration, my confidence, my absolute, my mother. I love you Mom.

# EXECUTIVE SUMMARY

Single particle impact breakage experiments provide essential data to aid in the fundamental understanding of rock fracture in comminution. Such experiments, conducted using devices such as the drop weight tester, split Hopkinson bars and more recently the rotary breakage tester, have been successfully used to characterize ore breakage properties in relation to measured fracture energies. Current theoretical understanding of impact breakage is that there are three important energy regimes to the process. Below a certain energy value, $E_0$, breakage will never occur for an infinite number of impacts. Second is an intermediate energy zone for which breakage occurs after a number of consecutive impacts and after a critical energy value, $E_{crit}$, is a regime where breakage typically occurs for a single impact.

This work was therefore undertaken in order to identify the energy values described for impact breakage of a chosen homogenous ore and a conventional mining gold ore. Drop weight tests on gold ore were used to calculate A and b hardness parameters using both the standard JK breakage model and the modified Shi-Kojovic model. The A x b values with the modified model gave consistently higher values than the standard model, typically increasing by 2-5%.

Split Hopkinson pressure bars were used to establish the ultimate compressive stress of blue stone through single impact breakage tests and the fraction of impact energy utilized to cause particle fracture. From these tests it was noted that less than 50% of available impact energy was utilized to cause fracture, with cylindrical specimens absorbing the highest fraction of 43%.

The rotary breakage tester was used to conduct incremental breakage experiments with blue stone and gold ore. The probability to breakage at the impact energies tested was found to remain relatively consistent over consecutive impacts. This showed that a model could be fitted between the cumulative probability to breakage and the number of impacts at these energy levels. The values of $E_0$ for blue stone and gold ore were calculated to be 0.0464 and 0.00366 respectively. $E_{crit}$ for 90% probability to first impact breakage for these two ores was 0.344 and 0.281 respectively. It was found that incremental breakage was much more inefficient than single impact breakage. From tests with both split Hopkinson pressure bars and the rotary breakage tester, breakage degrees for single impacts increased rapidly with increase in breakage energy whilst the breakage degrees obtained from incremental breakage tests for similar amounts of energy expended remained low.

## LIST OF ABBREVIATIONS AND NOMENCLATURE

DWT- Drop weight test

SHPB- Split Hopkinson pressure bar

RBT- Rotary breakage tester

CMR- Centre for Minerals Research

BISRU- Blast Impact and Survivability Research Unit

UCT- University of Cape Town, South Africa

DEM- Discrete Element Method

XRD- X- ray diffraction

UCS- Ultimate Compressive Stress

$K_{ic}$- Critical Stress intensity factor

$W_i$- Bond work index (kWh/t)

$P_{80}$- size at which 80% of the product passes ($\mu m$)

$F_{80}$- size at which 80% of the feed passes ($\mu m$)

$\sigma_p$- Particle strength

$F_c$- Force to failure

$d_p$ - Geometric mean size or distance between loading points

$k_p$- Particle stiffness

$Y_b$ - Young's modulus

$\mu_b$- Poisson's ratio

$E_f$- Particle fracture energy

$k_i$ – Breakage rate of size i per unit time

$s_i$ – mass of i present

$f_i$ – feed of size class i

$b_{ij}$ – breakage function

$p_i$ - product of size class i

$t_{10}$- Percentage material passing through a screen one tenth of the original geometric mean particle size

S- Breakage probability

$W_{min}$ or $E_0$- Minimum energy below which infinite impacts would never result in fracture

$W_{crit}$ or $E_{crit}$- Energy above which a solitary impact would almost certainly cause breakage

# LIST OF TABLES

## CHAPTER 2



## CHAPTER 3



## CHAPTER 4



## CHAPTER 5



## CHAPTER 6



## CHAPTER 7

# LIST OF FIGURES

## CHAPTER 2



## CHAPTER 3

## CHAPTER 4



## CHAPTER 5

## CHAPTER 6



## CHAPTER 7

# CHAPTER 1

# INTRODUCTON

## 1.1 BACKGROUND AND HYPOTHESES

Impact breakage has been identified to be the most elementary size reduction mechanism in comminution devices[13,43]. Machines such as crushers, mills and grinding rolls are understood to cause ore breakage via impact, abrasion and attrition, but of these impact breakage is known to be the most effective process[14]. A great deal of research has thus been devoted toward understanding particle fracture at a fundamental level, which has led to a number of devices being devised to conduct standard breakage characterization tests. Impact breakage has been described to occur by two common means[2]. In the first instance, the material to be broken is struck by a rigid object, while the second involves the material being launched against a static target.

Ore breakage has been interpreted using approaches based on both fracture mechanics and conventional engineering load analysis[7,11,38,39]. From fracture mechanics it has been put forward that compressive impact breakage results from loading forces causing weaknesses in the material microstructure to act as sites for stress concentrations. Following a material specific stress intensity about these flaws, crack initiation, propagation and eventual failure occurs[49]. Further work has suggested that 'preferential breakage', or a tendency for materials to fracture along weaker grains of the ore composition, may also occur[14]. Engineering load analysis describes fracture from a macro structure perspective in terms of strengths known as yield stress and ultimate tensile stress, which govern the maximum loads specific materials can be subjected to before irreversible inelastic deformation and complete fracture respectively occur[20].

Although both approaches describe impact breakage in terms of load, because comminution research is primarily concerned with the energy expended to cause particle size reduction, breakage theory in this field is defined in terms of relationships between energy utilization and breakage degree by size[36]. The main challenges of this approach have been quantifying the energy consumption of impact

breakage and defining standard parameters to accurately describe the overall process.

The discrete element method (DEM) has proven particularly valuable as a computational tool to simulate the energy spectra and collisions of particles in a milling environment[34,35]. With this method individual particles are assigned stiffness parameters and interact using Newtonian equations to calculate their position and trajectories. Impact interactions are then described by spring and dashpot particle mechanics to provide calculations for energy losses to direct impact and shear against other particles as well as the internal mill surface and liners[1]. After such data is validated through experimental measurement, results from such computational calculations can be used as a reasonable estimate of energy utilization in machines where direct measurement is not feasible[12].

Typically, DEM simulations provide frequencies or the number of occurrences of interactions at particular energy values. Over a variety of milling conditions the noted trend has been that a small minority in the region of less than 15 percent of impacts occur at energies expected to cause fracture, whilst the remainder occur at lower energies[25]. Based on this result it has been inferred that the greater influence behind impact breakage in mills is successive weakening of particles over several impacts, or incremental breakage, as opposed to resulting from solitary impacts at high forces[41].

An interpretation of particle breakage by impact has been put forward that the process occurs over three distinct regimes, separated by two defined parameters[25]. For a given particle size, below a certain minimum specific energy, termed $E_0$ or $W_{min}$, is a region in which breakage never occurs even for infinite impacts, as interactions at this energy level are insufficient to weaken the particle microstructure[52]. Following this is an intermediate regime for which a number of consecutive impacts gradually cause crack initiation and particle weakening until a final impact leads to complete fracture. The number of impacts required to cause fracture decreases with increase in energy until a critical value known as $E_{crit}$, defined in terms of particle breakage probability, at which energy a solitary impact is sufficient to cause breakage. Following this is the final regime in which single impacts are expected to cause immediate particle fracture.

Prior work by Whyte on incremental breakage has been carried out using drop weight tests, where it has been found that the value of $E_0$ may be size dependent and decrease marginally with each successive impact due to progressive particle weakening[50,56]. Drop weight tests have been commonly used for impact breakage research, which provide measurement of available potential energy to relate to subsequent product size. However, the energy range for which the machine is suited falls well outside the region of interest for incremental breakage, its operating minimum usually well higher than $E_{crit}$ for most sizes.

Many other breakage devices have been used in the past to study particle fracture. Split Hopkinson pressure bars allow for accurate measurement of the force-time response of specimens at high strain rates[28]. In addition to this, the device allows for calculation of both the available input energy and the amount of this that is absorbed by a particle under impact. In recent research the rotary breakage tester (RBT), a device designed at the Julius Kruttschnitt Minerals Research Centre (JKMRC), has been commissioned. This permits for rapid breakage experiments over wide energy ranges typically estimated to occur in comminution devices[46]. Results of such experiments have already been used to extend and validate current breakage models[44], and its success in carrying out a wide range of breakage experiments suggests that it may become a standard device to further breakage research.

Most experimental work with these devices has been conducted at very high energies in order to characterize the single impact breakage properties of particular materials. Little work has been devoted to understanding incremental breakage, or comparing the energy expended in breakage over several impacts against that of single impacts. It is also worth noting that comparisons between the breakage data obtained from different devices have not been previously investigated. As such, this thesis has been put forward in order to investigate two primary hypotheses:

## Hypotheses

- For a given material, values of $E_0$ and $E_{crit}$ exist and can be measured
- Single impact breakage is more efficient than incremental breakage

For this work, a number of objectives have been put forward which address these hypotheses as well as several noted aspects of ore impact breakage that require investigation. These will now be briefly discussed.

## 1.2 OBJECTIVES AND SCOPE

This study will investigate several aspects of impact breakage by addressing the following objectives:

- To use experimental data to calculate the values of $E_0$ and $E_{crit}$ for a chosen ore type.

- To determine and compare breakage energy/product size relationships across different devices.

- To compare the efficiency of single impact breakage against incremental breakage.

The drop weight test, split Hopkinson pressure bars and the rotary breakage tester are the three breakage devices chosen for this project. The drop weight test will be used to model the standard breakage degree by energy relationship and observe how it differs with particle size. Experiments using Hopkinson bars will be used to calculate strength parameters of ore and investigate the effects of impulse and loading geometry on the amount of energy absorbed by particles to cause breakage. Finally, tests with the rotary breakage tester will be used to determine particle breakage probabilities at energies between $E_0$ and $E_{crit}$. For the purpose of this work $E_0$ will be calculated from fitting incremental breakage data to a breakage model, while $E_{crit}$ will be defined as the energy calculated for a 90% probability of breakage. Breakage degree will be quantified by the $t_{10}$ breakage parameter.

The scope of this study will be limited to particle fracture by impact breakage. It has been considered that this mechanism of breakage is the most useful in identifying breakage patterns for comminution models[43]. The work in this thesis is thus meant to provide an overview of impact breakage comparisons, as opposed to a rigorous quantitative comparison. It is expected that this work will form the basis for future studies in this area.

A commonly found road aggregate has been selected as the primary test material for this work. Although conditioned particles from milling are mainly used as test specimens in order to negate the influence of rock geometry, angular specimens are also used for comparison.

Where possible, energies at which experiments are conducted are chosen from standard values, while tests at energies found to be below $E_{crit}$ are selected based on results from DEM. For the RBT, these energy values are chosen to be reproducible and shown for an energy value to be repeatable.

## 1.3 PLAN OF DEVELOPMENT

CHAPTER 1: This chapter provides a background to the thesis, which leads into the hypotheses and objectives of the study.

CHAPTER 2: This chapter briefly reviews the history of comminution research, discusses breakage theory and modeling, and in addition reviews several devices used for impact breakage experiments.

CHAPTER 3: A summary of ore types selected for this study, their mineralogy and sample preparation for the experimental work is given here. Tests with each breakage device are then explained and listed together with their individual experimental procedures.

CHAPTER 4: This Chapter discusses the theory behind the drop weight test method, which is followed by results and analyses of experiments conducted with this device.

CHAPTER 5: The Split Hopkinson pressure bar apparatus and theory is described and explained, after which results and analysis of the breakage data obtained is provided.

CHAPTER 6: A discussion of the technique and theory for the rotary breakage tester is found in this Chapter. Breakage data obtained from these experiments is then reviewed.

CHAPTER 7: This Chapter provides a summary of the breakage results from each device. Correlation in breakage data across the three devices is then discussed.

CHAPTER 8: Conclusions based on work from this thesis are provided, and recommendations for future experiments are listed.

# CHAPTER 2

# LITERATURE REVIEW

*Overview*
*This chapter presents a review of material relevant to the thesis. Theoretical descriptions of breakage and their adaptations to form comminution breakage equations are explained. Experimental techniques developed to test impact breakage are also reviewed, along with some of the breakage models that have then been put forward.*

## 2.1 BRIEF HISTORY OF COMMINUTION RESEARCH

Integrated into the operation of any minerals processing circuit is the size reduction of extracted ore, or comminution stage. Devices such as crushers, mills and grinding rolls typically account for about half the energy expended by modern plants[37], and have even been stated to take up to 70% in some circuits[21]. From the standpoint of both capital saving and power conservation, reducing or optimizing the energy requirements of this stage is therefore most beneficial. To this end, the drive in comminution research has mainly been to understand the causatives behind ore breakage[2,3,43].

Numerous studies have been conducted over the years concerning breakage in comminution machines[4,18,23,40]. Considering the tumbling mill (pictured in Figure 2.1), likely the most common industrial comminution device, the broad consensus reached is that particle size reduction occurs via three basic mechanisms[37]:

- Impact breakage – Which may take place in the form of single particle fracture or bed breakage. This would be primarily from cataracting charge falling at the base or toe in a mill, while in machines like grinding rolls this would involve beds of ore compacting against the action of rollers.

- Abrasion – Material grinding against itself results in surface damage, gradually wearing it down and reducing it in size, which is characteristic of ore behaviour at the base of mills.

- Attrition – When larger rock crushes against smaller pebbles, the tinier particles tend to grind down to finer sizes, a process which typically occurs at a faster rate than similar size material abrading against itself.

Figure 2.1: Tumbling mill in a comminution circuit

Concepts from rock mechanics research have been used to deal with interpreting the roles these three mechanisms play as breakage circuits become larger and more complex. Many well documented theories describing energy versus breakage size distributions have been put forward over the years[3,8,9], which have been extensively refined and modified to suit modern circuits[22,36]. While these relationships are useful in the design and operation of comminution equipment, they do not provide useful information to the fundamental understanding of the process of fracture.

As given by Klaus Schonert[43], the definition of comminution fundamentals is:

*"...usually understood to deal with aspects of particle breakage including fracture physics, deformation and breakage of particles under controlled stressing, interference of particles stressed in a layer or bed, the properties of the created surface and so on."*

Given that the field encapsulates such a broad spectrum, describing a fundamental relationship for overall particle breakage in comminution has thus proven difficult. As such, since impact breakage represents the simplest form of size reduction in this regard, fundamental theories of ore fracture have focused on describing this mechanism[13].

## 2.2 THEORIES OF IMPACT BREAKAGE

Impact breakage is one of the principal size reduction mechanisms in comminution[29], thus a great deal of research has been devoted to understanding this process. Impact breakage is defined to occur through either material struck by a rigid object or material launched against a static target[2]. Work in this area has traditionally considered both a macroscopic view of breakage through classic rock mechanics or process engineering approaches, and micro scale analyses of particle response using fracture physics or continuum damage mechanics. These two perspectives will now be highlighted further.

### *Rock mechanics*

Conventional engineering describes uniaxial loading using the stress/strain curve to define the material specific elongation (strain) of a material under force per unit area (stress)[20], a generic example of which is illustrated in Figure 2.2. Although both tensile and compressive behaviour can be described using the same idealized graph, it is the tensile properties of a material that govern its strength under load, and traditionally parameters such as yield stress, Young's modulus, Ultimate tensile stress and Poisson's ratio are used as comparative measures of material strength properties[37].

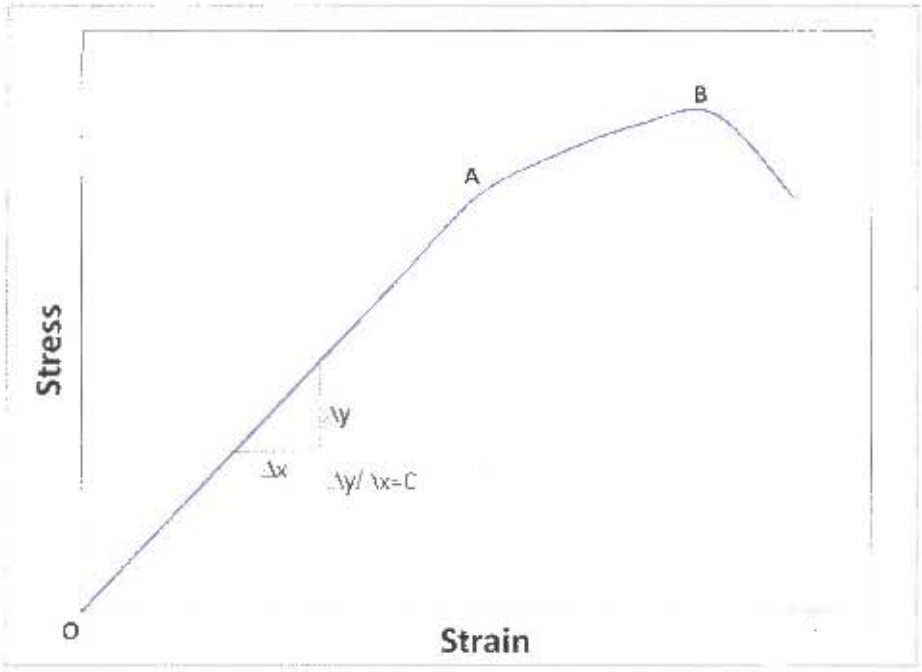


Figure 2.2: Simplified example of an engineering Stress vs. Strain curve

Under compressive loading, region OA depicts the elastic region for which stress is directly proportional to strain by a constant ratio known as the Young's modulus, a measure of material elasticity. Metals, being typically ductile in nature, tend to have lower values as their microstructure lends toward elastic deformation under load, whereas rocks typically exhibit brittle behaviour and thus have higher moduli. As the stress intensifies the material reaches the stress value at A known as the Yield stress, after which it enters a region of plastic deformation AB, whereby the material, although not having fractured, deforms irreversibly and does not return to its original microstructure when the load is removed. This region extends for a brief or longer period dependent on the material until the critical stress value at point B, the Ultimate Compressive Stress (UCS) which is the maximum stress a material can undergo before complete failure. Another commonly quoted value of interest is Poisson's ratio which is a ratio of the longitudinal strain or displacement to the transverse strain, to indicate the tendency of the material to displace in the direction of the load or shear under stress. Table 2.1 shows expected ranges of these values for mining ores, established from standardized slow compression rock mechanics tests of cylindrical specimens.

Table 2.1: Typical ranges of engineering strength parameters for mining ores[37]

| | |
|---|---|
| Ultimate Compressive Stress (MPa) | 50-450 |
| Young's Modulus (GPa) | 10-70 |
| Poisson's Ratio | 0.08-0.45 |

*Fracture mechanics*

The discipline of Linear Elastic Fracture Mechanics (LEFM) has arisen as a combination of fracture physics and continuum damage mechanics[37]. From conventional engineering fracture tests[48] it is already known that cracks and notches in materials act as stress raisers and for LEFM, an assumption is made that the stress at the edge of every crack can be represented as a multiple of a stress intensity factor K.

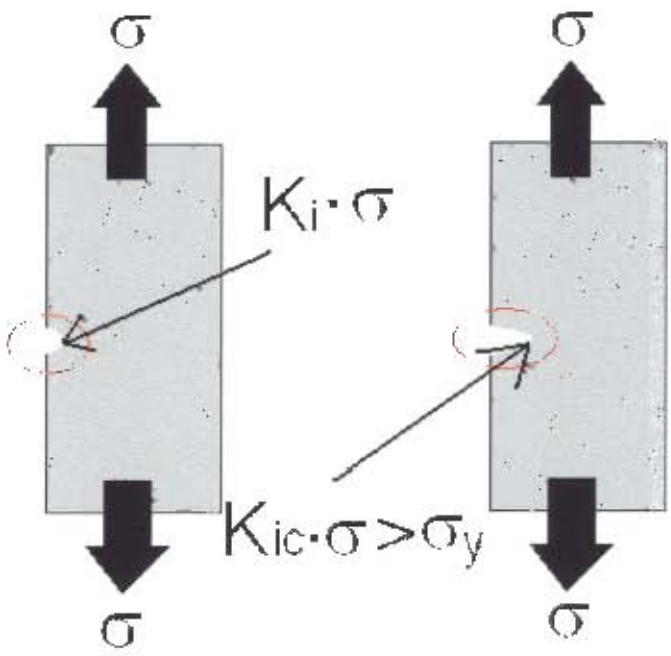


Figure 2.3: Simplified illustration of how stress intensity at a micro-crack under load leads to further crack propagation

For every material there exists a critical stress intensity factor designated $K_{IC}$, at which a given load will exceed the material's fracture strength and cause the crack to propagate as shown in Figure 2.3, leading to eventual failure. This value of $K_{IC}$, also known as fracture toughness, is used as a measure of the rock's resistance to weakening, or hardness, and is established through standardized rock mechanics tensile load testing, known as mode I fracture[49].

Mechanics of solids and continuum mechanics are further used to describe and predict particle interactions and weakening from crack inception until failure. Using mathematics derived from Hertzian theories of elastic contact, such models have

been used to define fracture strengths and breakage probabilities for both single impact fracture and breakage over successive impacts[49,50,51].

The force-compression profile from such mathematical modeling is seen to be similar to that from engineering considerations, as shown in Figure 2.4, which shows the profile of a typical experimental test compared with its damage mechanics model (Equations 1-3 in diagram) and a Hertzian model (given by Equation 1 in diagram) with a constant stiffness coefficient.

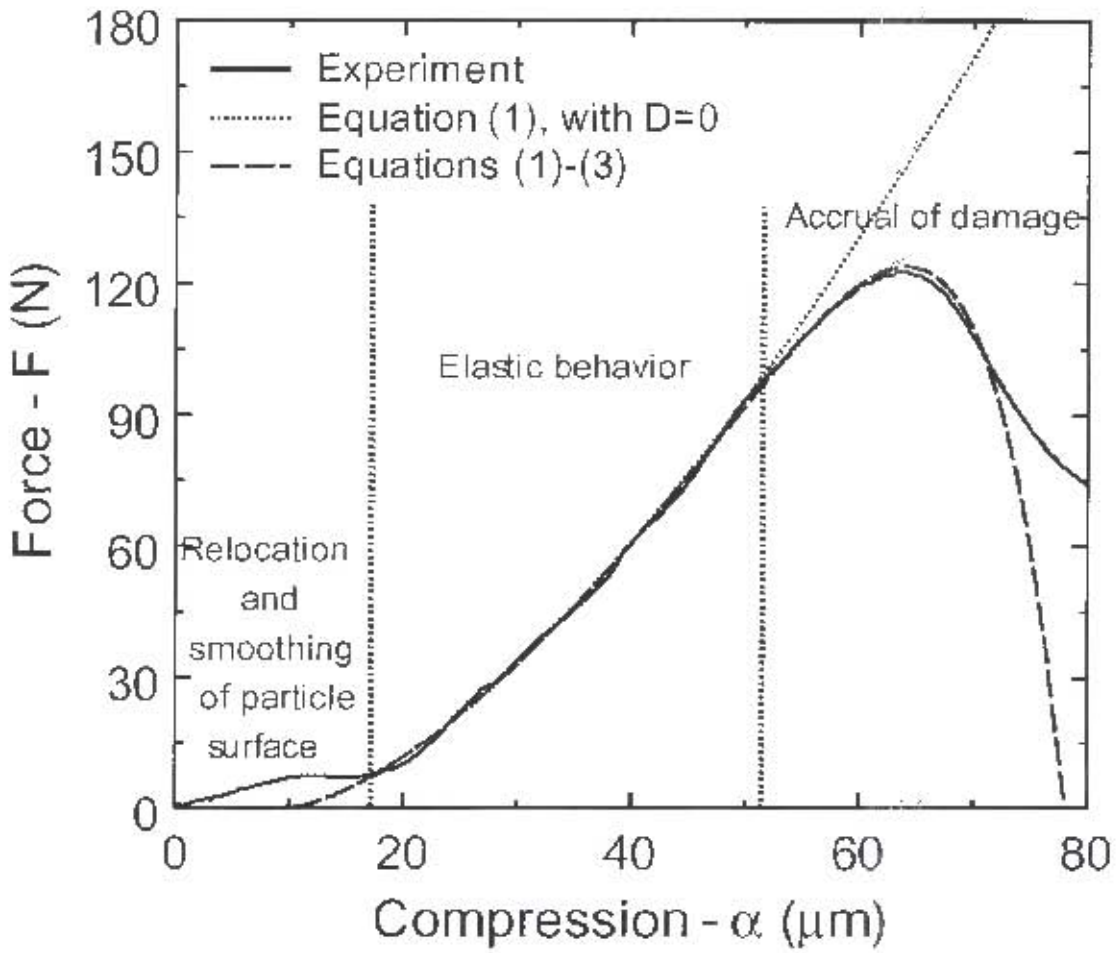


Figure 2.4: Force vs. Compression profile obtained from damage mechanics modeling of breakage[49]

Damage mechanics can therefore be used to quantify likely stresses in irregular shaped bodies under load where measurement is not possible. For this, a further assumption is made that unstable crack propagation is dictated by the so called 'Griffith criterion'[4] which states that for a crack to move through a structure the rate of energy release in the particle must be greater than the material's crack resistance,

a parameter calculated from its fracture energy. This available excess strain energy then drives the crack through two stages of failure. The first stage covers the period or energy expended from first impact to initial fracture. The second stage follows as the remaining or released energy that determines kinetic movement of particles, sound, and further breakage of progeny particles[51].

## 2.3 APPLICATION OF IMPACT BREAKAGE RESEARCH TO COMMINUTION

In order to apply information from the aforementioned analyses of breakage to comminution, several assumptions have had to be employed. Primarily because the main concern in this field is the energy expended to reduce particles to particular sizes, the most quoted values for measures of impact rock hardness and load response relate to measurements or predictions of these. Impact breakage research in comminution is then based on interpreting the power draw of a particular device and understanding the mechanics by which the energy transfer is used to achieve breakage[54].

An example of this is the standard ore hardness characterization parameter, the Bond work index[8]. The Bond work index is formally defined as the power required to reduce a material from a theoretically infinite size to 80% by mass of the original material passing through a screen of size matching the desired product size (75-150 $\mu m$ range). Thus by this method, the rate of energy input is proportional to the feed and product size of an ore by a constant named its work index, and this can be related to the feed and product size by the relationship in Equation 2.1.

$$W = 10 W_i \left( \frac{1}{\sqrt{P_{80}}} - \frac{1}{\sqrt{F_{80}}} \right) \qquad \text{Equation 2.1}$$

Where

W – Work input (kWh/t)

$W_i$ - Bond work index (kWh/t)

$P_{80}$ - size at which 80% of the product passes ($\mu m$)

$F_{80}$ - size at which 80% of the feed passes ($\mu m$)

The power of rod and ball mills calculated from Bond grindability tests has been found to correlate well using this relationship, and other relationships have been introduced to calculate the indices under other conditions[37].

Limitations of the method include the constraint that the slope of the feed and product size distributions must be approximately parallel otherwise taking a single point description would be inaccurate. Further, it has been found that Bond's equation does not hold over the size range -100 + 0.1mm[36].

As a measure of rock strength, this index has been found to relate broadly with the UCS (see Section 2.2) as shown in Table 2.2, although because different methods are employed to calculate either of these parameters, they are poor predictors of each other. Work indices for various modes of breakage are established through standardized experiments.

Table 2.2: Relationship between Work Index and UCS[37]

| Property | Soft | Medium | Hard | Very Hard |
|---|---|---|---|---|
| UCS (Mpa) | 50-100 | 100-150 | 150-250 | +250 |
| Work Index | 7-9 | 9-14 | 14-20 | +20 |

A number of parameters have been introduced to describe various fracture characteristics of ores. Based on work by Tavares and King[49], particle strength, particle stiffness, and particle fracture energy are measures that can be applied to impact breakage. Particle strength is derived from the ultimate tensile strength as the maximum stress a particle can withstand to failure. As stress is defined as force per unit cross sectional area, particle strength ($\sigma_p$) is thus taken to be the force to failure ($F_c$) divided by a nominal amount of the particle cross section whose diameter is given by the geometric mean size or distance between loading points ($d_p$). A simplified equation for this is shown in Equation 2.2.

$$\sigma_p = \frac{2.8F_c}{\pi d_p^2} \qquad \text{Equation 2.2}$$

Particle stiffness ($k_p$) is derived from Hertzain elastic contact[16] to give a theoretical estimate of the force deformation relationship for an idealized spherical particle,

which is useful to modelling. It has been found to show similarity to fracture toughness and can be roughly calculated through Equation 2.3 below, where $Y_b$ is the Young's modulus of the material and $\mu_b$ is its Poisson's ratio.

$$k_p = \frac{Y_b}{1-\mu_b^2} \qquad \text{Equation 2.3}$$

Particle fracture energy ($E_f$), or the total energy absorbed by a particle under impact until first fracture, is defined from the force deformation profile as the area under this curve until the point of initial breakage, which can be simply expressed by the integral in Equation 2.4.

$$E_f = \int_0^{\Delta_c} F_c d\Delta \qquad \text{Equation 2.4}$$

Here, $\Delta$ is the total deformation of the particle while $\Delta_c$ is the deformation at fracture. The amount of absorbed strain energy during impact is thought to be critical in predicting the extent to which fracture occurs[51]. Because this energy is dependent on a number of factors, including rate of energy transfer, method and duration of impact, ore geometry, size and strain rate, it is difficult to accurately quantify the amount of available impact energy a material under stressing actually absorbs. Methods used to estimate this have included performing lab scale measurements following which the results would be scaled up to approximate measurements in the machine concerned. Another method gaining acceptance is the use of computer simulation to calculate forces associated with impact interactions in large scale machines[17,34].

### *Discrete Element Method*

The Discrete Element Method (DEM) has increasingly gained in acceptance as a valuable tool to characterize the motion and energy spectra in comminution machines such as tumbling mills[27]. By using of simple elastic impact laws to perform numerical iterations of multi-particle interactions, this method can be used to simulate collision energy, surface behaviour, flow boundaries and deformations of particles or boundaries within a user defined environment[1,25,34,35].

When applied to tumbling mills, in its basic form the method involves assigning defined elements such as steel balls and rocks calculated stiffness parameters and using Newton's laws of motion to predict their trajectories. A spring and dashpot mechanism is then used to simulate the elastic collisions within the tumbling environment, where the forces and energies associated with every interaction can be numerically calculated in discrete time steps. Based on these values, calculations can be made to predict power draw, liner wear, and steel consumption of the mill as well as other useful data[12].

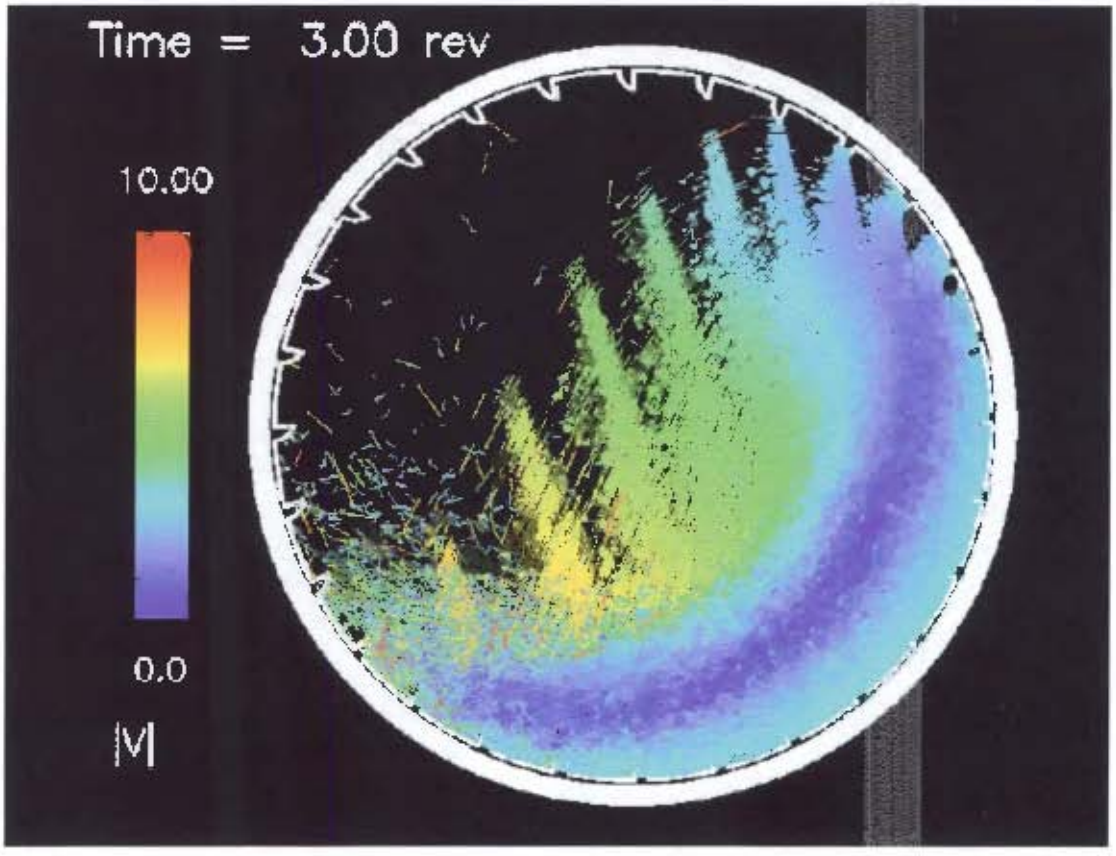


Figure 2.5: DEM visualization of anticlockwise charge revolution in a tumbling mill[12]

Figure 2.5 shows a typical visualization of charge motion during a time step for an anti clockwise mill revolution, with hues from blue to red used to distinguish ascending velocities. From this illustration it is observed that the highest impact velocity interactions occur at the toe or lowest falling position of cascading charge, which is in line with particle tracking imaging of real tumbling devices[34].

Collision frequencies of various impacts such as steel ball to ball, ball to rock, rock to rock, rock/ball to liner in both direct impact and shear can then be obtained. Figure 2.6 shows the collision frequencies of dashpot energy contacts in a typical time step against the calculated dissipated energy lost to these interactions, shown over a particle size range where 53mm represents the mean size.

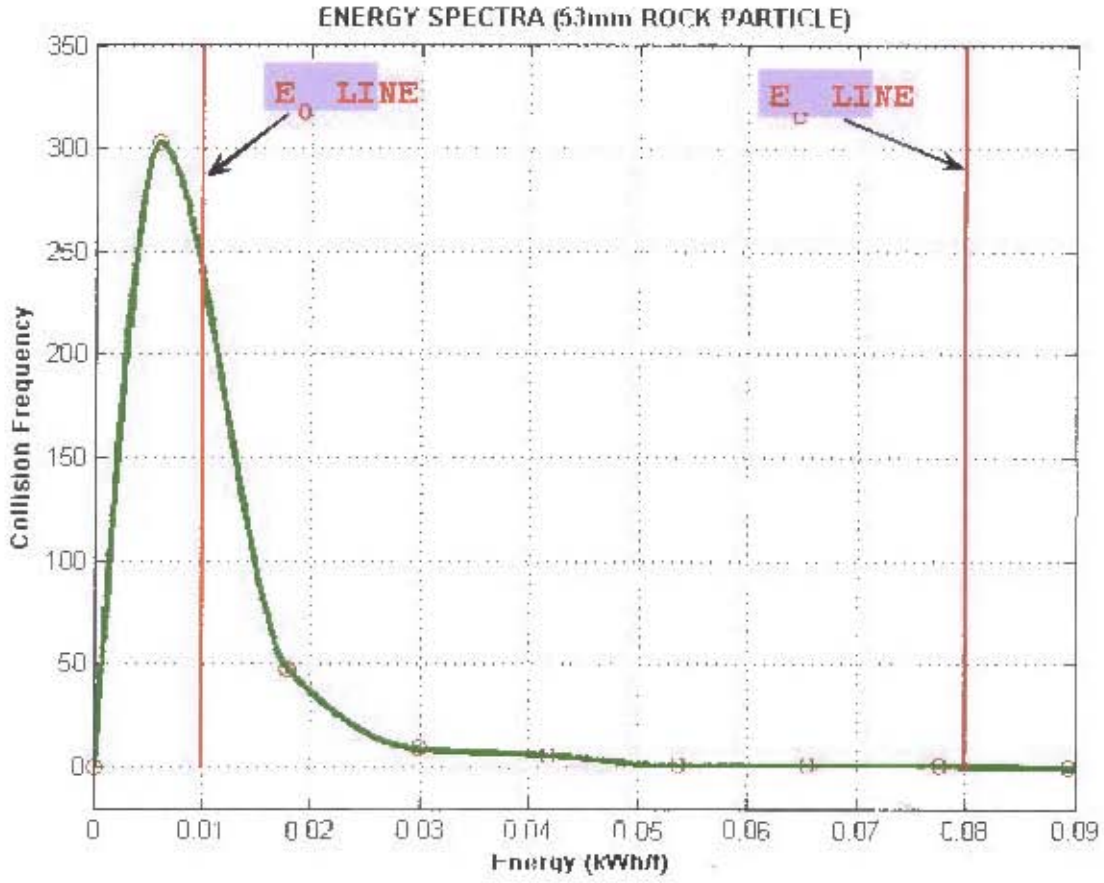


Figure 2.6: Graph illustrating collision frequencies vs. energy for 53mm mean rock particles in a DEM simulation[25]

A trend is observed here that has been used to define modern interpretations of energy/breakage relationships, in that a distinctly large majority of interactions occur at very low energies, whereas a small minority occur within the high impact energy regime estimated to be sufficient to cause fracture in single impacts. This conclusion agrees with the understanding that a large contributor to size reduction in mills is surface damage via modes such as abrasion and attrition. It also further also lends credence to the idea of 'progressive weakening', in that particles fracture more as a result of repeated stressing at low forces than single impacts at high forces.

It is important to note that while DEM provides a profile of the energy environment in a mill, it does not model the breakage or characterize the redistribution of the charge following the impact events. For this reason, breakage rate functions are introduced to computer simulations to calculate the particle size distributions resulting from the determined impact energies.

*Population balance model*

One of the most widely used statistical models of particle distribution is the population balance framework, whose inception is accredited to Epstein in 1947. While many variations of this model have been presented over the years, the original principles behind the model have remained largely the same. The simple principle behind this model is that it sums all the mass present in specific size classes and then uses breakage rate functions to provide the accumulation or loss of mass in each per breakage iteration[37].

An important assumption used in this model is that the rate of breakage of material is directly proportional to the mass of that material that is present in its given size class (i), and thus that for each size interval there exists a rate constant that governs the rate of breakage for that interval. Thus, as shown in Equation 2.5

$$\text{Breakage rate} = k_i \times s_i \qquad \text{Equation 2.5}$$

Where $k_i$ – Breakage rate of size i per unit time

$s_i$ – mass of i present

Derivation of the model is then based upon the conservation of mass about every size range present in the mill, so that for each size class

Feed in + Breakage in = Product out + breakage out

Which gives rise to the overall balance equation

$$f_i + \sum_{j=1}^{i-1} b_{ij} k_j s_j = p_i + k_i s_i \qquad \text{Equation 2.6}$$

Where f – feed of size class i

$b_{ij}$ – breakage function which determines the distribution of upper size fraction j that falls under i following breakage.

$p_i$ - product of size class i

Thus the breakage product can be expressed as a function of the feed rate, operating factors particular to the breakage device and chosen breakage parameters.

To define an idealized equation to relate product size to the available breakage energy provided by the device, the appearance function $b_{ij}$ is used. The parameters defined by the function have to be determined from actual impact breakage experiments. Many techniques have been developed to define impact breakage functions, the most common forms of which will now be discussed.

## 2.4 DEVICES USED FOR IMPACT BREAKAGE TESTS

As previously mentioned, single particle impact breakage represents the most elementary process in comminution[43]. In tumbling mills, the fundamental fracture process has been concluded to be as a result of the impact of falling media[38], and further research has also led to the belief that impact breakage is the most effective means of size reduction available in breakage machines[14].

Impact breakage experiments have thus been extensively used as a means to identify useful trends for comminution research, as well as provide statistical data to implement in functions for design and optimization of circuits[37]. Although much about fundamental mechanisms behind fracture response of materials under different forms of load is known from fracture physics and rock mechanics, single particle breakage tests in comminution are mainly concerned with characterizing ore hardness under impact load and using this data to provide predictive models to use in design simulations.

Some forms of such single particle impact breakage experiments include

- Drop weight tests
- Split Hopkinson bar tests
- Ultra fast load cell experiments
- Rotary breakage tests

Each of these will now be briefly highlighted

*Drop weight tests*

The drop weight test device, developed at the JKMRC, replaced the twin pendulum test as the standard measurement technique to characterize ore breakage in the early nineties[37]. An electric winch is used to control pneumatic pressure which raises lead weights along vertical guide rails to fixed heights, which after release fall under gravity to crush ore specimens mounted on an anvil. The device is installed in a Perspex enclosure as is pictured in Figure 2.7.

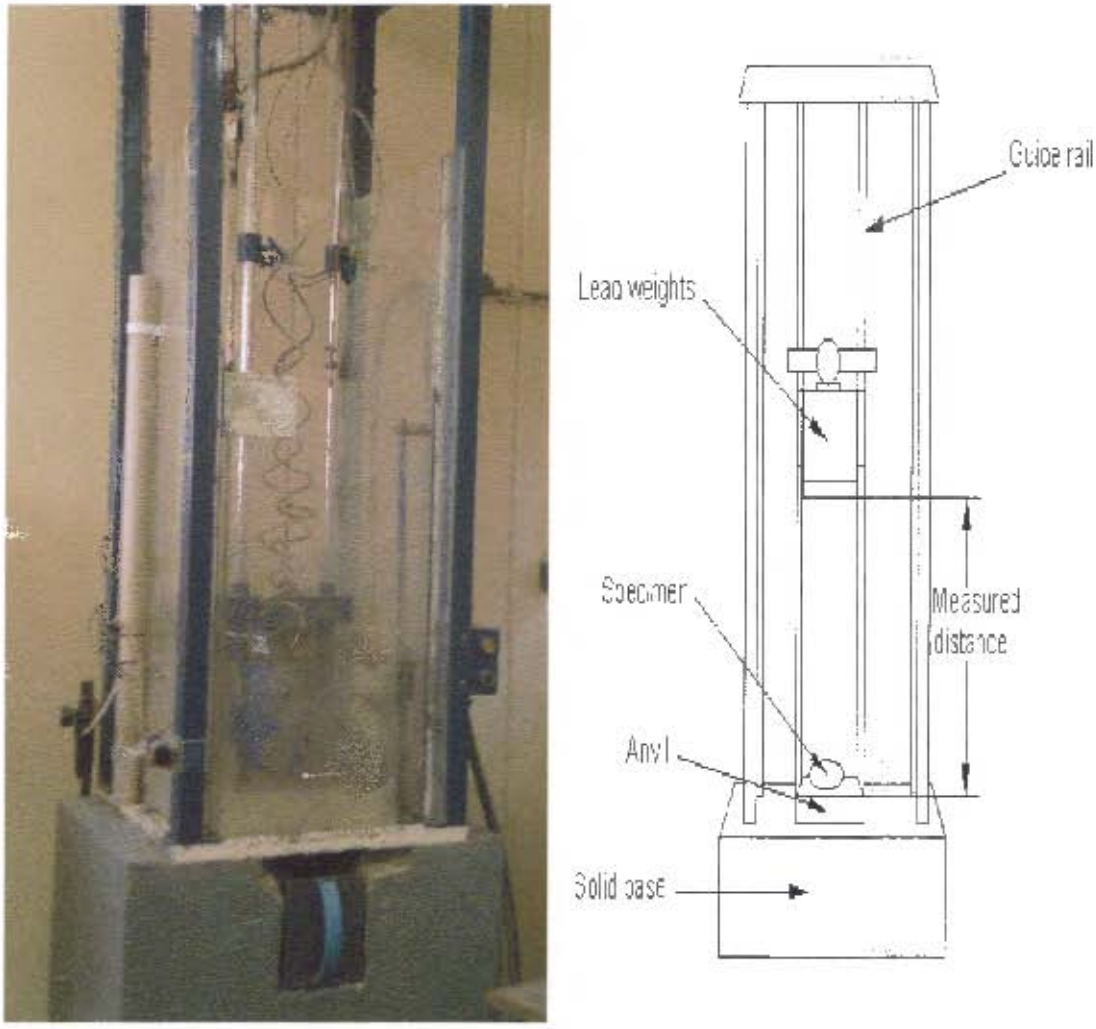


Figure 2.7: Picture and schematic of drop weight test apparatus

By conservation of energy, it is assumed that the available potential energy of the weight is converted to the kinetic energy at impact which is imparted to the specimen. Rock samples are usually prepared by screening to narrow size ranges and standard energy/size combinations are used for a specified number of specimens broken within each range. The mean mass ($\bar{m}$) of specimens is measured prior to the test and the drop height in centimetres ($h$) is calculated according to the formula in Equation 2.7[37].

$$h_i = \frac{\bar{m} E_{in}}{0.0272 M_d} \qquad \text{Equation 2.7}$$

The drop weight mass ($M_d$) is chosen according to the energy required for the particular experiment. It is generally considered better to have more mass than raise the height due to errors introduced by misalignment of the guide rails[57]. Also, as the drop weights do not come to rest squarely on the anvil due to the post breakage specimen remains, the offset height difference ($h_f$) has to be accounted for in calculating the available potential energy. This leads to the equation used to calculate the available impact energy which is:

$$E_{in} = \frac{0.0272 M_d (h_i - h_f)}{\bar{m}} \qquad \text{Equation 2.8}$$

The advantages of the drop weight test are that is has a wide energy/size range and is relatively easy to use. It has been successfully used to provide extensive data for single impact breakage as well as incremental damage experiments[37,56], and has for long proven useful to validating breakage models.

Possible shortcomings of the device mainly deal with its inaccuracies regarding energy measurement. The assumption that all the available energy goes to breakage is inaccurate, as it has been shown that frictional losses from the guide rails and rebounding velocities from weights at greater heights lead to miscalculations[42]. After having accounted for these, it is still well known that not all the available energy from an impact is imparted to a specimen[25], and the drop weight test provides no easy way of measuring this amount. Lastly, in conducting incremental breakage experiments its use has been found to be limited at lower energies,

*Split Hopkinson bars*

Split Hopkinson pressure bars (SHPB) are used to conduct ballistic impact experiments and obtain precise measurements of material load response at high

strain rates. Although many adaptations have followed his original work, design of the bars is accredited to Bertram Hopkinson, who developed the technique in the early forties to measure deformations from dynamic loading events at high velocities, such as the impact of bullets[28].

In its simplest from, the device consists of some form of launcher such as a gas gun, an impactor known as a striker, and two bars in series usually made out of rigid steel, with a specimen loaded in between them. The bars are mounted in a rigid framework and are restricted from movement except in the longitudinal direction where they move freely along bushings or bearings. Figure 2.8 shows a picture and simplified schematic of the arrangement as set up at the Blast Impact and Survivability Research Unit (BISRU), University of Cape Town.

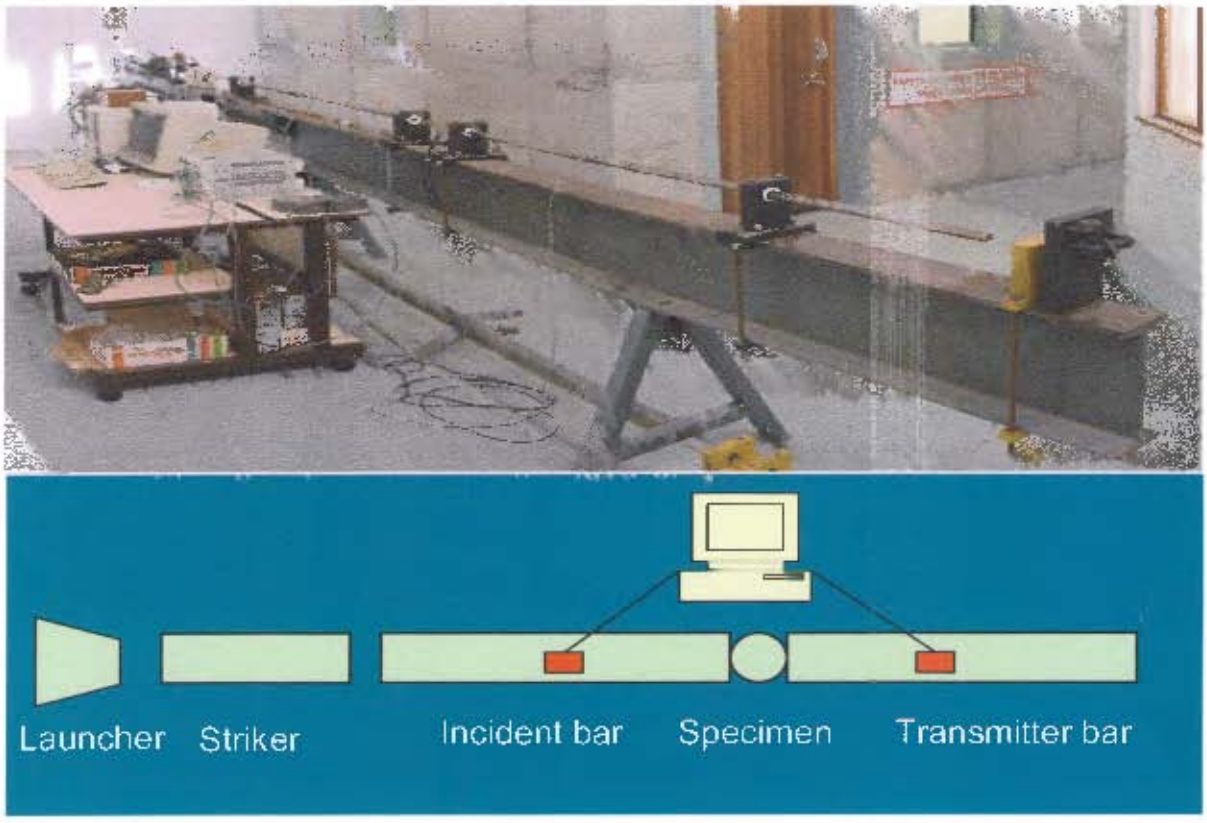


Figure 2.8: Picture and schematic of Hopkinson bar apparatus

When the launcher is fired, the striker shoots out of the barrel and impacts against the face of the first bar, called the incident bar, generating a longitudinal stress wave which propagates along it, and when it interacts with the specimen, a portion of this wave follows through to the second rod, known as the transmitter bar, while the remainder is reflected back along the incident bar. Both bars are mounted with strain

gauges, illustrated in red in the schematic above, and through electronic amplifiers these output voltage signals which are directly proportional to the instantaneous stress at their position.

These signals can be captured and recorded over the entire loading duration by computer and used to accurately resolve force to fracture, incident strain energy, and the fraction of this energy that is absorbed by the specimen during impact. For specimens of known dimensions, deformation characteristics can be calculated and through imaging techniques crack initiation and propagation can also be studied.

According to one dimensional stress wave theory[26,33], the stress ($\sigma_b$) experienced by the bars can be given by the relationship in Equation 2.9.

$$\sigma_b = \rho C V \qquad \text{Equation 2.9}$$

$\rho$ - Bar Density

C – Speed of stress wave transmission through the bar

V- Velocity of the bar

To derive the strain energy associated with each wave, the work done in discrete time steps is accumulated to give the squared integral of the wave as calculated in Equation 2.10. By conservation of energy, strain energy absorbed by the specimen can then be assumed to be the difference between the incoming and outgoing waves.

$$E_v = \sum_{t_0}^{t_{final}} \left( \frac{\left( \frac{\sigma_b(t_{n+1}) + \sigma_b(t_n)}{2} \right)^2 (t_{n+1} - t_n)(A_b)}{C\rho} \right) \qquad \text{Equation 2.10}$$

Where

$E_v$ - Strain energy of wave

$A_b$ - Cross-sectional area of the relevant bar

C – Wave transmission speed through the bar

$\rho$ - Bar density

This technique offers several advantages over conventional impact breakage testing in that it allows for precise measurement of loads and their interactions with specimens. Because it also provides data that can be used to assess exactly how stress and energy interactions lead to breakage, it has been used to establish rock properties and investigate various factors affecting degrees of breakage[4,5]. As its range of testing also allows for incremental breakage tests, it has also been successfully used to conduct multiple impact experiments[6].

The test is limited by the narrow size range that it allows for, as well as the lengthy time taken to perform experiments. Also, because it tests for single particles at a time, it cannot be used to feasibly perform multi particle experiments for most particle sizes.

*Ultra fast load cell*

The Ultra fast load cell (UFLC) is a unique combination of the drop weight and the Split Hopkinson bar. Developed at the Utah Comminution Center in 1986 by Weichert, it was an idea designed to combine the best attributes of the two testsing techniques into one[49,55]. By this technique, the vertical impact of a steel ball of known mass falling under gravity on a specimen from a fixed height is used to provide energy to the particle, while a long steel rod on which the particle rests is fitted with strain gauges to measure the load response of the particle. A schematic of the arrangement as described is provided in Figure 2.9.

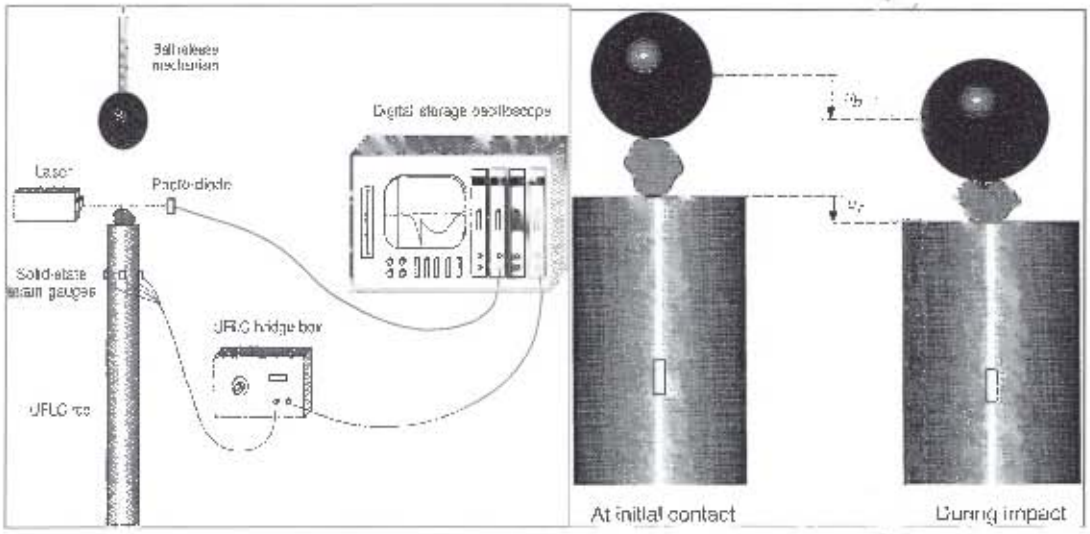


Figure 2.9: Schematic of the Ultra fast load cell[49]

A laser accelerometer set a millimeter or less above the particle is used to precisely measure the velocity of the falling steel ball just prior to impact, and from a momentum balance the relationship in
Equation 2.11 is established.

$$m_b \frac{d^2 u_b}{dt^2} = -F_b + m_b g \qquad \text{Equation 2.11}$$

$u_b$- Position of center of gravity of the ball

$m_b$- Ball's mass

$F_b$- Force exerted by the particle on the ball

g- Acceleration due to gravity

t- Measured time

One dimensional stress wave theory is used to determine the stress in the rod, and assuming negligible inertia of the steel ball and specimen, force-displacement Equation 2.12 is derived.

$$\alpha(t) \quad v_0 t + \frac{gt^2}{2} - \frac{1}{m_b} \int_0^t \int_0^\tau F(\hat{\tau}) d\hat{\tau} d\tau - \frac{1}{\rho A C} \int_0^t F(\tau) d\tau \qquad \text{Equation 2.12}$$

$\alpha$ is an expression for the overall deformation calculated as $u_0$-$u_1$, the distance between the centre of gravity and rod, as displayed in the schematic (Figure 2.9). As the equation only holds true until the return of the reflected wave, UFLC rods are usually at least 5m long to ensure the reflected wave causes no interference in the initial load signal.

Advantages of the UFLC are that it offers exact force time measurements, can be used for bed and single particle breakage and has a wide range of energies and sizes. A disadvantage of the technique is that highly sensitive measuring equipment is required, which may be expensive, and thus the method is not widely available.

A short, portable load cell was later designed by Bourgeois for measurement of breakage properties on site[9], to measure energy versus breakage relationships of industrial ores. Following a developed calibration technique to deconvolute the strain gauge signals from the device it was found that there was minimal loss in resolution in comparison with lab scale load cells. Thus this device could be used to provide quick and accurate in situ single impact breakage characterisation of industrial ores.

*The JK Rotary breakage tester*

The Rotary breakage tester RBT was developed at the Julius Kruttschnitt Minerals Research Centre as part of an Amira P9 project to design and build a new faster breakage characterization device[46]. The machine loads particles by a vibrating feeder through a channel to a variable speed rotor whose rotating action launches them against anvils mounted in a surrounding stator.

After impact, gravity causes product particles to fall along an incline into a collection bucket. A vacuum pump is also supplied to suction any additional progeny. Figure 2.10 shows the first commercial JKRBT, installed at Anglo Research labs, Germiston South Africa in its closed (ready) and open (product collection) positions respectively.

Figure 2.10: Photographs of JK rotary breakage tester

Test particles are fed through the hatch at the top of the device and are aided by the feed mechanism into the rotor-stator system. Two radial outlets in the rotating centrifuge release the particles into the impact chamber in which the anvils are mounted at 90-degree planes to the particle trajectory. A control panel alongside is used to alter both the feed rate and rotor speed, which determines the specific energy of impact. The specific breakage energy can be directly related to the particle velocity through Equation 2.13[46].

$$E_{cs} = 0.5 \cdot V_i^2 \qquad \text{Equation 2.13}$$

Where Vi is the velocity of the particle prior to impact. As this velocity resolved from both the tangential and radial components of the particle motion, calibration of the machine requires a determination of a proportionality constant C which relates the particle velocity to the known tangential velocity.

The RBT has the distinct advantage that it allows for rapid testing of numerous particles across a wide size range, and can be used for both single impact and incremental breakage as its energy requirements are relatively easy to modify. In

comparison with drop weight test data, the device has been found to correlate well across most sizes[46].

Disadvantages of the device at this stage are that firstly it is not commercially available as it has not yet become an accepted standard breakage device. Secondly, although it provides an accurate determination of impact velocity and thus available impact energy to test particles, like the drop weight test it cannot quantify how much of this is actually utilized to cause breakage.

In addition to the devices listed here, a number of other devices have been developed over the years to characterize particle breakage of ore specimens. Among these are experiments such as the Chevron bend test, Brazilian test and Twin pendulum test. The Chevron test is one of the standard methods of mode I fracture toughness testing as established by the International Society of Rock Mechanics (ISRM)[39]. Its apparatus is configured to induce tensile failure in specimens, from which the measured force at fracture and particle dimensions are used to calculate fracture toughness. The Brazilian test also measures tensile strength in rock by measuring stresses created by compression of rock disks[10]. The twin pendulum test was the developed at the JKMRC as the first device to conduct single particle breakage tests from which breakage functions for comminution models could be obtained[38].

## 2.5 DATA REPRESENTATION AND BREAKAGE MODELS

Comminution research is primarily concerned with linking the energy utilized in breakage and the particle size distribution which results[32]. Data provided from breakage experiments is therefore represented in forms which allow for quick interpretations of this relationship. In order to do so, several parameters have been introduced to define measures such as breakage degree, efficiency and fracture energy.

Progeny from breakage experiments is most often represented in terms of the mass fraction of the original particle size that segregates into sizes between a series of screens down to a chosen smallest aperture. Cubic splines can then be used to represent this product size distribution. The cumulative percentage material passing through a given screen deck size is plotted against the smallest to the largest screen sizes employed in the series, where an example is given in Figure 2.11[37].

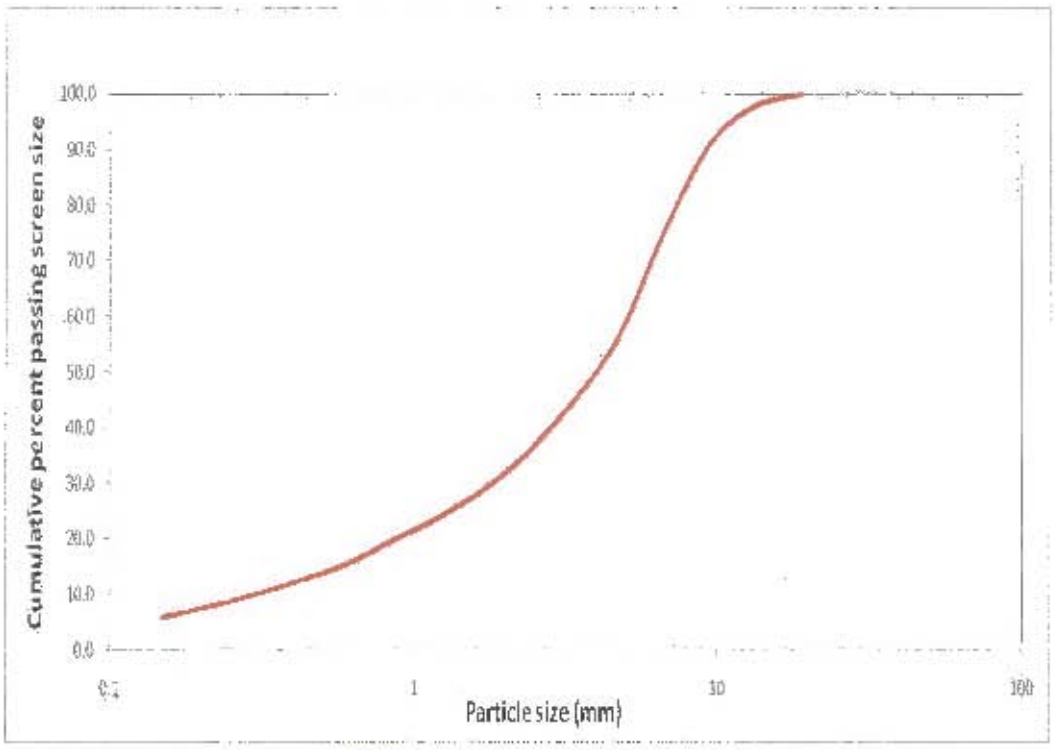


Figure 2.11: Example of cubic spline representation of breakage product from a drop weight test

If the original top screen size is used to define the 100% mark, the x-ordinate can be re-plotted to display the fractions of the original screen size Y and the corresponding percentage t that passes that particular size. Thus $t_n$ can be viewed to be the percentage of original size material passing through a screen an $n^{th}$ or Y/n of that size. Of these, a characteristic index $t_{-0}$ has been chosen as the quantity to measure the degree of breakage. It is defined as the percentage material passing through a screen whose aperture is one tenth of the original geometric mean particle size. Its value has been found to strongly correlate to the mode I fracture toughness $K_{IC}$ (see Section 2.2), although its main usefulness is that it can be used to reasonably estimate the full size distribution of any ore type from a set of curves known as the one parameter family developed by Naranayan and Whiten[38], shown in Figure 2.12, where if the data points in the graph can be obtained for an ore, they can be used to predict the full product size at any other $t_{10}$ value.

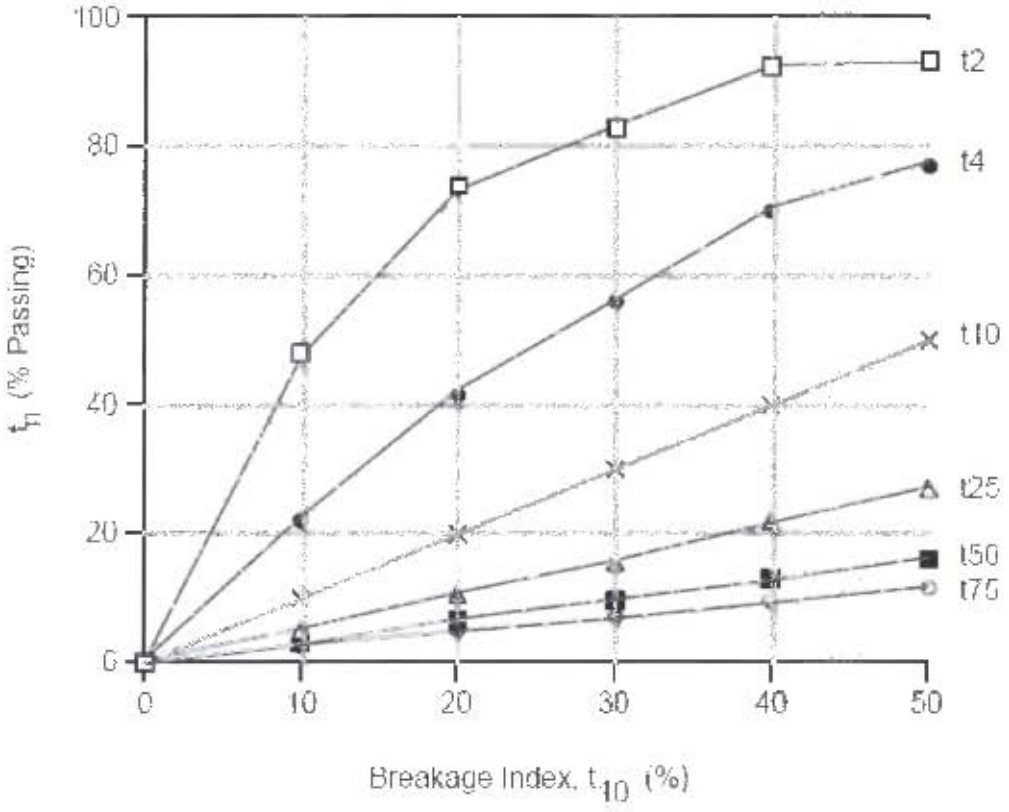


Figure 2.12: One parameter family of $t_{10}$ curves[37]

The $t_{10}$ breakage index is the size product parameter used in most breakage models to calculate the product distribution from breakage at given energies[44]. Many breakage models have been developed and modified in the past[2,45,52], a few of which will now be discussed.

*Breakage models*

A standard equation developed from JK pendulum tests which has long been in use in breakage modeling is the well known $t_{10}$-$E_{cs}$ function:

$$t_{10} = A\left(1 - e^{-b E_{cs}}\right) \qquad \text{Equation 2.14}$$

$E_{cs}$ is taken to be the specific comminution energy (kWh/t) or available energy to cause fracture per mass present, and A and b are impact breakage parameters which can be described through interpretation of a typical $t_{10}$-$E_{cs}$ curve as shown in Figure 2.13. The value of A corresponds to the asymptote or theoretical maximum

value of $t_{10}$ obtainable for an ore (approximately 55~60 in the graph shown), whose exact value is not of great importance as the energy typically required to meet this breakage degree is well above that anticipated in SAG mills. Factor b is related to the linear gradient of the curve at energies lower than 1 kWh/t. As the calculation of each value inevitably affects the other, the value of A.b is often reported as the single value representing an indication of impact breakage hardness, where a lower value indicates a reluctance to fracture for an ore characteristic of a harder tougher mineralogy whilst a higher A.b would indicate a readiness to fracture to high degree characteristic of a softer ore type. Typical ore hardness ranges as reported at the JKMRC are shown in Table 2.3.

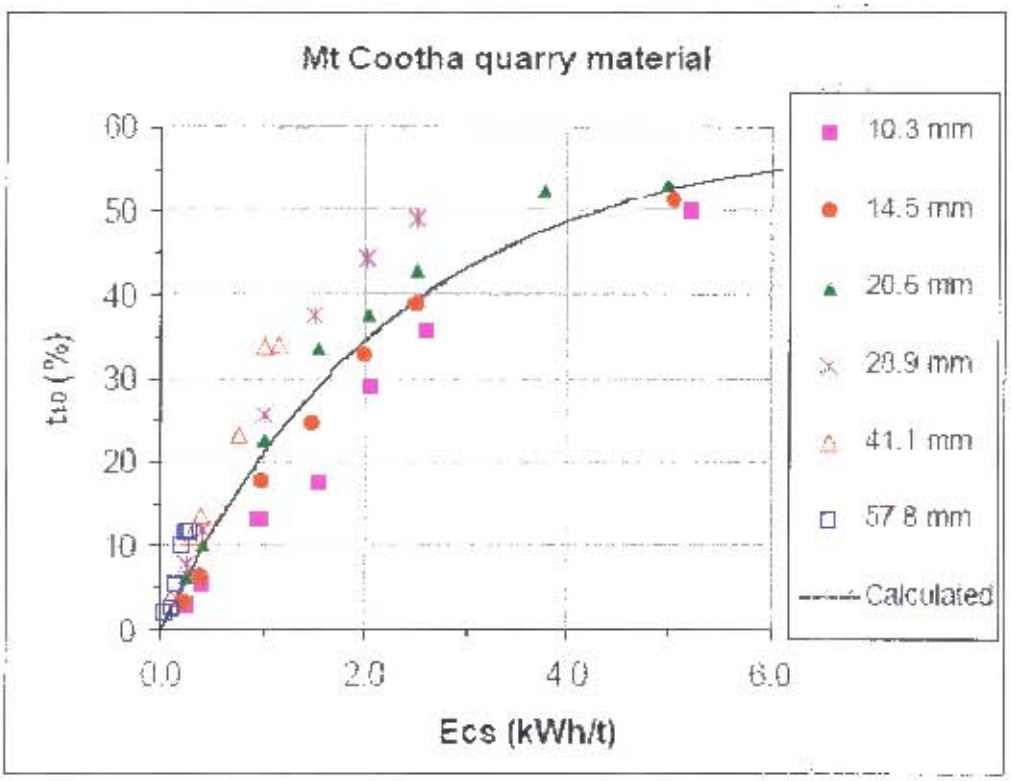


Figure 2.13: Example of a $t_{10}$ vs $E_{cs}$ curve[44]

Table 2.3: Typical reported ranges of A.b and $t_a$ impact breakage parameters

| Property | Very Hard | Hard | Mod. Hard | Medium | Mod. Soft | Soft | Very Soft |
|---|---|---|---|---|---|---|---|
| A*b | <30 | 30-38 | 38-43 | 43-56 | 56-67 | 67-127 | >127 |
| $t_a$ | <0.24 | 0.24-0.35 | 0.35-0.41 | 0.41-0.54 | 0.54-0.65 | 0.65-1.38 | >1.38 |

Although practical, this model has been found to have poor predictive capability particularly across a large range of particle sizes[44]. As illustrated, data across different sizes from the same ore gives different $t_{10}$ curves, and thus over time further parameters have been introduced to improve the model. One such function based on Bourgeois' drop weight data was that of George Banini[4] who developed a function incorporating particle size as seen in Equation 2.15.

$$t_{10} = 100 \times \left[ 1 - \left[ \frac{1}{\left( 1 + \left( \frac{\ln(E_{sv} + 1)}{\alpha_{\infty}^{-1} d^{-n}} \right)^{\beta_m} \right)} \right] \right] \qquad \text{Equation 2.15}$$

In this function, energy ($E_{sv}$) was expressed as volumetric specific input energy (kWh/m$^3$), d was the particle size (mm) while $\alpha_{\infty}$, $\beta_m$ and n where impact breakage parameters to be fitted to test data.

DEM simulations (see Section 2.2) further highlighted that particle fracture in mills did not necessarily occur as a result of solitary high energy impacts, but also very likely from repeated stressing of particles at low energies leading to eventual breakage. From continuum damage mechanics of particle fracture by Tavares and King[50], the following "Particle weakening" breakage model was developed.

$$D_n^* = \left[ \frac{2\gamma}{(2\gamma - 5D_n^* + 5)} \frac{E_{k_1 n}}{E_{n-1}} \right]^{\frac{2\gamma}{5}} \qquad \text{Equation 2.16}$$

Where: $D_n^*$ = The "damage" or fractional reduction in particle stiffness following the $n_{th}$ impact

$\gamma$ = Damage accumulation constant

$E_{k_1 n}$ = Specific strain energy absorbed by particle

$E_{n-1}$ = Energy required to disintegrate particle

Vogel and Peukert developed a model, based on Weibull statistics[52,55] combined with Hertzian theories of contact[16], to also investigate more factors that influenced breakage including ore properties, particle size and repeated stressing. This work provided a model which expressed breakage probability (S) in terms of a series of parameters given in Equation 2.17[52].

$$S = 1 - e^{\left[-f_{Mat} \cdot x \cdot k\left(W_{m,kin} - W_{m,\min}\right)\right]} \qquad \text{Equation 2.17}$$

This model introduced several terms to understanding breakage. A theoretical minimum energy ($W_{min}$ or $E_0$) was defined, below which infinite impacts would never result in fracture. After an intermediate energy region for which breakage occurred after a series of impacts a critical value of energy ($W_{crit}$ or $E_{crit}$) was also given, above which a solitary impact would almost certainly cause breakage. It considered the number of impacts to breakage (k) and particle size (x), while material specific properties were catered for using the parameter $f_{mat}$[53].

Because both Tavares' and Peukert's models expressed breakage in term of parameters that were difficult to define and measure, namely particle weakening and breakage probability, validation of these proved difficult and their usefulness to comminution was thus somewhat impractical[44]. Frank Shi and Tony Kojovic however, modified the Vogel and Peukert model to relate $t_{10}$ to impact energy by the following equation[44]:

$$t_{10} = M\left[1 - e^{\left[-f_{mat} \cdot x \cdot k\left(W_{m,kin} - W_{m,\min}\right)\right]}\right] \qquad \text{Equation 2.18}$$

A major advantage of the equation was that it could be directly correlated to the existing JK model in Equation 2.11 such that the value of A could be replaced by M, while b could be replaced by $f_{mat}.x$, and lastly $k(E_{cs}-E_0)$ could replace $E_{cs}$. This model was successfully validated by the authors in later work[45].

# CHAPTER 3

# SAMPLE PREPARATION, EXPERIMENTAL AND DATA ANALYSIS PROCEDURE

*Overview*
*This chapter describes the approach that was taken to address the objectives laid out in the introduction. It begins with a brief overview of the test objectives and proceeds to explain and list the tests conducted with each of the breakage devices used to meet these. In addition, it provides details of the techniques used in the experimental analysis of the data obtained.*

## 3.1 EXPERIMENTAL FRAMEWORK

In order to test the listed hypotheses and meet the objectives for this thesis a series of experiments were planned and conducted with the listed breakage devices. For the developed test program, experiments were divided into two groups as follows:

I – Single impact breakage:
These sets of experiments were carried out using the drop weight test, split Hopkinson pressure bars and the rotary breakage tester. Individual particles were subjected to impact breakage at standard breakage energies above $E_{crit}$ to characterize ore properties and compare the breakage across the devices.

II – Incremental breakage
Using the rotary breakage tester and split Hopkinson pressure bar, groups of particles were subjected to low energy impacts at several energies between $E_0$ and $E_{crit}$ to establish both breakage probability and predict the likely values of these two parameters for a given size.

To investigate the effect of particle size on breakage characteristics, tests were performed in the following three size classes named as follows:

Small (S) -16mm +13.2mm
Medium (M) -22.4mm +19mm
Large (L) -31.5mm +26.5mm

## 3.2 ORE MINERALOGY AND SAMPLE PREPARATION

Rock types from two sources were used for the experiments conducted across the breakage devices. A common road quarry commonly known as blue stone was the main test material and a gold ore obtained from a local Anglo Gold mine was also chosen. Blue stone was primarily selected as it was found to be an equigranular material which was thus thought likely to yield consistent breakage results. To compare this breakage data with a conventional mining ore, the gold ore was also investigated.

About 1 tonne of blue stone was collected from a local Holcim road and aggregate quarry deposit in sizes ranging from 11.2 to 63mm, while approximately half a tonne of gold ore was made available from an Anglo gold metallurgical laboratory for use in this work. Thus for both ore types material was limited by the amount made available from either source to carry out breakage experiments.

X-ray diffraction tests were carried out on the ores to establish their mineralogy and determine their differences in grain consistency. These tests were carried out at the XRD and XRF facility based at the University of Pretoria. Particles were first reduced to micro scale sizes in a micronising mill and prepared for analysis using a back loading preparation method. Samples were then analysed using an X'Pert Pro powder diffractometer using filtered radiation, and then identified using X'Pert's Highscore plus software.

Although both ores showed a high quartz content, blue stone was identified to have a high percentage of softer feldspars in the form of plagioclase. The gold ore was found to have little to no plagioclase, but had relatively high percentages of muscovites and softer talcacious minerals such as pyrophyllite. Differences in mineral composition for the two types of gold ore were assessed to investigate whether they would significantly influence the breakage behavior. Table 3.1 lists results of the mineralogy tests for the ores tested. Weight percentage relative phase amounts are listed together with three standard deviations of error to the right of each amount.

Table 3.1: Summary of XRD mineralogy tests on selected ores

| Mineral component | Sample 1 Gold ore | | Sample 2 Gold ore | | Blue stone | |
|---|---|---|---|---|---|---|
| | Relative % | Error | Relative % | Error | Relative % | Error |
| **Chalcopyrite** | 0.3 | 0.07 | 0.45 | 0.08 | - | - |
| **Chlorite IIb-2** | 3.19 | 0.42 | - | - | - | - |
| **Diopside** | 1.52 | 0.21 | 0.86 | 0.33 | 1.51 | 0.45 |
| **Enstatite** | 3.89 | 0.6 | 3.08 | 0.66 | 3.57 | 0.72 |
| **Microcline** | 2.62 | 0.69 | - | - | 5.32 | 0.81 |
| **Muscovite** | 19.59 | 0.57 | 20.43 | 0.69 | 8.08 | 0.63 |
| **Plagioclase** | 0.67 | 0.33 | - | - | 30.47 | 0.99 |
| **Pyrite** | - | - | 0.42 | 0.1 | 0.15 | 0.19 |
| **Pyrophyllite** | 1.69 | 0.51 | 8.39 | 0.81 | 2.5 | 0.78 |
| **Quartz** | 66.54 | 0.87 | 66.37 | 0.69 | 48.39 | 1.14 |

A sample of blue stone was examined under microscope and found to have a consistent grain structure. Figure 3.1 shows the particle structure of blue stone under magnification with a 1mm scale provided. Quartz is identified as the darker, fine grained material which forms a matrix around the gray grains, which consist of feldspars such as plagioclase. Muscovites are the brown substance found between surrounding edges of feldspar grains.

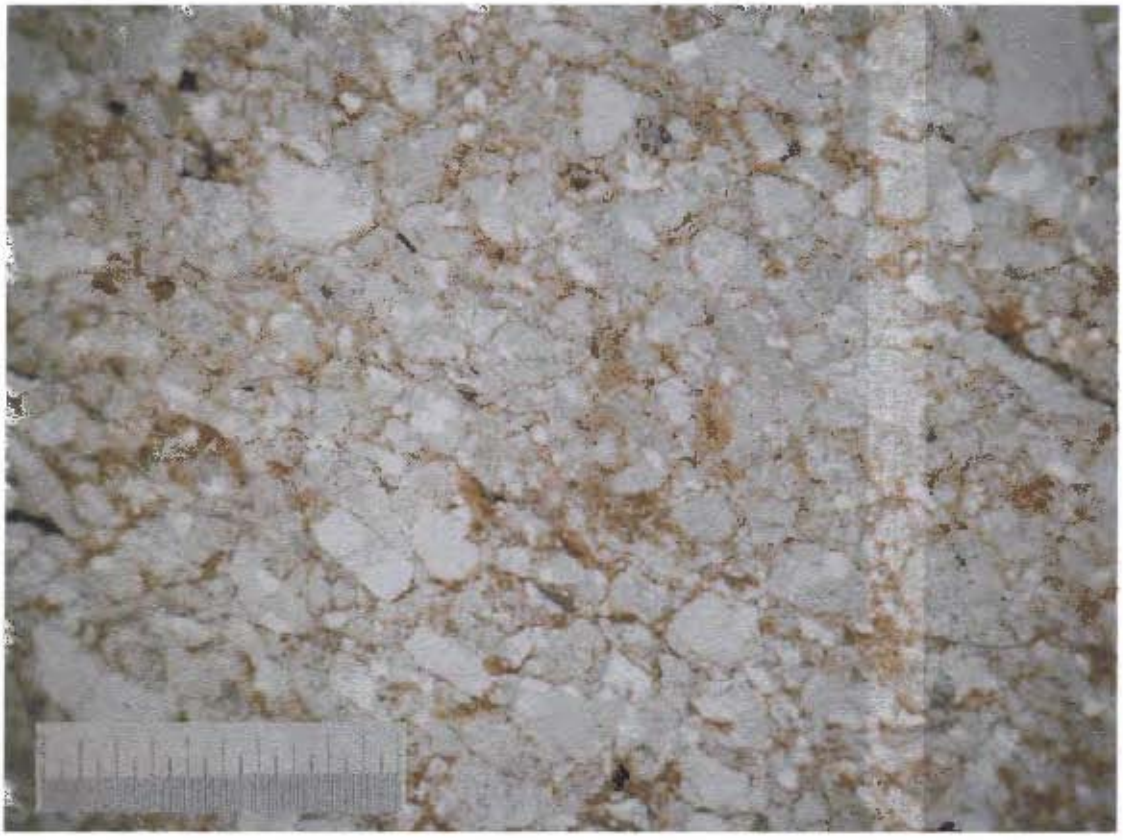

Figure 3.1: Magnified photograph of blue stone showing grain size

Prior experimental work by this author had shown that oval particles tended to absorb more energy than jagged particles[15], thus for this study these two distinct geometries were investigated. Particles that tended to have uneven, jagged edges were termed angular, and those of more oval, smooth shapes were named rounded. The difference in appearance of these two geometries is illustrated in Figure 3.2.

Angular specimens were collected in the three size ranges from a local quarry and depot. A sub-sample of these rocks was then taken to the University of Stellenbosch where a pilot mill was used to condition these into rounded pebbles.

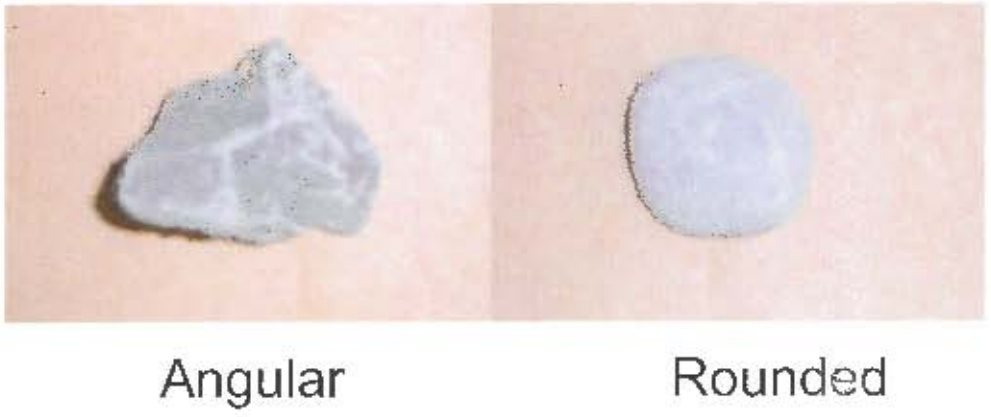


Figure 3.2: Two types of geometries investigated for breakage experiments

Conditioning of angular pebbles was accomplished by tumbling angular pebbles autogenously in a 300mm by 1m long mill at 40% loading. At 75% critical speed with high water content, it was observed that little fracture occurred whilst steady abrasion and gradual rounding or pebbles was achieved. Rounded particles were typically obtained after 4-5 hours of continuous milling under these conditions. Chosen angular and rounded pebbles in each size class were then individually weighed to make sure they fell in similar mass ranges.

The angular gold ores selected for breakage experiments were obtained from the feed belt of two industrial AG mills. Rounded gold ore particles were collected from the centre of the mill charge. These specimens had therefore been subjected to a high stress environment and it was sought to investigate how this would affect their breakage characteristics.

Each ore type was assigned a specific name to aid in distinguishing it during testing and subsequent sieving. Table 3.2 summarizes the ore types that were investigated in this work.

Table 3.2: List of abbreviations assigned to ore types used

| | Name | Geometry | Description |
|---|---|---|---|
| Blue Stone | BS-A | Angular | Coarse pebbles |
| | BS-R | Rounded | Oval particles from milling |
| Gold ore | AG1-A | Angular | Feed to 1st AG Mill (Sample 1) |
| | AG1-R | Rounded | Collected from centre of 1st Mill |
| | AG2-A | Angular | Feed to 2nd AG Mill (Sample 2) |
| | AG2-R | Rounded | Collected from centre of 2nd Mill |

To conduct standard Hopkinson bar strength tests using the blue stone ore, cylindrical specimens of 20mm diameter by 20mm length were also used. These were drilled using a cylindrical diamond drill core of 20mm inner diameter out of flat slabs of rock that had been cut to 20mm thickness. As the core bit and ore tended to heat up considerably during drilling, the procedure was carried out with the slab fully immersed in water mixed with coolant. Figure 3.3 shows an example of a cylindrical specimen used to carry out these experiments.


Figure 3.3: Example of cylindrical specimen used for Hopkinson bar strength tests

## 3.3 EXPERIMENTAL PROCEDURES USED FOR EACH DEVICE

Testwork carried out on each device was planned such that the tests would follow the standard procedures specific to each device as closely as possible. Experimental

methods applied for each device were drawn up such that comparisons could then be drawn between the specific information each would provide. As such, procedures for some experiments had to be developed where there was no standard method.

*Drop weight test*

No incremental breakage experiments were carried out using the drop weight. The tests were primarily done to establish ore breakage parameters using the standard breakage technique. The following is a summary of the procedure that was followed for experiments with this device. This procedure was based upon the standard JK test procedure given from the drop weight test manual[57].

1. Select appropriate drop weight head according to energy required and using extractor tool carefully remove or add lead weights until required mass is attained.

2. Adjust position of the height limiting stop on the device so that drop weight head will be lifted to required test height. Clamp limiting stops of both rails in place. Raise drop weight head slightly to create enough room to place the specimen.

3. Slide open the access door. Using a pair of tongs, place a test particle on the anvil. Close the access door.

4. Raise the drop weight head until it reaches the stop. Release the head and watch for any head bounce. Discontinue the test and recheck calculations if bounce is observed (unlikely below 3 kWh/t).

5. Open the door and measure the gap between the anvil and the face of the drop weight head for at least the first 10 particles in an energy/size combination. Lift the head clear of the anvil and brush the broken fragments aside. If more particles are to be broken within same energy/size range, return to step 3.

6. Record all relevant data from test into a notebook or sheet of paper.

7. Using brush provided collect all rock fragments and fines into collection bucket and transfer into a labeled plastic bag for identification. Keep aside for sizing procedure.

8. Return to step 1.

Gold ore particles in all the listed size ranges were subjected to impact breakage at standard drop weight energies in order to determine and compare values of impact breakage parameters such as A and b (see Section 2.5). Blue stone specimens were used to compare differences between rounded and angular geometries at four selected energy levels.

The influence of particle size on breakage distributions was also investigated for this data. This was done by comparing the breakage degree and particle size distributions at similar energies for the three size ranges listed. Due to a shortage of material, drop weight test data could not be obtained for all the ore types in the three size ranges chosen. A total of 33 drop weight tests were conducted for this thesis, which are summarized in Table 3.3.

Table 3.3: Summary of conducted drop weight tests

| | | ENERGY (kWh/t) | | | |
|---|---|---|---|---|---|
| Ore | Size | 0.25 | 1 | 2.5 | |
| AG1-A | 13.2 -16mm (S) | ✓ | ✓ | ✓ | |
| | 19 -22.4mm (M) | ✓ | ✓ | ✓ | |
| | 26.5 -31.5mm (L) | ✓ | ✓ | ✓ | |
| AG2-A | 13.2 -16mm (S) | ✓ | ✓ | ✓ | |
| | 19 -22.4mm (M) | ✓ | ✓ | ✓ | |
| | 26.5 -31.5mm (L) | ✓ | ✓ | ✓ | |
| AG2-R | 13.2 -16mm (S) | ✓ | ✓ | ✓ | |
| | 19 -22.4mm (M) | ✓ | ✓ | ✓ | |
| | 26.5 -31.5mm (L) | ✓ | ✗ | ✗ | |
| | | 0.2 | 0.6 | 1.6 | 2 |
| BS-A | 13.2 -16mm (S) | ✗ | ✗ | ✗ | ✗ |
| | 19 -22.4mm (M) | ✗ | ✗ | ✗ | ✗ |
| | 26.5 -31.5mm (L) | ✓ | ✓ | ✓ | ✓ |
| BS-R | 13.2 -16mm (S) | ✗ | ✗ | ✗ | ✗ |
| | 19 -22.4mm (M) | ✗ | ✗ | ✗ | ✗ |
| | 26.5 -31.5mm (L) | ✓ | ✓ | ✓ | ✓ |

*Split Hopkinson pressure bar*

Split Hopkinson pressure bars are designed to measure stress-time responses of ductile materials such as metals at high strain rates to characterize their strength by conventional engineering parameters. In order to adapt this device to ore breakage testing, several modifications to the standard set up were required. Generally, impact surfaces are machined flat for compressive pulse loading but because breaking and abrasive contact in mills typically occurs against rounded surfaces such as steel balls or other rocks, ends of the bars were threaded to allow for adjustable end effectors. Two types of end effectors were compared for this work, rounded end effectors of 25mm radius to mimic steel ball breakage in mills, and flat end effectors to match the impact conditions of the other test devices. As the bars were threaded these attachments could be easily screwed on and off as illustrated in Figure 3.4. A photograph of a loaded specimen with rounded end effectors is given in Figure 3.5.

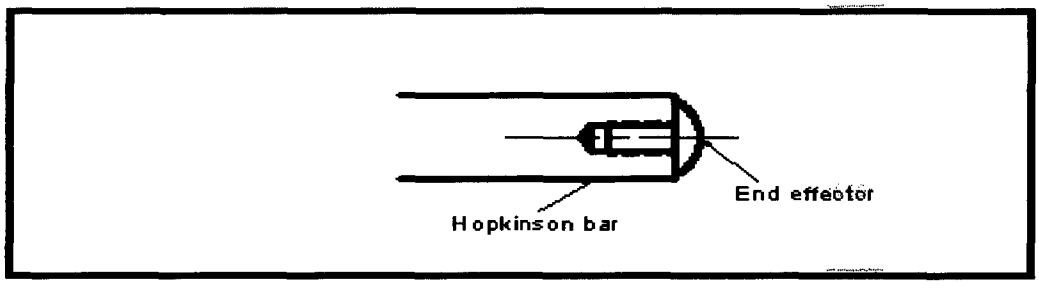


Figure 3.4: Sectioned view of a Hopkinson bar end effector

The end effectors were designed from the same grade of steel as the bars, and their back ends were machined flat to be flush against the bar surface such that pulse transmission through them would have negligible impedance.

To enable easy recovery of rock fragments after impact, a perspex chamber was designed to fit around the specimen and bars, with holes on either side which allowed for the bars to pass through with a large clearance. Figure 3.5 shows an angular specimen mounted with the 25mm end effectors and particle collection chamber. Table 3.4 provides the relevant dimensions and calculated properties from the set of bars used to carry out this work.

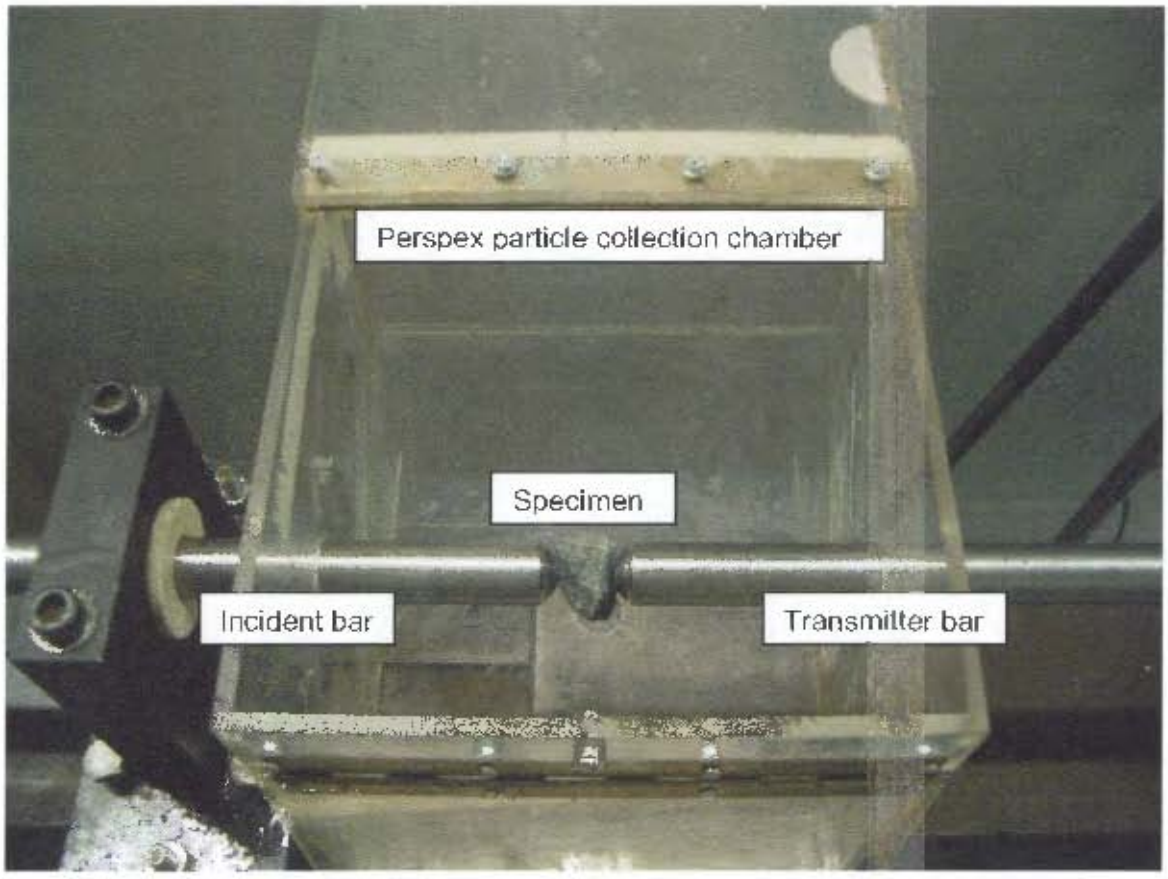


Figure 3.5: Hopkinson bars with 25mm end effectors and collection chamber

Table 3.4: Hopkinson bar dimensions and properties as used in breakage tests

| Property | Incident bar | Transmitted bar | Striker1 | Striker2 | Striker3 |
|---|---|---|---|---|---|
| Mass (kg) | 6.02 | 3.06 | 0.639 | 1.013 | 1.352 |
| Length (m) | 2 | 1.1 | 0.308 | 0.455 | 0.605 |
| Diameter (m) | 0.022 | 0.022 | 0.019 | 0.019 | 0.019 |
| Density (kg/ cubic metre) | 7918 | 7920 | | | |
| Young's Modulus (GPa) | 190 | 191 | | | |
| Strain gauge distance (m) | 0.95 | 0.8 | | | |
| Pulse speed (m/s) | 4904.5 | 4904.5 | | | |
| Strain gauge voltage (V) | 2.4 | 2.4 | | | |
| Amplifier voltage (V) | 8 | 8 | | | |

There was no available procedure for rock breakage testing with this device and as such one had to be developed. All breakage tests performed using the BISRU Split Hopkinson bars followed this procedure:

1. Initially open nitrogen cylinder knob to release pressurized air into gas gun system (done only at the beginning of experiments as a safety precaution to ensure no pressurized air remains in the firing chamber at the end of a run. Close knob at the end of experiments). Switch on trigger circuit.

2. Set/ensure back pressure in gas gun chamber is at least 8 bar, optimally set it to 10 bar (appx. 1Mpa).

3. Load striker into firing tube, using poking tool provided push it back to a selected initial position (for this project where the impact face of the striker lined up with the fifth lining hole of the tube).

4. Check photodiode signals on digital oscilloscope to make sure both signals are displayed on screen, with sufficient volts per division (vertical) to display the change of state from low (0V) to high (5V) of both diodes. LED lights should both be on when signal is low. Set time per division (horizontal) to at least 2ms per division or sufficient to capture change of state of both signals, typically in 10-15ms range. Push "trigger mode" and check trigger level is set to trip on rising edge of first photodiode from the face of the striker, and then press "single" to initiate the capture of a single event.

5. Ensure strain gauge circuitry is switched on. Check that circuit voltage is about 2.5V and amplifier voltage 8.5V, and that both signals are sensitive to movement on the computer software in "Continuous Acquisition" mode with no trigger set. Zero the strain gauge levels if necessary by turning the variable capacitors in the amplifier circuits using a screwdriver in the clockwise or anticlockwise for downward and upward movement respectively (This is only done as a visual aid and is not necessary for calculations). Set trigger to analog, use a suitable pre-trigger of 200 micro seconds or so, and set the trigger to trip at a suitably high voltage to ensure it does not get prematurely tripped by electrical noise or slight movement of the bars (0.8-1V usually sufficient for signals rising over 3V). Set recording time to about 1000 microseconds or sufficient to record entire first series of the three stress waves, with a recommended sampling rate of 1 Kilo samples per second.

6. Load the specimen by placing it in a random orientation between the two bars with the selected end effectors firmly screwed in. Push bars together to hold the specimen in place and close the inspection lid of the Perspex box.

7. Set the pressure in the gas gun to correspond to desired (calibrated) energy level by turning the handle clockwise. Monitor the chamber pressure with the provided gauge and let off any excess pressure with the outlet lever. When done click the "Arm" button in the computer software and raise the safety switch before depressing the fire button which launches the striker. Two rising change of state signals should be obtained on the oscilloscope, and the stress waves should be shown on screen.

8. Use the delta-x feature on the oscilloscope to accurately calculate the time between the photodiode signals. Enter this time along with all relevant data to the particular test in the space provided and save the data as a text file of a chosen name.

9. Open the front end and top lid of the housing and sweep all fragments into a labeled plastic bag for identification. Keep aside for sizing procedure.

10. Return to Step 2.

Both single impact and incremental breakage experiments were conducted according to this procedure, although the energies used were limited by the allowable ranges for the gas gun and strain gauges. Blue stone was the only material tested with this device, where tests with pebbles were limited to the large (L -31.5 +26.5mm) size range. Cylindrical specimens were used to perform standard strength measurement tests.

Single impact breakage tests with this device were primarily conducted to measure standard strength properties and characterize the hardness of the ore. Further tests were conducted to quantify the fraction of impact energy absorbed by particles to cause breakage and investigate its effect on breakage degree. In addition to this various other factors were investigated including the effect of impulse and geometry.

A series of experiments were performed with both angular and rounded specimens to investigate the number of specimens required to provide statistically reliable

information. Also, the same comparison tests were run using the two described different end effectors to measure this effect on energy absorption. As the length of the striker determines the duration of the impact pulse, a set of experiments was also conducted with three different strikers to examine the effect of impulse on particle breakage. In addition, standard Hopkinson bar material strength tests were conducted with cored cylindrical specimens of 20mm diameter and 20mm length to characterize the specimen hardness using engineering parameters. Table 3.5 shows the single impact breakage experiments that were carried out with Hopkinson bars.

Table 3.5: Summary of single impact HPB tests

| Type of test | # tests | Particle type |
|---|---|---|
| End effector comparison | 21 | Rounded |
| Geometry comparison | 37,44 | Angular, rounded |
| Impulse time comparison | 30 | Rounded |
| Energy-size profile | 25 | Rounded |
| Material strength tests | 10 | Cylindrical |

Incremental breakage experiments with the Hopkinson bar were carried out according the procedure developed in this thesis. Due to the lengthy time taken to set up experiments with the Hopkinson bar, as well as the difficulties regarding repeatability using the gas gun, a relatively small number of incremental breakage experiments were performed. 12 tests were conducted to compare the breakage degree resulting from single impact breakage against that from multiple impacts for similar amounts of energy.

At the lowest gas gun pressure of 3 bar, specimens were subjected to impact breakage and then grouped according to the number of impacts that was required to cause breakage. For the incremental breakage tests with this device performed for this thesis, breakage was defined as when a fragment of at least 1/3$^{rd}$ of the original specimen fractured from the original particle. This was determined by inspection following an impact event. After this, the breakage degrees could be calculated according to the number of impacts required to fracture the particles.

*Rotary breakage tester*

Both single impact and incremental breakage experiments were conducted with the rotary breakage tester. Single impact breakage experiments were performed using

the standard method as described in the operator's manual[58], whilst incremental breakage tests were carried out according to a procedure developed in this thesis.

Figure 3.6 shows the onboard control panel for the RBT. Status indicator lights show the status of the RBT and the various switches control the state of the vibrating feeder and vacuum pump. The digital display and interface below can be used to set motor speed and change settings associated with a particular test. When the green status indicator lights after the initial start up procedure, the machine is in its 'ready' state. The two mist separators at the back of the machine should be drained before starting up the rotor to ensure no moisture interferes with the running of the pneumatic circuit.

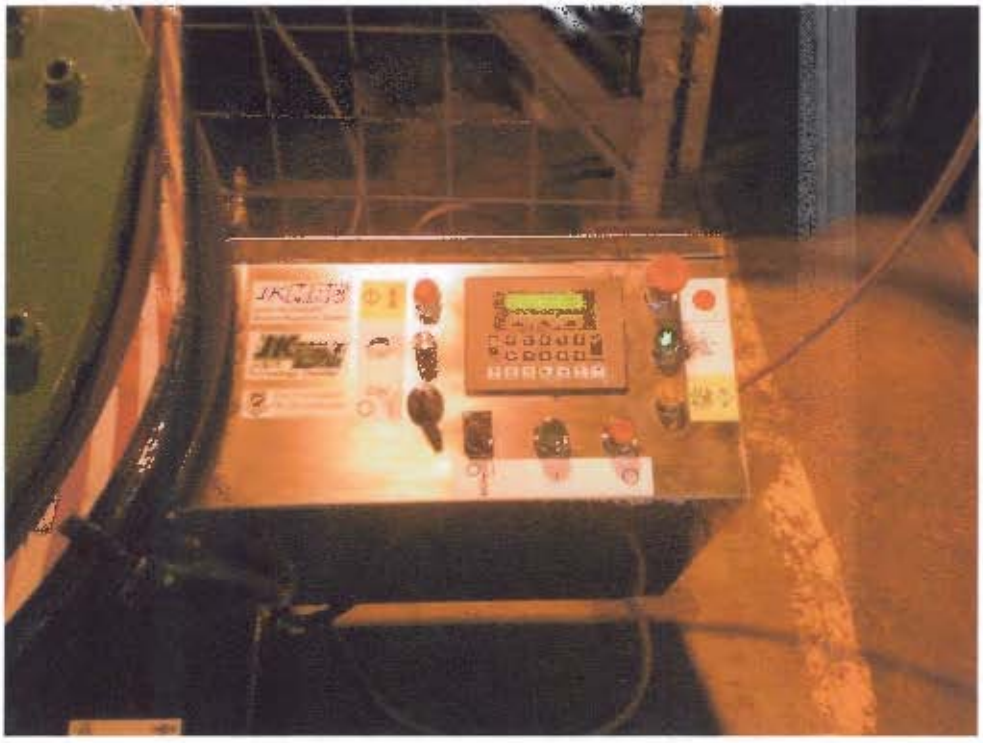

Figure 3.6: Photograph of RBT control panel

Tests with the RBT were conducted according to a similar routine to that provided in the manual[58]. For this work the procedure for an RBT test ran as follows:

1. After the initial start up procedure is complete, drain the mist separators and ensure the oil level is above the red line on the indicator.

2. Switch on the vibrating feeder by turning the knob to the 'on' position. Alter the frequency of its oscillations using the dial above the power knob to a desired position (usually maximum, unless the feeder vibrates heavily, in which case reduce the frequency until stable).

3. Scroll through the menu screen by pressing 'Next' or 'Prev' on the digital panel, until the 'Data input' option. Enter the desired energy input (in rpm; at the time of this project the validation study to enter energy as rpm directly had not been completed) using either the keypad or pressing 'increase' or 'decrease' until the value is reached. Table 3.6 lists the rotor speeds in rpm for standard breakage test energies.

Table 3.6: Calibrated RBT rotor speeds for standard breakage energies[58]

| Size Range (mm) | Number of particles/Test | Required rpm for Target Ecs values | | | |
|---|---|---|---|---|---|
| | | 0.1 | 0.25 | 1 | 2.5 |
| -45+37.5 | 30 | 874 | 1357 | 2641 | |
| -31.5+26.5 | 30 | | 1357 | 2641 | 4103 |
| -22.4+19 | 30 | | 1357 | 2641 | 4103 |
| -16+13.2 | 30 | | 1357 | 2641 | 4103 |

4. Push the green 'start' button and the rotor will accelerate to the chosen speed. The display button will indicate the actual rotor speed in relation to the selected speed above it. While the variable speed drive stabilizes at this rpm, select a sample and record the total mass to be fed to the RBT.

5. After having waited until the rotor speed is constant, insert the test particles into the top hatch at a steady rate of up to about 2 particles per second.

6. After processing the sample, push the red 'stop' button to bring the rotor to a stop. The vacuum pump should automatically turn on when the flywheel reduces below 500 rpm.

7. When the rotor has come to a halt, raise the lock handle and pull out the release pin. The green 'status ready' light should go off. Depress and hold the 'raise' button until the front lid of the RBT rises to a position which allows for access to the interior of the impact chamber.

8. Brush the remaining fragments into the collection bucket and if necessary use the vacuum hose to suction fine particles into the dust bag.

9. Raise the lock lever and pull out the recovery bucket. Withdraw the dust bag filter empty its contents into a tray. Brush the outside of the bag to recover any additional fines lodged in the filter. Empty the contents of the bin into the tray and weigh the total mass of the recovered product.

10. Place the filter bag back in the collection bin and replace the bucket in position, pushing the lever down to lock it in place.

11. Press and hold the 'lower' key on the panel to return the lid to its closed position. When it comes to a stop, raise the lid lock handle and insert the lock pin fully. The green 'status ready' light should turn on.

12. Return to step 3 or 4.

I – Single impact breakage:

For the RBT, standard energies identical to those of the drop weight test had been calibrated by setting the rotor speed to specific values. Tests with the two ore types took place at two selected energy levels to compare the degree of breakage achieved with that of the drop weight test. Both rounded and angular geometries were also investigated with the RBT.

It was sought to compare the scatter in size distribution between a select grouped set of specimens with that of a broad number. Thus tests were done to compare the scatter in data between groups of five specimens each with that of the standard 30 particles for a particular size range. As ore was limited following the drop weight tests, data could not be obtained across all energy levels for the ore types investigated in this study. A total of 45 tests were conducted with the RBT, which are summarized in Table 3.7.

Table 3.7: Summary of single impact RBT tests

| | | ENERGY (kWh/t) | | |
|---|---|---|---|---|
| Ore | Size | 0.25 | 1 | 2.5 |
| AG1-A | 13.2 -16mm (S) | ✗ | ✓ | ✓ |
| | 19 -22.4mm (M) | ✗ | ✓ | ✓ |
| | 26.5 -31.5mm (L) | ✗ | ✓ | ✓ |
| AG1-R | 13.2 -16mm (S) | ✗ | ✓ | ✓ |
| | 19 -22.4mm (M) | ✗ | ✓ | ✓ |
| | 26.5 -31.5mm (L) | ✗ | ✓ | ✓ |
| AG2-A | 13.2 -16mm (S) | ✗ | ✓ | ✓ |
| | 19 -22.4mm (M) | ✗ | ✗ | ✗ |
| | 26.5 -31.5mm (L) | ✗ | ✓ | ✓ |
| AG2-R | 13.2 -16mm (S) | ✗ | ✓ | ✓ |
| | 19 -22.4mm (M) | ✗ | ✓ | ✓ |
| | 26.5 -31.5mm (L) | ✓ | ✗ | ✗ |
| BS-A | 13.2 -16mm (S) | ✗ | ✓ | ✓ |
| | 19 -22.4mm (M) | ✗ | ✓ | ✓ |
| | 26.5 -31.5mm (L) | ✗ | ✓ | ✓ |
| 6 Groups of 5 particles each | 19 -22.4mm (M) | ✗ | ✓ | ✗ |
| BS-R | 13.2 -16mm (S) | ✗ | ✓ | ✓ |
| | 19 -22.4mm (M) | ✗ | ✓ | ✓ |
| | 26.5 -31.5mm (L) | ✗ | ✓ | ✓ |
| 6 Groups of 5 particles each | 19 -22.4mm (M) | ✗ | ✓ | ✗ |

II – Incremental breakage

The most significant incremental breakage work was done with the RBT, mainly to determine the values of $E_0$ and $E_{crit}$ for both blue stone and gold ore and investigate the probability to breakage at energy values below the critical energy value. Rounded specimens were primarily selected for these experiments as this geometry had been found from prior experimental work to give greater repeatability in breakage results[5,6]. For calculations of these breakage values the largest size range (26.5-31.5mm) was selected.

To establish the number of specimens per test needed for an acceptable statistical accuracy, a number of repeat experiments were performed using a chosen energy level. Five energy levels determined by scoping tests to fall between $E_0$ and $E_{crit}$ were selected and for each of these the total initial number of specimens would be fed into the RBT. Following the breakage procedure as outlined for single impact breakage

with this device, material passing the 2nd from bottom (22.4mm) screen size for a 26.5-31.5mm particle was classified as broken whilst anything in the 22.4-26.5mm range was categorized as chipped. For the RBT, material remaining in the original size fraction together with the chipped material would be fed back into the RBT for cumulative impacts and the process would be repeated for five impacts or until at least 70% of the total original starting mass was broken. Table 3.8 shows the incremental breakage experiments that were carried out.

Table 3.8: Summary of incremental breakage RBT tests

| Energy level (E) | Input E (kWh/t) | Rounded gold stone | Rounded blue stone |
|---|---|---|---|
| 1 | 0.013 | ✓ | ✗ |
| 2 | 0.047 | ✓ | ✗ |
| 3 | 0.091 | ✓ | ✓ |
| 4 | 0.167 | ✓ | ✓ |
| 5 | 0.273 | ✗ | ✓ |

## 3.4 DATA ANALYSIS PROCEDURE

A procedure to interpret the breakage data provided from each of the breakage devices had to be decided which would provide information relevant to the objectives of the work.

Product size distribution data was represented by cubic splines (see section 2.5) where the cumulative percentage material passing a given screen size was plotted against a logarithmic scale of screen size. The degree of breakage was defined by the $t_{10}$ parameter, in that the interpolated percentage mass of material calculated to pass through the screen size 1/10 of the specimen's original geometric mean size was the measure used to compare breakage degree. Breakage efficiency was then defined relatively as the breakage degree for a given energy, so that by comparison for identical impact energy the fracture resulting in a higher breakage degree was termed more efficient.

As the Hopkinson bars were restricted from movement in every direction but longitudinal, one dimensional stress wave theory was assumed for calculations from this strain gauge data. Microsoft Excel's solver function was used to find the optimal

fit for the breakage and probability models that were selected. The conditions used were that the root mean square error between the data points and calculated curve fit had to be as close to zero as possible, with the single constraint that $E_0$ had to be greater than 0. A forward biased Newton algorithm was selected to perform the calculation which provided the optimal solution that met the chosen criteria. For every iteration in the values calculated with this software all parameters were reset to zero.

Both the standard JK breakage model and the modified Shi-Kojovic breakage model (see Section 2.5) were fitted to the single impact breakage data obtained from the drop weight tests and the RBT. This fit would then give the values of the A and b parameters, and predict a value of $E_0$ for the modified equation. The Vogel-Peukert probability to breakage model was used to determine $E_0$ and $E_{crit}$ from the incremental breakage data from the Rotary breakage tester.

# CHAPTER 4

# DROP WEIGHT TESTS

*Overview*
*This chapter is devoted to the work done using the drop weight tester. A brief introduction of the design of the device and its contribution to comminution research is given, after which the technique and theory behind the method is provided. Experimental results and accompanying discussions are also presented.*

## 4.1 BACKGROUND AND CONTRIBUTION TO COMMINUTION

Many forms of gravity impact breakage devices have been designed in the past [37, 38,49], one of the most successful of which was the drop weight test (DWT). This was introduced in 1992 at the Julius Kruttschnitt Minerals Research Centre (JKMRC) primarily as a standard technique to determine ore properties for JK SimMet computer software[24,37].

The technique conveniently applied measurement of energy to directly quantify breakage degree and thus its data could be used to establish breakage characterization parameters for different ore types. Values such as the $t_{10}$, A and b value, previously developed to describe material breakage properties[38] could then be fitted to breakage models for use in mineral processing simulators.

Over the nineties, numerous drop weight experiments were conducted to create a database of product distributions for a series of standardized energies, from which established references such as the well known one parameter family of curves was developed[37] (see Section 2.5). Since then, the JK drop weight tester has become a standard characterization of ore hardness in impact breakage research.

## 4.2 DROP WEIGHT TEST TECHNIQUE AND THEORY

As discussed in the literature review (see Section 2.4), the impact breakage apparatus comprises of adjustable lead weights which move freely along vertical guide rails which are attached to a solid base on which is mounted a steel anvil. Using a pneumatic lift control circuit, the selected weights can be lifted to a fixed height by an electric winch. When released these fall under gravity to crush individual particles or beds of rock specimens on the anvil. After this the product can be gathered and swept into the collection bucket provided. A photograph together with a simplified schematic of the machine is given in Figure 2.7.

The mass of each component and drop weight should be carefully measured to ensure accurate determination of the potential energy to the particle. Components include the body, lead weights, steel disk washer and securing unit, which should also be thoroughly cleaned prior to each test to ensure no contamination from previous experiments. A lifting tool is typically used to engage and disengage lead disks to and from the drop weight body, as protection from injury under the heavy load and as they tend to deform easily under impact. Care is also taken never to release the drop weight without a test particle as this may result in damage to the steel impact faces[57].

An air supply of at least 100psi (0.689MPa) is required to provide compressed air to the air filter-regulator unit which controls the lift-release pneumatic mechanism. A lubricator unit is also provided to monitor that the oil level stays within an acceptable level. After the drop weight is lifted against the height limiting stop, which is fastened in place by the operator, the specimen can be placed onto the anvil. This should be done using tongs as a safety precaution. The inspection door must be slid shut for the actuator to become operational, whereupon the drop weight can be released by pushing the actuator release valve. According to laboratory safety standards, the device must be operated with gloves, safety goggles and ear protection as higher energies typically generate loud noise[57].

*Summary of relevant theory*[37]

No calibration is required to calculate the impact energy of the drop weight as the specific breakage energy is simply the potential energy of the falling drop weight.

These are assumed to be equal under the condition that the drop weight has negligible rebound velocity after impact. The height (in centimeters) to which drop weight is to be raised is calculated using Equation 4.1.

$$h_i = \frac{\bar{m} E_{in}}{0.0272 M_d} \qquad \text{Equation 4.1}$$

Because the drop weight does not come to rest squarely on the anvil due to the interference from post breakage fragments, this offset height has to be accounted for in the energy calculation. A standard convention is to regard this offset height to be half the geometric mean of the initial test particle size; thus for a particle of initial size –a cm +b cm the offset height would be calculated according to Equation 4.2.

$$h_f = 0.5\sqrt{a \times b} \qquad \text{Equation 4.2}$$

Hence the calculated specific impact energy is calculated to be given by the relationship in Equation 4.3.

$$E_{in} = \frac{0.0272 M_d (h_i - h_f)}{\bar{m}} \qquad \text{Equation 4.3}$$

Where

$M_d$- Drop weight mass

$\bar{m}$ - Mean particle mass of specimens

## 4.3 RESULTS AND DISCUSSION

Drop weight tests were performed based on available material from the six variations of the gold ore and blue stone ore types discussed in Chapter 3 (see section 3.2). Ores were distinguished based on metallurgical names assigned to them during testing (see Table 3.2) and separated into size fractions named small (-16mm +13.2mm), medium (-22.4mm +19mm) and large (-31.5mm +26.5mm). In line with

the standard experiment, drop weight test energies 0.25, 1 and 2.5 kilowatt hours/tone and 15 total particles per energy, were used on the gold ore types.

As the available material was limited, no drop weight tests could be performed on AG1-R ore, and only 1 energy was used for AG2-R in the large (-31.5 +26.5mm) size fraction. Tests with blue stone took place only in the large size fraction at 0.2, 0.6, 1.6 and 2 kilowatt hours/tonne, with the 15 particles used per energy. Breakage size distributions for the angular and rounded gold ores are displayed in Figure 4.1 to Figure 4.3. It can be observed that the distribution becomes gradually finer with increase in breakage energy and decrease in particle size as is to be expected.

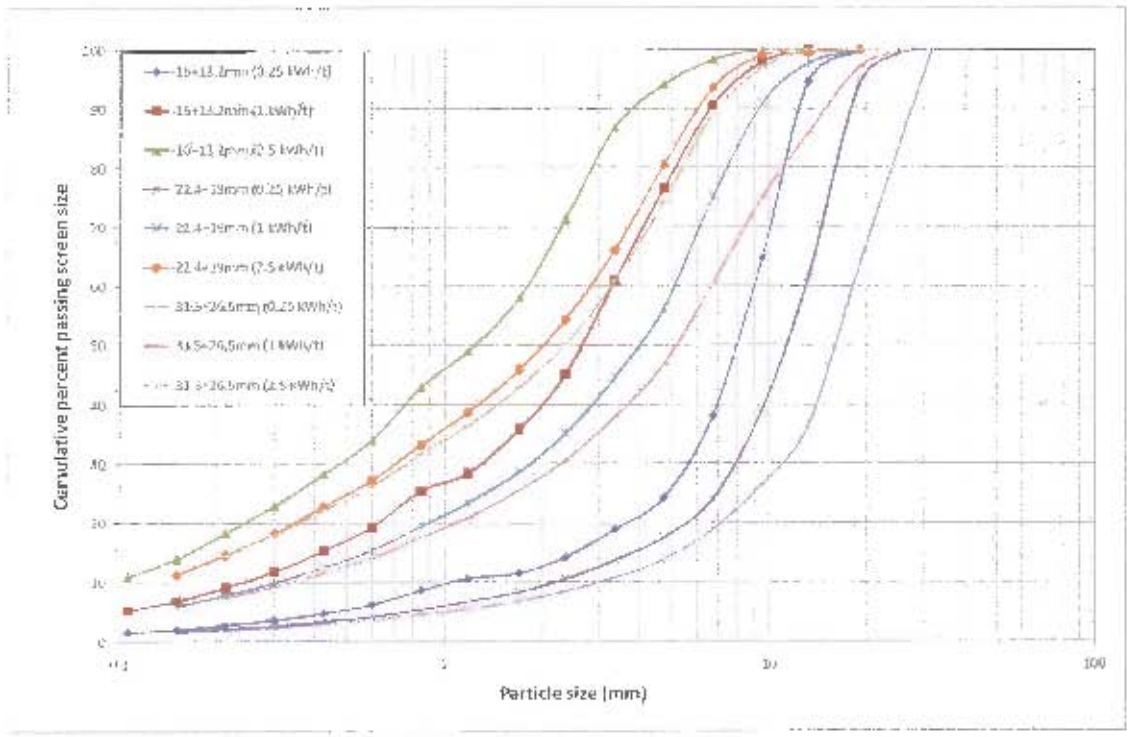


Figure 4.1: Drop weight test size distribution for AG1-R ore

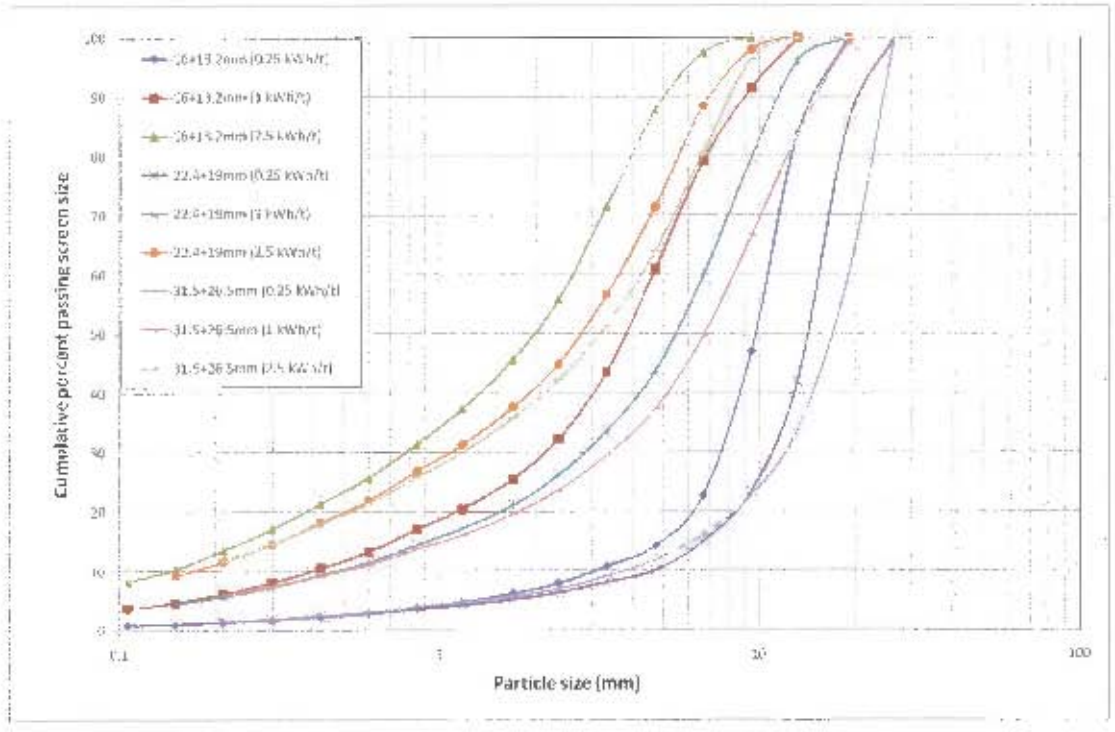


Figure 4.2: Drop weight test size distribution for AG2-A ore

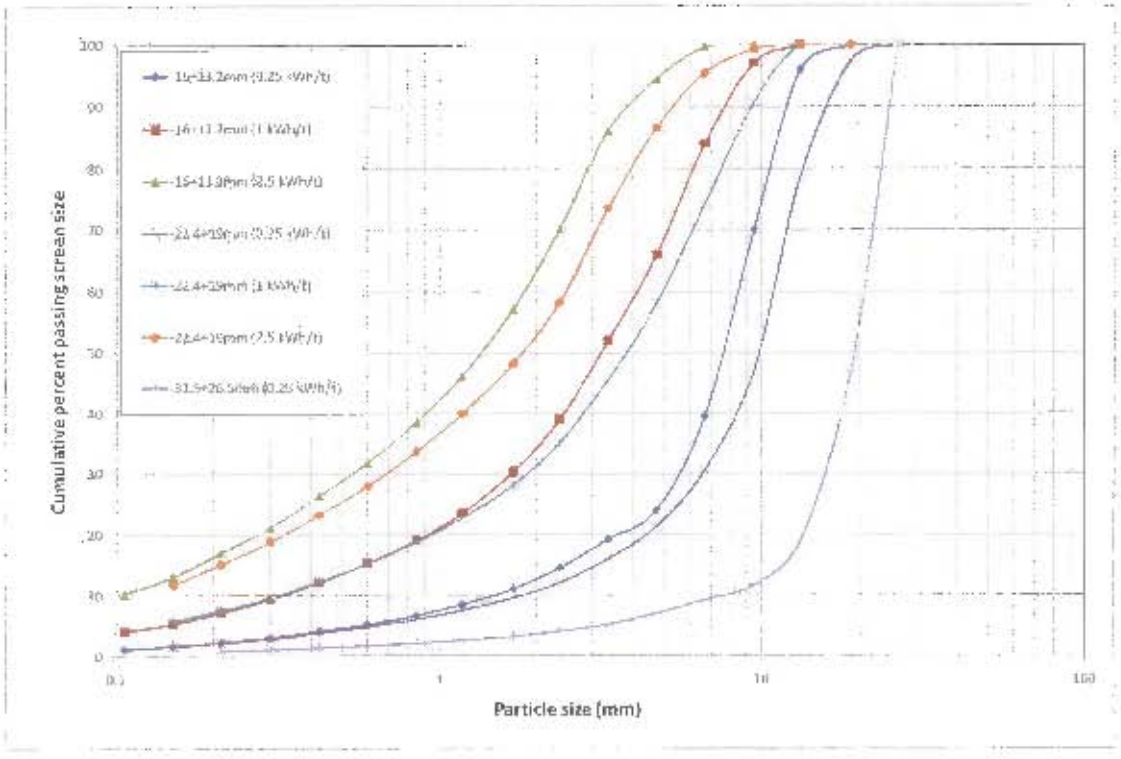


Figure 4.3: Drop weight test size distribution for AG2-R ore

The A.b parameters of all ore types were calculated according to the method described in Section 3.4, and these are provided in Table 4.1. Closely similar values were observed by fitting the standard breakage model and the modified model to

breakage data. The fit using the Shi-Kojovic breakage model however, was noted to yield consistently higher A.b hardness values, likely attributed to the offset introduced by the minimum energy to breakage $E_0$ in the equation. As the lowest energy for drop weight tests was 0.25 kWh/t the fitted values of $E_0$ were merely estimates for the particular ores types. The low A.b values indicated that all the ore types were of a brittle nature showing in the hard to medium hardness range (see Table 2.3).

Table 4.1: Relative % increase in calculated A.b parameters from Drop weight test

| | A.b results | | |
|---|---|---|---|
| MET no | Standard eq. | Modified eq. | % increase |
| AG1-A | 45.9 | 47.7 | 3.9 |
| AG2-A | 31.0 | 33.8 | 9.0 |
| AG2-R | 39.6 | 40.4 | 2.0 |
| BS-A | 44.4 | 46.7 | 5.2 |
| BS-R | 43.8 | 46.1 | 5.3 |

Table 4.1 shows the percentage increase between the A.b values obtained from fitting breakage data to the standard model with that of the modified model. As observed from these calculations, AG2-A ore showed the highest percentage increase in A.b while the other ore types showed 2-5% increase between the standard and modified model. This showed a good correlation between the two.

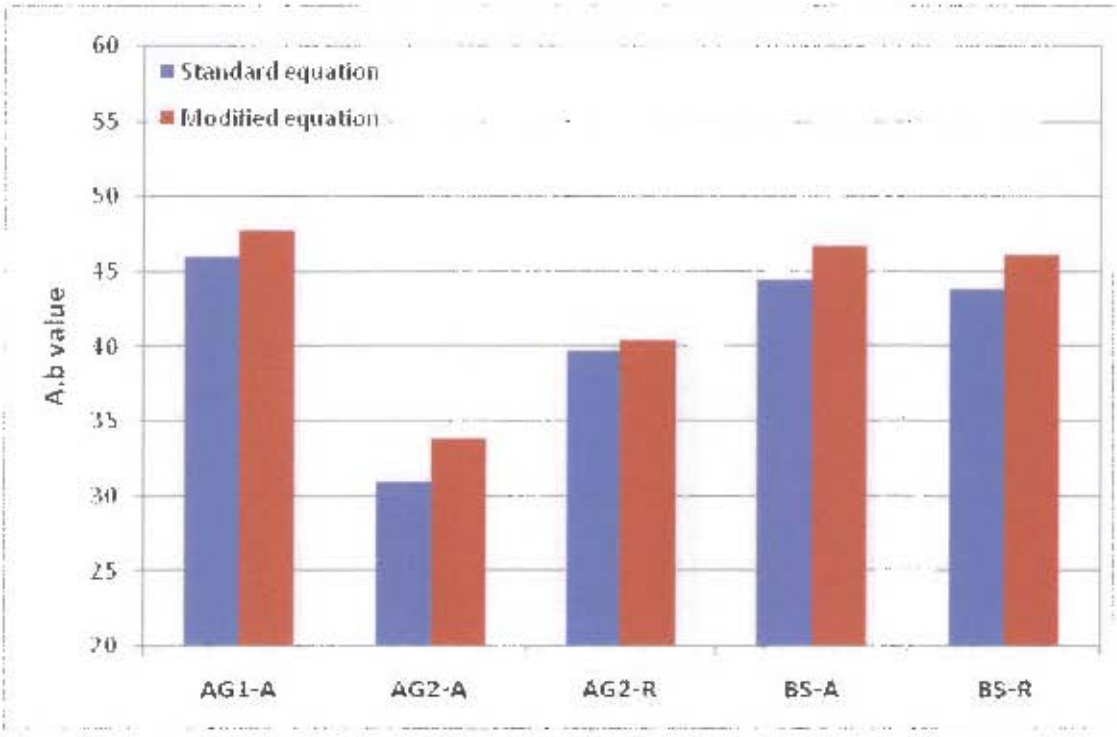


Figure 4.4: Bar graph of A.b values for drop weight data calculated from two models

The harder of the two angular ore types was the AG2-A ore. Results also showed that the rounded particles decreased in hardness from an A.b value of 31.0 to 39.6, which gave credence to the assumption of gradual particle weakening (see Section 2.5) as the ore was subjected to a high stress milling environment. For the blue stone, little difference was observed between the A.b values of the angular and rounded geometries. This showed that the milling environment under which these particles were rounded (see Section 3.2) did not significantly affect their hardness.

The value of A indicates the theoretical maximum breakage degree to which an ore can fracture, while the value of b indicates whether the ore fractures toward this maximum degree gradually over an increasing energy range or rapidly. These hardness parameters were calculated by fitting $t_{10}$ curves to breakage data following the procedure discussed in Section 3.4. As the A and b values for both equations were closely similar, these curves were found to closely overlap as shown in Figure 4.5 to Figure 4.7.

Figure 4.8 shows the best model curves fitted to data for the single size (-31.5 +26.5mm) tested for BS-A and BS-R. As observed in Table 4.2, because the A and b values obtained for each geometry were closely identical, a single curve could be used to fit both geometries using both the standard and modified breakage model.

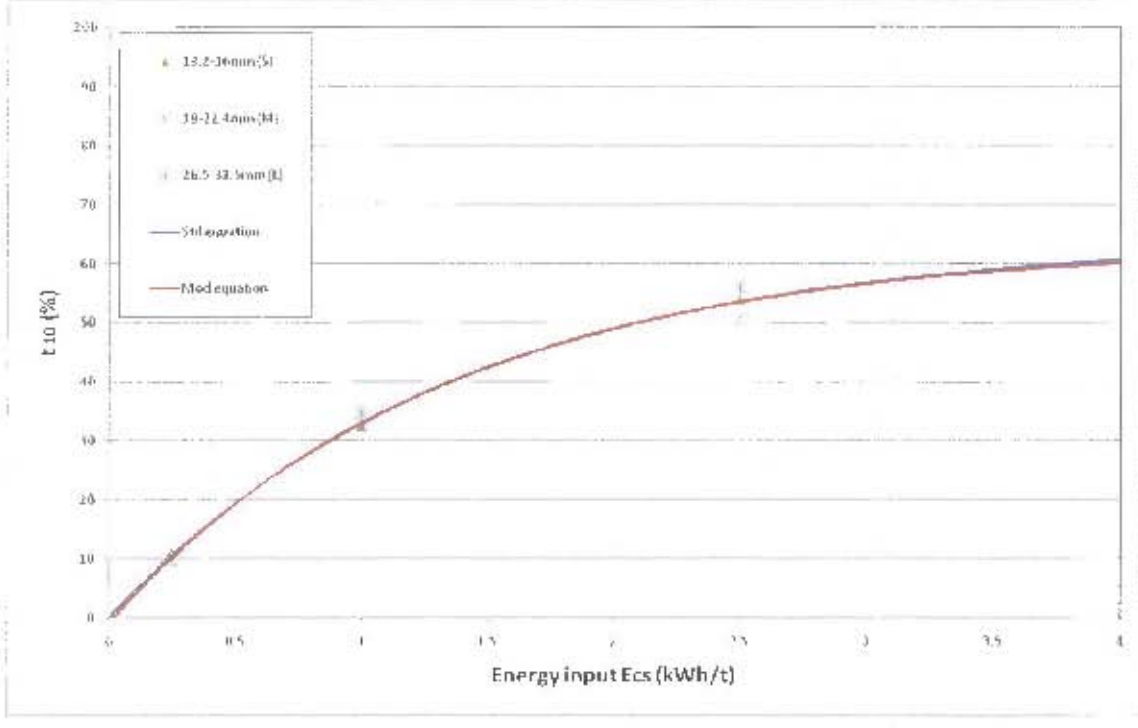


Figure 4.5: Drop weight test $t_{10}$ curves for AG1-A ore

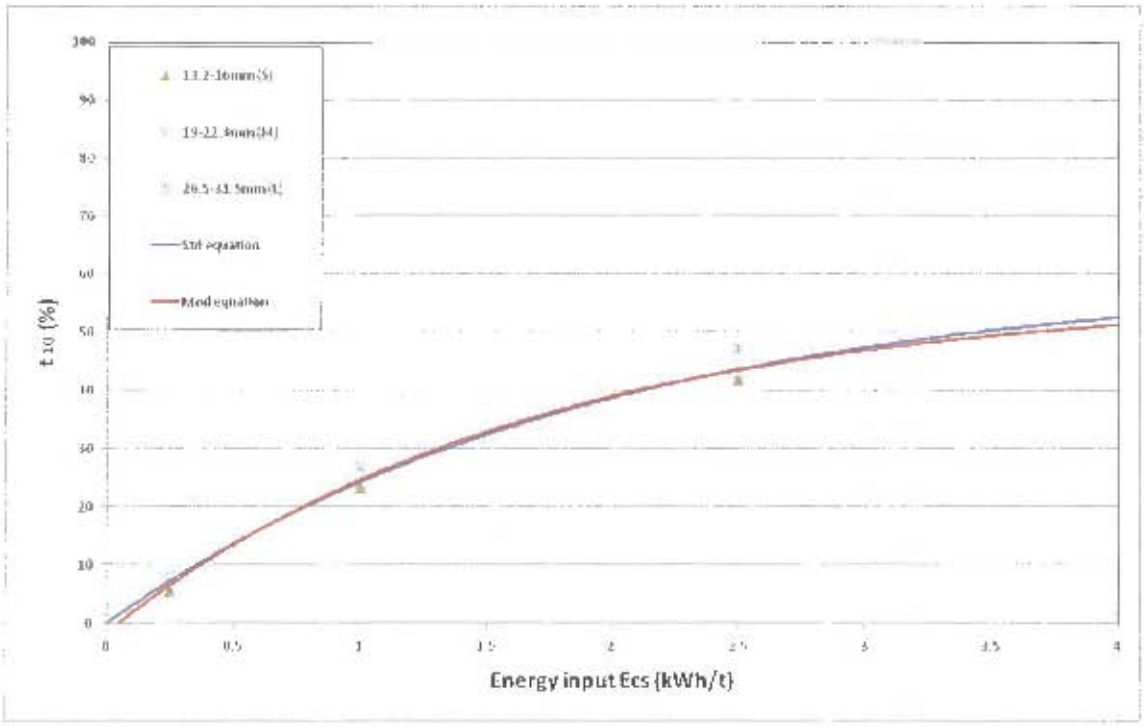


Figure 4.6: Drop weight test $t_{10}$ curves for AG2-A ore

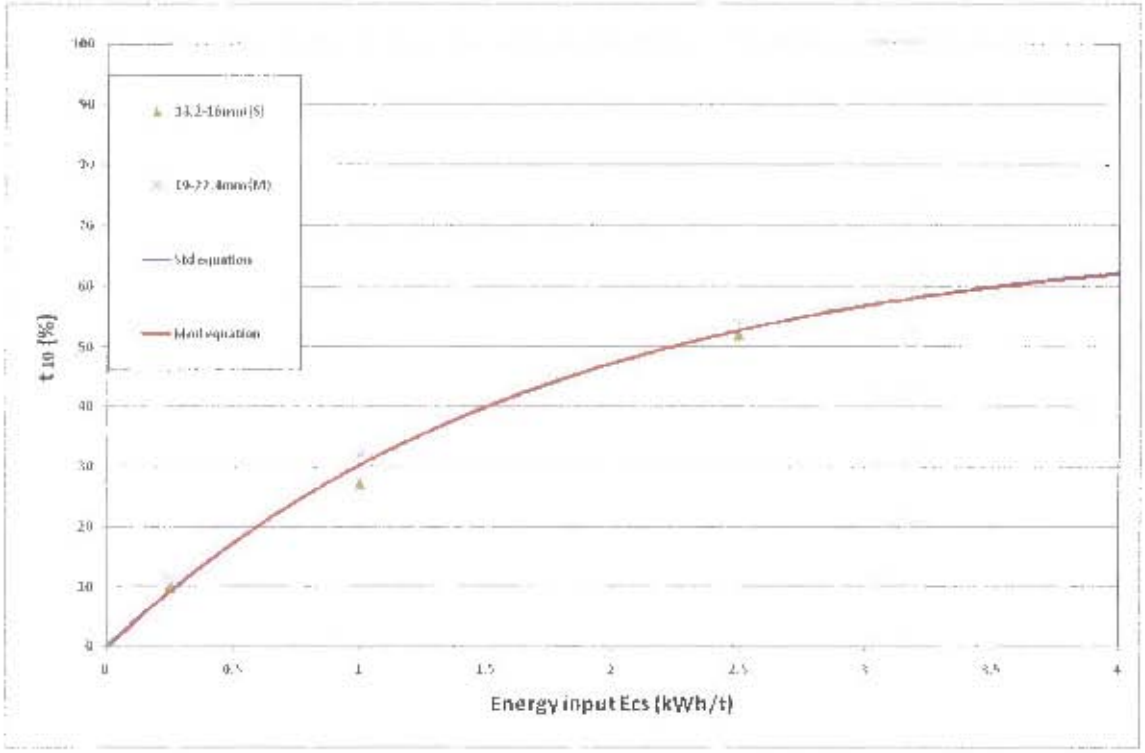


Figure 4.7: Drop weight test $t_{10}$ curves for AG2-R ore

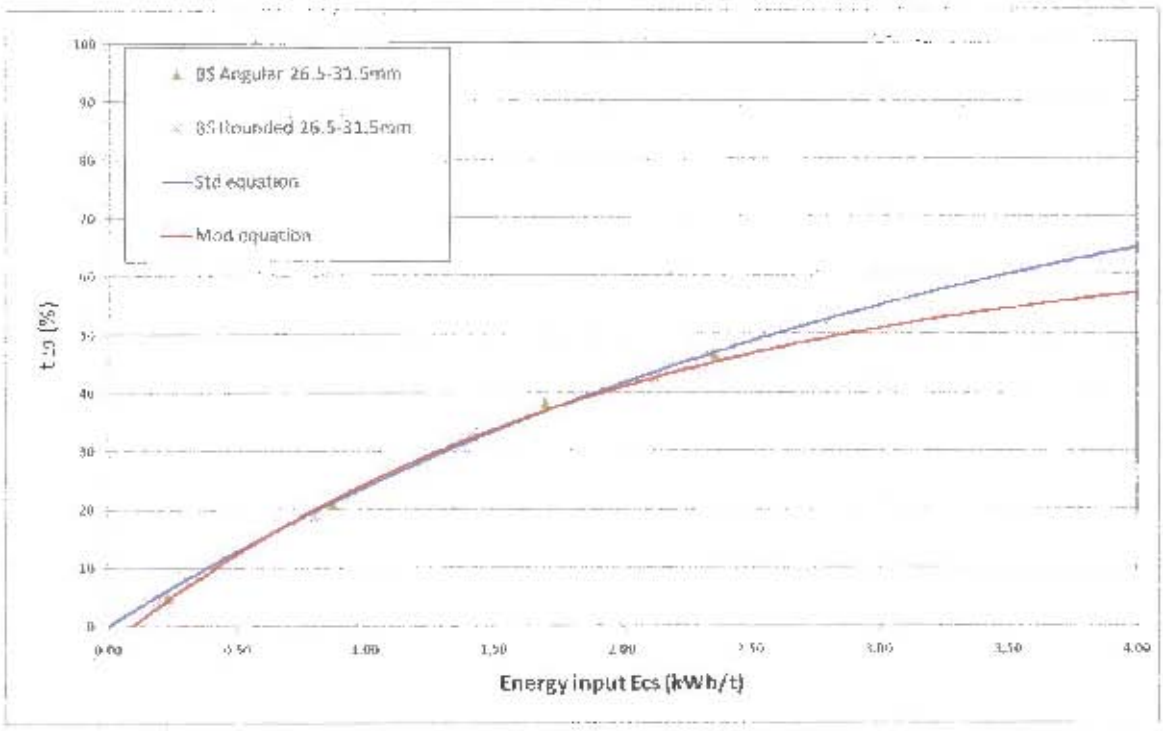


Figure 4.8: Drop weight test $t_{10}$ curves for BS-A and BS-R ore

Table 4.2: Calculated A and b breakage parameters for Drop weight test

| Gold ore | | A | b |
|---|---|---|---|
| AG1-A | 13.2 -16mm (S) | 64.39 | 0.75 |
| | 19 -22.4mm (M) | 64.38 | 0.65 |
| | 26.5 -31.5mm (L) | 64.78 | 0.76 |
| | Standard model fit | 64.39 | 0.71 |
| AG2-A | 13.2 -16mm (S) | 60.32 | 0.49 |
| | 19 -22.4mm (M) | 60.32 | 0.5 |
| | 26.5 -31.5mm (L) | 60.32 | 0.56 |
| | Standard model fit | 60.32 | 0.51 |
| AG2-R | 13.2 -16mm (S) | 76.04 | 0.46 |
| | 19 -22.4mm (M) | 68.92 | 0.64 |
| | 26.5 -31.5mm (L) | - | - |
| | Standard model fit | 69.31 | 0.57 |
| **Blue Stone** | **26.5 -31.5mm (L)** | A | b |
| BS1-A | Angular | 63.47 | 0.7 |
| BS2-R | Rounded | 63.44 | 0.69 |

Table 4.2 shows the values of A and b obtained with the standard JK breakage model. As the particle size effect is not considered in this model, independent curves were fitted for each particle size class so that the size specific values of A and b for this model could be compared against the conventional size independent values. It was noted that while the maximum breakage degree A remained relatively consistent

the value of b was different between sizes of individual ore types. The trend noted with gold ore types in the $t_{10}$ curves from Figure 4.7 to 4.8 was that for energies below 1 kWh/t breakage degree was similar across all three sizes. For 2.5 kWh/t larger breakage degrees were consistently obtained for the largest size and while the lowest value was for the smallest. Also noted was that the hardest ore AG2-A had the lowest maximum degree of fracture, indicated by the lowest A value, while AG1-A had the highest maximum degree of fracture. A bar graph of A.b values for each particle size compared against the standard fit are displayed in Figure 4.9.

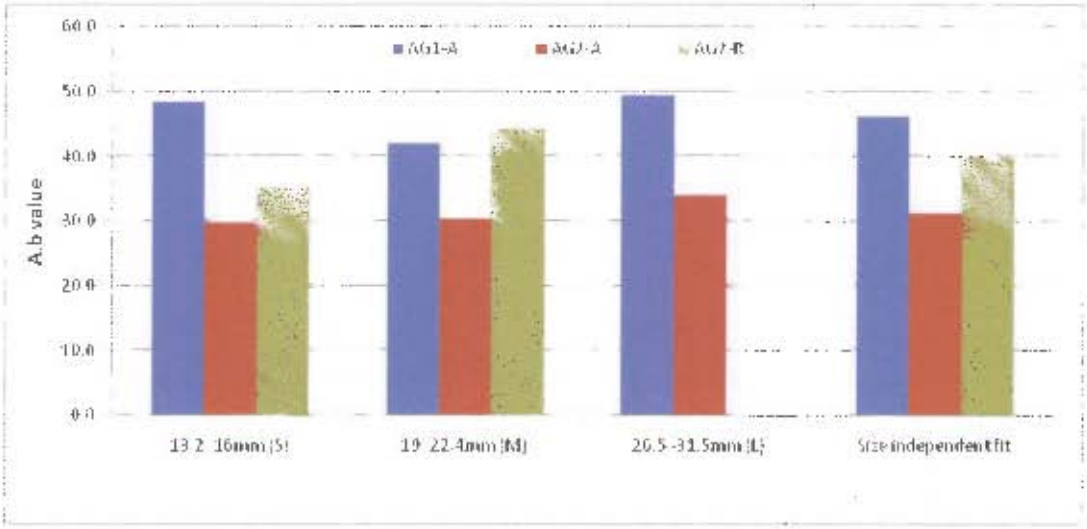


Figure 4.9: Bar graph of size specific A.b parameters from drop weight test

A plot of P80 values for each particle size was plotted to further investigate the size effect (Figure 4.10). It was observed that P80 increased steadily with particle size. All gold ore types exhibited this tendency particularly below 1 kWh/t where a sharp almost linear increase was obtained, whereas at higher energy levels this product size tended to level out with a lower gradient.

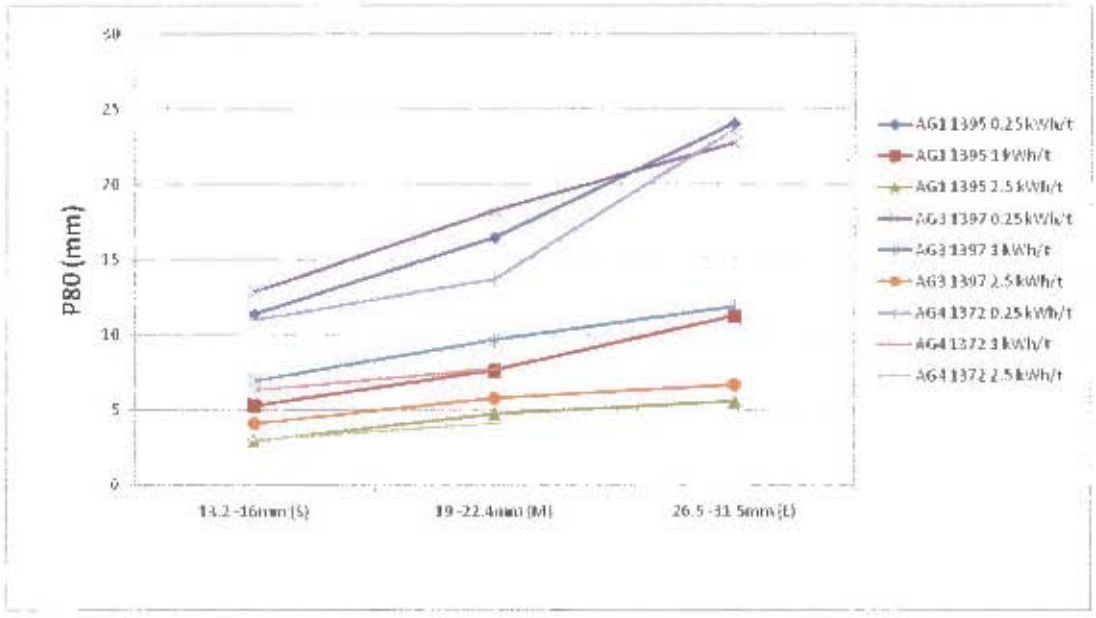


Figure 4.10: Graph of P80 sizes for gold ore obtained from drop weight experiments

Figure 4.11 shows a graph of P80 sizes for blue stone ore at the breakage energies tested to compare the effect of geometry on this size. The P80 decreased similarly between both geometries, highlighting further that ore geometry had little effect on breakage results for the drop weight test.

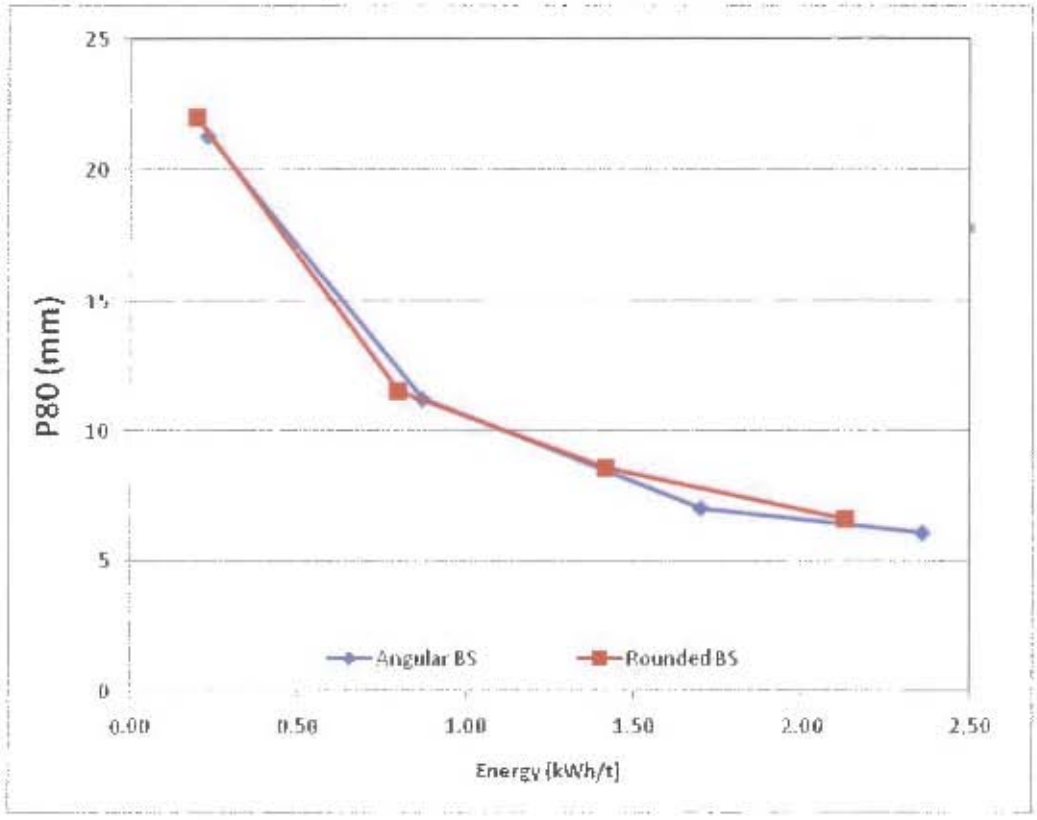


Figure 4.11: Graph of P80 sizes for blue stone ore from drop weight tests

To compare relative breakage fineness between gold ore types, breakage distributions for each size were plotted and displayed from Figure 4.12 to Figure 4.14, which showed similarity to results of the calculated hardness parameters (Table 4.1). The hardest ore AG2-A was seen to consistently fracture into coarser fractions at similar energies across all sizes, while the weakest ore AG1-A usually separated into the finest fractions. This result was observed across all three size fractions.

A summary of all drop weight test results can be found in Section 7.1.

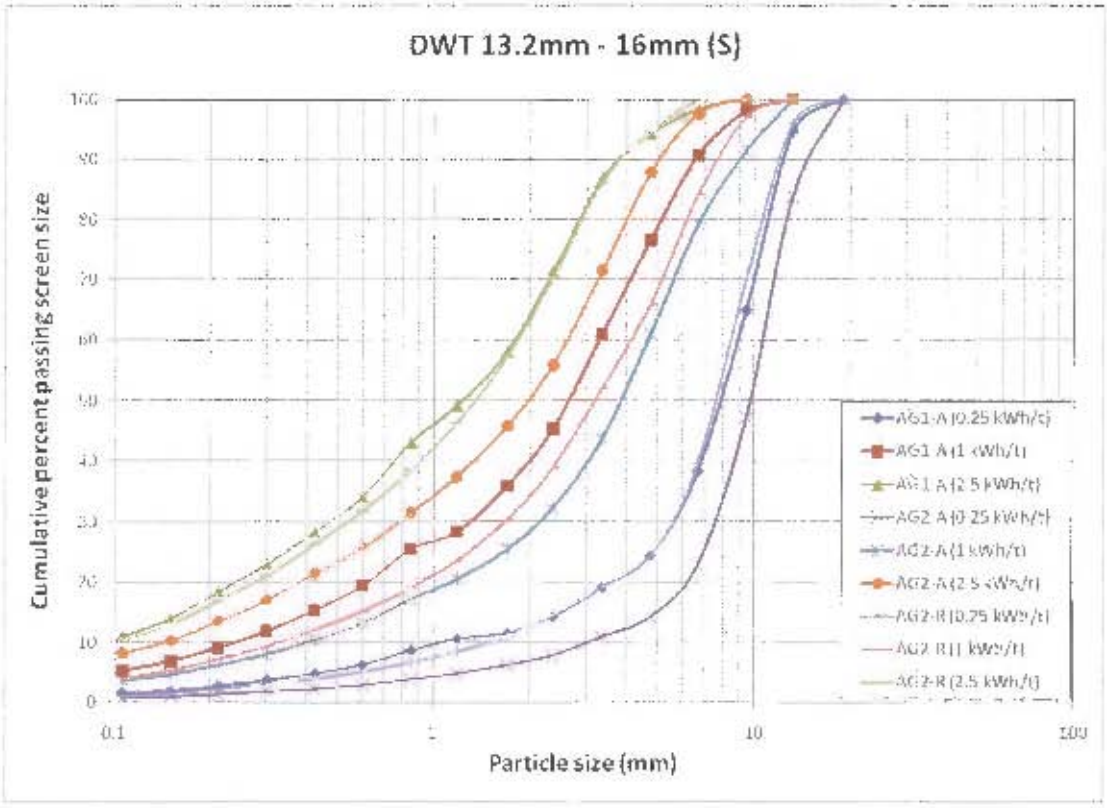


Figure 4.12: Drop weight test breakage distributions for gold ores in small size class

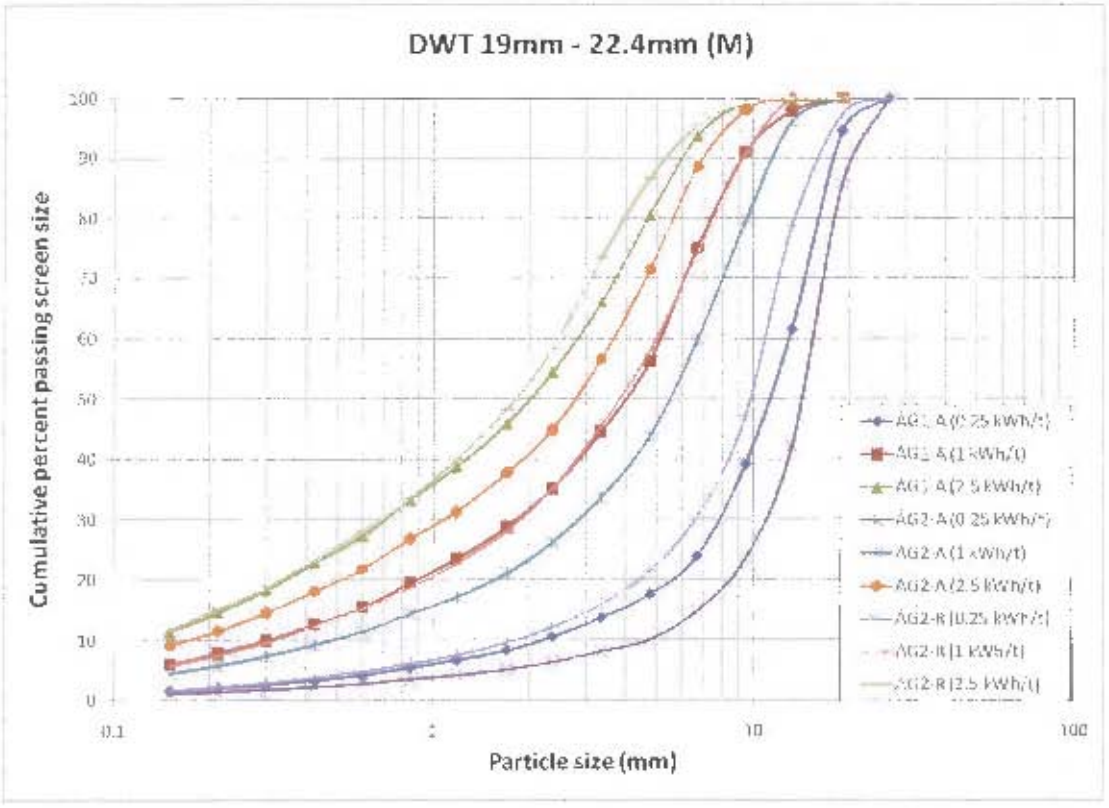


Figure 4.13: Drop weight test breakage distributions for gold ore in medium size class

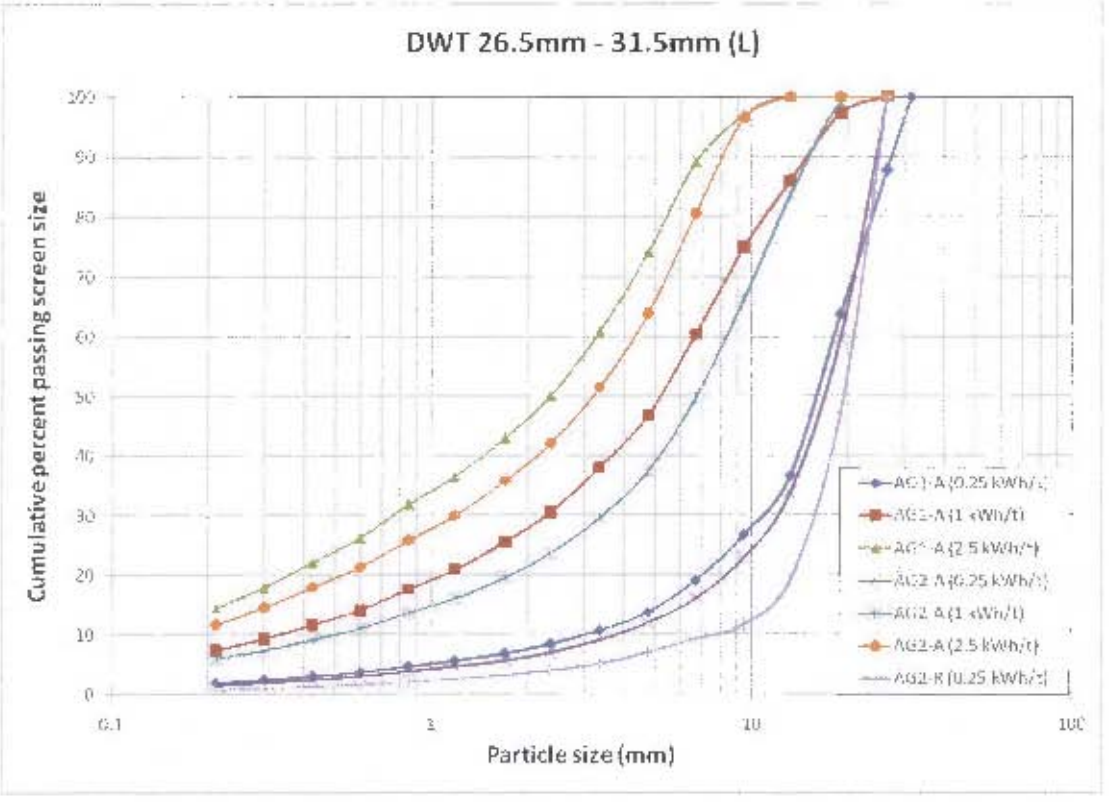


Figure 4.14: Drop weight test breakage distributions for gold ore in large size class

# CHAPTER 5

# SPLIT HOPKINSON PRESSURE BARS

*Overview*
*This chapter provides results of the work using split Hopkinson pressure bars. Following a brief introduction of the history behind the device and its use in comminution research, the technique and theory behind the method is discussed. The experimental procedure and results are then presented with accompanying discussions.*

## 5.1 BACK GROUND AND APPLICATION TO COMMINUTION

The basic principle behind the Hopkinson bar is originally accredited to Bertram Hopkinson, who following on from the work of his father, developed the technique to measure pressures from dynamic events such as the impact of bullets[28]. By the early forties, through a study of the shapes of stress waves propagating through metallic bars and the application of stress wave theory, he was able to refine the technique to accurately describe forces associated with high impact velocities.

Later, Davies[15] and Kolsky[30] extensively modified the method to utilize two bars with test pieces mounted in between to further classify stress/strain responses of materials under load through measures of true stress wave transmissions and reflections through either bar. Kolsky's work in particular led to the apparatus being renamed the Kolsky bar in some scientific circles[26], although the former is still more commonly employed as the standard name in tribute to Hopkinson's original work.

Hopkinson bars have been used in a wide range of configurations since then to measure tension, torsion and shear responses of materials at high strain rates, mainly in classifying deformation and failure properties of ductile materials such as metals and their alloys[15,47]. In comminution, the technique has proven useful as it allows for accurate description of forces, and in turn energies associated with both impact and the actual fraction of this that is absorbed by ore specimens. Thus, it has been used successfully in breakage experiments to determine properties from single samples, and has even been adapted for breakage of beds of particles using vertical bars[19,20,31].

## 5.2 HOPKINSON BAR TECHNIQUE AND THEORY

*Experimental technique*

As highlighted in the literature review (see Section 2.4), the apparatus in its basic form consists of some form of launcher in series with two (usually steel) bars, one known as the incident bar and the other the transmitter bar, both affixed with strain gauges, the sample loaded in between either bar. A photograph of the apparatus with an accompanying schematic is given in Figure 2.8.

At the Blast Impact and Survivability Research Unit (BISRU), University of Cape Town, a pressure controlled gas gun is used as the launching mechanism. The firing tube of aperture 20mm allows for a cylindrical striker of up to 800mm length to be loaded. To prevent misfire, a back pressure is set in the gun which closes the exit valve in the firing chamber. This pressure is typically set by the operator to about 10bar (1 Mpa), which is usually higher than the firing pressure, although if a greater firing pressure is required it should be set higher. An available gauge monitors this pressure as it tends to decrease slightly after several firings, hence it should be constantly maintained. Firing pressure is set using a winch handle and accompanying pressure gauge to a desired value, after which to launch the striker a pre-trigger switch is lifted and trigger button depressed. A digital oscilloscope in trigger mode captures signals from two photoelectric diodes mounted around the firing tube, each of which is coupled with a light emitting diode. The recorded time between the change of state of either diode when the light path is broken by the striker, together with the known trap gap distance, or length between either diode, can be used to calculate the striker velocity and hence the kinetic energy of the collision.

Impact of the striker face against the incident bar face, if the two cross-sectional areas are equal, generates an elastic collision where half of the available striker's kinetic energy is transferred to the bar in the same form. The remainder is converted to strain energy and propagates along the bar as a stress wave, with negligible rebound velocity of the striker[26]. The length of the striker dictates the length of the

stress pulse and thus the impulse of the wave, where according to theory the length of the generated stress pulse is equivalent to twice the length of the striking rod[33].

Both incident and transmitter bars are axially aligned in series with the gas gun and firing tube by clamps with adjustment bolts in both vertical and horizontal directions which hold the bars firmly to a rigid framework bolted level to the ground. These adjustment bolts are used together with a spirit level to ensure exact alignment of all apparatus and should be regularly tightened by the operator. Either bar is thus restricted in every direction but longitudinal in which lightly lubricated Teflon bushings housed firmly in the clamps and machined to a rolling fit with the bars allow for free movement with negligible friction.

Strain gauges are fastened on radially opposite sides of either bar's surface at fixed distances from the end of the bars to minimize damage to them during contact events. These provide voltage readings directly proportional to the instantaneous stress values at their mounting point along the bar surface, which can be assumed to be equal to the stress through the epicentre provided the bars are not larger than roughly 30mm in diameter[19]. Following amplification by electronic circuitry, these signals can be sent to a PCI card on computer which captures the readings as stress pulses fluctuate through the bars. LabView 7 Express, created by National Instruments, was the software used to provide continuous acquisitions of voltage readings, and can be configured to trigger mode to acquire and record a specified number of strain gauge readings over an entire loading duration. For a typical impact, the overall stress wave pattern from both strain gauges can be seen as illustrated in Figure 5.1. A text file is generated with all relevant test information, including the time from the start to end point against corresponding voltage values of either strain gauge.

Figure 5.1: LabView Express interface showing a typical loading event with the HPB

Because the bars are axially aligned with the striker and restricted from movement in all other directions but longitudinal, it is assumed that the stress wave generated propagates in only this measured direction and hence one dimensional stress wave theory can be applied[26]. By this interpretation instantaneous stress and strain in the specimen can be calculated, as well as the strain energy associated with the various generated waves.

Stress is proportional to the transmitted stress in the second bar, where the point of sudden rapid decline is the maximum or yield stress of the specimen, and the first and second kinks in this wave are the yield point and work hardening fracture points respectively[16]. As the specimen is now fractured, all subsequent stress waves past this point are caused by residual strain energy reverberating along the bars. Strain is calculated through integrating the reflected stress wave for known specimen dimensions while strain energy is found from the square of the integrated stress wave. Theory behind these calculations is now discussed further.

*Summary of relevant theory*

Figure 5.2 shows a typical plot of captured strain gauge readings during a breakage event. If the striker in this example moves from left to right, a positive convention is assigned to the voltage to describe a stress pulse in this direction whilst a negative sign is given to a stress pulse in the right to left direction. Thus, as observed from the signal obtained, the instantaneous voltage signal from the incident bar strain gauge generates both an incident wave toward the specimen and a reflected wave in the opposite direction. Interaction of the incident stress wave with the specimen occurs during the time between the end of the incident wave and the beginning of the reflected wave, and the strain gauge in the transmitter bar only receives the fraction of the incident wave that propagates through the test piece.

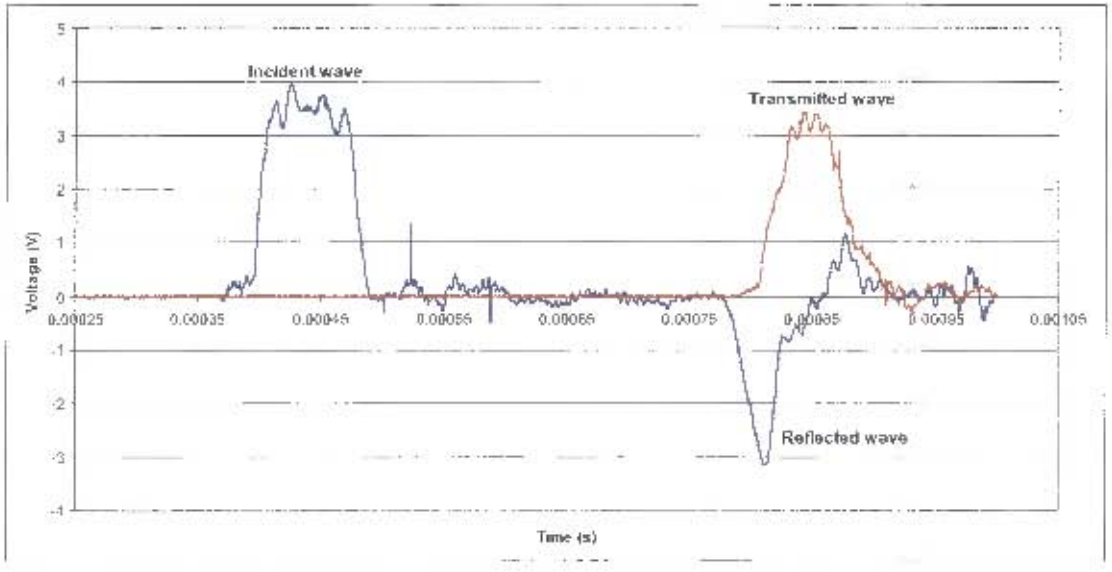


Figure 5.2: Typical HPB readout with labeled waves

Calibration of strain gauges can be done by several methods. For highly dispersive waves, or waves that show a great deal of variation under continuous measurement, a method that calculates the momentum balance between the striker and incident bar can be used. By using Fourier analysis, the scatter in these waves can be reduced following which the velocities of the striker and incident bar prior to and after impact are used for the momentum balance. This method, although found to be very accurate, is complicated and is usually applied when a great deal of wave dispersion is observed[33].

For steady waves with little scatter, the average value of the maximum incident bar voltage can be calculated and equated to the incident stress by a proportionality constant. Using this method, a striker of known dimensions and weight is launched against first the incident bar alone and then with the bar in direct contact with the transmitter bar. The two tests yield fully reflected and fully transmitted waves as shown in Figure 5.3 and Figure 5.4 which indicate in the first instance the maximum voltage pulse generated in the bar which should return in equal value as a reflected wave, and in the second scenario a fully transmitted wave with negligible reflection. If the wave shows partial transmission to the transmitter bar with notable reflection through the incident bar, this indicates an impedance between the bars from different grades of material for either bar, and hence both bars would have to be calibrated singly.

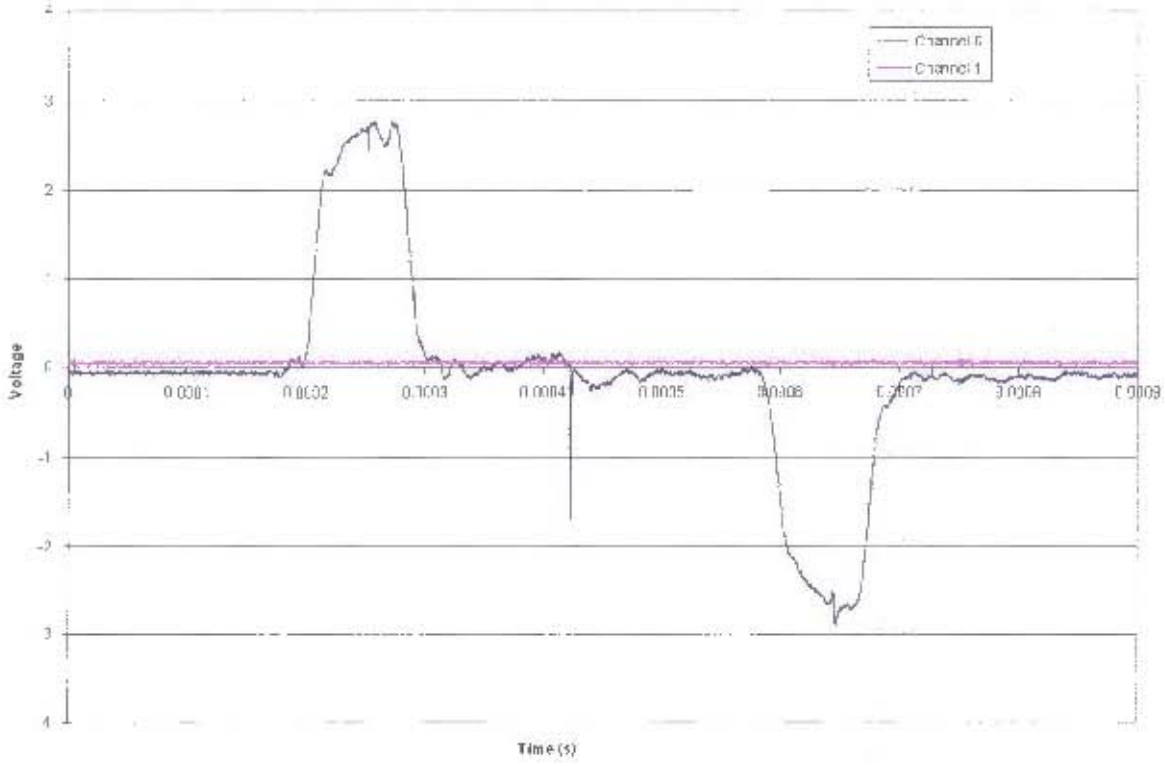


Figure 5.3: Fully reflected wave with a single Hopkinson bar

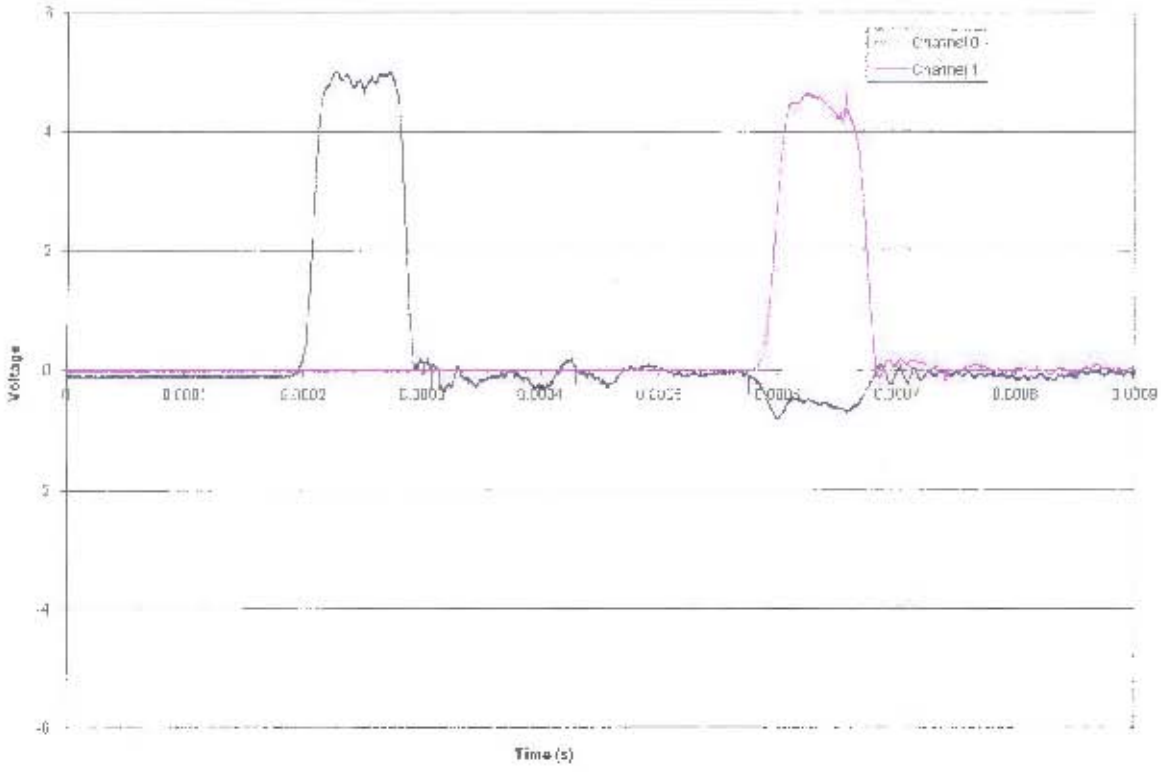


Figure 5.4: Fully reflected wave with two Hopkinson bars in direct contact

From measurement of the striker's velocity using the trap gap distance and digital oscilloscope as described earlier in this section, the velocity of the incident bar can be found by elastic contact theory[26] to be given by Equation 5.1.

$$V_b = V_o\left(\frac{A_s}{A_s + A_b}\right) \qquad \text{Equation 5.1}$$

$V_b$ - Incident bar's velocity

$V_o$ - Initial Striker velocity

$A_s$ - Cross-sectional area of the striker

$A_b$ - Cross-sectional area of the relevant bar (incident bar)

The incident bar's mass and dimensions are measured and used to find its density. Pulse speed is then the length of the bar divided by the time taken for the pulse to travel this distance, calculated as the time on the recorded signal from the last signal of the incident wave to the first signal of similar negative value on the reflected wave.

The fundamental equation of one dimensional stress wave theory[126] as shown in Equation 5.2 is used to calculate the maximum stress in the incident bar

$$\sigma_i = CV_b\rho \qquad \text{Equation 5.2}$$

$\sigma_i$ - Incident bar stress

$C$ - Pulse speed

$V_b$ - Incident bar velocity

$\rho$ - Bar density

From the recorded signal, the average maximum voltage can be calculated by taking the mean value of the signal over the time period when the incident wave is at its peak. The calculated incident bar stress can then be divided by this average maximum to find the proportionality constant K which will be used as a calibration of the stress per unit voltage of the strain gauge, as is given in Equation 5.3.

$$K = \frac{\sigma_i}{V_{max}} \qquad \text{Equation 5.3}$$

K – Proportionality constant

$V_{max}$ - Average maximum Voltage from the strain gauge

As a precaution the theoretical value of K should be calculated and compared to the experimental one, to ensure that the values do not deviate by more than 5%, which is the standard allowable error for most strain gauges[47]. The theoretical value of K can be calculated from Equation 5.4.

$$K_{th} = \frac{4E}{ABVF} \qquad \text{Equation 5.4}$$

| | |
|---|---|
| E - Young's Modulus of bars | $E=\rho C^2$ |
| A - Amplifier Gain | A gain of 1000 is usually the standard |
| B - Bridge factor | 2 for the Wheatstone bridge circuitry |
| V - Bridge Excitation Voltage | Twice the supply voltage across the gauge |
| F - Gauge factor | Usually given for specific strain gauges |

Because the transmitted stress is indicative of the portion of the stress wave that actually interacts with the sample and causes fracture, instantaneous stress in the specimen can be found by multiplying the voltage of this signal by the calibrated value of K. Instantaneous strains for these corresponding stresses can also be determined if dimensions of the test piece are known by first calculating the instantaneous length of the specimen over the duration of the stress wave. This is a sum of the original length added to the integrated wave velocities of both bars, as shown in Equation 5.5. Instantaneous strain at particular times is then found by taking the natural logarithm of the quotient between the instantaneous length at that time with the original length.

$$L(t) = L_o + \int V_1(t)dt + \int V_2(t)dt \qquad \text{Equation 5.5}$$

$L(t)$ - Instantaneous length

$L_o$ - Original specimen length

$V_1(t)$ - The velocity of the incident wave

$V_2(t)$ - The velocity of the transmitted wave

Velocities of these waves are found using the fundamental one dimensional stress wave Equation 5.2. It should be noted that the strain gauge signals obtained occur both prior (in the incident wave case) and after (the transmitted and reflected wave case). It is thus assumed that these stresses are equivalent measures of the actual pulse interaction with the specimen at the ends of either bar, and thus a time shift to move the incident wave forward and the transmitted and reflected waves backward must be operated on the three waves to provide an assessment of the real-time response of the test particle. The incident bar time is increased by adding its original time to the time obtained by dividing the strain gauge distance by the wave speed through the bar, while the transmitted and reflected wave times are shifted backward by their original times minus the relevant strain gauge distances divided by the wave speed. This results in a force time interaction profile of the stress waves with the specimen as shown in Figure 5.5.

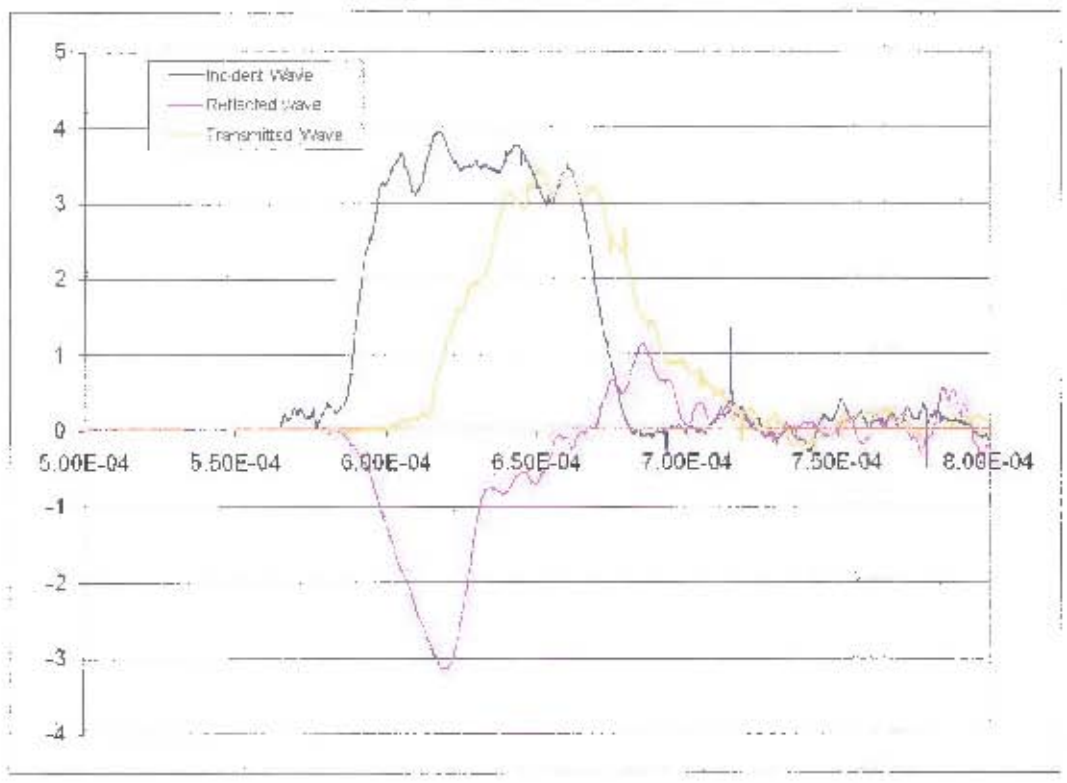


Figure 5.5: Stress time profile for all three times shifted HPB waves

Strain energy associated with each wave is found through calculating the work done by the wave for discrete time steps, which in summation lead to the squared integral of the wave as expressed in Equation 5.6.

$$E_v = \sum_{i}^{t_{end}} \left( \frac{\left( \frac{\sigma(t_{n+1}) + \sigma(t_n)}{2} \right)^2 (t_{n+1} - t_n)(A_b)}{C\rho} \right) \qquad \text{Equation 5.6}$$

$E_v$ - Strain energy of wave

$A_b$ - Cross-sectional area of the relevant bar

C – Wave transmission speed through the bar

$\rho$ - Bar density

Thus the strain energy available to the specimen to cause breakage is found by applying this equation to the incident wave, while the amount of this energy actually absorbed by the specimen during the contact event is assumed from conservation of energy to be the difference between the available energy and that of the outgoing transmitted and reflected stress waves.

## 5.4 RESULTS AND DISCUSSION

The following pressure energy graph was derived using a series of impact experiments with the incident bar in direct contact with the transmitter bar together with the flat end effectors.

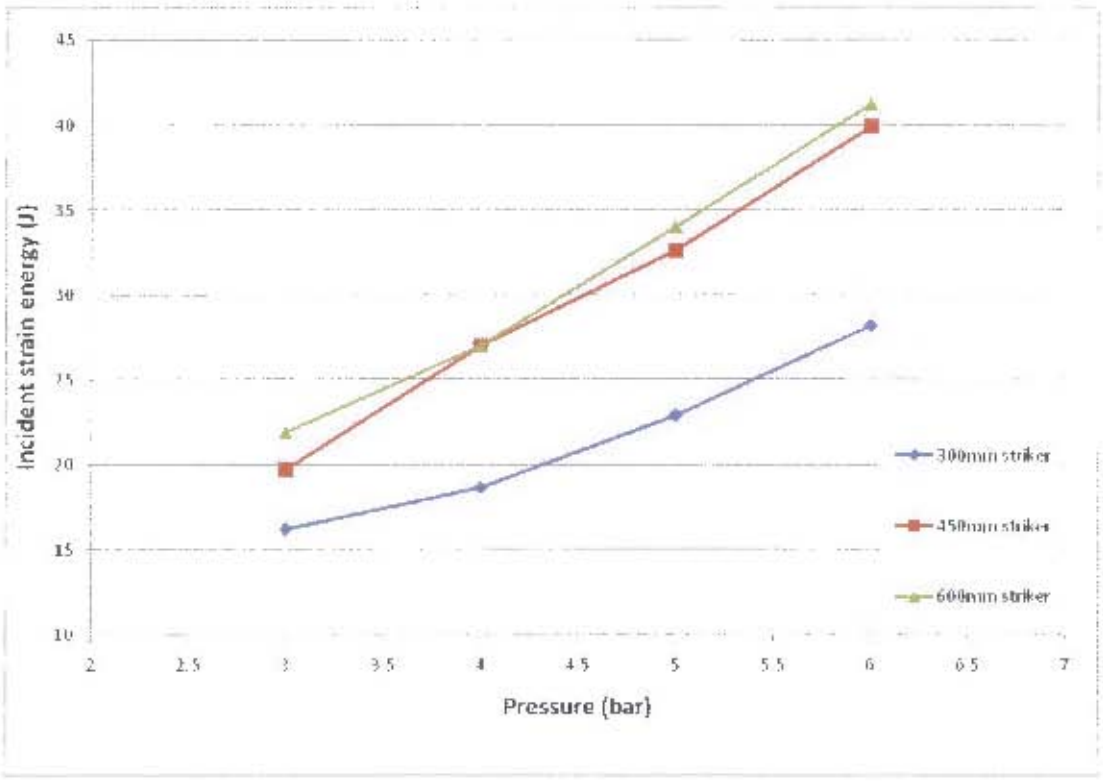


Figure 5.6: Pressure energy calibration graph for strikers used with HPB

Split Hopkinson bar experiments were conducted as explained in Section 3.3 on blue stone to calculate standard strength properties and investigate trends in breakage properties which could not be calculated from other standard breakage tests.

Experiments with cored cylindrical specimens of blue stone loaded co-axially with flat end effectors yielded stress strain data which could be used to calculate its fracture properties. Figure 5.7 shows the stress-strain relationship obtained for coaxial and transversely loaded specimens. It was determined that the curves followed the conventional compressive load stress- strain relationship (see Section 2.2), showing a initial yield strength of approximately 120 MPa before finally fracturing at a ultimate compressive stress of 138 MPa. Assuming a linear relationship over the elastic portion of the curve up to the yield point, the gradient of the curve or Young's

Modulus was calculated to be 22.4 GPa. By comparing the strain of transverse loaded specimens with this data the Poisson's ratio was found to be 0.3.

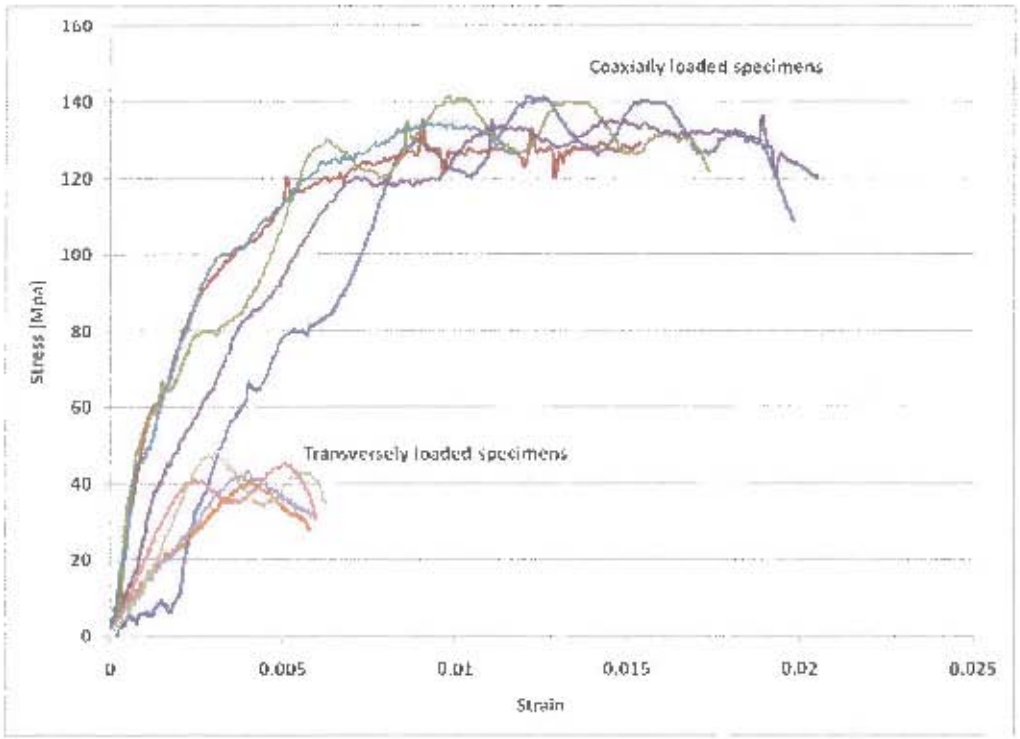


Figure 5.7: Compressive strength data obtained with HPB tests on blue stone ore

From these strength parameters, the particle breakage parameters as defined by Tavares and King[49] (see Section 2.3) were calculated as listed in Table 5.1. Particle strength of the specimen by the calculation is less than the yield stress of the material because the calculation considered the cross sectional area to be the geometric distance between loading points. The stiffness parameter calculated was within the range for brittle materials such as rock particles[51]. The particle fracture energy of 1.77 J for the average specimen weight of 40g meant an average specific energy of 44.25 J/kg.

Table 5.2 shows a number of quoted particle fracture energies for different materials. This showed that the fracture energy obtained for blue stone was between the expected ranges for quartz and marble specimens.

Table 5.1: Calculated fracture properties of blue stone ore

| Blue stone fracture properties from SHPB tests | |
|---|---|
| Particle strength | 87.57 MPa |
| Particle stiffness Gpa | 24.66 MPa |
| Particle fracture energy | 1.77 J |

Table 5.2: Quoted particle fracture energies for a number of materials[49]

| Material | $E_{m,c}$ (J/kg) | $d_{50,c}$ (mm) | b | Size range (mm) |
|---|---|---|---|---|
| Apatite | 1.50 | 19.3 | 1.62 | 0.25– 8.00 |
| Galena | 3.19 | 7.31 | 1.03 | 0.70– 7.60 |
| Gibsonite | 5.50 | 7.03 | 1.60 | 1.18–10.0 |
| Quartz | 43.4 | 3.48 | 1.61 | 0.25– 4.75 |
| Sphalerite | 7.00 | 8.24 | 1.16 | 0.35–10.0 |
| Magnetite | 9.56 | 3.93 | 1.96 | 0.25– 7.20 |
| Copper ore | 96.1 | 1.17 | 1.26 | 0.25–15.8 |
| Iron ore | 47.3 | 1.08 | 2.30 | 0.25–15.0 |
| Limestone | 114.2 | 0.490 | 2.05 | 0.35– 5.60 |
| Marble | 45.9 | 0.582 | 2.66 | 0.50–15.0 |
| Taconite (BM) | 235.9 | 0.303 | 1.42 | 0.35– 6.00 |
| Taconite (CC) | 163.3 | 0.356 | 1.76 | 0.35–10.0 |

From calculation of these strength parameters, the inherent inefficiency of particle breakage can be observed. Table 5.3 shows the average calculated input energy of the Hopkinson bar against the energy absorbed by the specimen and the particle fracture energy. These values show that only 42.6% of available energy actually goes to the particle whilst only 32.8% of this is actually required to cause first fracture, the remainder being used in further breakage of progeny particles, kinetic energy, heat and sound.

Table 5.3: Calculated utilization of impact energy with HPB (cored specimens)

| | Calculated (J) | Calculated (kWh/t) | % |
|---|---|---|---|
| Input Energy | 5.4 | 0.0375 | 100 |
| Absorbed energy | 2.3 | 0.0160 | 42.6 |
| Fracture energy | 1.77 | 0.0123 | 32.8 |

Table 5.4: Calculated utilization of impact energy with SHPB (blue stone particles)

| Geometry | Mean | | | | Standard deviations | | | |
|---|---|---|---|---|---|---|---|---|
| | Input E | E absorbed | $t_5$ | $t_{10}$ | Input E | E absorbed | $t_5$ | $t_{10}$ |
| | kWh/t | % | mm | mm | kWh/t | % | mm | mm |
| Ang | 0.2046 | 31.0 | 1.40 | 0.57 | 0.0113 | 5.5 | 1.04 | 0.42 |
| Rou | 0.2082 | 39.4 | 1.65 | 0.64 | 0.0111 | 3.6 | 1.14 | 0.42 |

Table 5.4 shows the average percentage energy absorbed by 37 angular and 44 rounded specimens for the same mean input energy range of 0.2 kWh/t. Similar to results with cored specimens, the values showed that for either geometry, less than 50% of the input energy was absorbed by the particles. Rounded geometries absorbed an average energy of 39 percent, with a lower deviation about this mean, while angular specimens absorbed 31 percent. As rounded specimens tended to

absorbed an average energy of 39 percent, with a lower deviation about this mean, while angular specimens absorbed 31 percent. As rounded specimens tended to absorb more energy for a given impact, a slight increase was observed in the $t_5$ and $t_{10}$ obtained for this geometry.

Normal distributions as shown in Figure 5.8 were plotted to further observe the trend in energy absorbed between the two geometries, where it was noted that rounded specimens tended to absorb more energy than angular specimens, and the fraction absorbed was of greater consistency as observed from the higher peak and tighter band about their distribution.

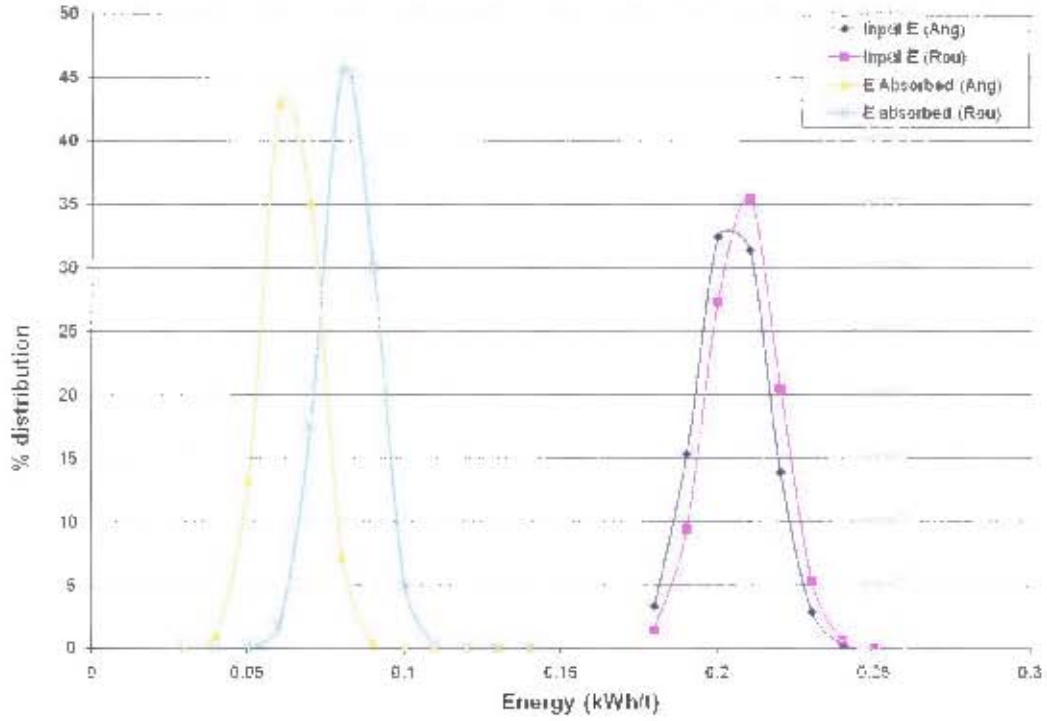


Figure 5.8: Normal distributions of energy ranges obtained from HPB tests

Figure 5.9 shows the results of tests conducted to measure the effect of end effectors on the amount of energy absorbed by rounded particles under impact. It was found that flat surfaces transferred slightly higher fractions of impact energy to specimens over an identical input energy range of 0.2 to 0.22 kWh/t. Either type of end effector transferred less than 50% percent of the impact energy to the specimen to cause fracture.

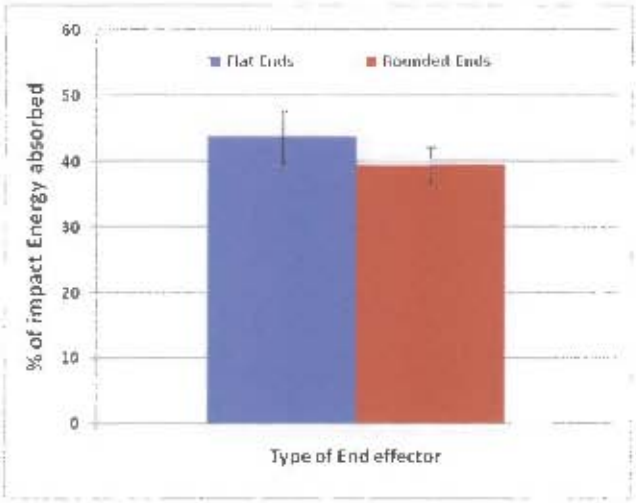


Figure 5.9: Percentage input energy absorbed with each HPB end effector

Experiments were carried out to investigate the duration of impact or impulse effect on the amount of energy absorbed by ore particles. This was calculated as the time period taken for the incident wave to initiate and fall at a cut off of 0.1V. Figure 5.10 shows the impulse profiles of approximately 0.18, 0.24 and 0.27milli seconds that were generated for the same firing pressure with the three strikers used. The profiles confirmed the result from stress wave theory that striker length was directly proportional to impulse[35]. It should be noted that these impulse times were the time taken to transfer the load and not the actual rate of particle deformation or strain rate.

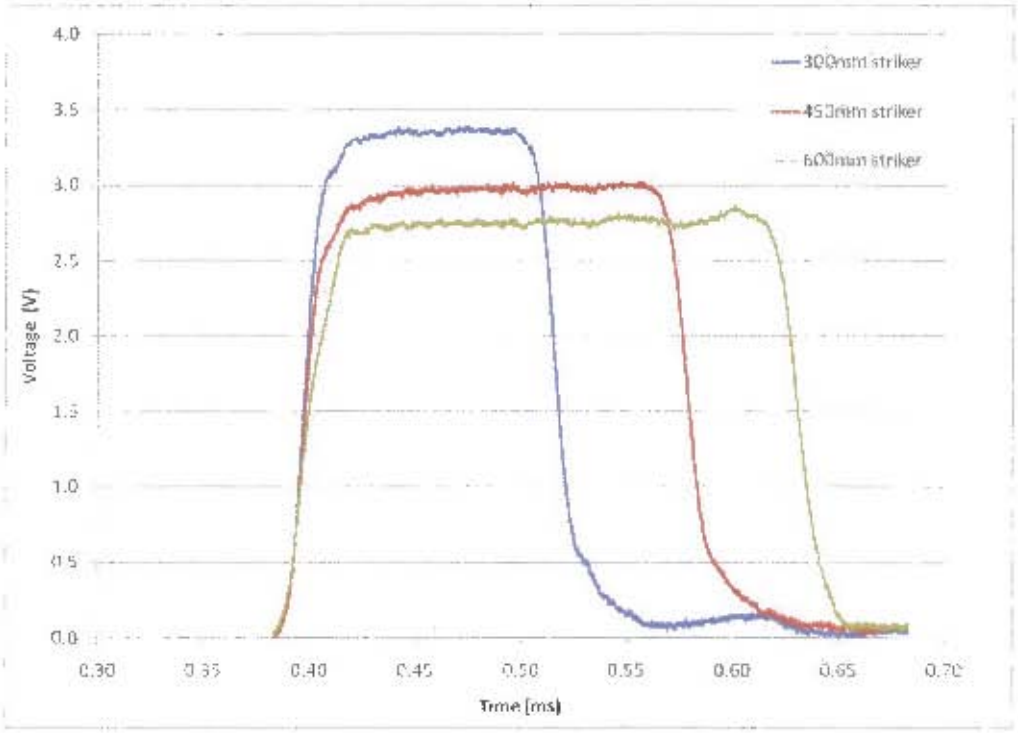


Figure 5.10: Typical Impulse profiles obtained with the three strikers used

For 10 specimens at the same calibrated energy range of 0.19-0.21 kWh/t, the mean amount of energy absorbed by each specimen was calculated and plotted as shown in Figure 5.11. The variation in the mean values obtained was shown by error bars of 1 standard deviation. The amount of energy absorbed by a specimen increased marginally with the duration of the time taken to transfer the load between the 300mm and 450mm striker, while it remained fairly constant between the 450mm and 600mm striker.

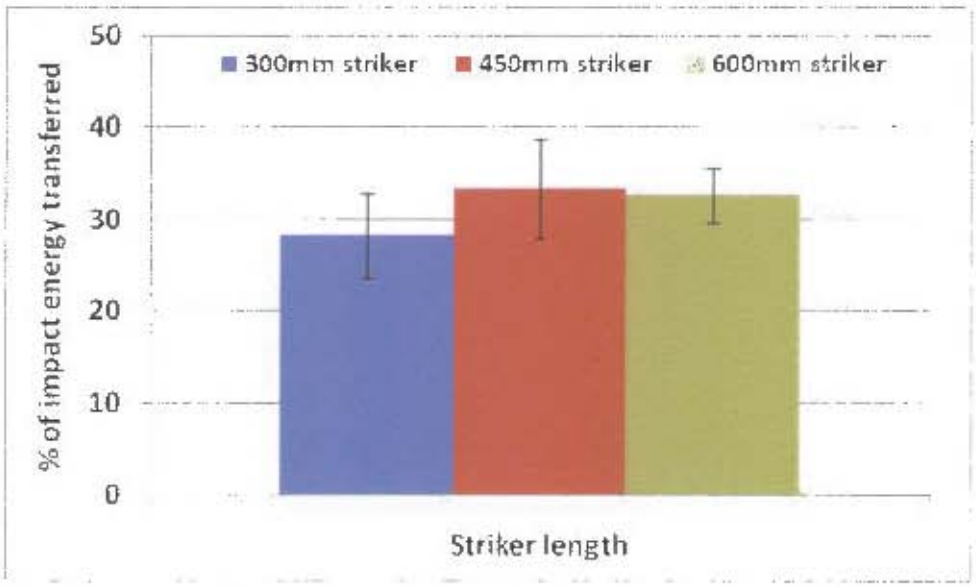


Figure 5.11: Comparison of percentage energies transferred with different strikers

The breakage degree from 70 single impact breakage experiments with rounded specimens was used to obtain the energy-size relationship shown in Figure 5.12. The $t_{10}$ was plotted against the calculated energy absorbed by the specimen and it was observed that the percentage increased as the amount of absorbed energy from the available impact energy increased. The tests were carried out over the permissible impact energy range of the Hopkinson bars used, which ranged from 0.17 to 0.56 kWh/t. The standard JK $t_{10}$ breakage model (Equation 2.14) was fitted to this data where A and b values of 2.3 and 5.4 were obtained. The maximum degree of breakage from Hopkinson bar tests from Hopkinson bar tests was noted to very low as breakage tests with this device generated little fine material.

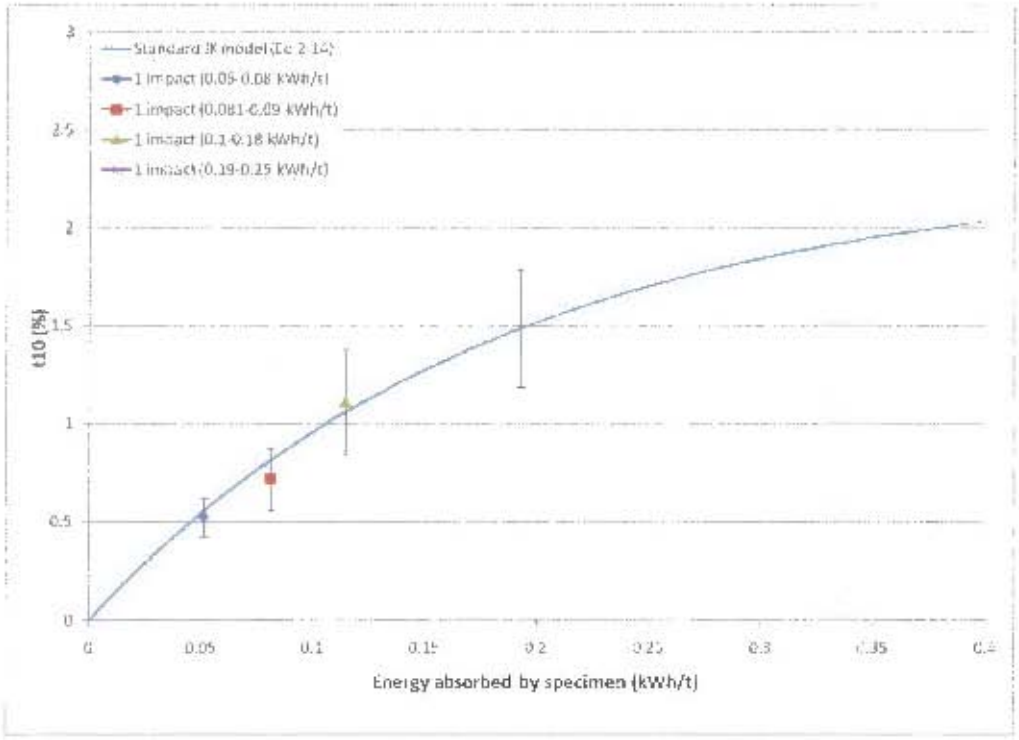


Figure 5.12: Plot of breakage degree against energy absorbed for rounded particles

A similar graph as shown in Figure 5.13 was plotted to compare the breakage degree from single impact and incremental breakage tests. A series of incremental breakage experiments were conducted using 12 particles according to the procedure in Section 3.3. 3 specimens were found to fracture in 2 impacts, with 4 specimens in 3-6 impacts, 3 specimens in 7-10 impacts and 2 which fractured in 12 and 13 impacts.

This data was used to compare the breakage degree between single impact and incremental breakage. The $t_{10}$ values from incremental breakage tests were plotted against the single impact breakage data for the cumulated total amount of energy expended to cause breakage (Figure 5.13). It was noted that although the $t_{10}$ noticeably increased with the absorbed energy for single impacts, the breakage degree from incremental impacts relatively constant for the total amount of energy that had been absorbed by the specimen until fracture.

As $t_{10}$ values obtained with the Hopkinson bars were low, the $t_5$ was also plotted to further compare this relationship (Figure 5.14), which better illustrated that for the same amount of energy expended, incremental breakage appeared much more inefficient than single impact fracture.

A summary of all Hopkinson bar results can be found in Section 7.1.

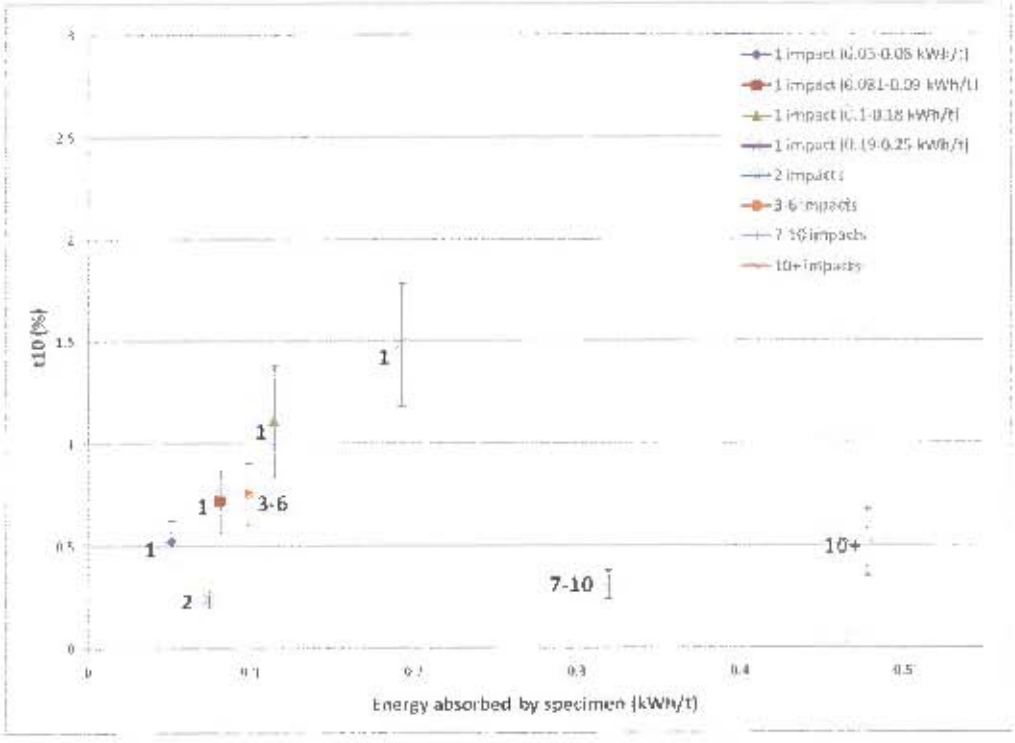


Figure 5.13: $t_{10}$ breakage data from HPB tests

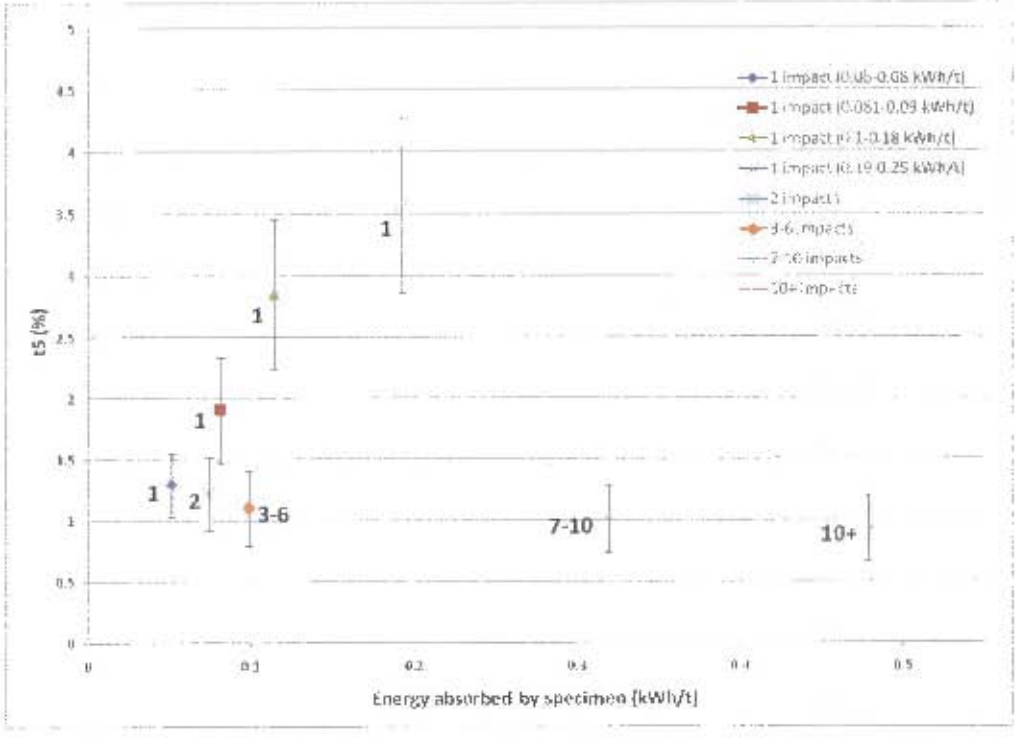


Figure 5.14: $t_5$ breakage data from HPB tests

# CHAPTER 6

# ROTARY BREAKAGE TESTER

*Overview*
*This chapter is dedicated to the work done using the Julius Kruttschnitt rotary breakage tester. A brief introduction of the design of the device and its intended role in comminution research is given, followed by a discussion of the technique and theory behind the method. Test results from both single impact and incremental breakage experiments with this device are then presented.*

## 6.1 BACK GROUND AND IMPLEMENTATION IN COMMINUTION RESEARCH

The rotary breakage tester (RBT) was developed at the JKMRC as part of a P9N project to introduce a new breakage characterization device to complement the drop weight test as an ore characterization tool[46]. It was designed primarily to overcome several noted limitations of the standard drop weight, mainly the lengthy time required to perform tests, and the limited range of input energies achievable. Its rotor-stator impactor design, as described in the literature review (see Section 2.4) allowed for expedient testing of ore particles in similar size ranges to the drop weight and over a wider energy range. With its automated breakage mechanism, many particles could be processed in breakage tests to improve the statistical number of specimens over which material parameters would be calculated.

As it has only recently been commissioned, its implementation in comminution research at this stage is minimal although initial experiments with the prototype have shown good correlation in breakage results with conventional drop weight tests[46].

## 6.2 ROTARY BREAKAGE TEST TECHNIQUE AND THEORY

The working of the JKRBT can be broken down into three basic systems, namely the feed mechanism, impactor and the collection system, all of which are controlled by an onboard control panel. Figure 6.1 shows the overall schematic of these systems.

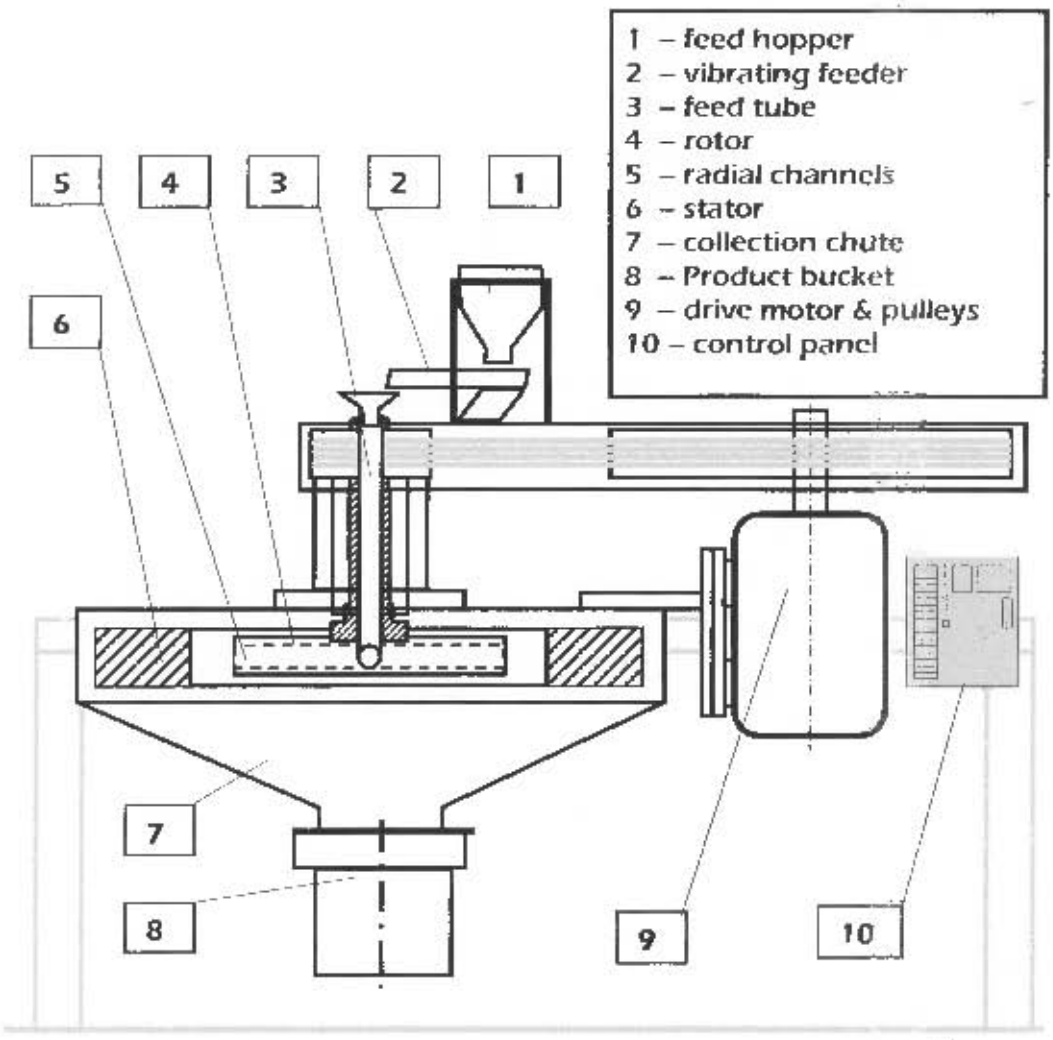


Figure 6.1: Labeled schematic of JK rotary breakage tester[46]

Particles are inserted at the top of the machine through the available hatch, which drops them onto a vibrating feeder and leads them into the feed tube. As the particles come to the bottom of the vertical feed tube, they are launched by the centrifugal force of the rotor along the horizontal radial channels until they impact against the anvil faces of the surrounding stator. The interior of the impact chamber is designed such that the series of impact plates face the exit of these radial channels. This ensures that the particles impact the anvils orthogonally to their direction of travel[46].

By gravity, product particles fall to the collection chute which is radially inclined toward a product collection bucket. A vacuum is also available to suction any finer material into the product bucket, which automatically switches on when the rotor is brought to a stop.

The main electronic circuit box requires a 3 phase power supply of 360V, which is used to supply power to all other components. The control panel is used to set rotor speed, which translates to impact energy, and can also be used to adjust the particle feed rate. At least 100psi (0.689 MPa) is required to supply compressed air to the pneumatic feeder. Lubricating oil is also required and should be maintained by monitoring the oil level indicator.

*Summary of relevant theory*[46]

Specific input energy for an impact with the RBT is the kinetic energy per unit mass of the particle. As kinetic energy ($0.5 \cdot m \cdot v^2$) has a mass component by definition, this means that for a given ore particle, its impact energy is independent of mass and only depends on the particle speed.

The rotor spins at a constant velocity and particles travel a relatively short distance after leaving the radial channels to the stator. Thus it is assumed that the velocity at which particles leave the rotor circumference ($V_p$) is the impact velocity of the specimen. If this velocity is also assumed to be horizontal, it can be resolved into two vector components, radial ($V_r$) and tangential ($V_t$).

$$V_p = \vec{V}_r + \vec{V}_t \qquad \text{Equation 6.1}$$

If the radial velocity is expressed as a fraction of the tangential velocity, the particle velocity can be represented by a constant C multiplied by the magnitude of the tangential velocity.

$$V_p = C \cdot |V_t| \qquad \text{Equation 6.2}$$

The tangential velocity of the particle is simply equal to the rotor speed, or as expressed in Equation 6.3, the expression for the particle speed in meters per second can be written as

$$V_t = \frac{2\pi Nr}{60}$$ Equation 6.3

Where N is the rotor speed in rpm, and r is the radius of the rotor. Equation 6.4, an overall expression for the specific energy of the impact in kilowatt hours/tonne, is then derived. Calibration of the machine requires determining the unknown constant C, which is done by high speed camera tracking of particles.

$$E_{cs} = \frac{0.5\left[C\left(\frac{2\pi Nr}{60}\right)\right]^2}{3600}$$ Equation 6.4

## 6.3 RESULTS AND DISCUSSION

Single impact and incremental breakage experiments with the rotary breakage tester were carried out according to the procedure outlined in Section 3.3. Single impact breakage tests were performed on two standard breakage energy levels to compare the breakage degree with that obtained from drop weight tests. Incremental breakage tests were conducted to determine the values of $E_0$ and $E_{crit}$ for blue stone and gold ore. Ores were segregated based on metallurgical names assigned to them during testing (see Table 3.2) and separated into three size fractions small (-16mm +13.2mm), medium (-22.4mm +19mm) and large (-31.5mm +26.5mm).

### *I- Single impact breakage*

Two energy levels (1 and 2.5 kWh/t) were selected from the standard RBT breakage values, with the conventional number of 30 particles used in each experiment. Figures 6.3 to 6.8 show the breakage distributions that were obtained for tests on all the ore types. Similar to results from the drop weight tests, it was observed that the distribution became gradually finer with increase in energy and decrease in particle size.

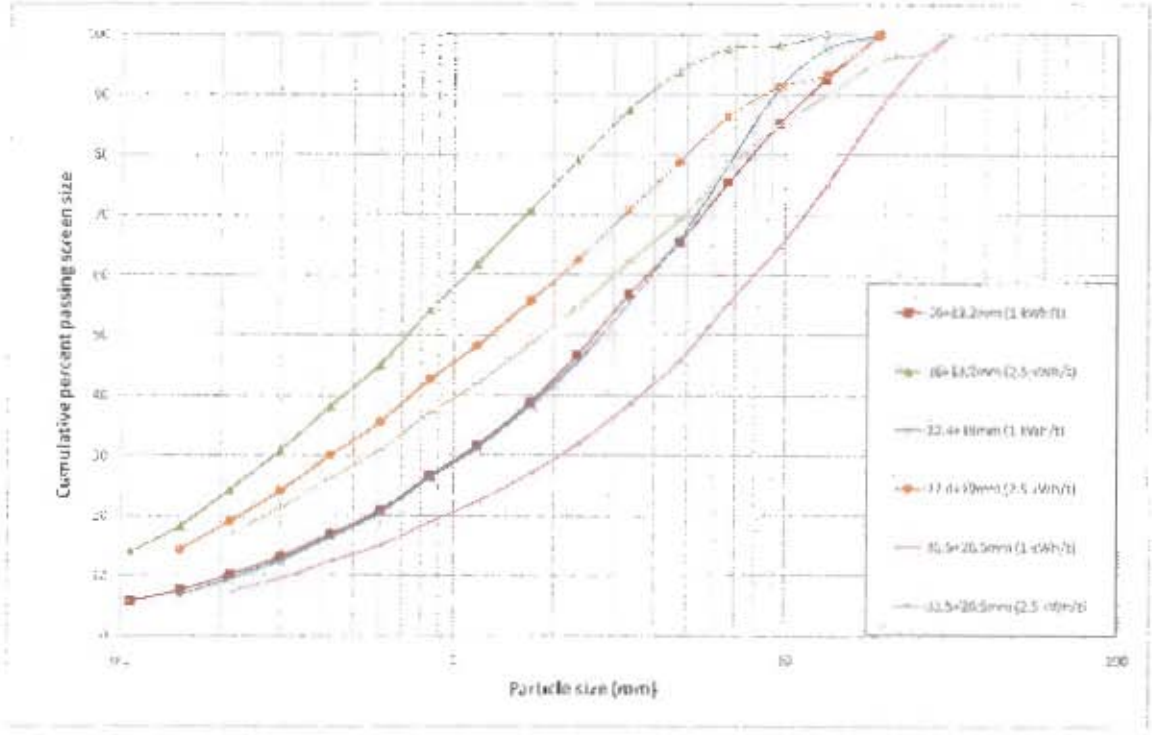


Figure 6.2: RBT particle size distributions for AG1-A ore

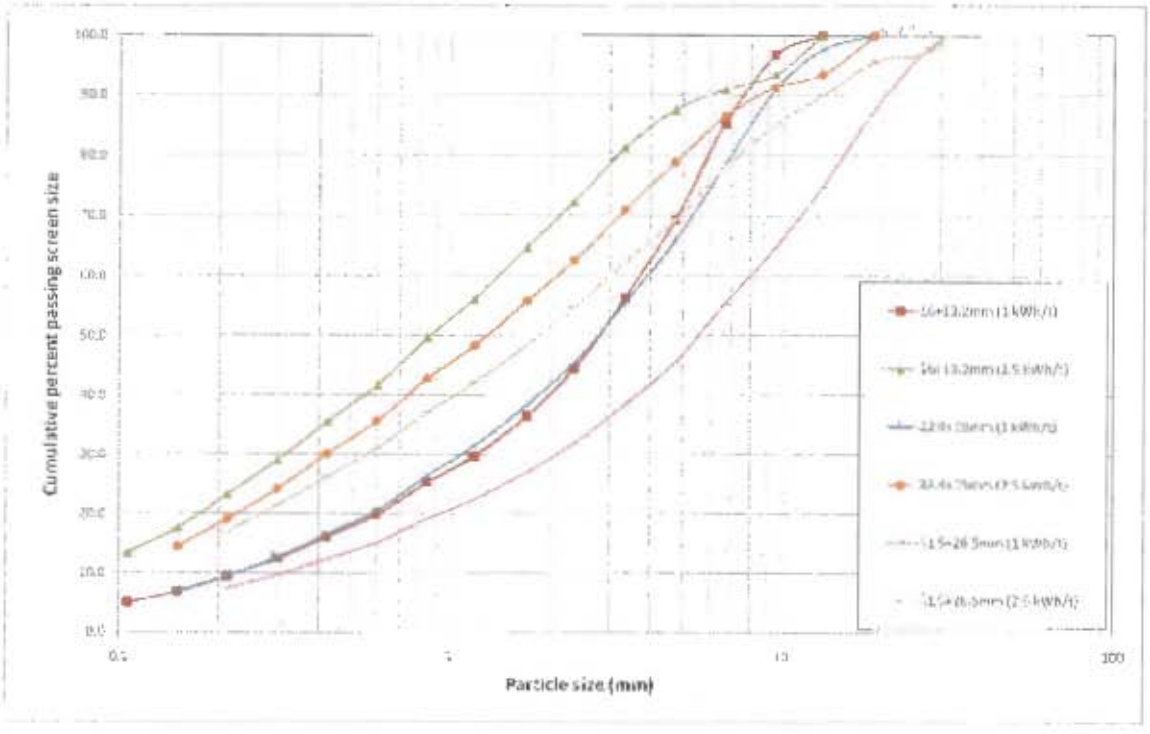


Figure 6.3: RBT particle size distributions for AG1-R ore

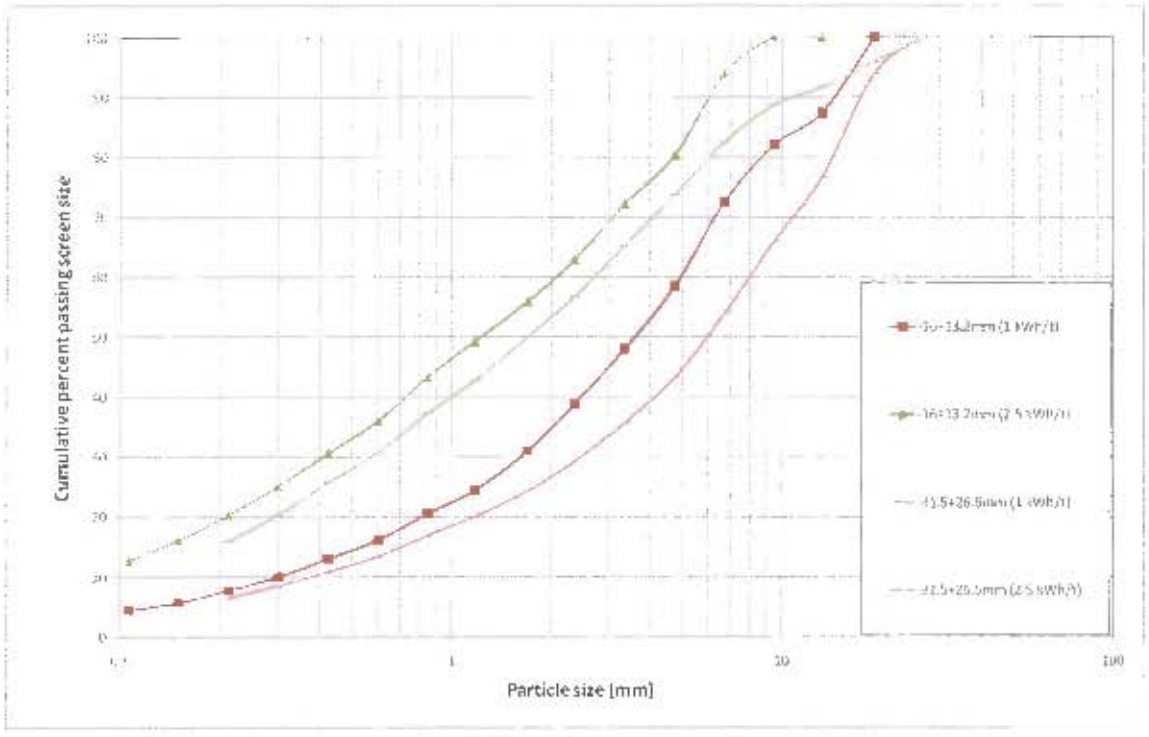


Figure 6.4: RBT particle size distributions for AG2-A ore

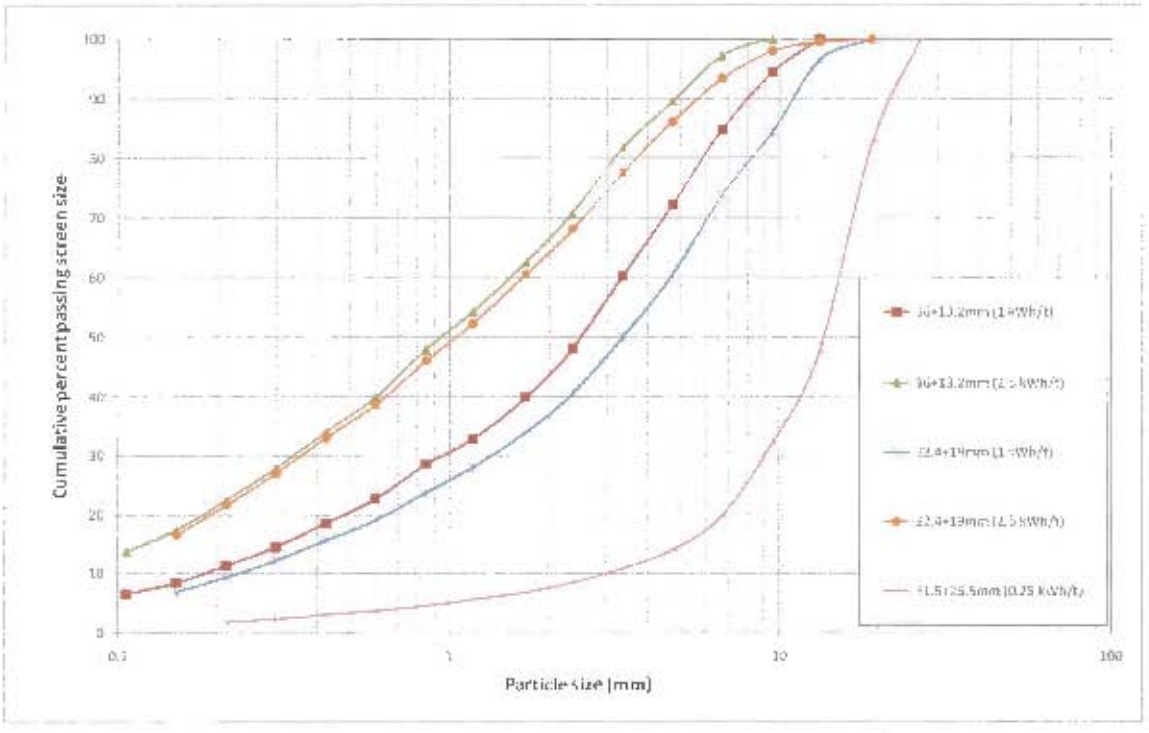


Figure 6.5: RBT particle size distributions for AG2-R ore

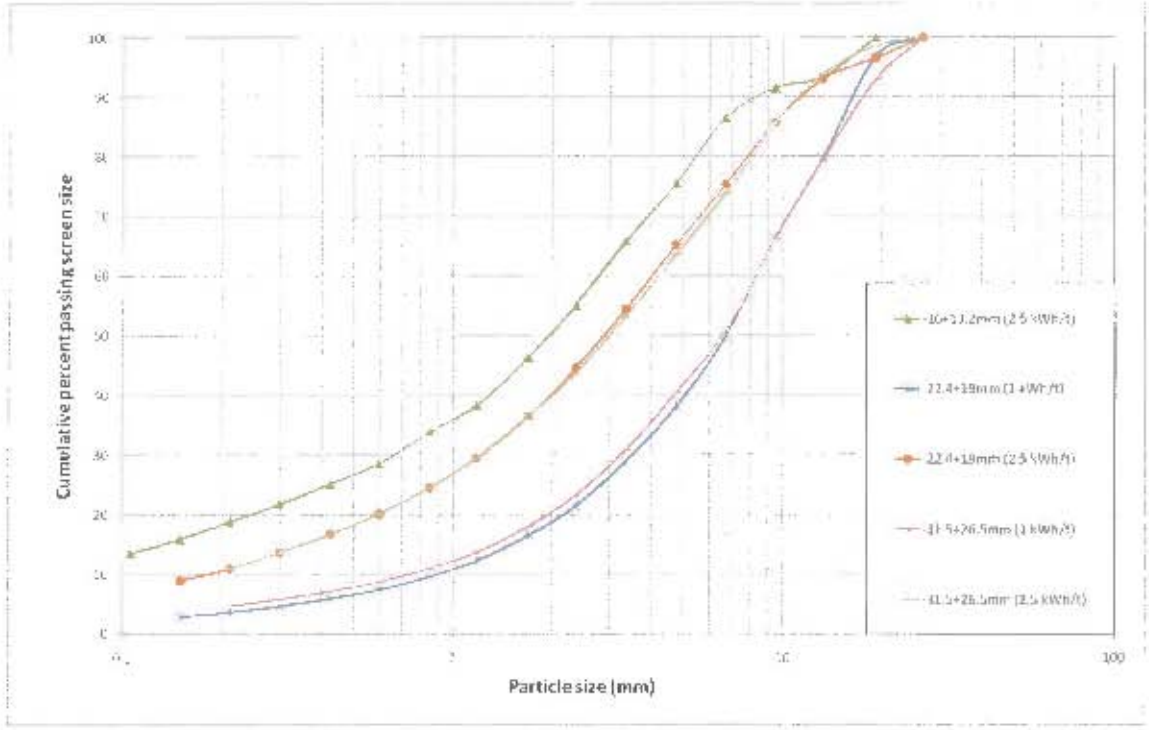


Figure 6.6: RBT particle size distributions for BS-A ore

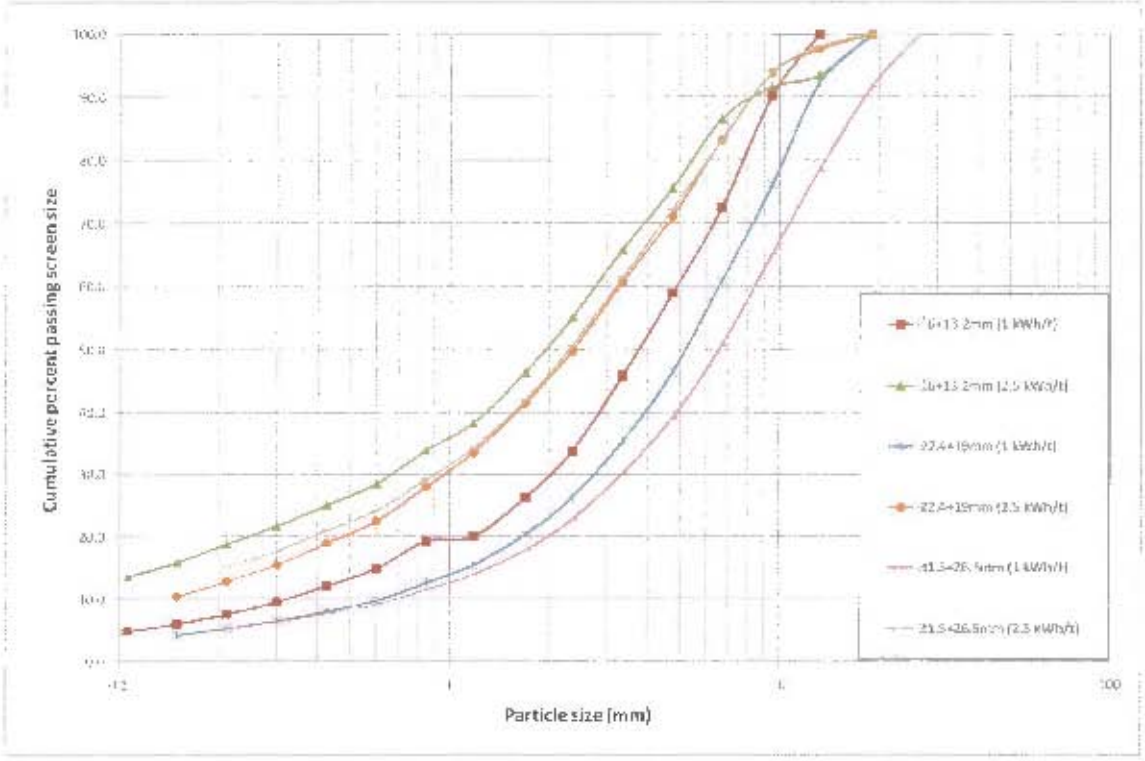


Figure 6.7: RBT particle size distributions for BS-R ore

For AG2-R ore sufficient material was available to perform experiments at the three standard breakage energy levels and determine the A.b hardness parameter. 45.6 was obtained using the standard equation[37], with a value of 47.6 with the modified

Shi-Kojovic equation[44] (see Section 2.5). As shown in Figure 6.8, both breakage models were fitted to the data obtained, and the modified equation was found to give a slightly higher gradient than the standard equation. As $E_0$ is incorporated in this model, the value of b marginally increased, which led to the observed dissimilarity at higher energy levels. Similar to drop weight test results, it was noted that breakage degrees at energies below 1kWh/t were consistent for all particle sizes while at higher energy levels larger particle sizes tended to generate higher values.

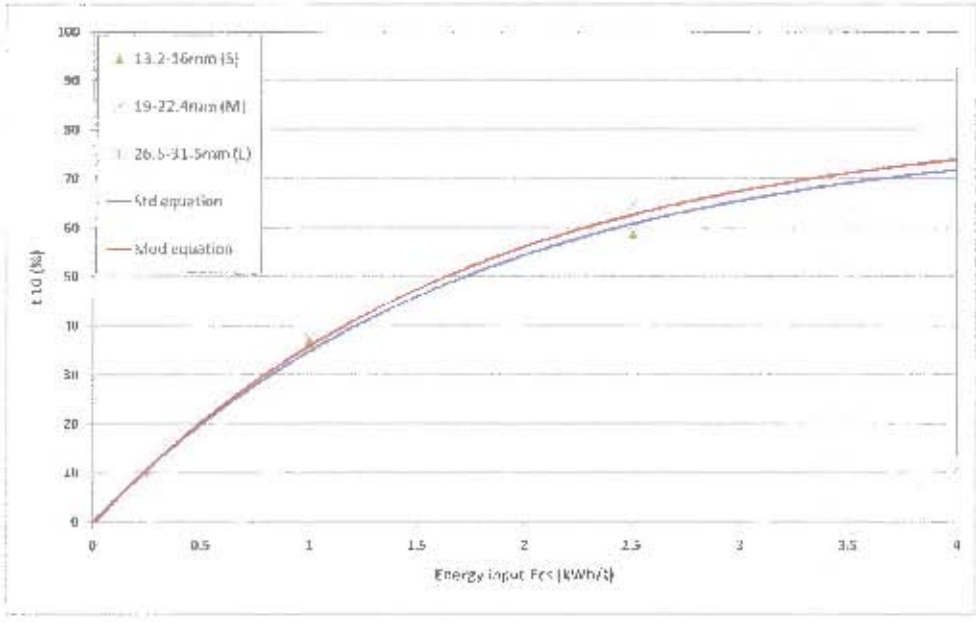


Figure 6.8: $t_{10}$ curve for AG2-R ore

A series of experiments were carried out with blue stone to investigate the deviation in size distribution from 6 groups of 5 particles each subjected to breakage. Each group of particles was screened and weighed independently and the total masses were added up to give the total average distribution for 30 particles. Table 6.1 shows the averages and standard deviations that were obtained for either of the two geometries.

Table 6.1: Mean and deviation in distributions of angular and rounded particles

| | | $t_2$ | $t_4$ | $t_5$ | $t_{10}$ |
|---|---|---|---|---|---|
| Angular | Mean | 60.2 | 44.8 | 34.6 | 27.2 |
| | Std dev | 12.3 | 9.9 | 12.2 | 10.6 |
| Rounded | Mean | 58.5 | 30.8 | 28.0 | 16.5 |
| | Std dev | 5.7 | 4.0 | 4.4 | 2.7 |

Figure 6.9 and Figure 6.10 were plotted to further observe the results for both rounded and angular geometries respectively. It was observed that the scatter from rounded specimens was much less than from angular specimens, which tended to give greater standard deviations in breakage results, as shown in Table 6.1. In these graphs the red square represented the average distribution for the particular degree of breakage of from the six tests. From these results the significance of the number of particles over which results were calculated was also highlighted.

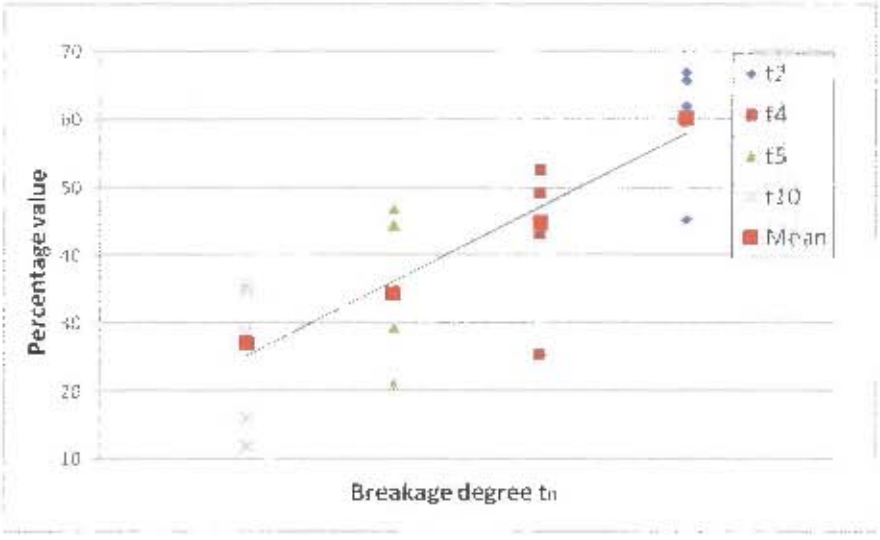


Figure 6.9: Comparison in PSD scatter of BS-A (Angular blue stone)

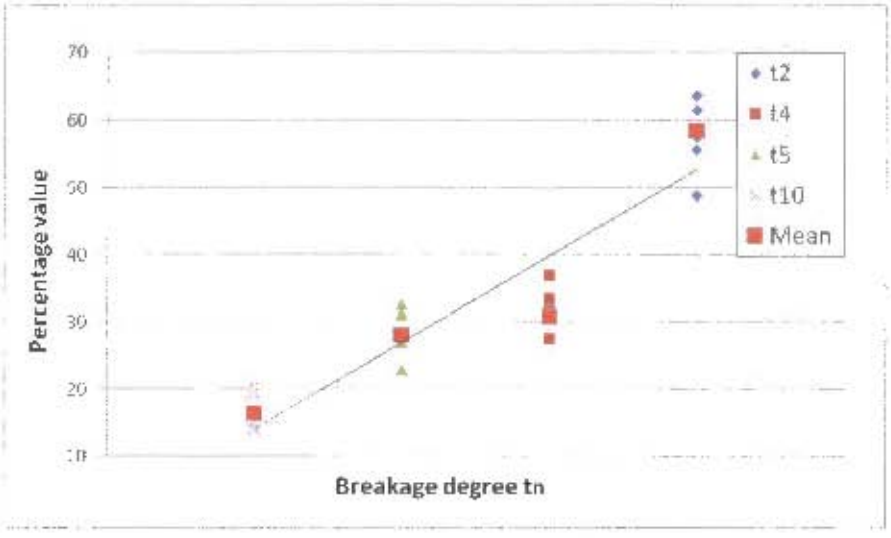


Figure 6.10: Comparison in PSD scatter of BS-R (Rounded blue stone)

*II- Incremental breakage*

As the procedure for incremental breakage tests was developed for this work, experiments were conducted to establish the number of specimens sufficient to provide statistically relevant breakage data. Rounded particles of blue stone were used for these tests as they had been found to give more consistent breakage data (see section 6.3 - I) and the same hardness as angular specimens (see section 4.3). For these experiments, five tests at 0.167 kWh/t, an intermediate energy level between $E_0$ and $E_{crit}$, were repeated with 100 particles in each test.

Table 6.2 shows results of the repeatability tests. The coefficient of variation (COV), or relative percentage of standard deviation over mean, from these repeatability experiments was calculated for the breakage probability, $t_{10}$, and P80 sizes. It was determined that 100 specimens gave an acceptable range of error in results, and thus for all incremental breakage tests this number of particles was used.

Table 6.2: Deviation in calculations from repeated RBT tests with 100 specimens

| | Probability (%) | $t_{10}$(%) | P80 (mm) |
|---|---|---|---|
| Mean | 68.70 | 4.47 | 24.80 |
| Standard deviation | 5.25 | 0.20 | 0.79 |
| COV Std dev/Mean (%) | 7.6 | 4.6 | 3.2 |

According to the procedure described in Section 3.3, incremental breakage tests were conducted on blue stone and gold ore across five energy levels determined to be below $E_{crit}$. For tests with AG2-R ore, the cumulative total breakage probability from the original starting mass was plotted against number of impacts as shown in Figure 6.11. For the energy levels and number of impacts tested, the total breakage probability increased steadily with each impact, which implied that a probability to breakage model could be established over a given number of impacts at a particular energy level. This model would then be used to define $E_{crit}$ as the energy calculated to cause single impact breakage for a particular breakage probability.

The model chosen to fit this data was based on the same form as the Vogel and Peukert relationship (Equation 2.17), modified to the form given in Equation 6.5. This was a simplified form which related the probability of breakage (S) to the number of impacts k, with the other parameters combined into a constant c.

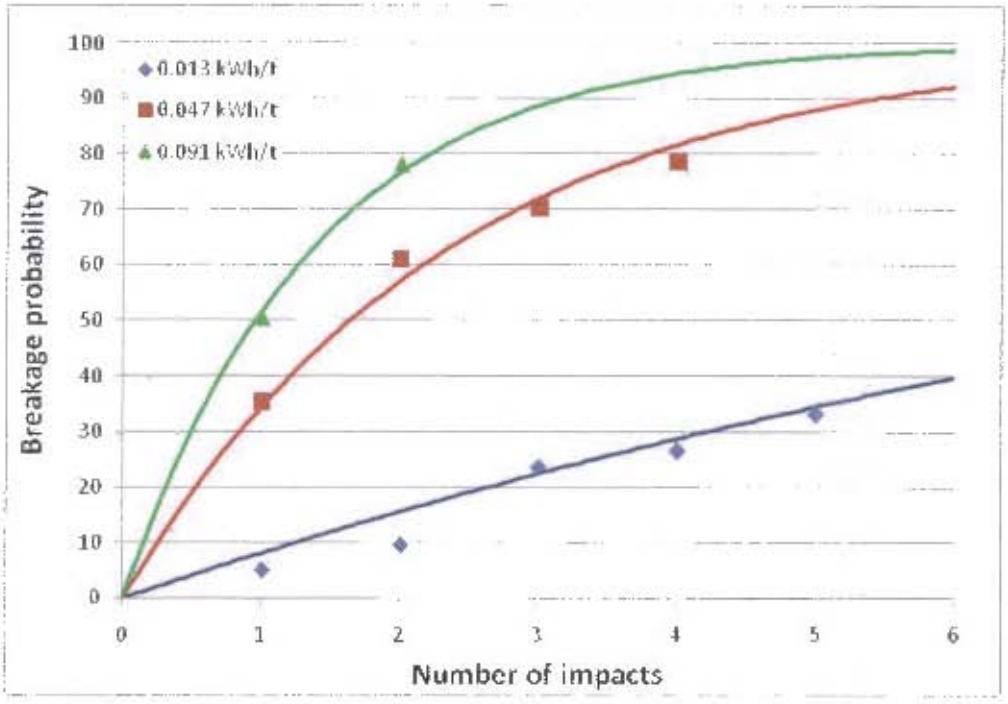


Figure 6.11: Cumulative total breakage probabilities at sub critical energy levels

$$S = 1 - e^{|-c \cdot k|} \qquad \text{Equation 6.5}$$

The value of c was found as a function of the input energy, where the values were calculated for the three energy levels as shown in Table 6.3. Parameter c was found to be a linear function of the input energy passing through the origin with a gradient of 8.2, as shown in Figure 6.12.

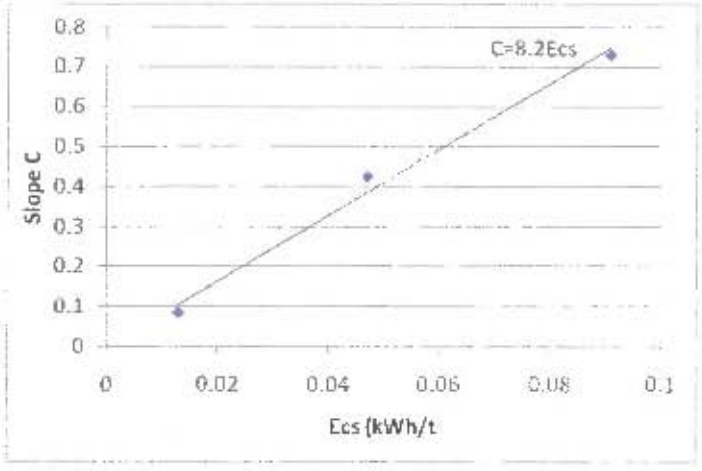


Figure 6.12: Relationship between c and input energy

Table 6.3: Calculated values of function c from breakage tests

| Energy | c |
|---|---|
| 0.013 | 0.0848 |
| 0.047 | 0.4248 |
| 0.091 | 0.7302 |

If the slope was defined as a constant *f* for a particular probability to breakage from a single impact (setting k=1), Equation 6.5 could be inverted to solve for the critical energy $E_{crit}$ as a function of breakage probability (S), as given in Equation 6.6.

$$E_{crit} = \frac{\ln(1-S)}{f} \qquad \text{Equation 6.6}$$

Thus for a probability of breakage of 90%, an $E_{crit}$ of 0.281 kWh/t was obtained for the AG2-R ore, where the slope *f* was 8.2. For the blue stone a slope of 6.7 was obtained which gave an $E_{crit}$ of 0.344 kWh/t.

The values of $E_0$ and $f_{mat}$ were calculated from fitting the Vogel-Peukert probability of breakage model (Equation 2.17) to RBT data. These were solved simultaneously for the full range of incremental impact data. Each set of curves for a different number of impacts intersected the x-axis at a slightly different point offset by the value of $E_0$ between each curve. In order to overcome this, the effective cumulative specific energy $E_{cs} - E_0$ was plotted against probability of breakage as shown in Figure 6.13. The curve showed a good fit to the experimental data.

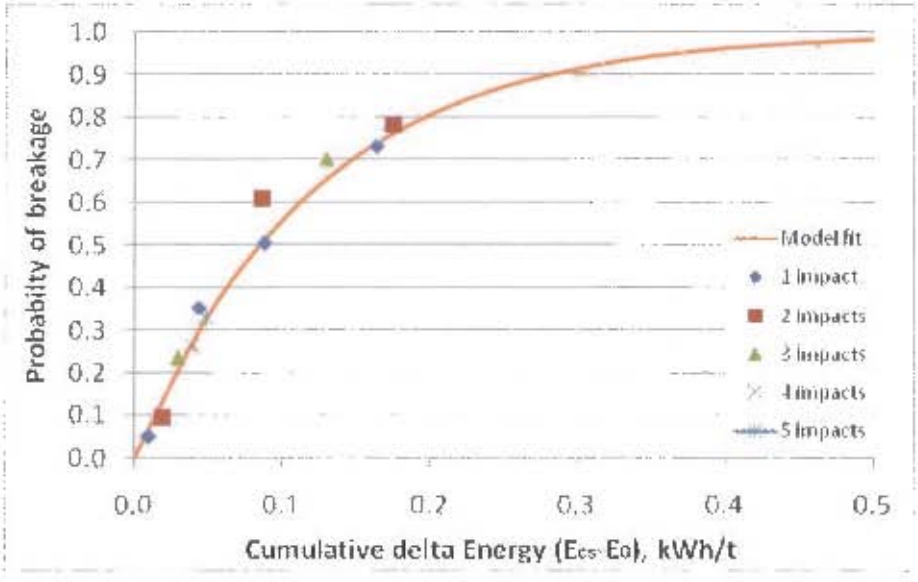


Figure 6.13: Probability to breakage model fitted to data from AG2-R

The same method was applied to fit breakage probability data of incremental breakage tests on blue stone as plotted in Figure 6.14. The curve for blue stone followed a similar trend although the data for this fit was limited.

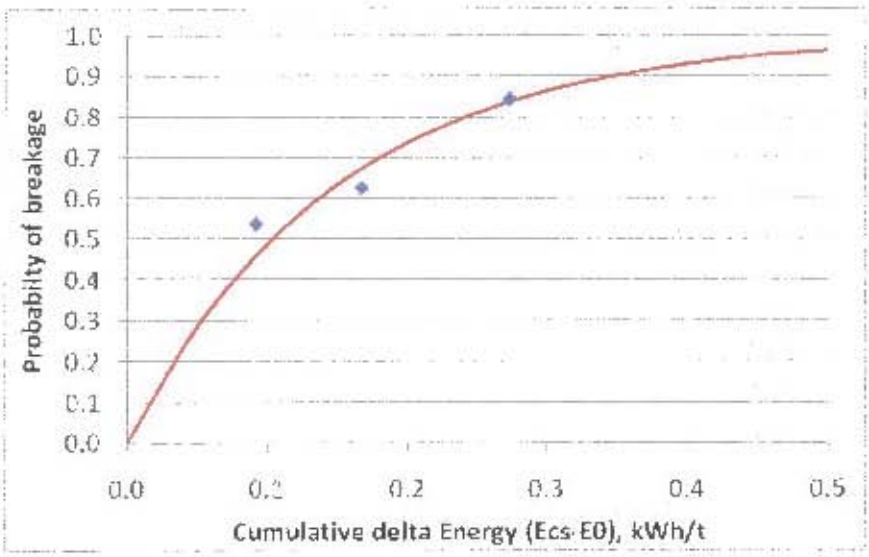


Figure 6.14: Probability to breakage model fitted to data from BS-R

A summary of these fitted parameters is provided in Table 6.4.

Table 6.4: Parameters used to fit probability of breakage data

| | c | $E_{cri}$ (kWh/t) | $f_{mat}$ (t/kwh/mm) | $E_0$-$W_{min}$ (kWh/t) |
|---|---|---|---|---|
| AG2-R | 8.2 | 0.281 | 0.312 | 0.00366 |
| BS-R | 6.7 | 0.334 | 0.284 | 0.0464 |

For AG2-R ore, Figure 6.15 was plotted to compare the degree of breakage of single impacts with that of incremental breakage. While the $t_{10}$ values from single impacts increased steadily with energy, these values for the same energy expended for incremental breakage remained low. It was thus observed that incremental breakage was much less efficient than single impact breakage, that is, it was considerably more beneficial to break a particle in a single impact rather than with a number of lower energy impacts. The modified $t_{10}$ equation (Equation 2.18) was fitted to the single impact breakage data to compare the value of $E_0$ from that obtained from fitting the full range of incremental breakage data. A value of 0.0098 was obtained for $E_0$, which highlighted that in order to accurately fit this parameter a full range of incremental breakage data was more beneficial.

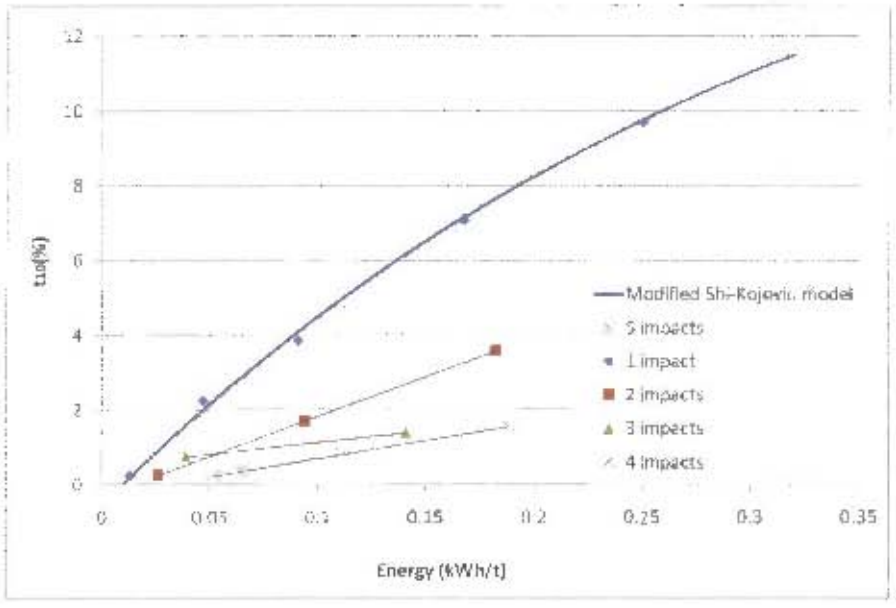


Figure 6.15: Plot of $t_{10}$ against expended energy for incremental breakage with RBT

Figure 6.16 was plotted to show the inverse ratio of $t_{10}$ values with an increasing number of impacts for the same cumulative energy input estimated by successive equal energy impacts. It emphasized the penalty associated with multiple impacts relative to single impact breakage, as exposing a particle to a distribution of smaller impacts expended the energy for negligible breakage.

A summary of all RBT results can be found in Section 7.1.

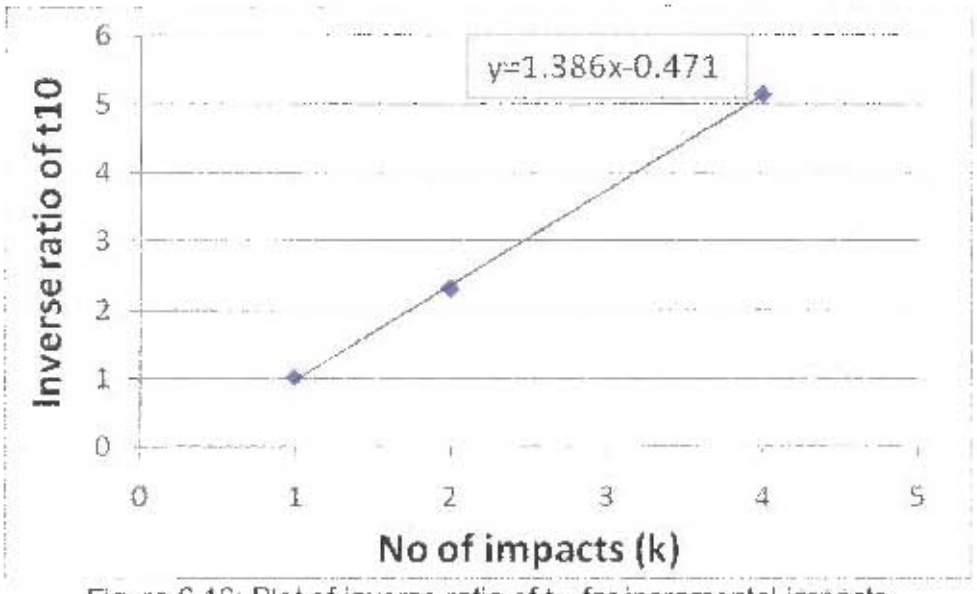


Figure 6.16: Plot of inverse ratio of $t_{10}$ for incremental impacts

# CHAPTER 7

# SUMMARY AND COMPARISON OF BREAKAGE RESULTS

*Overview*
*This chapter summarizes the results of the work carried out with all three devices. A comparison of the breakage data obtained across these is then discussed.*

## 7.1 SUMMARY OF RESULTS

Breakage experiments were carried out with all three devices to address the objectives outlined in Chapter 1. Single impact breakage tests were carried out on two rock types using the drop weight test, split Hopkinson pressure bars and rotary breakage tester. Incremental breakage experiments were also conducted on these two rock types with split Hopkinson pressure bars and the rotary breakage tester.

*Drop weight test*

Single impact breakage tests with the drop weight tests yielded the A and b hardness parameters for the ore types investigated (see Table 4.1). These were calculated using both the standard JK breakage model and the modified Shi-Kojovic model. A low percentage difference was found between the values obtained with either model, although the modified equation consistently gave higher A.b values than the standard equation. Hardness values with the conventional model were found to range between 31 and 46 which corresponded to between hard and medium according to the JKMRC database(see Table 2.3). AG2-A was found to be in the hard range of 30-38 with an A.b value of 31.0. The rounded variation of this ore, AG2-R (collected from the AG mill), was calculated to have a higher, moderately hard value ranked in the 38-43 range. This suggested that rounded pebbles which had been subjected to high stress rounding had become weaker than angular particles. A.b values for AG1-A, BS-A and BS-R were 45.9, 44.4 and 43.8 respectively, found to lie in the medium hardness range of 43-56.

Little difference in $t_{10}$ was observed at drop weight test energies below 1 kWh/t. At this energy, particles of the three sizes investigated were found to fracture to similar breakage degrees across all the ore types. For 2.5 kWh/t and above however, a

slight difference was observed in $t_{10}$ values for different particle sizes, with larger sizes always tending to fracture to higher breakage degrees. With the standard equation, size specific model fits were plotted and compared to the conventional size independent fit with this model. The differences between these showed the particle size effect to have an influence on breakage. P80 values for the gold ores at each size were compared over the energy ranges tested, and the noted trend was an increase in P80 as particle size increased. This further illustrated a particle size effect. Tests with blue stone to compare the effect of ore geometry on breakage degree showed no distinct difference in breakage degree between either geometry for the energy ranges tested. Both angular and rounded geometries gave similar breakage results over the full energy range tested, showing that the conditions under which angular particles were rounded did not affect ore hardness,

*Split Hopkinson pressure bars*

Experiments with cored cylindrical specimens were used to establish the ultimate compressive stress (UCS) of blue stone, which was found to be 138 MPa. By further calculations the Young's modulus and Poisson's ratio were found to be 22.4 and 0.3 respectively. Strength parameters as put forward by Tavares and King[49] were also calculated where the particle strength and stiffness and were found to be 87 MPa and 24 GPa respectively. The particle fracture energy was found to be 44.25 J/kg which was shown to be in the expected range for quartz and marble particles.

Single impact breakage tests with split Hopkinson pressure bars showed a difference between the mean energy absorbed by angular and rounded specimens of blue stone at identical energy ranges. Rounded geometries absorbed 39% whilst angular particles absorbed 31% of available impact energy to cause fracture. Rounded specimens were also found to give greater consistency in the fraction of energy absorbed during impact relative to angular specimens. For all specimens tested with the Hopkinson bar, it was observed that specimens absorbed less than 50% of available energy to cause fracture.

The effect of end effector geometry on the energy transfer to the particle using Hopkinson bars was investigated using rounded specimens of blue stone. It was found that flat surfaces transferred marginally higher percentages of impact energy than rounded ends over an identical input energy range.

Single impact breakage tests were also carried out using strikers of three different lengths to investigate the role of impulse, or duration of impact, on particle breakage. The amount of energy absorbed by a specimen for similar impact energy increased with the duration of the time taken to transfer the load between the 300mm and 450mm strikers, while it remained fairly constant between the 450mm and 600mm strikers.

Breakage degree was found to increase with increase in absorbed impact energy. To compare the efficiency of single impacts against incremental impact fracture, breakage degrees were plotted against the total energy absorbed by particles for the number of impacts required to cause breakage. Breakage degrees steadily increased with absorbed energy for single impact breakage whilst these values remained similar for the same cumulative energy absorbed over several impacts. It was concluded that incremental breakage was an inefficient method of breakage relative to single impact fracture.

*Rotary breakage tester*

Single impact breakage experiments were conducted with the rotary breakage tester at 1 and 2.5 kWh/t to investigate the breakage degree versus impact energy relationship with the device. It was observed that breakage distributions from these tests became gradually finer with increase in energy and decrease in particle size. For rounded AG2-R gold ore, A.b values of 45.6 and 47.6 were obtained with the standard and modified models respectively. Below 1 kWh/t little difference was observed in breakage degree between particle sizes, whilst at 2.5 kWh/t larger sizes showed distinctly higher $t_{10}$ values.

To investigate the statistical significance of the number of specimens used for breakage tests, 6 groups of 5 particles each were subjected to breakage against the standard number of 30 particles in each test using blue stone. It was observed that the scatter from rounded specimens was much less than from angular specimens, which tended to give greater breakage consistency. From these results the significance of the number of particles over which results were calculated was also highlighted.

Incremental breakage experiments on AG2-R were conducted at energy levels between $E_0$ and $E_{crit}$ and it was found that the probability of breakage at a particular energy for each impact remained relatively consistent. A model (Equation 6.5) similar to the Vogel-Peukert relationship was fitted to this data and it was established that the gradient from this model was a linear function of the input energy. This model was then used to define $E_{crit}$ as a function of breakage probability.

$E_{crit}$ was calculated at 90% breakage probability by fitting this model to the whole range of incremental breakage data for AG2-R ore. An $E_{crit}$ of 0.281 kWh/t was obtained for the AG2-R, while an $E_{crit}$ of 0.344 kWh/t was calculated for blue stone by fitting this model to a single set of single impact breakage data. The values of $E_0$ and $f_{mat}$ were calculated from fitting the Vogel-Peukert probability of breakage model (Equation 2.17) to RBT data. AG2-R was found to have an $E_0$ of 0.00366 whilst $E_0$ for BS-R was 0.0464.

The rotary breakage tester further illustrated the inefficiency of incremental breakage relative to single impact breakage. For similar amounts of energy expended, the breakage degree from multiple impacts was observed to remain fairly low while that of single impacts steadily increased.

## 7.2 COMPARISON OF BREAKAGE RESULTS ACROSS THE THREE DEVICES

For the three devices in this work, distinctly different methods were employed to calculate particle fracture properties from their breakage data. The basis for comparison between these devices therefore was chosen to be the $t_{10}$ breakage degree obtained over similar energy ranges.

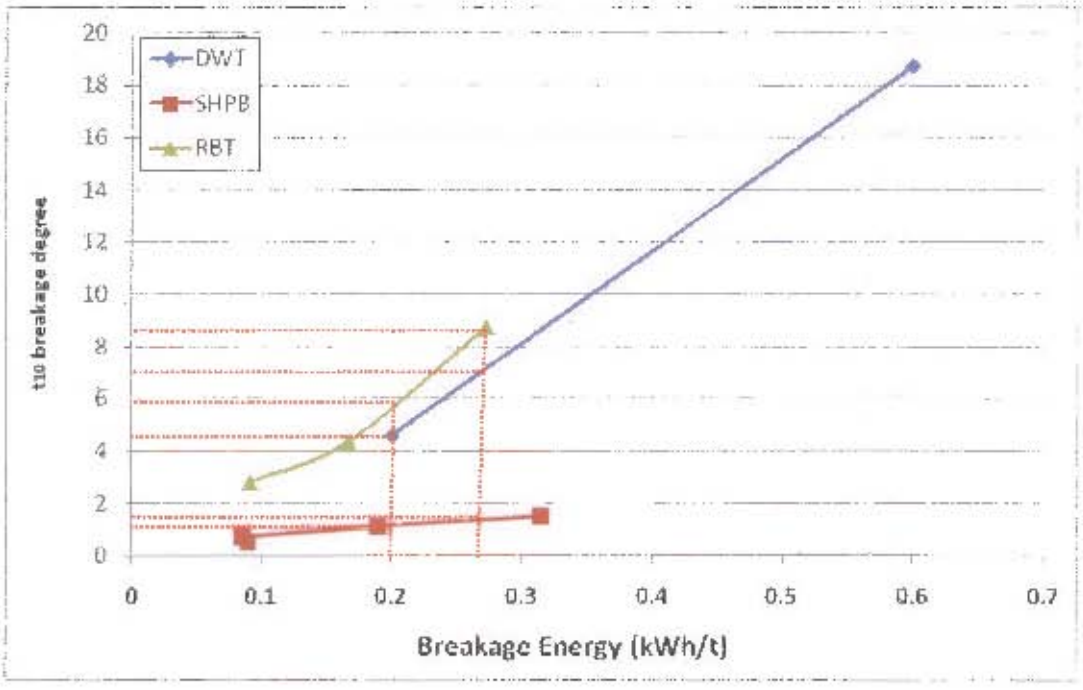


Figure 7.1: Overlap in impact breakage energies across the devices for blue stone

Figure 7.1 shows a plot of breakage energies at which single impact breakage tests with the -31.5 +26.5mm size of BS-R overlapped. The $t_{10}$ was plotted against this as the basis to compare breakage between the devices. From the values calculated for 0.2 and 0.26 kWh/t (Table 7.1), the breakage degree for the split Hopkinson pressure bars was found to be much lower than for the other two devices. From the tests carried out with the two devices used for this work the RBT was found to give consistently higher $t_{10}$ values than the drop weight test. It is not known whether this device was part of a Round Robin test series at any time. The drop weight test was routinely used for routine experiments verified by the JKMRC. The RBT that was used for this work was newly commissioned.

Table 7.1: Comparison of $t_{10}$ values for similar breakage energies with the three devices

| Energy (kWh/t) | 0.2 | 0.25 |
|---|---|---|
| **Device** | **t10** | **t10** |
| | (%) | (%) |
| DWT | 4.60 | 7.1 |
| SHPB | 1.40 | 1.6 |
| RBT | 5.80 | 8.7 |

Product distributions for the three devices at this similar energy level were plotted in Figure 7.2. It was observed that although the Hopkinson bar had a smaller top size, little material fractured beyond the 10mm screen size relative to the drop weight and rotary breakage tester.

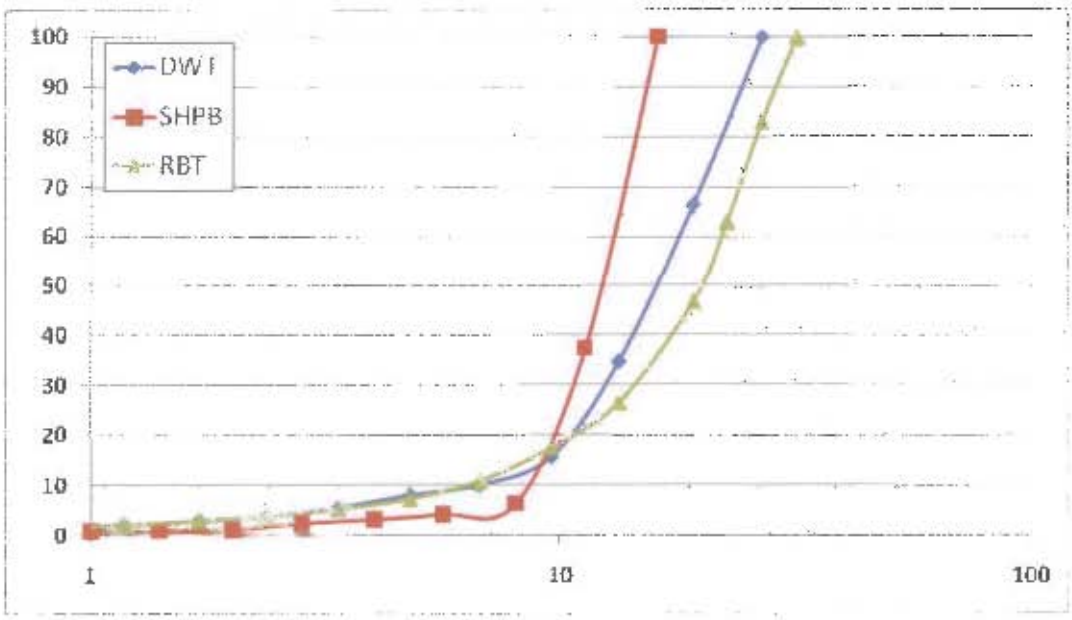


Figure 7.2: Comparison of size distributions for each device over a similar range

This result was attributed to the mode of loading by the Hopkinson bar. As the particle was subjected to point loading with this device, it showed a high degree of initial fracture. For the other devices however, the particles fractured against a static surface, which resulted in finer product while for Hopkinson bars, after initial fracture the remaining energy dissipated through kinetic energy of the transmitter bar and reverberating stress pulses in the bars.

To compare the degree of breakage between the drop weight test and rotary breakage tester, the standard deviation over the mean of the $t_{10}$ values was calculated. This relative variation in $t_{10}$ values was calculated at identical energies for gold ores as shown in Table 7.2. From tests with the two devices used, the RBT was observed to consistently generate higher $t_{10}$ values across all sizes and energies.

Table 7.2: Percentage values of $t_{10}$ and variation between Drop Weight and RBT tests

| | | 1 kWh/t | | Std dev/ Mean | 2 kWh/t | | Std dev/ Mean |
|---|---|---|---|---|---|---|---|
| | | DWT | RBT | | DWT | RBT | |
| Size (mm) | Ore type | $t_{10}$ | $t_{10}$ | | $t_{10}$ | $t_{10}$ | |
| Small (-16 +11.2) | AG1-A | 32.3 | 35.4 | 6.4 | 53.8 | 66.6 | 15.0 |
| | AG2-A | 23.1 | 28.0 | 13.5 | 41.8 | 52.8 | 16.5 |
| | AG2-R | 27.1 | 36.5 | 20.9 | 52.0 | 58.6 | 8.4 |
| Medium (-22.4 +19) | AG1-A | 32.3 | 42.4 | 19.1 | 50.9 | 59.5 | 11.0 |
| | AG2-R | 32.0 | 37.6 | 11.3 | 53.7 | 64.7 | 13.0 |
| Large (-31.5 +26.5) | AG1-A | 34.6 | 35.4 | 1.6 | 55.9 | 58.7 | 3.5 |
| | AG1-A | 26.8 | 32.7 | 14.2 | 47.2 | 61.4 | 18.5 |

Although the $t_{10}$ was consistently higher with the RBT, overall particle size distributions generated by either of them for identical energies were seen to vary as shown in Figure 7.3 and 7.4. Distributions of AG1-A gold ore were compared as it was the only ore type for which all sizes were tested with both devices at identical energy. Differences were observed in distributions above the P50, while below this mark they grew gradually similar, with the RBT consistently generating finer material. Due to this result, the standard model A.b parameter found with the RBT for this rounded gold ore type was higher, with a value of 45.6 obtained compared to 39.6 with the drop weight.

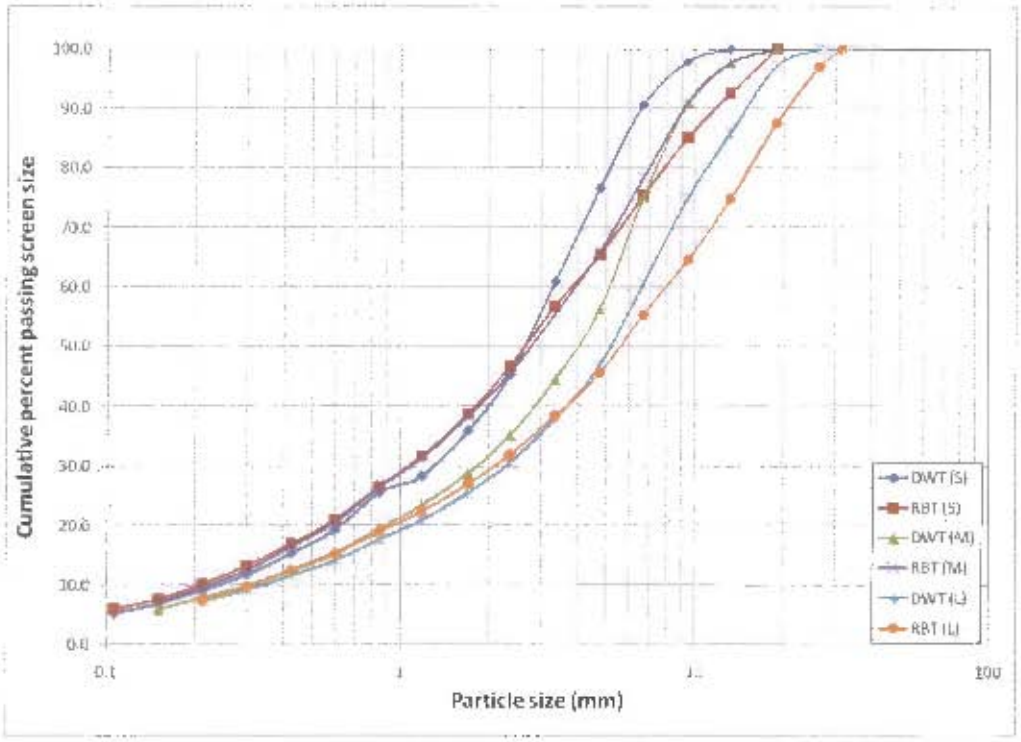


Figure 7.3: Particle size distributions of AG1-A ore for DWT and RBT at 1kWh/t

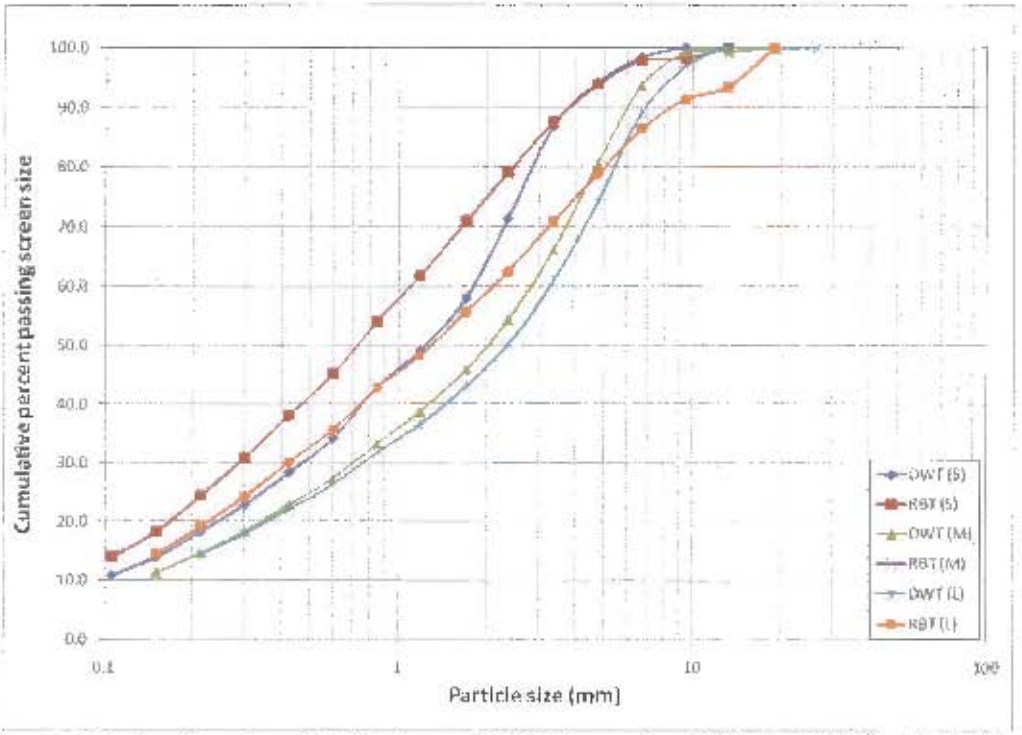


Figure 7.4: Particle size distributions of AG1-A ore for DWT and RBT at 2.5kWh/t

# CHAPTER 8

# CONCLUSIONS AND RECOMMENDATIONS

*Overview*
*This chapter concludes the thesis and offers recommendations for future work.*

## 8.1 OBSERVATIONS MADE FROM EXPERIMENTAL WORK

The objective of this thesis was to test two hypotheses related to assessment of impact breakage in comminution. For this work, single impact breakage tests were carried out on two rock types with the drop weight test, split Hopkinson bars and the rotary breakage tester. Incremental breakage experiments were also conducted on these ores with split Hopkinson pressure bars and the rotary breakage tester.

Drop weight tests on gold ore were used to calculate the A and b hardness parameters using both the standard JK breakage model and the modified Shi-Kojovic model. The modified equation gave consistently higher A.b values for all ore sizes and energies tested, although little difference was found between fitting the two models. A 2-5 % percent increase was found in the A.b value with the modified equation for all ores except AG2-A which gave the highest difference of 9%.

Split Hopkinson pressure bars were used to establish the ultimate compressive stress of blue stone through single impact breakage tests. From calculations using one dimensional stress wave theory, particles were found to absorb less than 50% of the available impact energy during fracture. Cylindrical specimens had the highest mean percentage of absorbed impact energy of 42.6%, followed by rounded and angular specimens which absorbed 39.4% and 31.0% respectively.

The rotary breakage tester was used to conduct incremental breakage experiments with blue stone and gold ore. The probability to breakage at the impact energies tested was found to remain relatively consistent over consecutive impacts. This showed that a model could be fitted between the cumulative probability to breakage and the number of impacts at these energy levels. This showed that a model could be used to establish the probability of breakage as a function of input energy and define an equation for $E_{crit}$.

The values of $E_0$ for blue stone and gold ore were calculated to be 0.0464 and 0.00366 respectively. $E_{crit}$ for 90% probability to first impact breakage for these two ores was 0.344 and 0.281 respectively.

It was found that incremental breakage was much more inefficient than single impact breakage. From tests with both split Hopkinson pressure bars and the rotary breakage tester, breakage degrees for single impacts increased rapidly with increase in breakage energy whilst the breakage degrees obtained from incremental breakage tests for similar amounts of energy expended remained low.

In comparing breakage data from the three devices, Hopkinson bars were found to have the lowest breakage degree for similar impact energies. Although it showed the highest degree of initial fracture, the subsequent $t_{10}$ values from this device were found to be very low compared to those of the drop weight and rotary breakage tester for the same energy. The RBT was found to give consistently finer product distributions below the P50 mark, which resulted in higher t10 values with this device than the drop weight test.

## 8.2 CONCLUSIONS

The work in this thesis was conducted to address two hypotheses as presented in the introduction, namely:

- For a given material, values of $E_0$ and $E_{crit}$ exist and can be measured
- Single impact breakage is more efficient than incremental breakage

Based on objectives from these hypotheses given in the introduction, the following conclusions were reached through experimental tests with the drop weight test, split Hopkinson pressure bars and the rotary breakage tester:

- The value of $E_0$ for -31.5 +26.5mm size was 0.046kWh/t for blue stone and 0.0037 kWh/t for gold ore. This indicated that the Blue stone is more resistant to breakage.

- Values of $E_{crit}$ were calculated for a 90% probability of breakage in a single impact. For blue stone and gold ore these were 0.334 and 0.281 kWh/t respectively. As only one size was tested in this set of work, the size dependency derived by Vogel and Peukert could not be tested. The harder blue stone will fracture in a single impact at a higher energy than the gold ore.

- The degree of breakage achievable by a particular device depends on the method of impact. Split Hopkinson pressure bars, which use point loading, gave the highest initial particle fracture, but gave much coarser size distributions below P20. Below P50, the rotary breakage tester gave consistently finer product distributions than the drop weight test.

- Incremental breakage is less efficient than single impact breakage. This was investigated with split Hopkinson pressure bars and established with the rotary breakage tester. The $t_{10}$ value dropped off dramatically for equivalent cumulative energy applied over multiple impacts versus a single impact to breakage. This was shown to equate to 1.4 times the amount of energy expended using incremental breakage relative to the energy needed for single impact fracture.

## 8.3 RECOMMENDATIONS FOR FUTURE WORK

Several limitations prevented a number of investigations from being carried out. Tests with Hopkinson bars were limited to the energy range of 0.1 to 0.6 kWh/t. Energies below 0.1 kWh/t could not be obtained as the firing mechanism would not launch below the minimum back pressure of 3 bar (appx 0.3 MPa), while energies higher than 0.6 kWh/t were found to damage strain gauges.

Incremental breakage tests with the rotary breakage tester could not be carried out for lower energy values than those conducted as the lowest possible breakage energy was dictated by the minimum rotor speed of 300rpm. Incremental breakage tests at lower energies would allow for more accurate experimental determination of $E_0$.

Calculation of $E_{crit}$ was limited to the available size range of -31.5 + 26.5 mm. As incremental breakage tests with the RBT required a relatively high number of

particles per test, only this size range was investigated as a basis for the methodology in future experiments. Incremental breakage tests for a greater number of impacts and up to higher percentages of mass broken would allow for more accurate experimental determination of $E_{crit}$.

Thus, from the breakage tests carried out across the three breakage devices selected for this project, the following recommendations are put forward for future work in this area:

- Values of $E_0$ and $E_{crit}$ can be calculated for other ore types from the methodology developed for this project. The effect of particle size on these values can be investigated by conducting similar experiments with the RBT across a range of sizes.

- Further breakage experiments can be carried out on the rotary breakage tester to characterize the breakage behavior at energies between $E_0$ and $E_{crit}$. With a lower rotor speed, $E_0$ can be experimentally determined through tests at very low energies. Lower energies between $E_0$ and $E_{crit}$ can also be selected to establish the relationship between cumulative breakage probability and the number of impacts at lower energies.

- The scatter from results of breakage experiments on angular specimens relative to that of rounded particles using Hopkinson bars suggests that uniform specimen geometries would be better suited for this test. These tests could be used to develop breakage models which quantify the energy absorption of particles under impact.

- Standard static compression tests could be performed to compare the strength parameters from such tests with those obtained from the impact breakage parameters calculated in this work, which was not part of this scope.

- Rounding specimens of gold ore in the same manner as the blue stone particles can be done to investigate the mechanical coupling of the drop weight relative to the Hopkinson bars

# REFERENCES


1. Agrawala, S., Rajamani, R.K., Songfack, P., Mishra, B.K., *Mechanics of media motion in tumbling mills with 3d discrete element method.* Minerals Engineering, 1997. **10**(2): p. 215-227.

2. Austin, L.G., *A treatment of impact breakage of particles.* Powder Technology, 2002. **126**: p. 85-90.

3. Austin, L.G. and Luckie, P.T., *Methods for determination of breakage distribution parameters.* Powder Technology, 1971. **5**: p. 215-222.

4. Banini, G.A., *An integrated description of rock breakage in comminution machines.* Julius Kruttschnitt Mineral Research Centre, Department of Mining, Metallurgical and Materials Engineering, University of Queensland, 2000. **PhD thesis**.

5. Bbosa, L.S. and Powell, M., *An investigation of impact breakage of rocks using the split Hopkinson pressure bar.* Journal of the South African Institute of Mining and Metallurgy, 2006. **106**(4): p. 291-296.

6. Bbosa, L.S. and Powell, M., *Measuring the input and absorbed energy of impact breakage using split Hopkinson pressure bars.* AMIRA Project P9N Mineral Processing, 2006. **6th Technical Report**: p. 197-206.

7. Bearman, R.A., Briggs, C.A. and Kojovic, T., *The application of rock mechanics parameters to the prediction of comminution behaviour.* Minerals Engineering, 1997. **10**(3): p. 255-264.

8. Bond, F.C., *The third theory of comminution.* Transaction AIME (Mining), 1952. **193**: p. 484-494.

9. Bourgeois, F., King, R.P. and Herbst, J.A., *Low-impact-energy single particle fracture.* Ed: Kawatra, 1992. **Chapter 8**: p. 99-108.

10. Cai, M. and Kaiser, P.K., *Numerical simulation of the Brazilian test and the tensile strength of anisotropic rocks and rocks with pre-existing cracks.* international Journal of Rock Mechanics and Mining Sciences, 2004. **41**(3): p. 450-451.

11. Cho, H. and Austin, L.G., *An Equation for the breakage of particles under impact.* Powder Technology, 2003: p. 161-166.

12. Cleary, P.W., *Predicting charge motion, Power draw, Segregation, and wear in ball mills using Discrete Element Methods.* Minerals Engineering, 1998. **11**(11): p. 1061-1080.

13. Crabtree, D.D., Kinasevich, R.S., Mular, A.L., Meloy, T.P., Fuerstenau, D.W., *Mechanisms of size reduction in comminution systems* Society of Mining Engineeers, 1964. **229**: p. 201-210.

14. Daniel, M., *Comminution energy efficiency, essential to the development of future sustainable energy.* AMIRA Project P9N Mineral Processing, 2005. **4th P9N Technical report**: p. 2-44.

15. Davies, E.D.H. and Hunter, S.C., *The dynamic compression testing of solids by the method of the spit Hopkinson pressure bar.* Journal of the Mechanics and Physics of Solids, 1963. **11**(3): p. 155-179.

16. Deeg, W., *New algorithms for calculating Hertzian stresses, deformations, and contact zone parameters.* AMP Journal of technology, 1992. **2**: p. 14-24.

17. Djordjevic, N., Morrison, R.D., Loveday, B., Cleary, P.W., *Modelling comminution patterns within a pilot scale AG/SAG mill.* Minerals Engineering, 2006. **19**: p. 1505-1516.

18. Fandrich, R.G., *Mineral liberation through confined particle bed breakage.* Julius Kruttschnitt Mineral Research Centre, Department of Mining, Metallurgical and Materials Engineering, University of Queensland, 1998. **PhD thesis**.

19. Fandrich, R.G., Clout, J.M.F. and Bourgeois, F.S., *The CSIRO Hopkinson Bar Facility for large diameter particle breakage.* Minerals Engineering, 1998. **11**(9): p. 861-869.

20. Frew, D.J., Forrestal M.J., and Chen, W., *A split Hopkinson bar technique to determine compressive stress strain data for rock materials.* Experimental Mechanics, 2001. **41**: p. 40-46.

21. Fuerstenau, D.W. and Abouzeid, A.-Z.M., *The energy efficiency of ball milling in comminution.* International Journal of Mineral Processing, 2002. **67**: p. 161-185.

22. Fuerstenau, D.W. and Kapur, P.C., *Newer energy-efficient approach to particle by comminution.* Powder Technology, 1995. **82**: p. 51-57.

23. Fuerstenau, D.W., Lutch J.J., and De, A., *The effect of ball size on the energy efficiency of hybrid high-pressure roll mill/ball mill grinding.* Powder Technology, 1999. **105**: p. 199-204.

24. Genc, O., Ergun L., and Benzer, H., *Single particle impact breakage characterization of materials by drop weight testing.* Physicochemical Problems of Mineral Processing, 2004. **38**: p. 241-255.

25. Govender, I. and Powell, M., *Mathematical framework of the Unified Comminution model.* AMIRA Project P9N Mineral Processing, 2006. **5th Technical report**: p. 97-104.

26. Gray, G., *Classic Split-Hopkinson Pressure Bar Technique.* ASM Handbook, Mechanical Testing and Evaluation, 2000. **Volume 8**: p462-477

27. Herbst, J.A., *Making a Discrete Grain Breakage model practical for comminution equipment performance simulation.* Powder Technology, 2004. **143-144**: p. 144-150.

28. Hopkinson, B., *A method for measuring the pressure produced in the detonation of high explosives or by the impact of bullets.* Philosophical transactions of the Royal Society, 1914. **213**: p. 437-456.

29. Kapur, P.C., Pande D., and Fuerstenau D.W., *Analysis of single-particle breakage by impact grinding.* International Journal of Mineral Processing, 1997. **49**: p. 233-236.

30. Kolsky, H., *An investigation of the Mechanical Properties of Materials at very High Rates of Loading.* Proc. Phys. Society, 1949. **62**: p. 676-700.

31. Li, Q.M. and Meng H., *About the dynamic strength enhancement of concrete-like materials in a split Hopkinson pressure bar test.* International Journal of Solids and Structures, 2003. **40**: p. 343-360.

32. Liu, J. and Schonert K., *Modelling of interparticle breakage.* International Journal of Mineral Processing, 1996. **44-45**: p. 101-115.

33. Marais, S., Tait, R.B., Cloete, T.J., Nurick, G. *Material testing at high strain rate using the split Hopkinson pressure bar.* 2004. Latin American Journal of Solids and Structures, **1**: p319-339

34. Mishra, B.K., *A review of computer simulation of tumbling mills by the discrete element method: Part II- Practical applications.* International Journal of Mineral Processing, 2003. **71**(1-4): p. 95-112.

35. Mishra, B.K. and Rajamani, R.K., *The discrete element method for the simulation of ball mills.* Applied Mathematical Modelling, 1990. **16**(11): p. 598-604.

36. Morell, S., *An alternative energy-size relationship to that proposed by Bond for the design and optimisation of grinding circuits.* International Journal of Mineral Processing, 2004. **74**: p. 133-141.

37. Napier-Munn, T.J., Morell, S., R.D. Morrison, and T. Kojovic, *Minerals Comminution Circuits: Their operation and optimization.* 1999. **Published by JKMRC**

38. Naranayan, S.S., *Modelling the performance of industrial ball mills using single particle breakage data.* International Journal of Mineral Processing, 1987. **20**(3-4): p. 211-228.

39. Ouchterlony, F., *Fracture toughness of rock with core based specimens.* Engineering Fracture Mechanics, 1990. **35**(1-3): p. 351-366.

40. Powell, M. and Nurick G., *A study of charge motion in rotary mills Part2- Experimental work.* Minerals Engineering, 1995. **9, No. 3**: p. 343-350.

41. Powell, M. and Morrison, R. D. *A new look at Breakage testing.* 11th European Symposium on Comminution, 9-12 Oct 2006, Budapest, Hungary. Published by European Federation of Chemical Engineers. 6pp.

42. Radziszewski, P. and Laplante A., *Exploring the effect of friction losses on drop weight breakage results.* AMIRA Project P9N Mineral Processing, 2006. **5th P9N Technical Report**: p. 42-49.

43. Schonert, K., *Advances in Comminution fundamentals and impacts on technology.* Aufbereitungs-Technik, 1991. **32**(9): p. 487-494.

44. Shi, F. and Kojovic. T., *Investigation of a model for impact breakage incorporating particle size effect.* AMIRA Project P9N Mineral Processing, 2005. **4th Technical report**: p. 45-53.

45. Shi, F. and Kojovic. T., *Validation of a model for impact breakage incorporating particle size effect.* International Journal of Mineral Processing, 2007. **82** p. 156-163.

46. Shi, F., Kojovic, T., Larbi-Bram, S., Manlapig, E., *Development of a new breakage characterisation device.* AMIRA Project P9N Mineral Processing, 2006. **5th technical report**: p. 55-66.

47. Song, B. and Chen, W., *Loading and unloading split Hopkinson pressure bar pulse shaping techniques for dynamic hysteretic loops.* Society for Experimental Mechanics, 2004. **44, No.6**: p. 622-627.

48. Tait, R.B., *Fracture and Fracture Mechanics- Case Studies.* 1985. Personal Communication University of Cape Town

49. Tavares, L.M. and King, R.P., *Single-particle fracture under impact loading.* International Journal of Mineral Processing, 1998. **54**: p. 1-28.

50. Tavares, L.M. and King, R.P., *Modeling of particle fracture by repeated impacts using continuum damage mechanics.* Powder Technology, 2002. **123**: p. 138-146.

51. Tavares, L.M. and King, R.P., *Measurement of the load-deformation response from impact-breakage of particles.* International Journal of Mineral Processing, 2004. **74S**: p. 267-277.

52. Vogel, L. and Peukert, W., *Breakage behaviour of different materials-construction of a mastercurve for the breakage probability.* Powder Technology, 2003. **129**: p. 101-110.

53. Vogel, L. and Peukert, W., *Determination of material properties relevant to grinding by practicable labscale milling tests.* International Journal of Mineral Processing, 2004. **74S**: p. 329-338.

54. Vogel, L. and Peukert, W., *From single particle impact behaviour to modelling of impact mills.* Chemical Engineering Science, 2005. **60**: p. 5164-5176.

55. Weichert, R., *Corelation between probability of breakage and fragment size distribution of mineral particles.* International Journal of Mineral Processing, 1988. **22**(1-4): p. 1-8.

56. Whyte, R., *Measuring incremental damage in rock breakage by impact.* Julius Kruttschnitt Mineral Research Centre, Department of Mining, Metallurgical and Materials Engineering, University of Queensland, 2005. **Undergraduate thesis**.

## MANUALS AND WEBSITES

57. JKMRC Drop Weight Tester: Breakage test procedure. Machine manual. **Published by JKMRC**

58. JKMRC Rotary Breakage Tester: Breakage test procedure. Section 9 Machine manual. **Published by JKMRC**

59. PANanalytical X-ray Powder Diffractometer http://www.panalytical.com

60. National Instruments LabView Express http://www.ni.com/labview

# Appendix A- Drop Weight test data

# Appendix B- Split Hopkinson Pressure bar data

# Appendix C- Rotary Breakage Test data

## AG 1-A: Angular Gold ore

Energy calculations

| Size (mm) | 13.2 -16mm (S) | | | 19 -22.4mm (M) | | | 26.5 -31.5mm (L) | | |
|---|---|---|---|---|---|---|---|---|---|
| Energy targeted (kWh/t) | 0.25 | 1 | 2.5 | 0.25 | 1 | 2.5 | 0.25 | 1 | 2.5 |
| Drop weight mass required (kg) | 2.75 | 2.75 | 6.724 | 2.75 | 14.933 | 24.918 | 4.726 | 24.918 | 44.913 |
| Drop weight mass used (kg) | 2.75 | 2.75 | 6.724 | 2.75 | 14.933 | 24.918 | 4.726 | 24.918 | 44.913 |
| Height required (cm) | 23.5 | 91.2 | 92.4 | 68.9 | 50.4 | 75.1 | 87.5 | 66.0 | 90.9 |
| Height used (cm) | 23.5 | 91.2 | 92.4 | 68.9 | 50.4 | 75.1 | 87.5 | 66 | 90.9 |
| Measured residual gaps (mm) | 8 | 1 | 1 | 9 | 4 | 6.5 | 18 | 10.5 | 1 |
| | 6 | 1 | 1 | 9 | 11 | 0.5 | 17 | 14 | 4.5 |
| | 8 | 3 | 3 | 13 | 4 | 2 | 11 | 3.5 | 9 |
| | 9 | 6 | 1 | 15 | 7 | 4 | 14 | 15.5 | 3.5 |
| | 6 | 2 | 1 | 17 | 5.5 | 0.5 | 15 | 7.5 | 3 |
| | 6 | 4 | 1 | 10 | 5.5 | 4 | 18 | 8 | 3.5 |
| | 7 | 1 | 1 | 9 | 10.5 | 2.5 | 12 | 6.5 | 3.5 |
| | 13 | 2 | 4 | 13 | 3 | 3.5 | 23 | 9.5 | 3.5 |
| | 6 | 2 | 1 | 12 | 5 | 4.5 | 11 | 8 | 3 |
| | 8 | 1 | 1 | 10 | 5.5 | 4.5 | 13 | 4.5 | 6.5 |
| Average offset height (cm) | 0.77 | 0.23 | 0.15 | 1.17 | 0.61 | 0.325 | 1.52 | 0.875 | 0.41 |
| Adjusted drop height (cm) | 22.73 | 90.97 | 92.25 | 67.73 | 49.79 | 74.775 | 85.98 | 65.125 | 90.49 |
| Sample total mass (g) | 203.5 | 203.5 | 202.3 | 608.4 | 607.5 | 607.7 | 1322.6 | 1323.6 | 1325.2 |
| No of particles | 30 | 30 | 30 | 30 | 30 | 30 | 30 | 30 | 30 |
| Average particle mass (g) | 6.8 | 6.8 | 6.7 | 20.3 | 20.3 | 20.3 | 44.1 | 44.1 | 44.2 |
| Actual impact energy (kWh/t) | 0.25 | 1.00 | 2.50 | 0.25 | 1.00 | 2.50 | 0.25 | 1.00 | 2.50 |

| Particle size distributions | 13.2 -16mm (S) | | | | | | | | |
|---|---|---|---|---|---|---|---|---|---|
| **ENERGY (kWh/t)** | 0.25 | | | 1 | | | 2.5 | | |
| Size (mm) | Wt above | %retained | Cumu %passing | Wt above | %retained | Cumu %passing | Wt above | %retained | Cumu %passing |
| 13.2 | 11 | 5.4 | 94.6 | 0 | 0.0 | 100.0 | 0 | 0.0 | 100.0 |
| 9.5 | 60.4 | 29.7 | 64.9 | 4 | 2.0 | 98.0 | 0 | 0.0 | 100.0 |
| 6.7 | 54.2 | 26.6 | 38.2 | 14.8 | 7.4 | 90.7 | 3.2 | 1.6 | 98.4 |
| 4.75 | 28.2 | 13.9 | 24.4 | 28.3 | 14.1 | 76.6 | 8.4 | 4.2 | 94.2 |
| 3.35 | 11 | 5.4 | 19.0 | 31.7 | 15.7 | 60.9 | 14.6 | 7.3 | 86.9 |
| 2.36 | 9.6 | 4.7 | 14.3 | 31.5 | 15.6 | 45.2 | 31 | 15.5 | 71.4 |
| 1.7 | 5.4 | 2.7 | 11.6 | 18.7 | 9.3 | 35.9 | 26.5 | 13.3 | 58.1 |
| 1.18 | 2 | 1.0 | 10.6 | 15.2 | 7.6 | 28.4 | 18 | 9.0 | 49.1 |
| 0.85 | 4.1 | 2.0 | 8.6 | 5.8 | 2.9 | 25.5 | 12.2 | 6.1 | 43.0 |
| 0.6 | 4.8 | 2.4 | 6.2 | 12.4 | 6.2 | 19.3 | 17.7 | 8.9 | 34.1 |
| 0.425 | 2.9 | 1.4 | 4.8 | 8 | 4.0 | 15.4 | 11.5 | 5.8 | 28.3 |
| 0.3 | 2.4 | 1.2 | 3.6 | 7.2 | 3.6 | 11.8 | 10.9 | 5.5 | 22.9 |
| 0.212 | 1.8 | 0.9 | 2.8 | 5.4 | 2.7 | 9.1 | 9.1 | 4.6 | 18.3 |
| 0.15 | 1.5 | 0.7 | 2.0 | 4.5 | 2.2 | 6.9 | 8.7 | 4.4 | 14.0 |
| 0.106 | 0.9 | 0.4 | 1.6 | 3.2 | 1.6 | 5.3 | 6.1 | 3.1 | 10.9 |
| Pan | 3.2 | 1.6 | 0.0 | 10.6 | 5.3 | 0.0 | 21.8 | 10.9 | 0.0 |
| Totals | 203.4 | 100 | | 201.3 | 100 | | 199.7 | 100 | |
| Mass discrepancy | 0.1 | | | 2.2 | | | 2.6 | | |
| t2 | | | 43.6 | | | 92.1 | | | 98.7 |
| t4 | | | 20.1 | | | 64.0 | | | 88.4 |
| t5 | | | 16.9 | | | 53.8 | | | 79.9 |
| t10 | | | 11.1 | | | 32.3 | | | 53.8 |
| P80 size | | | 11.38 | | | 5.22 | | | 2.91 |

| Particle size distributions | 19 -22.4mm (M) | | | | | | | | |
|---|---|---|---|---|---|---|---|---|---|
| **ENERGY (kWh/t)** | **0.25** | | | **1** | | | **2.5** | | |
| Size (mm) | Wt above | %retained | Cumu %passing | Wt above | %retained | Cumu %passing | Wt above | %retained | Cumu %passing |
| 19 | 33.7 | 5.5 | 94.5 | 0 | 0.0 | 100.0 | 0 | 0.0 | 100.0 |
| 13.2 | 199.8 | 32.9 | 61.6 | 13.5 | 2.2 | 97.8 | 3.1 | 0.5 | 99.5 |
| 9.5 | 135.7 | 22.3 | 39.3 | 41.2 | 6.8 | 91.0 | 2 | 0.3 | 99.2 |
| 6.7 | 92.4 | 15.2 | 24.1 | 96.3 | 15.8 | 75.2 | 33.3 | 5.5 | 93.7 |
| 4.75 | 39.4 | 6.5 | 17.6 | 114.6 | 18.9 | 56.3 | 79.6 | 13.1 | 80.6 |
| 3.35 | 23.2 | 3.8 | 13.8 | 71.1 | 11.7 | 44.6 | 87.9 | 14.5 | 66.1 |
| 2.36 | 19.7 | 3.2 | 10.5 | 57.2 | 9.4 | 35.2 | 71.2 | 11.7 | 54.4 |
| 1.7 | 13.3 | 2.2 | 8.3 | 39.2 | 6.4 | 28.7 | 51.2 | 8.4 | 45.9 |
| 1.18 | 10 | 1.6 | 6.7 | 32.1 | 5.3 | 23.5 | 43.8 | 7.2 | 38.7 |
| 0.85 | 7.8 | 1.3 | 5.4 | 24 | 3.9 | 19.5 | 33.4 | 5.5 | 33.2 |
| 0.6 | 7.4 | 1.2 | 4.2 | 24.9 | 4.1 | 15.4 | 36.3 | 6.0 | 27.3 |
| 0.425 | 4.9 | 0.8 | 3.4 | 17 | 2.8 | 12.6 | 26.7 | 4.4 | 22.9 |
| 0.3 | 4.5 | 0.7 | 2.6 | 16.6 | 2.7 | 9.9 | 27.6 | 4.5 | 18.3 |
| 0.212 | 3.6 | 0.6 | 2.0 | 12.5 | 2.1 | 7.8 | 22.6 | 3.7 | 14.6 |
| 0.15 | 3 | 0.5 | 1.5 | 11.3 | 1.9 | 6.0 | 20 | 3.3 | 11.3 |
| Pan | 9.4 | 1.5 | 0.0 | 36.3 | 6.0 | 0.0 | 68.6 | 11.3 | 0.0 |
| Totals | 607.8 | 100 | | 607.8 | 100 | | 607.3 | 100 | |
| Mass discrepancy | 0.6 | | | -0.3 | | | 0.4 | | |
| | | | | | | | | | |
| t2 | | | 44.2 | | | 92.5 | | | 99.2 |
| t4 | | | 18.9 | | | 60.2 | | | 83.3 |
| t5 | | | 15.9 | | | 51.1 | | | 76.4 |
| t10 | | | 9.5 | | | 32.3 | | | 50.9 |
| P80 size | | | 16.45 | | | 7.56 | | | 4.69 |

| Particle size distributions | 26.5 -31.5mm (L) | | | | | | | | |
|---|---|---|---|---|---|---|---|---|---|
| **ENERGY (kWh/t)** | **0.25** | | | **1** | | | **2.5** | | |
| Size (mm) | Wt above | %retained | Cumu %passing | Wt above | %retained | Cumu %passing | Wt above | %retained | Cumu %passing |
| 26.5 | 161.2 | 12.2 | 87.8 | | 0.0 | 100.0 | | 0.0 | 100.0 |
| 19 | 317.3 | 24.0 | 63.8 | 37.7 | 2.9 | 97.1 | | 0.0 | 100.0 |
| 13.2 | 358.1 | 27.1 | 36.7 | 148.2 | 11.2 | 85.9 | | 0.0 | 100.0 |
| 9.5 | 131.7 | 10.0 | 26.7 | 145.3 | 11.0 | 75.0 | 41 | 3.1 | 96.9 |
| 6.7 | 101.2 | 7.7 | 19.0 | 191 | 14.4 | 60.5 | 103.2 | 7.8 | 89.1 |
| 4.75 | 68.7 | 5.2 | 13.8 | 180.2 | 13.6 | 46.9 | 196.9 | 14.9 | 74.2 |
| 3.35 | 40.1 | 3.0 | 10.8 | 116.4 | 8.8 | 38.1 | 176.7 | 13.3 | 60.9 |
| 2.36 | 31.3 | 2.4 | 8.4 | 99.5 | 7.5 | 30.6 | 142.8 | 10.8 | 50.1 |
| 1.7 | 20 | 1.5 | 6.9 | 66 | 5.0 | 25.6 | 94.2 | 7.1 | 43.0 |
| 1.18 | 18 | 1.4 | 5.5 | 62 | 4.7 | 20.9 | 86.1 | 6.5 | 36.5 |
| 0.85 | 11.4 | 0.9 | 4.7 | 42.4 | 3.2 | 17.7 | 62.4 | 4.7 | 31.8 |
| 0.6 | 13.4 | 1.0 | 3.7 | 47.1 | 3.6 | 14.1 | 74 | 5.6 | 26.2 |
| 0.425 | 8.8 | 0.7 | 3.0 | 32.5 | 2.5 | 11.6 | 53.9 | 4.1 | 22.2 |
| 0.3 | 8.4 | 0.6 | 2.4 | 31.4 | 2.4 | 9.3 | 55.9 | 4.2 | 17.9 |
| 0.212 | 6.5 | 0.5 | 1.9 | 25.7 | 1.9 | 7.3 | 45.9 | 3.5 | 14.5 |
| Pan | 24.7 | 1.9 | 0.0 | 96.9 | 7.3 | 0.0 | 191.6 | 14.5 | 0.0 |
| Totals | 1320.8 | 100 | | 1322.3 | 100 | | 1324.6 | 100 | |
| Mass discrepancy | 1.8 | | | 1.3 | | | 0.6 | | |
| | | | | | | | | | |
| t2 | | | 42.5 | | | 88.3 | | | 100.0 |
| t4 | | | 20.5 | | | 63.2 | | | 90.6 |
| t5 | | | 16.6 | | | 54.1 | | | 82.1 |
| t10 | | | 9.7 | | | 34.6 | | | 55.9 |
| P80 size | | | 24.07 | | | 11.20 | | | 5.50 |

## AG 2-A: Angular Gold ore

Energy calculations

| Size (mm) | 13.2 -16mm (S) | | | 19 -22.4mm (M) | | | 26.5 -31.5mm (L) | | |
|---|---|---|---|---|---|---|---|---|---|
| Energy targeted (kWh/t) | 0.25 | 1 | 2.5 | 0.25 | 1 | 2.5 | 0.25 | 1 | 2.5 |
| Drop weight mass required (kg) | 2.75 | 4.726 | 14.933 | 2.75 | 14.933 | 24.918 | 4.726 | 24.918 | 39.928 |
| Drop weight mass used (kg) | 2.75 | 4.726 | 14.933 | 2.75 | 14.933 | 24.918 | 4.726 | 24.918 | 39.928 |
| Height required (cm) | 26.3 | 59.7 | 47.1 | 68.8 | 50.5 | 75.2 | 85.7 | 64.4 | 99.8 |
| Height used (cm) | 26.3 | 59.7 | 47.1 | 68.8 | 50.5 | 75.2 | 85.7 | 64.4 | 99.8 |
| | | | | | | | | | |
| Measured residual gaps (mm) | 9 | 7 | 7.5 | 16 | 11 | 6 | 17 | 15 | 7 |
| | 8 | 5 | 4 | 16 | 12 | 7 | 18 | 21 | 7 |
| | 10 | 10 | 2 | 15 | 9 | 6 | 23 | 10 | 6 |
| | 7 | 8 | 3 | 16 | 14 | 7 | 21 | 13 | 6 |
| | 8 | 4 | 4 | 12 | 6 | 5 | 26 | 20 | 8 |
| | 8 | 5 | 3 | 12 | 13 | 5 | 21 | 12 | 6 |
| | 9 | 6 | 3 | 14 | 14 | 5 | 16 | 12 | 9 |
| | 10 | 5 | 4 | 16 | 7 | 7 | 15 | 13 | 7 |
| | 9 | 6 | 3.5 | 16 | 9 | 5 | 16 | 13.5 | 6 |
| | 7 | 5 | 3 | 17 | 10 | 7 | 22 | 13 | 6 |
| | | | | | | | | | |
| Average offset height (cm) | 0.85 | 0.61 | 0.37 | 1.5 | 1.05 | 0.6 | 1.95 | 1.425 | 0.68 |
| Adjusted drop height (cm) | 25.45 | 59.09 | 46.73 | 67.3 | 49.45 | 74.6 | 83.75 | 62.975 | 99.12 |
| | | | | | | | | | |
| Sample total mass (g) | 228.5 | 228.1 | 228.1 | 607.4 | 608.5 | 608.9 | 1293.7 | 1292.2 | 1293.8 |
| No of particles | 30 | 30 | 30 | 30 | 30 | 30 | 30 | 30 | 30 |
| Average particle mass (g) | 7.6 | 7.6 | 7.6 | 20.2 | 20.3 | 20.3 | 43.1 | 43.1 | 43.1 |
| | | | | | | | | | |
| Actual impact energy (kWh/t) | 0.25 | 1.00 | 2.50 | 0.25 | 0.99 | 2.49 | 0.25 | 0.99 | 2.50 |

| Particle size distributions | 13.2 -16mm (S) | | | | | | | | |
|---|---|---|---|---|---|---|---|---|---|
| **ENERGY (kWh/t)** | 0.25 | | | 1 | | | 2.5 | | |
| Size (mm) | Wt above | %retained | Cumu %passing | Wt above | %retained | Cumu %passing | Wt above | %retained | Cumu %passing |
| 13.2 | 37 | 16.3 | 83.7 | | 0.0 | 100.0 | | 0.0 | 100.0 |
| 9.5 | 83.5 | 36.7 | 47.1 | 19.2 | 8.5 | 91.5 | | 0.0 | 100.0 |
| 6.7 | 55.2 | 24.3 | 22.8 | 27.9 | 12.3 | 79.2 | 5.8 | 2.5 | 97.5 |
| 4.75 | 19.6 | 8.6 | 14.2 | 41.2 | 18.2 | 61.0 | 22 | 9.7 | 87.8 |
| 3.35 | 7.6 | 3.3 | 10.9 | 39.2 | 17.3 | 43.6 | 37.1 | 16.3 | 71.5 |
| 2.36 | 6.8 | 3.0 | 7.9 | 25.6 | 11.3 | 32.3 | 35.7 | 15.7 | 55.8 |
| 1.7 | 3.8 | 1.7 | 6.2 | 15.4 | 6.8 | 25.5 | 22.9 | 10.1 | 45.7 |
| 1.18 | 3.3 | 1.4 | 4.7 | 11.5 | 5.1 | 20.4 | 19 | 8.4 | 37.4 |
| 0.85 | 2.1 | 0.9 | 3.8 | 7.6 | 3.4 | 17.1 | 13.4 | 5.9 | 31.5 |
| 0.6 | 2.1 | 0.9 | 2.9 | 8.8 | 3.9 | 13.2 | 13.2 | 5.8 | 25.7 |
| 0.425 | 1.3 | 0.6 | 2.3 | 6.1 | 2.7 | 10.5 | 9.8 | 4.3 | 21.4 |
| 0.3 | 1.2 | 0.5 | 1.8 | 5.6 | 2.5 | 8.0 | 9.9 | 4.4 | 17.0 |
| 0.212 | 0.9 | 0.4 | 1.4 | 4.1 | 1.8 | 6.2 | 8 | 3.5 | 13.5 |
| 0.15 | 0.8 | 0.4 | 1.1 | 3.4 | 1.5 | 4.7 | 7.2 | 3.2 | 10.3 |
| 0.106 | 0.5 | 0.2 | 0.8 | 2.2 | 1.0 | 3.7 | 4.8 | 2.1 | 8.2 |
| Pan | 1.9 | 0.8 | 0.0 | 8.4 | 3.7 | 0.0 | 18.7 | 8.2 | 0.0 |
| Totals | 227.6 | 100 | | 226.2 | 100 | | 227.5 | 100 | |
| Mass discrepancy | 0.9 | | | 1.9 | | | 0.6 | | |
| | | | | | | | | | |
| t2 | | | 27.7 | | | 81.7 | | | 98.0 |
| t4 | | | 11.5 | | | 47.1 | | | 74.8 |
| t5 | | | 9.5 | | | 38.6 | | | 64.4 |
| t10 | | | 5.5 | | | 23.1 | | | 41.8 |
| P80 size | | | 12.82 | | | 6.89 | | | 4.08 |

| Particle size distributions | 19 -22.4mm (M) | | | | | | | | |
|---|---|---|---|---|---|---|---|---|---|
| **ENERGY (kWh/t)** | **0.25** | | | **1** | | | **2.5** | | |
| Size (mm) | Wt above | %retained | Cumu %passin | Wt above | %retained | Cumu %passing | Wt above | %retained | Cumu %passing |
| 19 | 86.2 | 14.2 | 85.8 | | 0.0 | 100.0 | | 0.0 | 100.0 |
| 13.2 | 265.1 | 43.8 | 42.0 | 23.6 | 3.9 | 96.1 | | 0.0 | 100.0 |
| 9.5 | 112 | 18.5 | 23.5 | 99.8 | 16.4 | 79.7 | 12.2 | 2.0 | 98.0 |
| 6.7 | 51.7 | 8.5 | 15.0 | 120.1 | 19.8 | 59.9 | 57.7 | 9.5 | 88.5 |
| 4.75 | 29.4 | 4.9 | 10.1 | 97.4 | 16.1 | 43.8 | 103.3 | 17.0 | 71.5 |
| 3.35 | 12 | 2.0 | 8.1 | 61.5 | 10.1 | 33.7 | 90 | 14.8 | 56.7 |
| 2.36 | 10.8 | 1.8 | 6.3 | 45.6 | 7.5 | 26.2 | 71.7 | 11.8 | 44.9 |
| 1.7 | 7.2 | 1.2 | 5.2 | 30.4 | 5.0 | 21.1 | 43.5 | 7.2 | 37.7 |
| 1.18 | 5.6 | 0.9 | 4.2 | 24.1 | 4.0 | 17.2 | 38.7 | 6.4 | 31.4 |
| 0.85 | 4.2 | 0.7 | 3.5 | 17 | 2.8 | 14.4 | 27.3 | 4.5 | 26.9 |
| 0.6 | 4.6 | 0.8 | 2.8 | 18 | 3.0 | 11.4 | 30.6 | 5.0 | 21.8 |
| 0.425 | 3.1 | 0.5 | 2.3 | 12.8 | 2.1 | 9.3 | 22.4 | 3.7 | 18.1 |
| 0.3 | 2.9 | 0.5 | 1.8 | 12.1 | 2.0 | 7.3 | 22.1 | 3.6 | 14.5 |
| 0.212 | 2.2 | 0.4 | 1.4 | 9.4 | 1.5 | 5.8 | 17.6 | 2.9 | 11.6 |
| 0.15 | 1.9 | 0.3 | 1.1 | 8 | 1.3 | 4.4 | 14.6 | 2.4 | 9.2 |
| Pan | 6.7 | 1.1 | 0.0 | 26.9 | 4.4 | 0.0 | 55.9 | 9.2 | 0.0 |
| Totals | 605.6 | 100 | | 606.7 | 100 | | 607.6 | 100 | |
| Mass discrepancy | 1.8 | | | 1.8 | | | 1.3 | | |
| | | | | | | | | | |
| t2 | | | 27.6 | | | 83.3 | | | 98.4 |
| t4 | | | 11.1 | | | 47.2 | | | 75.0 |
| t5 | | | 9.2 | | | 39.3 | | | 64.9 |
| t10 | | | 5.8 | | | 23.9 | | | 41.7 |
| P80 size | | | 18.24 | | | 9.58 | | | 5.73 |

| **Particle size distributions** | **26.5 -31.5mm (L)** | | | | | | | | |
|---|---|---|---|---|---|---|---|---|---|
| Size (mm) | Wt above | %retained | Cumu %passing | Wt above | %retained | Cumu %passing | Wt above | %retained | Cumu %passing |
| 26.5 | | 0.0 | 100.0 | | 0.0 | 100.0 | | 0.0 | 100.0 |
| 19 | 520.1 | 40.2 | 59.8 | 14.3 | 1.1 | 98.9 | | 0.0 | 100.0 |
| 13.2 | 335.6 | 26.0 | 33.8 | 197.3 | 15.3 | 83.6 | | 0.0 | 100.0 |
| 9.5 | 141 | 10.9 | 22.9 | 222.6 | 17.2 | 66.4 | 45.8 | 3.5 | 96.5 |
| 6.7 | 88.5 | 6.8 | 16.1 | 216 | 16.7 | 49.7 | 205.3 | 15.9 | 80.5 |
| 4.75 | 53.2 | 4.1 | 12.0 | 158.8 | 12.3 | 37.4 | 214.1 | 16.6 | 63.9 |
| 3.35 | 35.7 | 2.8 | 9.2 | 101.2 | 7.8 | 29.5 | 159.9 | 12.4 | 51.6 |
| 2.36 | 27.9 | 2.2 | 7.0 | 76.5 | 5.9 | 23.6 | 121.5 | 9.4 | 42.1 |
| 1.7 | 17.7 | 1.4 | 5.7 | 52.4 | 4.1 | 19.6 | 80.8 | 6.3 | 35.9 |
| 1.18 | 12.6 | 1.0 | 4.7 | 45.6 | 3.5 | 16.0 | 76.1 | 5.9 | 30.0 |
| 0.85 | 10.3 | 0.8 | 3.9 | 30.3 | 2.3 | 13.7 | 53.5 | 4.1 | 25.8 |
| 0.6 | 11.2 | 0.9 | 3.0 | 33.6 | 2.6 | 11.1 | 58.1 | 4.5 | 21.3 |
| 0.425 | 7.5 | 0.6 | 2.5 | 24.4 | 1.9 | 9.2 | 43.5 | 3.4 | 18.0 |
| 0.3 | 6.9 | 0.5 | 1.9 | 23.8 | 1.8 | 7.3 | 44 | 3.4 | 14.5 |
| 0.212 | 5.3 | 0.4 | 1.5 | 19 | 1.5 | 5.9 | 36.8 | 2.9 | 11.7 |
| Pan | 19.6 | 1.5 | 0.0 | 75.9 | 5.9 | 0.0 | 150.9 | 11.7 | 0.0 |
| Totals | 1293.1 | 100 | | 1291.7 | 100 | | 1290.3 | 100 | |
| Mass discrepancy | 0.6 | | | 0.5 | | | 3.5 | | |
| | | | | | | | | | |
| t2 | | | 39.4 | | | 86.9 | | | 100.0 |
| t4 | | | 17.4 | | | 52.8 | | | 83.5 |
| t5 | | | 14.1 | | | 43.9 | | | 72.7 |
| t10 | | | 8.2 | | | 26.8 | | | 47.2 |
| P80 size | | | 22.77 | | | 11.83 | | | 6.64 |

## AG 2-R: Rounded Gold ore

Energy calculations

| Size (mm) | 13.2 -16mm (S) | | | 19 -22.4mm (M) | | | 26.5 -31.5mm (L) | | |
|---|---|---|---|---|---|---|---|---|---|
| Energy targeted (kWh/t) | 0.25 | 1 | 2.5 | 0.25 | 1 | 2.5 | 0.25 | 1 | 2.5 |
| Drop weight mass required (kg) | 2.75 | 2.75 | 6.724 | 2.75 | 6.724 | 24.918 | 2.75 | 24.918 | 44.913 |
| Drop weight mass used (kg) | 2.75 | 2.75 | 6.724 | 2.75 | 6.724 | 24.918 | 2.75 | | |
| Height required (cm) | 23.5 | 91.2 | 92.4 | 68.9 | 93.2 | 75.1 | 87.5 | 66.0 | 90.9 |
| Height used (cm) | 23.5 | 91.8 | 95.0 | 57.5 | 93.2 | 62.7 | 73.9 | | |
| Measured residual gaps (mm) | 6 | 3 | 1 | 10 | 4 | 3.5 | 20 | | |
| | 9 | 2 | 1 | 10 | 5 | 3.5 | 24 | | |
| | 5 | 3 | 1 | 11 | 6 | 4.5 | 15 | | |
| | 6 | 2 | 1 | 5 | 2 | 3 | 10 | | |
| | 5 | 3 | 1 | 12 | 4 | 3 | 20 | | |
| | 5 | 4 | 2 | 12 | 3 | 2.5 | 14 | | |
| | 10 | 2 | 2 | 9 | 5 | 2.5 | 15 | | |
| | 5 | 1 | 1 | 7 | 7 | 5 | 17 | | |
| | 7 | 2 | 2 | 13 | 4 | 3.5 | 16 | | |
| | 5 | 4 | 1 | 4 | 2 | 2 | 12 | | |
| Average offset height (cm) | 0.63 | 0.26 | 0.13 | 0.93 | 0.42 | 0.33 | 1.63 | | |
| Adjusted drop height (cm) | 22.87 | 91.50976381 | 94.9156859 | 56.57 | 92.78 | 62.37 | 72.27 | | |
| Sample total mass (g) | 204.4 | 204.8 | 208 | 506.2 | 508.2 | 507 | 646.9 | | |
| No of particles | 30 | 30 | 30 | 30 | 30 | 30 | 30 | | |
| Average particle mass (g) | 6.8 | 6.8 | 6.9 | 16.9 | 16.9 | 16.9 | 21.6 | | |
| Actual impact energy (kWh/t) | 0.25 | 1.00 | 2.50 | 0.25 | 1.00 | 2.50 | 0.25 | | |

| Particle size distributions | 13.2 -16mm (S) | | | | | | | | |
|---|---|---|---|---|---|---|---|---|---|
| **ENERGY (kWh/t)** | **0.25** | | | **1** | | | **2.5** | | |
| Size (mm) | Wt above | %retained | Cumu %passing | Wt above | %retained | Cumu %passing | Wt above | %retained | Cumu %passing |
| 13.2 | 8.4 | 4.1 | 95.9 | | 0.0 | 100.0 | | 0.0 | 100.0 |
| 9.5 | 52.9 | 25.9 | 70.0 | 6 | 2.9 | 97.1 | | 0.0 | 100.0 |
| 6.7 | 62.1 | 30.4 | 39.5 | 26.5 | 13.0 | 84.1 | 0.9 | 0.4 | 99.6 |
| 4.75 | 31.4 | 15.4 | 24.2 | 36.9 | 18.1 | 65.9 | 10.6 | 5.1 | 94.4 |
| 3.35 | 10.2 | 5.0 | 19.2 | 28.4 | 13.9 | 52.0 | 17.1 | 8.3 | 86.2 |
| 2.36 | 9.4 | 4.6 | 14.6 | 26.7 | 13.1 | 38.9 | 33 | 16.0 | 70.2 |
| 1.7 | 7.1 | 3.5 | 11.1 | 17.4 | 8.5 | 30.4 | 26.9 | 13.0 | 57.2 |
| 1.18 | 5.2 | 2.5 | 8.5 | 13.9 | 6.8 | 23.6 | 22.7 | 11.0 | 46.2 |
| 0.85 | 3.7 | 1.8 | 6.7 | 9.2 | 4.5 | 19.0 | 15.8 | 7.6 | 38.6 |
| 0.6 | 3.1 | 1.5 | 5.2 | 7.8 | 3.8 | 15.2 | 13.8 | 6.7 | 31.9 |
| 0.425 | 2.3 | 1.1 | 4.1 | 6.3 | 3.1 | 12.1 | 11.4 | 5.5 | 26.4 |
| 0.3 | 2.1 | 1.0 | 3.0 | 5.7 | 2.8 | 9.3 | 10.8 | 5.2 | 21.1 |
| 0.212 | 1.6 | 0.8 | 2.3 | 4.3 | 2.1 | 7.2 | 8.6 | 4.2 | 17.0 |
| 0.15 | 1.3 | 0.6 | 1.6 | 3.9 | 1.9 | 5.3 | 8.2 | 4.0 | 13.0 |
| 0.106 | 0.9 | 0.4 | 1.2 | 2.5 | 1.2 | 4.1 | 5.7 | 2.8 | 10.3 |
| Pan | 2.4 | 1.2 | 0.0 | 8.3 | 4.1 | 0.0 | 21.2 | 10.3 | 0.0 |
| Totals | 204.1 | 100 | | 203.8 | 100 | | 206.7 | 100 | |
| Mass discrepancy | 0.3 | | | 1 | | | 1.3 | | |
| | | | | | | | | | |
| t2 | | | 45.7 | | | 86.7 | | | 99.7 |
| t4 | | | 20.2 | | | 54.8 | | | 87.8 |
| t5 | | | 17.1 | | | 46.1 | | | 79.0 |
| t10 | | | 9.9 | | | 27.1 | | | 52.0 |
| P80 size | | | 10.93 | | | 6.26 | | | 2.97 |

| Particle size distributions | 19 -22.4mm (M) | | | | | | | | |
|---|---|---|---|---|---|---|---|---|---|
| **ENERGY (kWh/t)** | 0.25 | | | 1 | | | 2.5 | | |
| Size (mm) | Wt above | %retained | Cumu %passin | Wt above | %retained | Cumu %passing | Wt above | %retained | Cumu %passing |
| 19 | 13.1 | 2.6 | 97.4 | | 0.0 | 100.0 | | 0.0 | 100.0 |
| 13.2 | 94.5 | 18.7 | 78.7 | | 0.0 | 100.0 | | 0.0 | 100.0 |
| 9.5 | 159 | 31.5 | 47.1 | 47 | 9.3 | 90.7 | 3.6 | 0.7 | 99.3 |
| 6.7 | 83.3 | 16.5 | 30.6 | 84 | 16.6 | 74.2 | 19.5 | 3.9 | 95.4 |
| 4.75 | 46.6 | 9.2 | 21.4 | 81.4 | 16.1 | 58.1 | 44.4 | 8.8 | 86.6 |
| 3.35 | 26.9 | 5.3 | 16.1 | 63.6 | 12.5 | 45.6 | 66.4 | 13.2 | 73.5 |
| 2.36 | 19.9 | 3.9 | 12.1 | 52.5 | 10.4 | 35.2 | 76.9 | 15.2 | 58.2 |
| 1.7 | 12.6 | 2.5 | 9.6 | 35.6 | 7.0 | 28.2 | 50.5 | 10.0 | 48.2 |
| 1.18 | 10.3 | 2.0 | 7.6 | 27.5 | 5.4 | 22.8 | 42.1 | 8.3 | 39.9 |
| 0.85 | 7.3 | 1.4 | 6.1 | 20.2 | 4.0 | 18.8 | 31.6 | 6.3 | 33.7 |
| 0.6 | 6.4 | 1.3 | 4.9 | 18.1 | 3.6 | 15.2 | 28.7 | 5.7 | 28.0 |
| 0.425 | 5.2 | 1.0 | 3.8 | 14.5 | 2.9 | 12.3 | 23.5 | 4.7 | 23.3 |
| 0.3 | 4.6 | 0.9 | 2.9 | 13.7 | 2.7 | 9.6 | 22.9 | 4.5 | 18.8 |
| 0.212 | 3.5 | 0.7 | 2.2 | 10.5 | 2.1 | 7.6 | 18.3 | 3.6 | 15.2 |
| 0.15 | 3.1 | 0.6 | 1.6 | 9.5 | 1.9 | 5.7 | 17.1 | 3.4 | 11.8 |
| Pan | 8.1 | 1.6 | 0.0 | 28.9 | 5.7 | 0.0 | 59.4 | 11.8 | 0.0 |
| Totals | 504.4 | 100 | | 507 | 100 | | 504.9 | 100 | |
| Mass discrepancy | 1.8 | | | 1.2 | | | 2.1 | | |
| | | | | | | | | | |
| t2 | | | 54.1 | | | 92.8 | | | 99.4 |
| t4 | | | 23.3 | | | 61.5 | | | 88.5 |
| t5 | | | 19.0 | | | 52.5 | | | 80.8 |
| t10 | | | 11.0 | | | 32.0 | | | 53.7 |
| P80 size | | | 13.61 | | | 7.69 | | | 4.04 |

| Particle size distributions | 26.5 -31.5mm (L) | | |
|---|---|---|---|
| **ENERGY (kWh/t)** | **0.25** | | |
| Size (mm) | Wt above | %retained | Cumu %passing |
| 26.5 | | 0.0 | 100.0 |
| 19 | 341.5 | 52.8 | 47.2 |
| 13.2 | 182.2 | 28.2 | 19.0 |
| 9.5 | 47.1 | 7.3 | 11.7 |
| 6.7 | 15.3 | 2.4 | 9.3 |
| 4.75 | 14.9 | 2.3 | 7.0 |
| 3.35 | 12 | 1.9 | 5.2 |
| 2.36 | 6.9 | 1.1 | 4.1 |
| 1.7 | 5.1 | 0.8 | 3.3 |
| 1.18 | 4.6 | 0.7 | 2.6 |
| 0.85 | 3.1 | 0.5 | 2.1 |
| 0.6 | 2.7 | 0.4 | 1.7 |
| 0.425 | 2.2 | 0.3 | 1.3 |
| 0.3 | 2.1 | 0.3 | 1.0 |
| 0.212 | 1.5 | 0.2 | 0.8 |
| Pan | 5.1 | 0.8 | 0.0 |
| Totals | 646.3 | 100 | |
| Mass discrepancy | 0.6 | | |
| | | | |
| t2 | | | 25.0 |
| t4 | | | 9.8 |
| t5 | | | 8.2 |
| t10 | | | 4.7 |
| P80 size | | | 23.66 |

## BLUE STONE ORE: BS1-A and BS2-R data

Energy calculations

| Size (mm) | ANGULAR 26.5 -31.5mm (L) | | | | ROUNDED 26.5 -31.5mm (L) | | | |
|---|---|---|---|---|---|---|---|---|
| Energy targeted (kWh/t) | 0.2 | 0.6 | 1.6 | 2 | 0.2 | 0.6 | 1.6 | 2 |
| Drop weight mass required (kg) | 4.998 | 14.945 | 24.928 | 34.971 | 4.998 | 14.945 | 24.928 | 34.971 |
| Drop weight mass used (kg) | 4.998 | 14.945 | 24.928 | 34.971 | 4.998 | 14.945 | 24.928 | 34.971 |
| Height required (cm) | 50.0 | 60.0 | 70 | 70.0 | 50.0 | 60.0 | 70 | 70.0 |
| Height used (cm) | 50 | 60 | 70 | 70 | 50 | 60 | 70 | 70 |
| Measured residual gaps (mm) | 15 | 8 | 7 | 4 | 16 | 7 | 7 | 2 |
| | 16 | 9 | 4 | 4 | 16 | 12 | 7 | 5 |
| | 18 | 8 | 6 | 6 | 18 | 9 | 7 | 3 |
| | 16 | 12 | 5 | 5 | 19 | 8 | 6 | 3 |
| | 17 | 9 | 6 | 6 | 15 | 8 | 5 | 3 |
| | 14 | 9 | 5 | 5 | 19 | 7 | 5 | 4 |
| | 19 | 9 | 3 | 4 | 18 | 8 | 5 | 7 |
| | 16 | 7 | 5 | 3 | 16 | 10 | 6 | 5 |
| | 14 | 5 | 6 | 3 | 12 | 9 | 6 | 4 |
| | 17 | 6 | 3 | 3 | 19 | 7 | 6 | 6 |
| Average offset height (cm) | 1.62 | 0.82 | 0.5 | 0.43 | 1.68 | 0.85 | 0.6 | 0.42 |
| Adjusted drop height (cm) | 48.38 | 59.18 | 69.5 | 69.57 | 48.32 | 59.15 | 69.4 | 69.58 |
| Sample total mass (g) | 424 | 414 | 416 | 421 | 492 | 451 | 498 | 466 |
| No of particles | 15 | 15 | 15 | 15 | 15 | 15 | 15 | 15 |
| Average particle mass (g) | 28.3 | 27.6 | 27.7 | 28.1 | 32.8 | 30.1 | 33.2 | 31.1 |
| Actual impact energy (kWh/t) | 0.23 | 0.87 | 1.70 | 2.36 | 0.20 | 0.80 | 1.42 | 2.13 |

## BS1-A- Angular Blue Stone ore

| Particle size distributions | ANGULAR 26.5 -31.5mm (L) | | | | | | | | | | | |
|---|---|---|---|---|---|---|---|---|---|---|---|---|
| ENERGY (kWh/t) | 0.2 | | | 0.6 | | | 1.6 | | | 2 | | |
| Size (mm) | Wt above | %retained | Cumu %passing | Wt above | %retained | Cumu %passing | Wt above | %retained | Cumu %passing | Wt above | %retained | Cumu %passing |
| 26.5 | 0 | 0.0 | 100.0 | 0 | 0.0 | 100.0 | 0 | 0.0 | 100.0 | 0 | 0.0 | 100.0 |
| 19 | 122.4 | 28.9 | 71.1 | 0 | 0.0 | 100.0 | 0 | 0.0 | 100.0 | 0 | 0.0 | 100.0 |
| 13.2 | 161.3 | 38.1 | 32.9 | 36.9 | 8.9 | 91.1 | 0 | 0.0 | 100.0 | 0 | 0.0 | 100.0 |
| 9.5 | 52 | 12.3 | 20.7 | 86.2 | 20.9 | 70.2 | 18.9 | 4.6 | 95.4 | 9.7 | 2.3 | 97.7 |
| 6.7 | 38.1 | 9.0 | 11.7 | 104.5 | 25.3 | 44.9 | 72.4 | 17.4 | 78.0 | 54.2 | 12.9 | 84.8 |
| 4.75 | 14.9 | 3.5 | 8.1 | 46.3 | 11.2 | 33.7 | 74.6 | 18.0 | 60.0 | 62.5 | 14.9 | 69.9 |
| 3.35 | 10.8 | 2.6 | 5.6 | 38.6 | 9.3 | 24.4 | 66.8 | 16.1 | 43.9 | 71.1 | 16.9 | 52.9 |
| 2.36 | 7.2 | 1.7 | 3.9 | 30.6 | 7.4 | 16.9 | 50.8 | 12.2 | 31.7 | 57.3 | 13.7 | 39.3 |
| 1.7 | 3.7 | 0.9 | 3.0 | 13.8 | 3.3 | 13.6 | 24.8 | 6.0 | 25.7 | 28.5 | 6.8 | 32.5 |
| 1.18 | 3.2 | 0.8 | 2.2 | 14 | 3.4 | 10.2 | 25.5 | 6.1 | 19.6 | 30.9 | 7.4 | 25.1 |
| 0.85 | 2.2 | 0.5 | 1.7 | 9.5 | 2.3 | 7.9 | 16.9 | 4.1 | 15.5 | 19.9 | 4.7 | 20.4 |
| 0.6 | 1.8 | 0.4 | 1.3 | 7.6 | 1.8 | 6.1 | 14.1 | 3.4 | 12.1 | 18 | 4.3 | 16.1 |
| 0.425 | 1 | 0.2 | 1.1 | 4.5 | 1.1 | 5.0 | 8.4 | 2.0 | 10.1 | 10.7 | 2.6 | 13.5 |
| 0.3 | 1 | 0.2 | 0.8 | 4.6 | 1.1 | 3.9 | 8.5 | 2.0 | 8.0 | 11 | 2.6 | 10.9 |
| 0.212 | 0.9 | 0.2 | 0.6 | 3.3 | 0.8 | 3.1 | 6.4 | 1.5 | 6.5 | 8.4 | 2.0 | 8.9 |
| Pan | 2.6 | 0.6 | 0.0 | 12.7 | 3.1 | 0.0 | 27 | 6.5 | 0.0 | 37.3 | 8.9 | 0.0 |
| Totals | 423.1 | 100 | | 413.1 | 100 | | 415.1 | 100 | | 419.5 | 100 | |
| Mass discrepancy | 0.9 | | | 0.9 | | | 0.9 | | | 1.5 | | |
| t2 | | | 41.1 | | | 93.0 | | | 100.0 | | | 100.0 |
| t4 | | | 13.3 | | | 49.6 | | | 81.3 | | | 87.2 |
| t5 | | | 10.0 | | | 39.6 | | | 69.5 | | | 77.7 |
| t10 | | | 4.8 | | | 20.9 | | | 38.2 | | | 46.6 |
| P80 size | | | 21.31 | | | 11.24 | | | 7.02 | | | 6.08 |

## BS2-R- Rounded Blue Stone ore

| Particle size distributions | ROUNDED 26.5 -31.5mm (L) | | | | | | | | | | | |
|---|---|---|---|---|---|---|---|---|---|---|---|---|
| ENERGY (kWh/t) | 0.2 | | | 0.6 | | | 1.6 | | | 2 | | |
| Size (mm) | Wt above | %retained | Cumu %passing | Wt above | %retained | Cumu %passing | Wt above | %retained | Cumu %passing | Wt above | %retained | Cumu %passing |
| 26.5 | 0 | 0.0 | 100.0 | 0 | 0.0 | 100.0 | 0 | 0.0 | 100.0 | 0 | 0.0 | 100.0 |
| 19 | 163.7 | 33.4 | 66.6 | 0 | 0.0 | 100.0 | 0 | 0.0 | 100.0 | 0 | 0.0 | 100.0 |
| 13.2 | 157.2 | 32.1 | 34.6 | 48.7 | 10.8 | 89.2 | 4.1 | 0.8 | 99.2 | 0 | 0.0 | 100.0 |
| 9.5 | 93 | 19.0 | 15.6 | 92 | 20.4 | 68.8 | 61.2 | 12.3 | 86.9 | 19.3 | 4.2 | 95.8 |
| 6.7 | 27.3 | 5.6 | 10.0 | 118.7 | 26.4 | 42.4 | 107.5 | 21.6 | 65.3 | 70.5 | 15.2 | 80.7 |
| 4.75 | 10.5 | 2.1 | 7.9 | 48.9 | 10.9 | 31.5 | 73.4 | 14.7 | 50.6 | 77.5 | 16.7 | 64.0 |
| 3.35 | 12.1 | 2.5 | 5.4 | 43.9 | 9.7 | 21.8 | 63.7 | 12.8 | 37.8 | 73.9 | 15.9 | 48.1 |
| 2.36 | 8.9 | 1.8 | 3.6 | 29.9 | 6.6 | 15.2 | 49.3 | 9.9 | 27.9 | 56.4 | 12.1 | 35.9 |
| 1.7 | 4 | 0.8 | 2.8 | 14.9 | 3.3 | 11.9 | 25.4 | 5.1 | 22.8 | 30.2 | 6.5 | 29.4 |
| 1.18 | 3.9 | 0.8 | 2.0 | 14.7 | 3.3 | 8.6 | 26.7 | 5.4 | 17.5 | 32.2 | 6.9 | 22.5 |
| 0.85 | 2.2 | 0.4 | 1.5 | 9.3 | 2.1 | 6.5 | 17.5 | 3.5 | 14.0 | 22.3 | 4.8 | 17.7 |
| 0.6 | 2 | 0.4 | 1.1 | 7.6 | 1.7 | 4.8 | 15.2 | 3.0 | 10.9 | 19.2 | 4.1 | 13.6 |
| 0.425 | 1.1 | 0.2 | 0.9 | 4.8 | 1.1 | 3.8 | 9.3 | 1.9 | 9.1 | 11.6 | 2.5 | 11.1 |
| 0.3 | 1.1 | 0.2 | 0.7 | 4.3 | 1.0 | 2.8 | 9.3 | 1.9 | 7.2 | 11 | 2.4 | 8.7 |
| 0.212 | 0.9 | 0.2 | 0.5 | 3 | 0.7 | 2.2 | 7 | 1.4 | 5.8 | 8 | 1.7 | 7.0 |
| Pan | 2.5 | 0.5 | 0.0 | 9.7 | 2.2 | 0.0 | 28.9 | 5.8 | 0.0 | 32.5 | 7.0 | 0.0 |
| Totals | 490.4 | 100 | | 450.4 | 100 | | 498.5 | 100 | | 464.6 | 100 | |
| Mass discrepancy | 1.6 | | | 0.6 | | | -0.5 | | | 1.4 | | |
| t2 | | | 41.5 | | | 91.5 | | | 99.4 | | | 100.0 |
| t4 | | | 11.1 | | | 47.3 | | | 69.4 | | | 83.5 |
| t5 | | | 9.0 | | | 37.3 | | | 58.4 | | | 72.8 |
| t10 | | | 4.6 | | | 18.7 | | | 33.2 | | | 42.4 |
| P80 size | | | 22.01 | | | 11.54 | | | 8.60 | | | 6.62 |

Calculated A and b parameters from standard $t_{10}$ equation $t_{10} = A\left(1 - e^{-b.E_{cs}}\right)$

| | | A | b |
|---|---|---|---|
| AG1-A | **13.2 -16mm (S)** | 64.39 | 0.75 |
| | **19 -22.4mm (M)** | 64.38 | 0.65 |
| | **26.5 -31.5mm (L)** | 64.78 | 0.76 |
| | **Size independent fit** | 64.39 | 0.71 |

| | | A | b |
|---|---|---|---|
| AG2-A | **13.2 -16mm (S)** | 60.32 | 0.49 |
| | **19 -22.4mm (M)** | 60.32 | 0.5 |
| | **26.5 -31.5mm (L)** | 60.32 | 0.56 |
| | **Size independent fit** | 60.32 | 0.51 |

| | | A | b |
|---|---|---|---|
| AG2-R | **13.2 -16mm (S)** | 76.04 | 0.46 |
| | **19 -22.4mm (M)** | 68.92 | 0.64 |
| | **26.5 -31.5mm (L)** | - | - |
| | **Size independent fit** | 69.31 | 0.57 |

| | **26.5 -31.5mm (L)** | A | b |
|---|---|---|---|
| BS1 A | Angular | 63.47 | 0.7 |
| BS2 R | Rounded | 63.44 | 0.69 |

Calculated A and b parameters from modified $t_{10}$ equation $t_{10} = A\left(1 - e^{-b(E_{cs} - E_0)}\right)$

| | | A | b | A.b | E0 |
|---|---|---|---|---|---|
| AG1-A | **13.2 -16mm (S)** | 63.27 | 0.75 | 47.5 | 0.03 |
| | **19 -22.4mm (M)** | 63.27 | 0.71 | 44.9 | 0.03 |
| | **26.5 -31.5mm (L)** | 63.47 | 0.80 | 50.8 | 0.01 |
| | **Size independent fit** | 63.27 | 0.75 | 47.7 | 0.02 |
| | | A | b | A.b | E0 |
| AG2-A | **13.2 -16mm (S)** | 62.44 | 0.48 | 30.0 | 0.04 |
| | **19 -22.4mm (M)** | 62.44 | 0.45 | 28.1 | 0.02 |
| | **26.5 -31.5mm (L)** | 62.44 | 0.53 | 33.1 | 0.00 |
| | **Size independent fit** | 56.58 | 0.60 | 33.8 | 0.05 |
| | | A | b | A.b | E0 |
| AG2-R | **13.2 -16mm (S)** | 74.85 | 0.47 | 35.2 | 0.01 |
| | **19 -22.4mm (M)** | 68.11 | 0.66 | 45.0 | 0.01 |
| | **26.5 -31.5mm (L)** | | | | |
| | **Size independent fit** | 68.48 | 0.59 | 40.4 | 0.01 |
| Blue Stone | **26.5 -31.5mm (L)** | A | b | A.b | E0 |
| | Angular | 62.26 | 0.75 | 46.7 | 0.02 |
| | Rounded | 62.26 | 0.74 | 46.1 | 0.02 |
| | Geometry independent fit | 68.48 | 0.59 | 40.4 | 0.01 |

## SHPB DATA CALCULATION- SIMPLIFIED EXAMPLE

### Calibration data (calibrate strain gauge voltage to stress by ratio K)

| Bar data | | | |
|---|---|---|---|
| Mass (kg) | 4.98 | | |
| Diameter (m) | 0.02 | C.S. Area Ab (m^2) | 0.000314 |
| Length (m) | 2 | | |
| Volume (m^3) | 0.000628 | | |
| Density (kg/m^3) | 7926 | | |
| Young's mod (E) | 1.90061E+11 | | |
| | | | |
| Pulse time (s) | 0.00039 | | |
| Strain gauge dist-Incident bar (m) | 0.95 | | |
| Pulse speed C (m/s) | 4896.9 | | |
| | | | |
| Strain Gauge dist -Transmitted bar (m) | 0.6 | | |

| Scaling factor calculation | |
|---|---|
| Bar Stress (MPa) | 145.36 |
| Vmax | 3.99 |
| K (Mpa/V) | 36.43 |
| | |
| **Theoretical K calculation** | |
| Amplifier gain | 1000 |
| Bridge factor | 2 |
| Excitation voltage | 5.02 |
| Gauge factor | 2.11 |
| K theoretical | 35.89 |
| | |
| Percentage error in K | 1.51 |

**Obtain from Calibration test with single or two bars**

| | |
|---|---|
| Initial striker velocity (m/s) | 7.895 |
| Striker CS area (m^2) | 0.0003 |
| Average maximum voltage | 3.99 |

## GENERATED DATA

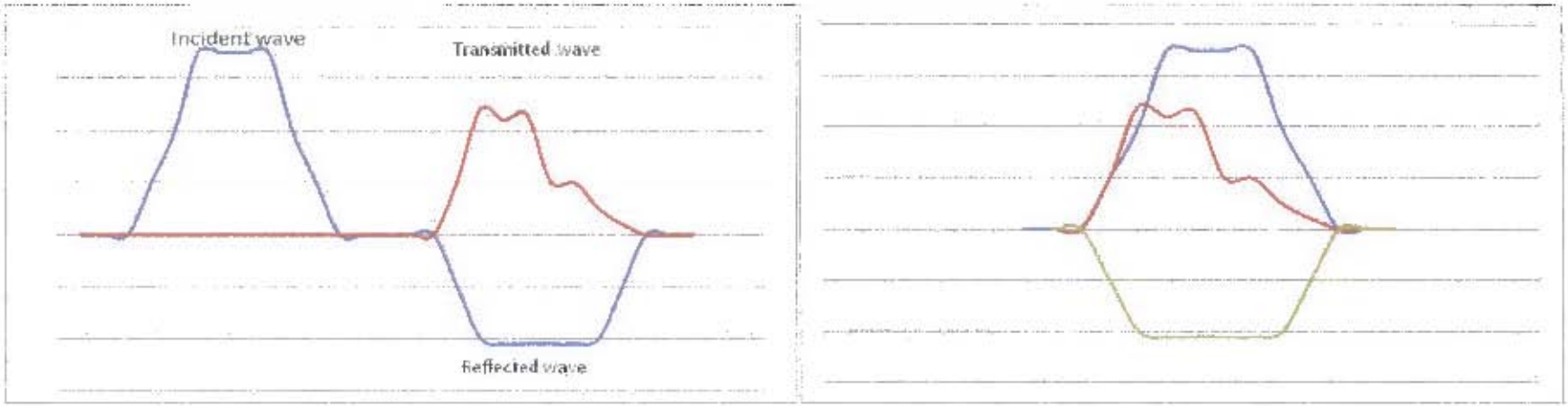


(A) (B)

**(A)**

Stress through specimen corresponds to transmitted stress wave

Point of sudden rapid decline in transmitted wave is yield stress of specimen, energy under curve to this point is particle strength

2nd kink in transmitted wave is 'work hardening' yield point of failure

**(B)**

Incident wave shifted time shifted forward by t+(bar1 strain gauge dist/pulse speed)
Reflected wave shifted back by t-(bar1 strain gauge dist/pulse speed)
Transmitted wave shifted back by t-(bar2 strain gauge dist/pulse speed)

Maximum stress in specimen = Highest value of transmitted stress wave
Maximum force transmitted to specimen = Maximum stress X Cross sectional area of HPB
Strain in specimen of known dimensions can be found by integration of instantaneous changes in length for small time steps (Eq.5.5)
Energy associated with each the waves can be found by integration of instantaneous work done for discrete time steps (Eq. 5.6)

**BS 1495 and 1496- Rounded and Angular blue stone SHPB data**

End effector comparison experiments-data

| Test name | Rock type (R or A) | Weight (g) | Energy Input (J) | Energy Input (kWh/t) | Energy absorbed (J) | Energy absorbed (kWh/t) | % Input E absorbed |
|---|---|---|---|---|---|---|---|
| Flat end eff 1 | R | 29.39 | 22.0 | 0.2079 | 9.6 | 0.0911 | 43.8 |
| Flat end eff 2 | R | 28.13 | 21.4 | 0.2112 | 7.4 | 0.0734 | 34.8 |
| Flat end eff 3 | R | 27.71 | 20.9 | 0.2096 | 8.7 | 0.0875 | 41.8 |
| Flat end eff 4 | R | 28.8 | 20.6 | 0.1988 | 9.8 | 0.0950 | 47.8 |
| Flat end eff 5 | R | 29.44 | 21.7 | 0.2047 | 9.2 | 0.0866 | 42.3 |
| Flat end eff 6 | R | 28.22 | 21.1 | 0.2075 | 9.1 | 0.0900 | 43.4 |
| Flat end eff 7 | R | 30.21 | 22.7 | 0.2086 | 11.1 | 0.1022 | 49.0 |
| Flat end eff 8 | R | 29.4 | 21.7 | 0.2046 | 10.0 | 0.0944 | 46.1 |
| Flat end eff 9 | R | 28.72 | 21.2 | 0.2049 | 8.8 | 0.0850 | 41.5 |
| Flat end eff 10 | R | 28.66 | 22.3 | 0.2162 | 10.4 | 0.1011 | 46.8 |
| | | | | | | | |
| Round end 1 | R | 29.88 | 22.95 | 0.2134 | 9.2 | 0.0856 | 40.1 |
| Round end 2 | R | 30.49 | 21.97 | 0.2002 | 9.2 | 0.0840 | 42.0 |
| Round end 3 | R | 30.37 | 22.36 | 0.2045 | 7.6 | 0.0694 | 33.9 |
| Round end 4 | R | 28.45 | 20.83 | 0.2034 | 8.6 | 0.0844 | 41.5 |
| Round end 5 | R | 29.31 | 21.62 | 0.2049 | 8.5 | 0.0810 | 39.5 |
| Round end 6 | R | 29.13 | 23 | 0.2193 | 8.2 | 0.0784 | 35.8 |
| Round end 7 | R | 30.22 | 22.38 | 0.2057 | 9.0 | 0.0829 | 40.3 |
| Round end 8 | R | 27.49 | 21.81 | 0.2204 | 8.8 | 0.0889 | 40.4 |
| Round end 9 | R | 28.76 | 21.998 | 0.2125 | 8.7 | 0.0840 | 39.6 |
| Round end 10 | R | 29.11 | 21.57 | 0.2058 | 9.2 | 0.0875 | 42.5 |

## Impulse time comparison data

300mm striker

| Test name | Rock type (R or A) | Weight (g) | Energy Input (J) | Energy Input (kWh/t) | Energy absorbed (J) | Energy absorbed (kWh/t) | % Input E absorbed |
|---|---|---|---|---|---|---|---|
| larr22-10-0.1 | R | 28.8 | 20.61 | 0.1988 | 6.05 | 0.0584 | 29.4 |
| larr22-10-0.2 | R | 30.81 | 22.02 | 0.1985 | 6.67 | 0.0601 | 30.3 |
| larr22-10-0.3 | R | 29.97 | 21.37 | 0.1981 | 4.9 | 0.0454 | 22.9 |
| larr22-10-0.4 | R | 28.94 | 20.67 | 0.1984 | 6.21 | 0.0596 | 30.0 |
| larr22-10-0.5 | R | 30.49 | 21.97 | 0.2002 | 5.16 | 0.0470 | 23.5 |
| larr22-10-0.6 | R | 28.45 | 20.83 | 0.2034 | 5.34 | 0.0521 | 25.6 |
| larr22-10-0.7 | R | 29.77 | 21.2 | 0.1978 | 7.57 | 0.0706 | 35.7 |
| larr22-10-0.8 | R | 30.42 | 21.6 | 0.1973 | 4.6 | 0.0420 | 21.3 |
| larr22-10-0.9 | R | 29.49 | 21.01 | 0.1979 | 6.45 | 0.0608 | 30.7 |
| larr22-10-0.10 | R | 29.84 | 21.23 | 0.1976 | 6.86 | 0.0639 | 32.3 |

450mm striker

| Test name | Rock type (R or A) | Weight (g) | Energy Input (J) | Energy Input (kWh/t) | Energy absorbed (J) | Energy absorbed (kWh/t) | % Input E absorbed |
|---|---|---|---|---|---|---|---|
| larr22-10-1.1 | R | 29.39 | 21.99 | 0.2079 | 9.14 | 0.0864 | 41.6 |
| larr22-10-1.2 | R | 29.11 | 21.57 | 0.2058 | 7.51 | 0.0717 | 34.8 |
| larr22-10-1.3 | R | 30.21 | 22.68 | 0.2086 | 7.49 | 0.0689 | 33.0 |
| larr22-10-1.4 | R | 28.72 | 21.18 | 0.2049 | 6.73 | 0.0651 | 31.8 |
| larr22-10-1.5 | R | 28.22 | 21.08 | 0.2075 | 5.5 | 0.0541 | 26.1 |
| larr22-10-1.6 | R | 30.22 | 22.38 | 0.2057 | 8.85 | 0.0814 | 39.5 |
| larr22-10-1.7 | R | 29.31 | 21.62 | 0.2049 | 5.95 | 0.0564 | 27.5 |
| larr22-10-1.8 | R | 30.37 | 22.36 | 0.2045 | 7.03 | 0.0643 | 31.4 |
| larr22-10-1.9 | R | 29.4 | 21.65 | 0.2046 | 6.17 | 0.0583 | 28.5 |
| larr22-10-1.10 | R | 29.44 | 21.69 | 0.2047 | 8.51 | 0.0803 | 39.2 |

600mm striker

| Test name | Rock type (R or A) | Weight (g) | Energy Input (J) | Energy Input (kWh/t) | Energy absorbed (J) | Energy absorbed (kWh/t) | % Input E absorbed |
|---|---|---|---|---|---|---|---|
| larr22-10-02.1 | R | 27.71 | 20.91 | 0.2096 | 6.2 | 0.0622 | 29.7 |
| larr22-10-02.2 | R | 27.49 | 21.81 | 0.2204 | 5.92 | 0.0598 | 27.1 |
| larr22-10-02.3 | R | 28.13 | 21.39 | 0.2112 | 5.08 | 0.0502 | 23.7 |
| larr22-10-02.4 | R | 28.36 | 23.18 | 0.2271 | 8.03 | 0.0787 | 34.6 |
| larr22-10-02.5 | R | 28.23 | 23.61 | 0.2323 | 8.9 | 0.0876 | 37.7 |
| larr22-10-02.6 | R | 29.88 | 22.95 | 0.2134 | 9.26 | 0.0861 | 40.3 |
| larr22-10-02.7 | R | 28.66 | 22.30 | 0.2162 | 8.21 | 0.0796 | 36.8 |
| larr22-10-02.8 | R | 29.13 | 23.00 | 0.2193 | 6.44 | 0.0614 | 28.0 |
| larr22-10-02.9 | R | 28.76 | 22.00 | 0.2125 | 8.87 | 0.0857 | 40.3 |
| larr22-10-02.10 | R | 28.46 | 23.43 | 0.2287 | 6.46 | 0.0631 | 27.6 |

**Specimen strength tests-Cylindrical specimens**

| | | | | | |
|---|---|---|---|---|---|
| Max stress (Mpa) | 141.6 | 135.4 | 141.4 | 136.3 | 138.4 |
| HPB abs energy (J) | 2.3 | 2.0 | 2.9 | 3.2 | 2.7 |
| Young's Modulus (GPa) | 13.9 | 27.9 | 21.6 | 18.6 | 30.2 |
| Yield Strain | 0.012 | 0.01 | 0.01 | 0.01 | 0.01 |

## Geometry comparison tests- Angular specimens

| Test no | Test name | Rock type (R or A) | Weight (g) | Energy Input (J) | Energy Input (kWh/t) | Energy absorbed (J) | Energy absorbed (kWh/t) | % Input energy absorbed |
|---|---|---|---|---|---|---|---|---|
| 1 | 17-02-33 | A | 30.45 | 20.1 | 0.1836 | 5.36 | 0.0489 | 26.6 |
| 2 | 17-02-32 | A | 30.13 | 20.2 | 0.1865 | 7.05 | 0.0650 | 34.8 |
| 3 | 15-02-17 | A | 30.27 | 20.6 | 0.1888 | 5.22 | 0.0479 | 25.4 |
| 4 | 15-02-10 | A | 29.56 | 20.2 | 0.1898 | 5.17 | 0.0486 | 25.6 |
| 5 | 15-02-11 | A | 30.1 | 20.9 | 0.1926 | 5.47 | 0.0505 | 26.2 |
| 6 | 15-02-06 | A | 30.08 | 21.1 | 0.1944 | 7.19 | 0.0664 | 34.2 |
| 7 | 15-02-35 | A | 30.18 | 21.3 | 0.1956 | 6.74 | 0.0620 | 31.7 |
| 8 | 15-02-33 | A | 30.42 | 21.6 | 0.1973 | 4.6 | 0.0420 | 21.3 |
| 9 | 17-02-34 | A | 29.84 | 21.2 | 0.1976 | 6.86 | 0.0639 | 32.3 |
| 10 | 15-02-31 | A | 29.77 | 21.2 | 0.1978 | 7.57 | 0.0706 | 35.7 |
| 11 | 17-02-31 | A | 29.49 | 21.0 | 0.1979 | 6.45 | 0.0608 | 30.7 |
| 12 | 14-02-23 | A | 29.97 | 21.4 | 0.1981 | 4.9 | 0.0454 | 22.9 |
| 13 | 14-02-26 | A | 28.94 | 20.7 | 0.1984 | 6.21 | 0.0596 | 30.0 |
| 14 | 14-02-17 | A | 30.81 | 22.0 | 0.1985 | 6.67 | 0.0601 | 30.3 |
| 15 | 14-02-13 | A | 28.8 | 20.6 | 0.1988 | 6.05 | 0.0584 | 29.4 |
| 16 | 15-02-18 | A | 30.49 | 22.0 | 0.2002 | 5.16 | 0.0470 | 23.5 |
| 17 | 15-02-30 | A | 28.45 | 20.8 | 0.2034 | 5.34 | 0.0521 | 25.6 |
| 18 | 17-02-20 | A | 30.37 | 22.4 | 0.2045 | 7.03 | 0.0643 | 31.4 |
| 19 | 17-02-36 | A | 29.4 | 21.7 | 0.2046 | 6.17 | 0.0583 | 28.5 |
| 20 | 17-02-37 | A | 29.44 | 21.7 | 0.2047 | 8.51 | 0.0803 | 39.2 |
| 21 | 15-02-19 | A | 28.72 | 21.2 | 0.2049 | 6.73 | 0.0651 | 31.8 |
| 22 | 17-02-19 | A | 29.31 | 21.6 | 0.2049 | 5.95 | 0.0564 | 27.5 |
| 23 | 17-02-14 | A | 30.22 | 22.4 | 0.2057 | 8.85 | 0.0814 | 39.5 |
| 24 | 14-02-25 | A | 29.11 | 21.6 | 0.2058 | 7.51 | 0.0717 | 34.8 |
| 25 | 15-02-34 | A | 28.22 | 21.1 | 0.2075 | 5.5 | 0.0541 | 26.1 |
| 26 | 14-02-24 | A | 29.39 | 22.0 | 0.2079 | 9.14 | 0.0864 | 41.6 |

| Test no | Test name | Rock type | Weight | Energy Input | Energy Input | Energy absorbed | Energy absorbed | % Input energy absorbed |
|---|---|---|---|---|---|---|---|---|
| 28 | 14-02-02 | A | 27.71 | 20.9 | 0.2096 | 6.2 | 0.0622 | 29.7 |
| 29 | 14-02-16 | A | 28.13 | 21.4 | 0.2112 | 5.08 | 0.0502 | 23.7 |
| 30 | 17-02-44 | A | 28.76 | 22.0 | 0.2125 | 8.87 | 0.0857 | 40.3 |
| 31 | 17-02-18 | A | 29.88 | 23.0 | 0.2134 | 9.26 | 0.0861 | 40.3 |
| 32 | 17-02-35 | A | 28.66 | 22.3 | 0.2162 | 8.21 | 0.0796 | 36.8 |
| 33 | 17-02-38 | A | 29.13 | 23.0 | 0.2193 | 6.44 | 0.0614 | 28.0 |
| 34 | 14-02-03 | A | 27.49 | 21.8 | 0.2204 | 5.92 | 0.0598 | 27.1 |
| 35 | 14-02-18 | A | 28.36 | 23.2 | 0.2271 | 8.03 | 0.0787 | 34.6 |
| 36 | 17-02-45 | A | 28.46 | 23.4 | 0.2287 | 6.46 | 0.0631 | 27.6 |
| 37 | 17-02-12 | A | 28.23 | 23.6 | 0.2323 | 8.9 | 0.0876 | 37.7 |

**Geometry comparison tests- Rounded specimens**

| Test no | Test name | Rock type (R or A) | Weight (g) | Energy Input (J) | Energy Input (kWh/t) | Energy absorbed (J) | Energy absorbed (kWh/t) | % Input energy absorbed |
|---|---|---|---|---|---|---|---|---|
| 1 | 14-02-21 | R | 29.58 | 18.5 | 0.1737 | 6.8 | 0.0638 | 36.7 |
| 2 | 14-02-07 | R | 29.91 | 20.4 | 0.1893 | 8.0 | 0.0746 | 39.4 |
| 3 | 14-02-11 | R | 30.43 | 20.9 | 0.1906 | 8.7 | 0.0796 | 41.8 |
| 4 | 15-02-09 | R | 29.71 | 20.6 | 0.1923 | 7.8 | 0.0733 | 38.1 |
| 5 | 15-02-38 | R | 28.69 | 20.0 | 0.1936 | 7.8 | 0.0757 | 39.1 |
| 6 | 17-02-10 | R | 30.72 | 21.6 | 0.1955 | 9.3 | 0.0840 | 43.0 |
| 7 | 14-02-19 | R | 29.15 | 20.7 | 0.1976 | 7.7 | 0.0729 | 36.9 |
| 8 | 14-02-12 | R | 29.4 | 20.9 | 0.1976 | 9.0 | 0.0849 | 42.9 |
| 9 | 14-02-20 | R | 30.27 | 21.6 | 0.1983 | 7.7 | 0.0704 | 35.5 |
| 10 | 15-02-26 | R | 29.85 | 21.7 | 0.2017 | 8.7 | 0.0812 | 40.3 |

| Test no | Test name | Rock type | Weight | Energy Input | Energy Input | Energy absorbed | Energy absorbed | % Input energy absorbed |
|---|---|---|---|---|---|---|---|---|
| 12 | 14-02-04 | R | 28.81 | 21.0 | 0.2021 | 9.3 | 0.0897 | 44.4 |
| 13 | 17-02-21 | R | 28.86 | 21.2 | 0.2042 | 8.7 | 0.0838 | 41.1 |
| 14 | 17-02-28 | R | 30.87 | 22.7 | 0.2043 | 10.0 | 0.0896 | 43.9 |
| 15 | 15-02-39 | R | 28.57 | 21.1 | 0.2053 | 8.8 | 0.0859 | 41.8 |
| 16 | 15-02-27 | R | 28.44 | 21.0 | 0.2055 | 8.1 | 0.0794 | 38.6 |
| 17 | 14-02-10 | R | 28.44 | 21.1 | 0.2058 | 7.7 | 0.0756 | 36.7 |
| 18 | 15-02-24 | R | 28.17 | 20.9 | 0.2059 | 8.4 | 0.0825 | 40.1 |
| 19 | 17-02-27 | R | 29.22 | 21.7 | 0.2059 | 5.4 | 0.0513 | 24.9 |
| 20 | 14-02-22 | R | 28.87 | 21.5 | 0.2069 | 9.5 | 0.0913 | 44.1 |
| 21 | 17-02-25 | R | 29.93 | 22.3 | 0.2069 | 8.8 | 0.0819 | 39.6 |
| 22 | 17-02-30 | R | 28.64 | 21.4 | 0.2073 | 8.0 | 0.0774 | 37.3 |
| 23 | 17-02-09 | R | 30.79 | 23.0 | 0.2074 | 10.9 | 0.0986 | 47.5 |
| 24 | 15-02-40 | R | 28.22 | 21.1 | 0.2076 | 8.5 | 0.0832 | 40.1 |
| 25 | 15-02-36 | R | 28.08 | 21.1 | 0.2083 | 7.7 | 0.0766 | 36.8 |
| 26 | 15-02-37 | R | 28.23 | 21.2 | 0.2085 | 8.2 | 0.0805 | 38.6 |
| 27 | 14-02-08 | R | 28.11 | 21.2 | 0.2095 | 8.5 | 0.0844 | 40.3 |
| 28 | 15-02-25 | R | 28.2 | 21.3 | 0.2100 | 8.5 | 0.0840 | 40.0 |
| 29 | 17-02-06 | R | 29.47 | 22.4 | 0.2108 | 8.8 | 0.0830 | 39.4 |
| 30 | 17-02-22 | R | 28.6 | 22.1 | 0.2150 | 8.6 | 0.0835 | 38.9 |
| 31 | 17-02-26 | R | 28.23 | 22.1 | 0.2176 | 8.6 | 0.0841 | 38.7 |
| 32 | 17-02-24 | R | 29.22 | 22.9 | 0.2179 | 8.1 | 0.0767 | 35.2 |
| 33 | 17-02-02 | R | 29.09 | 22.9 | 0.2182 | 7.9 | 0.0753 | 34.5 |
| 34 | 17-02-23 | R | 28.23 | 22.3 | 0.2190 | 9.2 | 0.0901 | 41.2 |
| 35 | 17-02-04 | R | 29.14 | 23.0 | 0.2196 | 9.2 | 0.0881 | 40.1 |
| 36 | 17-02-43 | R | 28.32 | 22.4 | 0.2201 | 9.4 | 0.0924 | 42.0 |
| 37 | 15-02-05 | R | 28.09 | 22.3 | 0.2202 | 7.6 | 0.0748 | 33.9 |

| | | | | | | | | |
|---|---|---|---|---|---|---|---|---|
| 38 | 17-02-42 | R | 28.21 | 22.4 | 0.2206 | 9.3 | 0.0916 | 41.5 |
| 39 | 17-02-05 | R | 28.14 | 22.4 | 0.2210 | 8.9 | 0.0874 | 39.5 |
| 40 | 17-02-11 | R | 28 | 22.4 | 0.2219 | 8.0 | 0.0794 | 35.8 |
| 41 | 14-02-01 | R | 29 | 23.2 | 0.2225 | 9.4 | 0.0897 | 40.3 |
| 42 | 17-02-39 | R | 28.7 | 23.0 | 0.2228 | 9.3 | 0.0899 | 40.4 |
| 43 | 17-02-01 | R | 29.09 | 23.4 | 0.2231 | 9.2 | 0.0882 | 39.6 |
| 44 | 17-02-03 | R | 30.2 | 24.6 | 0.2262 | 10.5 | 0.0961 | 42.5 |

## SHPB Incremental breakage data- BS-R

| Energy input kWh/t | Energy absorbed kWh/t | No of impacts to fracture | t2 | t5 | t10 |
|---|---|---|---|---|---|
| 0.2117 | 0.0742 | 2 | 26.08 | 2.25 | 0.39 |
| 0.2179 | 0.0813 | 2 | 2.84 | 0.92 | 0.15 |
| 0.2116 | 0.0770 | 2 | 0.48 | 0.48 | 0.18 |
| 0.3055 | 0.0988 | 3 | 0.22 | 0.22 | 0.25 |
| 0.4229 | 0.1643 | 4 | 0.54 | 0.54 | 0.54 |
| 0.6783 | 0.2410 | 5 | 13.90 | 2.26 | 1.30 |
| 0.5474 | 0.1799 | 5 | 10.26 | 1.40 | 0.94 |
| 0.8771 | 0.3196 | 8 | 14.12 | 0.07 | 0.07 |
| 0.7843 | 0.2405 | 9 | 2.00 | 2.00 | 0.40 |
| 1.0583 | 0.3829 | 10 | 2.38 | 0.97 | 0.46 |
| 1.3375 | 0.4784 | 11 | 22.88 | 1.51 | 0.88 |
| 1.2852 | 0.4758 | 12 | 14.71 | 0.36 | 0.16 |

## Particle size distributions of blue stone- Single impact breakage data - Angular specimens

| Test name | 14-02-02 | 14-02-03 | 14-02-13 | 14-02-16 | 14-02-17 | 14-02-18 | 14-02-23 | 14-02-24 | 14-02-26 | 15-02-06 | 15-02-10 |
|---|---|---|---|---|---|---|---|---|---|---|---|
| Specimen type | A | A | A | A | A | A | A | A | A | A | A |
| Weight (g) | 27.71 | 27.49 | 28.8 | 28.13 | 30.81 | 28.36 | 29.97 | 29.39 | 28.94 | 30.08 | 29.56 |
| Input Energy (J) | 20.91 | 21.81 | 20.61 | 21.39 | 22.02 | 23.18 | 21.37 | 21.99 | 20.67 | 21.05 | 20.2 |
| Input Energy(kWh/t) | 0.2096 | 0.2204 | 0.1988 | 0.2112 | 0.1985 | 0.2271 | 0.1981 | 0.2079 | 0.1984 | 0.1944 | 0.1898 |
| Absorbed Energy Energy (J) | 6.2 | 5.92 | 6.05 | 5.08 | 6.67 | 8.03 | 4.9 | 9.14 | 6.21 | 7.19 | 5.17 |
| Absorbed Energy(kWh/t) | 0.0622 | 0.0598 | 0.0584 | 0.0502 | 0.0601 | 0.0787 | 0.0454 | 0.0864 | 0.0596 | 0.0664 | 0.0486 |
| % energy absorbed | 29.7 | 27.1 | 29.4 | 23.7 | 30.3 | 34.6 | 22.9 | 41.6 | 30.0 | 34.2 | 25.6 |
| **Size fractions (mm)** | | | | | | | | | | | |
| **22.4** | 0 | 0 | 0 | 18.29 | 0 | 0 | 25.69 | 0 | 15.63 | 0 | 15.51 |
| **16** | 14.04 | 17.11 | 16.5 | 5.31 | 26.55 | 26.11 | 2.2 | 14.51 | 7 | 29.73 | 9.62 |
| **11.2** | 11.25 | 9.2 | 10.4 | 4.2 | 3.62 | 0 | 1.03 | 13.52 | 2.29 | 0 | 1.89 |
| **8** | 1.74 | 1 | 0.5 | 0 | 0.33 | 1.15 | 0.54 | 0.69 | 2.68 | 0 | 0.72 |
| **5.6** | 0 | 0 | 0 | 0 | 0.09 | 0.45 | 0.1 | 0 | 0.94 | 0 | 1.05 |
| **4** | 0 | 0.12 | 0.17 | 0 | 0 | 0.07 | 0 | 0 | 0.1 | 0 | 0.22 |
| **2.8** | 0.017 | 0.1 | 0.04 | 0 | 0.11 | 0.13 | 0 | 0.2 | 0.11 | 0.03 | 0.1 |
| **2** | 0 | 0.1 | 0.1 | 0.1 | 0 | 0.04 | 0 | 0.02 | 0.11 | 0.01 | 0.02 |
| **1.4** | 0.02 | 0 | 0 | 0 | 0.08 | 0.04 | 0.05 | 0 | 0.03 | 0.02 | 0 |
| **1** | 0.03 | 0 | 0.03 | 0.02 | 0.06 | 0.02 | 0 | 0 | 0.02 | 0 | 0.01 |
| **-1** | 0.03 | 0.04 | 0.09 | 0.08 | 0.06 | 0.1 | 0.12 | 0.1 | 0.11 | 0.02 | 0.1 |
| Total mass recovered | 27.1 | 27.7 | 27.8 | 28.0 | 30.9 | 28.1 | 29.7 | 29.0 | 29.0 | 29.8 | 29.2 |
| Mass discrepancy | 0.6 | -0.2 | 1.0 | 0.1 | -0.1 | 0.3 | 0.2 | 0.3 | -0.1 | 0.3 | 0.3 |

| Test name | 15-02-11 | 15-02-12 | 15-02-18 | 15-02-19 | 15-02-30 | 15-02-31 | 15-02-33 | 15-02-34 | 15-02-35 | 17-02-12 | 17-02-14 |
|---|---|---|---|---|---|---|---|---|---|---|---|
| Specimen type | A | A | A | A | A | A | A | A | A | A | A |
| Weight (g) | 30.1 | 30.21 | 30.49 | 28.72 | 28.45 | 29.77 | 30.42 | 28.22 | 30.18 | 28.23 | 30.22 |
| Input Energy (J) | 20.87 | 22.68 | 21.97 | 21.18 | 20.83 | 21.2 | 21.6 | 21.08 | 21.25 | 23.61 | 22.38 |
| Input Energy(kWh/t) | 0.1926 | 0.2086 | 0.2002 | 0.2049 | 0.2034 | 0.1978 | 0.1973 | 0.2075 | 0.1956 | 0.2323 | 0.2057 |
| Absorbed Energy Energy (J) | 5.47 | 7.49 | 5.16 | 6.73 | 5.34 | 7.57 | 4.6 | 5.5 | 6.74 | 8.9 | 8.85 |
| Absorbed Energy(kWh/t) | 0.0505 | 0.0689 | 0.0470 | 0.0651 | 0.0521 | 0.0706 | 0.0420 | 0.0541 | 0.0620 | 0.0876 | 0.0814 |
| % energy absorbed | 26.2 | 33.0 | 23.5 | 31.8 | 25.6 | 35.7 | 21.3 | 26.1 | 31.7 | 37.7 | 39.5 |
| **Size fractions (mm)** | | | | | | | | | | | |
| **22.4** | 0 | 14.51 | 18.1 | 27.69 | 0 | 12.64 | 0 | 0 | 0 | 0 | 0 |
| **16** | 27.37 | 15.53 | 7.98 | 0 | 28.22 | 13.83 | 24.95 | 28.07 | 29.69 | 9.78 | 11.08 |
| **11.2** | 0 | 0 | 2.39 | 0 | 0 | 2.02 | 3.56 | 0 | 0 | 12.35 | 15.26 |
| **8** | 1.81 | 0 | 0.93 | 0 | 0 | 0.1 | 1.17 | 0 | 0 | 3.83 | 2.24 |
| **5.6** | 0.43 | 0 | 0 | 0 | 0 | 0.38 | 0.09 | 0 | 0 | 0.7 | 0.52 |
| **4** | 0.15 | 0 | 0.03 | 0.4 | 0 | 0 | 0.06 | 0 | 0.23 | 0.34 | 0.39 |
| **2.8** | 0.09 | 0.11 | 0.04 | 0.08 | 0.04 | 0.28 | 0.14 | 0 | 0.04 | 0.48 | 0.2 |
| **2** | 0 | 0 | 0 | 0.04 | 0 | 0.06 | 0.02 | 0.03 | 0.03 | 0.12 | 0.1 |
| **1.4** | 0.01 | 0 | 0.03 | 0.03 | 0 | 0.07 | 0.05 | 0.06 | 0 | 0.15 | 0.17 |
| **1** | 0 | 0 | 0.02 | 0 | 0.03 | 0.04 | 0.03 | 0.01 | 0 | 0.04 | 0.11 |
| **-1** | 0.08 | 0.02 | 0.05 | 0.04 | 0.06 | 0.13 | 0.08 | 0.03 | 0.01 | 0.03 | 0.21 |
| Total mass recovered | 29.9 | 30.2 | 29.6 | 28.3 | 28.4 | 29.6 | 30.2 | 28.2 | 30.0 | 27.8 | 30.3 |
| Mass discrepancy | 0.2 | 0.0 | 0.9 | 0.4 | 0.1 | 0.2 | 0.3 | 0.0 | 0.2 | 0.4 | -0.1 |

| Test name | 17-02-18 | 17-02-19 | 17-02-20 | 17-02-31 | 17-02-32 | 17-02-33 | 17-02-34 | 17-02-35 | 17-02-36 | 17-02-37 | 17-02-44 | 17-02-45 |
|---|---|---|---|---|---|---|---|---|---|---|---|---|
| Specimen type | A | A | A | A | A | A | A | A | A | A | A | A |
| Weight (g) | 29.88 | 29.31 | 30.37 | 29.49 | 30.13 | 30.45 | 29.84 | 28.66 | 29.4 | 29.44 | 28.76 | 28.46 |
| Input Energy (J) | 22.95 | 21.62 | 22.36 | 21.01 | 20.23 | 20.13 | 21.23 | 22.3 | 21.65 | 21.69 | 21.998 | 23.43 |
| Input Energy(kWh/t) | 0.2134 | 0.2049 | 0.2045 | 0.1979 | 0.1865 | 0.1836 | 0.1976 | 0.2162 | 0.2046 | 0.2047 | 0.2125 | 0.2287 |
| Absorbed Energy Energy (J) | 9.26 | 5.95 | 7.03 | 6.45 | 7.05 | 5.36 | 6.86 | 8.21 | 6.17 | 8.51 | 8.87 | 6.46 |
| Absorbed Energy(kWh/t) | 0.0861 | 0.0564 | 0.0643 | 0.0608 | 0.0650 | 0.0489 | 0.0639 | 0.0796 | 0.0583 | 0.0803 | 0.0857 | 0.0631 |
| % energy absorbed | 40.3 | 27.5 | 31.4 | 30.7 | 34.8 | 26.6 | 32.3 | 36.8 | 28.5 | 39.2 | 40.3 | 27.6 |
| **Size fractions (mm)** | | | | | | | | | | | | |
| **22.4** | 0 | 0 | 0 | 0 | 17.03 | 0 | 25.01 | 0 | 0 | 0 | 0 | 0 |
| **16** | 18.54 | 29.2 | 26.62 | 28.77 | 10.92 | 29.9 | 0 | 27.34 | 24.98 | 22.88 | 26.9 | 7.21 |
| **11.2** | 6.94 | 0 | 1.83 | 0 | 0 | 0 | 3.32 | 0 | 1.98 | 5.55 | 0.57 | 19.89 |
| **8** | 1.98 | 0 | 1.13 | 0.32 | 1.64 | 0 | 0.55 | 0 | 1.85 | 0 | 0.74 | 0 |
| **5.6** | 1.2 | 0 | 0.17 | 0.1 | 0 | 0 | 0.1 | 0.67 | 0.34 | 0.38 | 0 | 0 |
| **4** | 0.32 | 0 | 0.21 | 0.13 | 0.02 | 0.09 | 0.32 | 0.25 | 0 | 0.39 | 0.25 | 0.51 |
| **2.8** | 0.09 | 0.01 | 0 | 0 | 0.13 | 0.04 | 0.1 | 0.04 | 0.05 | 0.1 | 0 | 0.19 |
| **2** | 0.01 | 0.03 | 0 | 0.01 | 0.03 | 0.14 | 0.01 | 0.05 | 0.03 | 0.03 | 0 | 0.15 |
| **1.4** | 0.01 | 0 | 0.03 | 0 | 0.03 | 0.08 | 0 | 0.04 | 0.04 | 0 | 0 | 0.13 |
| **1** | 0 | 0 | 0 | 0 | 0 | 0.03 | 0 | 0.04 | 0.03 | 0 | 0 | 0 |
| **-1** | 0.1 | 0.01 | 0.06 | 0.03 | 0.09 | 0.01 | 0.09 | 0.04 | 0.01 | 0.01 | 0.03 | 0.09 |
| Total mass recovered | 29.2 | 29.3 | 30.1 | 29.4 | 29.9 | 30.3 | 29.5 | 28.5 | 29.3 | 29.3 | 28.5 | 28.2 |
| Mass discrepancy | 0.7 | 0.1 | 0.3 | 0.1 | 0.2 | 0.2 | 0.3 | 0.2 | 0.1 | 0.1 | 0.3 | 0.3 |

## Particle size distributions of blue stone- Single impact breakage data - Rounded specimens

| Test name | 17-02-27 | 14-02-21 | 14-02-20 | 14-02-19 | 15-02-09 | 14-02-07 | 15-02-05 | 17-02-02 | 14-02-10 | 15-02-38 | 15-02-36 | 17-02-24 |
|---|---|---|---|---|---|---|---|---|---|---|---|---|
| Specimen type | R | R | R | R | R | R | R | R | R | R | R | R |
| Weight (g) | 29.22 | 29.58 | 30.27 | 29.15 | 29.71 | 29.91 | 28.09 | 29.09 | 28.44 | 28.69 | 28.08 | 29.22 |
| Input Energy (J) | 21.66 | 18.5 | 21.61 | 20.73 | 20.57 | 20.38 | 22.27 | 22.85 | 21.07 | 19.99 | 21.05 | 22.92 |
| Input Energy(kWh/t) | 0.2059 | 0.1737 | 0.1983 | 0.1976 | 0.1923 | 0.1893 | 0.2202 | 0.2182 | 0.2058 | 0.1936 | 0.2083 | 0.2179 |
| Absorbed Energy (J) | 5.4 | 6.79 | 7.67 | 7.65 | 7.84 | 8.03 | 7.56 | 7.88 | 7.74 | 7.82 | 7.74 | 8.07 |
| Absorbed Energy(kWh/t) | 0.0513 | 0.0638 | 0.0704 | 0.0729 | 0.0733 | 0.0746 | 0.0748 | 0.0753 | 0.0756 | 0.0757 | 0.0766 | 0.0767 |
| % energy absorbed | 24.9 | 36.7 | 35.5 | 36.9 | 38.1 | 39.4 | 33.9 | 34.5 | 36.7 | 39.1 | 36.8 | 35.2 |
| **Size fractions (mm)** | | | | | | | | | | | | |
| **22.4** | 0 | 0 | 0 | 0 | 0 | 0 | 0 | 0 | 0 | 0 | 0 | 0 |
| **16** | 24.85 | 28.43 | 9.28 | 25.16 | 14.49 | 11.32 | 14.37 | 18.6 | 27.26 | 22.61 | 27.37 | 28.18 |
| **11.2** | 3.97 | 0 | 19.22 | 3.14 | 14.33 | 17.2 | 12.44 | 9.83 | 0 | 5.01 | 0 | 2.63 |
| **8** | 0 | 0.54 | 0.73 | 0 | 0 | 0 | 0.48 | 0 | 0 | 0 | 0 | 0 |
| **5.6** | 0 | 0.22 | 0.17 | 0.28 | 0.61 | 0.6 | 0.35 | 0 | 0.17 | 0.3 | 0 | 0 |
| **4** | 0 | 0.04 | 0.43 | 0 | 0 | 0.13 | 0.04 | 0 | 0.29 | 0.26 | 0 | 0 |
| **2.8** | 0.12 | 0.12 | 0.06 | 0.11 | 0 | 0.17 | 0 | 0.22 | 0.18 | 0.13 | 0.31 | 0 |
| **2** | 0.06 | 0.06 | 0 | 0.09 | 0 | 0.07 | 0.08 | 0 | 0.05 | 0.08 | 0 | 0 |
| **1.4** | 0 | 0 | 0.03 | 0.07 | 0 | 0.05 | 0 | 0 | 0 | 0 | 0.02 | 0 |
| **1** | 0 | 0.05 | 0.03 | 0 | 0.01 | 0.05 | 0 | 0 | 0 | 0 | 0.02 | 0.01 |
| **-1** | 0.03 | 0.07 | 0.11 | 0.13 | 0.04 | 0.11 | 0.1 | 0.09 | 0.04 | 0.1 | 0.05 | 0 |
| Total mass recovered | 29.0 | 29.5 | 30.1 | 29.0 | 29.5 | 29.7 | 27.9 | 28.7 | 28.0 | 28.5 | 27.8 | 30.8 |
| Mass discrepancy | 0.2 | 0.1 | 0.2 | 0.2 | 0.2 | 0.2 | 0.2 | 0.4 | 0.4 | 0.2 | 0.3 | -1.6 |

| Test name | 17-02-30 | 17-02-11 | 17-02-29 | 15-02-27 | 14-02-11 | 15-02-37 | 15-02-26 | 17-02-25 | 15-02-24 | 17-02-06 | 15-02-40 | 17-02-22 |
|---|---|---|---|---|---|---|---|---|---|---|---|---|
| Specimen type | R | R | R | R | R | R | R | R | R | R | R | R |
| Weight (g) | 28.64 | 28 | 30.03 | 28.44 | 30.43 | 28.23 | 29.85 | 29.93 | 28.17 | 29.47 | 28.22 | 28.6 |
| Input Energy (J) | 21.37 | 22.37 | 21.84 | 21.04 | 20.88 | 21.19 | 21.67 | 22.29 | 20.88 | 22.36 | 21.09 | 22.13 |
| Input Energy(kWh/t) | 0.2073 | 0.2219 | 0.2020 | 0.2055 | 0.1906 | 0.2085 | 0.2017 | 0.2069 | 0.2059 | 0.2108 | 0.2076 | 0.2150 |
| Absorbed Energy (J) | 7.98 | 8 | 8.58 | 8.13 | 8.72 | 8.18 | 8.73 | 8.82 | 8.37 | 8.8 | 8.45 | 8.6 |
| Absorbed Energy(kWh/t) | 0.0774 | 0.0794 | 0.0794 | 0.0794 | 0.0796 | 0.0805 | 0.0812 | 0.0819 | 0.0825 | 0.0830 | 0.0832 | 0.0835 |
| % energy absorbed | 37.3 | 35.8 | 39.3 | 38.6 | 41.8 | 38.6 | 40.3 | 39.6 | 40.1 | 39.4 | 40.1 | 38.9 |
| **Size fractions (mm)** | | | | | | | | | | | | |
| **22.4** | 0 | 0 | 0 | 0 | 0 | 0 | 0 | 0 | 0 | 0 | 0 | 0 |
| **16** | 19.81 | 27.3 | 25.42 | 14.83 | 15.96 | 15.87 | 25.89 | 28.63 | 11.41 | 22.33 | 22.53 | 22.14 |
| **11.2** | 8.45 | 0 | 0 | 11.89 | 13.99 | 11.68 | 0 | 0 | 16.04 | 6.37 | 2.7 | 5.56 |
| **8** | 0.1 | 0 | 3.52 | 0 | 0 | 0 | 2.1 | 0.39 | 0 | 0 | 1.05 | 0.5 |
| **5.6** | 0 | 0.43 | 0.2 | 0.64 | 0 | 0 | 1.16 | 0.1 | 0.16 | 0.3 | 0.8 | 0 |
| **4** | 0.03 | 0.1 | 0.32 | 0.25 | 0.11 | 0 | 0 | 0.18 | 0 | 0.08 | 0.06 | 0 |
| **2.8** | 0 | 0 | 0.11 | 0.2 | 0.08 | 0.1 | 0.18 | 0.11 | 0.03 | 0.03 | 0.43 | 0.04 |
| **2** | 0 | 0 | 0.03 | 0.08 | 0.06 | 0.06 | 0.08 | 0.05 | 0 | 0.03 | 0.16 | 0 |
| **1.4** | 0 | 0 | 0.05 | 0.02 | 0.04 | 0.07 | 0 | 0 | 0 | 0.02 | 0.06 | 0.05 |
| **1** | 0 | 0 | 0.05 | 0.02 | 0.05 | 0.01 | 0.05 | 0.04 | 0 | 0.02 | 0.06 | 0 |
| **-1** | 0.02 | 0.05 | 0 | 0.12 | 0.07 | 0.05 | 0.09 | 0.13 | 0.03 | 0.07 | 0.12 | 0.11 |
| Total mass recovered | 28.4 | 27.9 | 29.7 | 28.1 | 30.4 | 27.8 | 29.6 | 29.6 | 27.7 | 29.3 | 28.0 | 28.4 |
| Mass discrepancy | 0.2 | 0.1 | 0.3 | 0.4 | 0.1 | 0.4 | 0.3 | 0.3 | 0.5 | 0.2 | 0.3 | 0.2 |

| Test name | 17-02-21 | 17-02-10 | 15-02-25 | 17-02-26 | 14-02-08 | 14-02-12 | 15-02-39 | 17-02-05 | 17-02-04 | 17-02-01 | 17-02-28 | 14-02-01 |
|---|---|---|---|---|---|---|---|---|---|---|---|---|
| Specimen type | R | R | R | R | R | R | R | R | R | R | R | R |
| Weight (g) | 28.86 | 30.72 | 28.2 | 28.23 | 28.11 | 29.4 | 28.57 | 28.14 | 29.14 | 29.09 | 30.87 | 29 |
| Input Energy (J) | 21.21 | 21.62 | 21.32 | 22.11 | 21.2 | 20.91 | 21.11 | 22.39 | 23.04 | 23.36 | 22.7 | 23.23 |
| Input Energy(kWh/t) | 0.2042 | 0.1955 | 0.2100 | 0.2176 | 0.2095 | 0.1976 | 0.2053 | 0.2210 | 0.2196 | 0.2231 | 0.2043 | 0.2225 |
| Absorbed Energy (J) | 8.71 | 9.29 | 8.53 | 8.55 | 8.54 | 8.98 | 8.83 | 8.85 | 9.24 | 9.24 | 9.96 | 9.36 |
| Absorbed Energy(kWh/t) | 0.0838 | 0.0840 | 0.0840 | 0.0841 | 0.0844 | 0.0849 | 0.0859 | 0.0874 | 0.0881 | 0.0882 | 0.0896 | 0.0897 |
| % energy absorbed | 41.1 | 43.0 | 40.0 | 38.7 | 40.3 | 42.9 | 41.8 | 39.5 | 40.1 | 39.6 | 43.9 | 40.3 |
| **Size fractions (mm)** | | | | | | | | | | | | |
| **22.4** | | 0 | 0 | 0 | 0 | 24.19 | 0 | 0 | 0 | 0 | 0 | 0 |
| **16** | | 30.48 | 23.34 | 26.52 | 27.82 | 3.9 | 19.83 | 17.66 | 20.59 | 25.05 | 30.2 | 9.29 |
| **11.2** | | 0 | 3.78 | 0 | 0 | 0 | 7.35 | 10.54 | 7.42 | 4.27 | 0 | 14.78 |
| **8** | | 0 | 0 | 0 | 0 | 0 | 0 | 0 | 0 | 0 | 0 | 2.91 |
| **5.6** | | 0 | 0.24 | 0.123 | 0 | 0.72 | 0.66 | 0.23 | 0.38 | 0 | 0 | 0.58 |
| **4** | | 0 | 0.2 | 0.12 | 0.03 | 0.14 | 0.19 | 0 | 0.21 | 0.06 | 0 | 0.53 |
| **2.8** | | 0.06 | 0.17 | 0.07 | 0 | 0.05 | 0.24 | 0.09 | 0.07 | 0.06 | 0.26 | 0.47 |
| **2** | | 0.02 | 0 | 0 | 0 | 0.05 | 0.05 | 0 | 0.07 | 0.02 | 0.06 | 0.07 |
| **1.4** | | 0.03 | 0.02 | 0 | 0.02 | 0.05 | 0.02 | 0.01 | 0 | 0.01 | 0 | 0.03 |
| **1** | | 0 | 0 | 0 | 0 | 0 | 0.02 | 0 | 0 | 0 | 0 | 0 |
| **-1** | | 0.05 | 0.07 | 0.07 | 0.06 | 0.14 | 0.01 | 0.05 | 0.12 | 0.07 | 0.03 | 0.05 |
| Total mass recovered | 0.0 | 30.6 | 27.8 | 26.9 | 27.9 | 29.2 | 28.4 | 28.6 | 28.9 | 29.5 | 30.6 | 28.7 |
| Mass discrepancy | 28.9 | 0.1 | 0.4 | 1.3 | 0.2 | 0.2 | 0.2 | -0.4 | 0.3 | -0.4 | 0.3 | 0.3 |

| Test name | 14-02-04 | 17-02-39 | 17-02-23 | 14-02-22 | 17-02-42 | 17-02-43 | 17-02-03 | 17-02-09 |
|---|---|---|---|---|---|---|---|---|
| Specimen type | R | R | R | R | R | R | R | R |
| Weight (g) | 28.81 | 28.7 | 28.23 | 28.87 | 28.21 | 28.32 | 30.2 | 30.79 |
| Input Energy (J) | 20.96 | 23.02 | 22.25 | 21.5 | 22.4 | 22.44 | 24.59 | 22.99 |
| Input Energy(kWh/t) | 0.2021 | 0.2228 | 0.2190 | 0.2069 | 0.2206 | 0.2201 | 0.2262 | 0.2074 |
| Absorbed Energy (J) | 9.3 | 9.29 | 9.16 | 9.49 | 9.3 | 9.42 | 10.45 | 10.93 |
| Absorbed Energy(kWh/t) | 0.0897 | 0.0899 | 0.0901 | 0.0913 | 0.0916 | 0.0924 | 0.0961 | 0.0986 |
| % energy absorbed | 44.4 | 40.4 | 41.2 | 44.1 | 41.5 | 42.0 | 42.5 | 47.5 |
| **Size fractions (mm)** | | | | | | | | |
| **22.4** | 0 | 0 | 0 | 0 | 0 | 0 | 0 | 0 |
| **16** | 16.75 | 9.78 | 0 | 28.21 | 21.99 | 17.62 | 12.72 | 27.7 |
| **11.2** | 10.25 | 16.86 | 27.51 | 0 | 5.86 | 9.23 | 12.29 | 0 |
| **8** | 0.29 | 0 | 0 | 0 | 0 | 0 | 2.46 | 0.75 |
| **5.6** | 0.62 | 0.88 | 0 | 0 | 0 | 0.43 | 0.95 | 0.69 |
| **4** | 0.19 | 0.15 | 0.24 | 0.34 | 0.49 | 0.19 | 0.77 | 0.39 |
| **2.8** | 0.2 | 0.16 | 0.16 | 0.04 | 0.04 | 0.37 | 0.31 | 0.06 |
| **2** | 0.09 | 0.12 | 0.06 | 0 | 0.03 | 0.03 | 0.08 | 0.11 |
| **1.4** | 0 | 0.04 | 0.04 | 0.04 | 0.07 | 0.04 | 0.14 | 0.06 |
| **1** | 0 | 0.1 | 0.02 | 0.04 | 0.06 | 0.04 | 0.04 | 0.03 |
| **-1** | 0.17 | 0.25 | 0.03 | 0.08 | 0.05 | 0.16 | 0.24 | 0.15 |
| Total mass recovered | 28.6 | 28.3 | 28.1 | 28.8 | 28.6 | 28.1 | 30.0 | 29.9 |
| Mass discrepancy | 0.2 | 0.4 | 0.2 | 0.1 | -0.4 | 0.2 | 0.2 | 0.9 |

## Particle size distributions of blue stone- Incremental breakage data - Rounded specimens

| Rock type | (R or A) | rou | rou | rou | rou | rou | rou | rou | rou | rou | rou | rou | rou |
|---|---|---|---|---|---|---|---|---|---|---|---|---|---|
| Weight | (g) | 26.83 | 27.4 | 27.48 | 27.74 | 25.82 | 25.26 | 26.56 | 26.99 | 26.25 | 27.48 | 27.55 | 27.53 |
| Energy Inp | (J) | 65.51 | 77.36 | 30.22 | 105.67 | 19.68 | 116.86 | 20.84 | 85.21 | 51.72 | 20.93 | 41.93 | 132.54 |
| Energy Inp | (kWh/t) | 0.6783 | 0.7843 | 0.3055 | 1.0583 | 0.2117 | 1.2852 | 0.2179 | 0.8771 | 0.5474 | 0.2116 | 0.4229 | 1.3375 |
| Energy abs | (J) | 23.27 | 23.72 | 9.77 | 38.23 | 6.90 | 43.26 | 7.78 | 31.05 | 17.00 | 7.62 | 16.29 | 47.41 |
| Energy abs | (kWh/t) | 0.2410 | 0.2405 | 0.0988 | 0.3829 | 0.0742 | 0.4758 | 0.0813 | 0.3196 | 0.1799 | 0.0770 | 0.1643 | 0.4784 |
| % Input energy absorb | | 35.5 | 30.7 | 32.3 | 36.2 | 35.1 | 37.0 | 37.3 | 36.4 | 32.9 | 36.4 | 38.8 | 35.8 |
| No hits to breakage | | 5 | 9 | 3 | 10 | 2 | 12 | 2 | 8 | 5 | 2 | 4 | 11 |
| PSD data | **31.5** | 0 | 0 | 0 | 0 | 0 | 0 | 0 | 0 | 0 | 0 | 0 | 0 |
| | **22.4** | 0 | 0 | 0 | 0 | 0 | 0 | 0 | 0 | 0 | 0 | 0 | 0 |
| | **16** | 21.53 | 26.5 | 27.27 | 25.03 | 17.53 | 19.85 | 25.69 | 21.38 | 22.99 | 27.15 | 27.4 | 19.36 |
| | **11.2** | 4.38 | 0 | 0 | 0 | 5.04 | 5.1 | 0 | 5.33 | 2.71 | 0 | 0 | 5.97 |
| | **8** | 0 | 0 | 0 | 0 | 2.58 | 0 | 0 | 0 | 0.44 | 0 | 0 | 1.51 |
| | **5.6** | 0 | 0 | 0 | 0.4 | 0 | 0 | 0.56 | 0 | 0 | 0 | 0 | 0.15 |
| | **4** | 0.16 | 0.2 | 0 | 0.05 | 0.34 | 0 | 0.15 | 0 | 0.08 | 0 | 0 | 0.12 |
| | **2.8** | 0.11 | 0.24 | 0 | 0.05 | 0.14 | 0.05 | 0 | 0 | 0.05 | 0.08 | 0 | 0.05 |
| | **2** | 0.1 | 0.05 | 0.06 | 0.06 | 0 | 0 | 0 | 0 | 0.06 | 0 | 0 | 0.07 |
| | **1.4** | 0.07 | 0.01 | 0 | 0.01 | 0 | 0 | 0.02 | 0 | 0 | 0 | 0 | 0 |
| | **-1.4** | 0.07 | 0.02 | 0 | 0 | 0 | 0 | 0 | 0 | 0 | 0 | 0.1 | 0.05 |
| | | 0.09 | 0.02 | 0 | 0.04 | 0.1 | 0.04 | 0.02 | 0.02 | 0.18 | 0.05 | 0.05 | 0.11 |
| | **Total mas** | 26.51 | 27.04 | 27.33 | 25.64 | 25.73 | 25.04 | 26.44 | 26.73 | 26.51 | 27.28 | 27.55 | 27.39 |
| | **Mass disc** | 0.32 | 0.36 | 0.15 | 2.1 | 0.09 | 0.22 | 0.12 | 0.26 | -0.26 | 0.2 | 0 | 0.14 |

# RBT SINGLE IMPACT BREAKAGE DATA

## AG1-A: Angular Gold ore

Energy calculations

| Size (mm) | 13.2 -16mm (S) | | | 19 -22.4mm (M) | | | 26.5 -31.5mm (L) | | |
|---|---|---|---|---|---|---|---|---|---|
| Energy targeted (kWh/t) | 0.25 | 1 | 2.5 | 0.25 | 1 | 2.5 | 0.25 | 1 | 2.5 |
| Calibrated RPM required | 1357 | 2641 | 4103 | 1357 | 2641 | 4103 | 1357 | 2641 | 4103 |
| RPM Used | | 2641 | 4103 | | 2641 | 4103 | | 2641 | 4103 |
| | | | | | | | | | |
| Sample total mass (g) | | 138.9 | 146.6 | | 406.8 | 446.2 | | 1300.5 | 965.3 |
| No of particles | | 30 | 30 | | 30 | 30 | | 30 | 30 |
| Average particle mass (g) | | 4.6 | 4.9 | | 13.6 | 14.9 | | 43.4 | 32.2 |
| | | | | | | | | | |
| Actual impact energy (kWh/t) | | 1.03 | 2.49 | | 1.03 | 2.49 | | 1.03 | 2.49 |

| Particle size distributions | 13.2 -16mm (S) | | | | | | | | |
|---|---|---|---|---|---|---|---|---|---|
| ENERGY (kWh/t) | 0.25 | | | 1 | | | 2.5 | | |
| Size (mm) | Wt above | %retained | Cumu %passing | Wt above | %retained | Cumu %passing | Wt above | %retained | Cumu %passing |
| 13.2 | | | | 10.2 | 7.4 | 92.6 | 0 | 0.0 | 100.0 |
| 9.5 | | | | 10.4 | 7.5 | 85.1 | 2.6 | 1.8 | 98.2 |
| 6.7 | | | | 13.5 | 9.7 | 75.4 | 0.7 | 0.5 | 97.8 |
| 4.75 | | | | 13.9 | 10.0 | 65.4 | 5.7 | 3.9 | 93.9 |
| 3.35 | | | | 11.9 | 8.6 | 56.8 | 9.3 | 6.3 | 87.5 |
| 2.36 | | | | 14 | 10.1 | 46.7 | 12.4 | 8.5 | 79.1 |
| 1.7 | | | | 11 | 7.9 | 38.8 | 12 | 8.2 | 70.9 |
| 1.18 | | | | 9.9 | 7.1 | 31.7 | 13.4 | 9.1 | 61.8 |
| 0.85 | | | | 7 | 5.0 | 26.6 | 11.1 | 7.6 | 54.2 |
| 0.6 | | | | 7.9 | 5.7 | 20.9 | 13.3 | 9.1 | 45.1 |
| 0.425 | | | | 5.5 | 4.0 | 16.9 | 10.2 | 7.0 | 38.2 |
| 0.3 | | | | 5.2 | 3.7 | 13.2 | 10.8 | 7.4 | 30.8 |
| 0.212 | | | | 4.2 | 3.0 | 10.2 | 9.4 | 6.4 | 24.4 |
| 0.15 | | | | 3.5 | 2.5 | 7.6 | 8.9 | 6.1 | 18.3 |
| 0.106 | | | | 2.4 | 1.7 | 5.9 | 6.3 | 4.3 | 14.0 |
| Pan | | | | 8.2 | 5.9 | 0.0 | 20.6 | 14.0 | 0.0 |
| Totals | | | | 138.7 | 100 | | 146.7 | 100 | |
| Mass discrepancy | | | | 0.2 | | | -0.1 | | |
| | | | | | | | | | |
| t2 | | | | | | 77.4 | | | 97.8 |
| t4 | | | | | | 58.5 | | | 88.8 |
| t5 | | | | | | 52.3 | | | 83.7 |
| t10 | | | | | | 35.4 | | | 66.6 |
| P80 size | | | | | | 8.02 | | | 2.47 |

| Particle size distributions | 19 -22.4mm (M) | | | | | | | | |
|---|---|---|---|---|---|---|---|---|---|
| **ENERGY (kWh/t)** | **0.25** | | | **1** | | | **2.5** | | |
| Size (mm) | Wt above | %retained | Cumu %passing | Wt above | %retained | Cumu %passing | Wt above | %retained | Cumu %passing |
| 19 | | | | 0 | 0.0 | 100.0 | 0 | 0.0 | 100.0 |
| 13.2 | | | | 9.6 | 2.4 | 97.6 | 29.1 | 6.6 | 93.4 |
| 9.5 | | | | 26.9 | 6.6 | 91.0 | 9.2 | 2.1 | 91.4 |
| 6.7 | | | | 51.3 | 12.6 | 78.4 | 22 | 5.0 | 86.4 |
| 4.75 | | | | 51 | 12.5 | 65.9 | 33.6 | 7.6 | 78.9 |
| 3.35 | | | | 41.9 | 10.3 | 55.5 | 35.4 | 8.0 | 70.9 |
| 2.36 | | | | 40.5 | 10.0 | 45.6 | 37.3 | 8.4 | 62.5 |
| 1.7 | | | | 29.2 | 7.2 | 38.4 | 29.8 | 6.7 | 55.8 |
| 1.18 | | | | 28.7 | 7.1 | 31.3 | 33.2 | 7.5 | 48.3 |
| 0.85 | | | | 20.2 | 5.0 | 26.4 | 24.5 | 5.5 | 42.8 |
| 0.6 | | | | 23.7 | 5.8 | 20.5 | 31.8 | 7.2 | 35.6 |
| 0.425 | | | | 16.4 | 4.0 | 16.5 | 24.6 | 5.5 | 30.1 |
| 0.3 | | | | 16.1 | 4.0 | 12.5 | 26.3 | 5.9 | 24.2 |
| 0.212 | | | | 12.3 | 3.0 | 9.5 | 22.4 | 5.0 | 19.1 |
| 0.15 | | | | 10.4 | 2.6 | 7.0 | 20.7 | 4.7 | 14.5 |
| Pan | | | | 28.3 | 7.0 | 0.0 | 64.2 | 14.5 | 0.0 |
| Totals | | | | 406.5 | 100 | | 444.1 | 100 | |
| Mass discrepancy | | | | 0.3 | | | 2.1 | | |
| | | | | | | | | | |
| t2 | | | | | | 92.5 | | | 91.8 |
| t4 | | | | | | 68.5 | | | 80.4 |
| t5 | | | | | | 61.3 | | | 75.3 |
| t10 | | | | | | 42.4 | | | 59.5 |
| P80 size | | | | | | 7.05 | | | 5.04 |

| Particle size distributions | 26.5 -31.5mm (L) | | | | | | | | |
|---|---|---|---|---|---|---|---|---|---|
| **ENERGY (kWh/t)** | **0.25** | | | **1** | | | **2.5** | | |
| Size (mm) | Wt above | %retained | Cumu %passing | Wt above | %retained | Cumu %passing | Wt above | %retained | Cumu %passing |
| 26.5 | | | | 38.7 | 3.0 | 97.0 | 30.3 | 3.1 | 96.9 |
| 19 | | | | 122.2 | 9.4 | 87.6 | 12.3 | 1.3 | 95.6 |
| 13.2 | | | | 167.5 | 12.9 | 74.7 | 54.3 | 5.6 | 89.9 |
| 9.5 | | | | 132.7 | 10.2 | 64.5 | 46.7 | 4.8 | 85.1 |
| 6.7 | | | | 119.6 | 9.2 | 55.3 | 68.8 | 7.1 | 78.0 |
| 4.75 | | | | 126.4 | 9.7 | 45.6 | 83.8 | 8.7 | 69.3 |
| 3.35 | | | | 93.7 | 7.2 | 38.4 | 67.3 | 7.0 | 62.3 |
| 2.36 | | | | 84.8 | 6.5 | 31.9 | 73.6 | 7.6 | 54.6 |
| 1.7 | | | | 62.8 | 4.8 | 27.1 | 58.8 | 6.1 | 48.5 |
| 1.18 | | | | 60.9 | 4.7 | 22.4 | 63 | 6.5 | 42.0 |
| 0.85 | | | | 43.2 | 3.3 | 19.0 | 47.2 | 4.9 | 37.1 |
| 0.6 | | | | 50.7 | 3.9 | 15.1 | 59.3 | 6.2 | 30.9 |
| 0.425 | | | | 35.7 | 2.7 | 12.4 | 44.9 | 4.7 | 26.3 |
| 0.3 | | | | 36.1 | 2.8 | 9.6 | 48 | 5.0 | 21.3 |
| 0.212 | | | | 28.4 | 2.2 | 7.4 | 41.7 | 4.3 | 17.0 |
| Pan | | | | 96.7 | 7.4 | 0.0 | 163.6 | 17.0 | 0.0 |
| Totals | | | | 1300.1 | 100 | | 963.6 | 100 | |
| Mass discrepancy | | | | 0.4 | | | 1.7 | | |
| | | | | | | | | | |
| t2 | | | | | | 77.5 | | | 91.2 |
| t4 | | | | | | 57.1 | | | 79.3 |
| t5 | | | | | | 50.7 | | | 73.8 |
| t10 | | | | | | 35.4 | | | 58.7 |
| P80 size | | | | | | 15.57 | | | 7.50 |

**AG2-1396: Angular Gold ore**

## AG1-R: Rounded Gold ore

Energy calculations

| Size (mm) | 13.2 -16mm (S) | | | 19 -22.4mm (M) | | | 26.5 -31.5mm (L) | | |
|---|---|---|---|---|---|---|---|---|---|
| Energy targeted (kWh/t) | 0.25 | 1 | 2.5 | 0.25 | 1 | 2.5 | 0.25 | 1 | 2.5 |
| Calibrated RPM required | 1357 | 2641 | 4103 | 1357 | 2641 | 4103 | 1357 | 2641 | 4103 |
| RPM Used | 1357 | 2641 | 4103 | 1357 | 2641 | 4103 | 1357 | 2641 | 4103 |
| Sample total mass (g) | | 165.9 | 161.4 | | 406.8 | 446.2 | | 1300.5 | 965.3 |
| No of particles | | 30 | 30 | | 30 | 30 | | 30 | 30 |
| Average particle mass (g) | | 5.5 | 5.4 | | 13.6 | 14.9 | | 43.4 | 32.2 |
| Actual impact energy (kWh/t) | | 1.03 | 2.49 | | 1.03 | 2.49 | | 1.03 | 2.49 |

| Particle size distributions | 13.2 -16mm (S) | | | | | | | | |
|---|---|---|---|---|---|---|---|---|---|
| ENERGY (kWh/t) | 0.25 | | | 1 | | | 2.5 | | |
| Size (mm) | Wt above | %retained | Cumu %passing | Wt above | %retained | Cumu %passing | Wt above | %retained | Cumu %passing |
| 13.2 | | | | 0 | 0.0 | 100.0 | 0 | 0.0 | 100.0 |
| 9.5 | | | | 5.3 | 3.2 | 96.8 | 10.5 | 6.5 | 93.5 |
| 6.7 | | | | 19.2 | 11.6 | 85.2 | 4.1 | 2.5 | 90.9 |
| 4.75 | | | | 26.4 | 15.9 | 69.3 | 5.4 | 3.4 | 87.6 |
| 3.35 | | | | 21.6 | 13.0 | 56.2 | 10.3 | 6.4 | 81.2 |
| 2.36 | | | | 19.5 | 11.8 | 44.5 | 14.2 | 8.8 | 72.3 |
| 1.7 | | | | 13.3 | 8.0 | 36.5 | 12.3 | 7.6 | 64.7 |
| 1.18 | | | | 11.3 | 6.8 | 29.6 | 14 | 8.7 | 56.0 |
| 0.85 | | | | 7.2 | 4.3 | 25.3 | 10.3 | 6.4 | 49.6 |
| 0.6 | | | | 9 | 5.4 | 19.9 | 12.7 | 7.9 | 41.7 |
| 0.425 | | | | 6.3 | 3.8 | 16.1 | 9.9 | 6.2 | 35.6 |
| 0.3 | | | | 6.1 | 3.7 | 12.4 | 10.6 | 6.6 | 29.0 |
| 0.212 | | | | 4.9 | 3.0 | 9.4 | 9.2 | 5.7 | 23.2 |
| 0.15 | | | | 4.2 | 2.5 | 6.9 | 9 | 5.6 | 17.7 |
| 0.106 | | | | 3 | 1.8 | 5.1 | 6.8 | 4.2 | 13.4 |
| Pan | | | | 8.4 | 5.1 | 0.0 | 21.6 | 13.4 | 0.0 |
| Totals | | | | 165.7 | 100 | | 160.9 | 100 | |
| Mass discrepancy | | | | 0.2 | | | 0.5 | | |
| | | | | | | | | | |
| t2 | | | | | | 87.6 | | | 91.4 |
| t4 | | | | | | 58.9 | | | 82.5 |
| t5 | | | | | | 51.0 | | | 77.2 |
| t10 | | | | | | 33.2 | | | 60.6 |
| P80 size | | | | | | 6.06 | | | 3.22 |

| Particle size distributions | 19 -22.4mm (M) | | | | | | | | |
|---|---|---|---|---|---|---|---|---|---|
| **ENERGY (kWh/t)** | **0.25** | | | **1** | | | **2.5** | | |
| Size (mm) | Wt above | %retained | Cumu %passing | Wt above | %retained | Cumu %passing | Wt above | %retained | Cumu %passing |
| 19 | | | | 0 | 0.0 | 100.0 | 0 | 0.0 | 100.0 |
| 13.2 | | | | 9.6 | 2.4 | 97.6 | 29.1 | 6.6 | 93.4 |
| 9.5 | | | | 26.9 | 6.6 | 91.0 | 9.2 | 2.1 | 91.4 |
| 6.7 | | | | 51.3 | 12.6 | 78.4 | 22 | 5.0 | 86.4 |
| 4.75 | | | | 51 | 12.5 | 65.9 | 33.6 | 7.6 | 78.9 |
| 3.35 | | | | 41.9 | 10.3 | 55.5 | 35.4 | 8.0 | 70.9 |
| 2.36 | | | | 40.5 | 10.0 | 45.6 | 37.3 | 8.4 | 62.5 |
| 1.7 | | | | 29.2 | 7.2 | 38.4 | 29.8 | 6.7 | 55.8 |
| 1.18 | | | | 28.7 | 7.1 | 31.3 | 33.2 | 7.5 | 48.3 |
| 0.85 | | | | 20.2 | 5.0 | 26.4 | 24.5 | 5.5 | 42.8 |
| 0.6 | | | | 23.7 | 5.8 | 20.5 | 31.8 | 7.2 | 35.6 |
| 0.425 | | | | 16.4 | 4.0 | 16.5 | 24.6 | 5.5 | 30.1 |
| 0.3 | | | | 16.1 | 4.0 | 12.5 | 26.3 | 5.9 | 24.2 |
| 0.212 | | | | 12.3 | 3.0 | 9.5 | 22.4 | 5.0 | 19.1 |
| 0.15 | | | | 10.4 | 2.6 | 7.0 | 20.7 | 4.7 | 14.5 |
| Pan | | | | 28.3 | 7.0 | 0.0 | 64.2 | 14.5 | 0.0 |
| Totals | | | | 406.5 | 100 | | 444.1 | 100 | |
| Mass discrepancy | | | | 0.3 | | | 2.1 | | |
| | | | | | | | | | |
| t2 | | | | | | 92.5 | | | 91.8 |
| t4 | | | | | | 68.5 | | | 80.4 |
| t5 | | | | | | 61.3 | | | 75.3 |
| t10 | | | | | | 42.4 | | | 59.5 |
| P80 size | | | | | | 7.05 | | | 5.04 |

| Particle size distributions | 26.5 -31.5mm (L) | | | | | | | | |
|---|---|---|---|---|---|---|---|---|---|
| **ENERGY (kWh/t)** | 0.25 | | | 1 | | | 2.5 | | |
| Size (mm) | Wt above | %retained | Cumu %passing | Wt above | %retained | Cumu %passing | Wt above | %retained | Cumu %passing |
| 26.5 | | | | 38.7 | 3.0 | 97.0 | 30.3 | 3.1 | 96.9 |
| 19 | | | | 122.2 | 9.4 | 87.6 | 12.3 | 1.3 | 95.6 |
| 13.2 | | | | 167.5 | 12.9 | 74.7 | 54.3 | 5.6 | 89.9 |
| 9.5 | | | | 132.7 | 10.2 | 64.5 | 46.7 | 4.8 | 85.1 |
| 6.7 | | | | 119.6 | 9.2 | 55.3 | 68.8 | 7.1 | 78.0 |
| 4.75 | | | | 126.4 | 9.7 | 45.6 | 83.8 | 8.7 | 69.3 |
| 3.35 | | | | 93.7 | 7.2 | 38.4 | 67.3 | 7.0 | 62.3 |
| 2.36 | | | | 84.8 | 6.5 | 31.9 | 73.6 | 7.6 | 54.6 |
| 1.7 | | | | 62.8 | 4.8 | 27.1 | 58.8 | 6.1 | 48.5 |
| 1.18 | | | | 60.9 | 4.7 | 22.4 | 63 | 6.5 | 42.0 |
| 0.85 | | | | 43.2 | 3.3 | 19.0 | 47.2 | 4.9 | 37.1 |
| 0.6 | | | | 50.7 | 3.9 | 15.1 | 59.3 | 6.2 | 30.9 |
| 0.425 | | | | 35.7 | 2.7 | 12.4 | 44.9 | 4.7 | 26.3 |
| 0.3 | | | | 36.1 | 2.8 | 9.6 | 48 | 5.0 | 21.3 |
| 0.212 | | | | 28.4 | 2.2 | 7.4 | 41.7 | 4.3 | 17.0 |
| Pan | | | | 96.7 | 7.4 | 0.0 | 163.6 | 17.0 | 0.0 |
| Totals | | | | 1300.1 | 100 | | 963.6 | 100 | |
| Mass discrepancy | | | | 0.4 | | | 1.7 | | |
| | | | | | | | | | |
| t2 | | | | | | 77.5 | | | 91.2 |
| t4 | | | | | | 57.1 | | | 79.3 |
| t5 | | | | | | 50.7 | | | 73.8 |
| t10 | | | | | | 35.4 | | | 58.7 |
| P80 size | | | | | | 15.57 | | | 7.50 |

**AG3-1397: Angular Gold ore**

**AG2-A: Angular Gold ore**
Energy calculations

| Size (mm) | 13.2 -16mm (S) | | | 19 -22.4mm (M) | | | 26.5 -31.5mm (L) | | |
|---|---|---|---|---|---|---|---|---|---|
| Energy targeted (kWh/t) | 0.25 | 1 | 2.5 | 0.25 | 1 | 2.5 | 0.25 | 1 | 2.5 |
| Calibrated RPM required | 1357 | 2641 | 4103 | 1357 | 2641 | 4103 | 1357 | 2641 | 4103 |
| RPM Used | | 2641 | 4103 | | | | | 2641 | 4103 |
| | | | | | | | | | |
| Sample total mass (g) | | 140.4 | 163.2 | | | | | 980.7 | 963.1 |
| No of particles | | 30 | 30 | | | | | 30 | 30 |
| Average particle mass (g) | | 4.7 | 5.4 | | | | | 32.7 | 32.1 |
| | | | | | | | | | |
| Actual impact energy (kWh/t) | | 1.03 | 2.49 | | | | | 1.03 | 2.49 |

| Particle size distributions | 13.2 -16mm (S) | | | | | | | | |
|---|---|---|---|---|---|---|---|---|---|
| **ENERGY (kWh/t)** | 0.25 | | | 1 | | | 2.5 | | |
| Size (mm) | Wt above | %retained | Cumu %passing | Wt above | | | Wt above | | |
| 13.2 | | | | 17.6 | 12.5 | 87.5 | 0 | 0.0 | 100.0 |
| 9.5 | | | | 7.5 | 5.3 | 82.1 | 0 | 0.0 | 100.0 |
| 6.7 | | | | 13.5 | 9.6 | 72.5 | 9.7 | 6.0 | 94.0 |
| 4.75 | | | | 19.7 | 14.0 | 58.5 | 22.2 | 13.7 | 80.4 |
| 3.35 | | | | 14.7 | 10.5 | 48.0 | 13.3 | 8.2 | 72.2 |
| 2.36 | | | | 12.8 | 9.1 | 38.9 | 15.1 | 9.3 | 62.9 |
| 1.7 | | | | 10.9 | 7.8 | 31.1 | 11.3 | 7.0 | 55.9 |
| 1.18 | | | | 9.3 | 6.6 | 24.5 | 10.8 | 6.6 | 49.3 |
| 0.85 | | | | 5.4 | 3.8 | 20.7 | 9.6 | 5.9 | 43.4 |
| 0.6 | | | | 6.3 | 4.5 | 16.2 | 11.9 | 7.3 | 36.1 |
| 0.425 | | | | 4.3 | 3.1 | 13.1 | 8.7 | 5.4 | 30.7 |
| 0.3 | | | | 4.2 | 3.0 | 10.1 | 9.1 | 5.6 | 25.1 |
| 0.212 | | | | 3.3 | 2.4 | 7.8 | 7.7 | 4.7 | 20.4 |
| 0.15 | | | | 2.7 | 1.9 | 5.8 | 7 | 4.3 | 16.1 |
| 0.106 | | | | 1.8 | 1.3 | 4.6 | 5.3 | 3.3 | 12.8 |
| Pan | | | | 6.4 | 4.6 | 0.0 | 20.8 | 12.8 | 0.0 |
| Totals | | | | 140.4 | 100 | | 162.5 | 100 | |
| Mass discrepancy | | | | 0 | | | 0.7 | | |
| | | | | | | | | | |
| t2 | | | | | | 74.5 | | | 95.2 |
| t4 | | | | | | 50.1 | | | 73.8 |
| t5 | | | | | | 43.9 | | | 68.0 |
| t10 | | | | | | 28.0 | | | 52.8 |
| P80 size | | | | | | 8.88 | | | 4.69 |

| Particle size distributions | 26.5 -31.5mm (L) | | | | | | | | |
|---|---|---|---|---|---|---|---|---|---|
| ENERGY (kWh/t) | 0.25 | | | 1 | | | 2.5 | | |
| Size (mm) | Wt above | %retained | Cumu %passing | Wt above | | | Wt above | | |
| 26.5 | | | | 0 | 0.0 | 100.0 | 0 | 0.0 | 100.0 |
| 19 | | | | 58.2 | 5.9 | 94.1 | 38.5 | 4.0 | 96.0 |
| 13.2 | | | | 171.2 | 17.5 | 76.6 | 40.7 | 4.2 | 91.8 |
| 9.5 | | | | 103.6 | 10.6 | 66.0 | 27.8 | 2.9 | 88.9 |
| 6.7 | | | | 119.9 | 12.2 | 53.8 | 60.8 | 6.3 | 82.5 |
| 4.75 | | | | 103.7 | 10.6 | 43.2 | 84 | 8.7 | 73.8 |
| 3.35 | | | | 73.1 | 7.5 | 35.8 | 81.1 | 8.4 | 65.4 |
| 2.36 | | | | 63.9 | 6.5 | 29.3 | 82.5 | 8.6 | 56.8 |
| 1.7 | | | | 48.1 | 4.9 | 24.4 | 64.2 | 6.7 | 50.1 |
| 1.18 | | | | 41.3 | 4.2 | 20.1 | 70.1 | 7.3 | 42.8 |
| 0.85 | | | | 31 | 3.2 | 17.0 | 52.8 | 5.5 | 37.3 |
| 0.6 | | | | 34.9 | 3.6 | 13.4 | 62.4 | 6.5 | 30.8 |
| 0.425 | | | | 24.2 | 2.5 | 11.0 | 48.7 | 5.1 | 25.8 |
| 0.3 | | | | 23.9 | 2.4 | 8.5 | 51.6 | 5.4 | 20.4 |
| 0.212 | | | | 19.2 | 2.0 | 6.6 | 42.8 | 4.5 | 15.9 |
| Pan | | | | 64.3 | 6.6 | 0.0 | 153.2 | 15.9 | 0.0 |
| Totals | | | | 980.5 | 100 | | 961.2 | 100 | |
| Mass discrepancy | | | | 0.2 | | | 1.9 | | |
| t2 | | | | | | 80.4 | | | 92.7 |
| t4 | | | | | | 56.1 | | | 83.7 |
| t5 | | | | | | 48.8 | | | 78.4 |
| t10 | | | | | | 32.7 | | | 61.4 |
| P80 size | | | | | | 14.33 | | | 6.13 |

**AG4-1372: Angular Gold ore**

**AG2-R: Rounded Gold ore**
Energy calculations

| Size (mm) | 13.2 -16mm (S) | | | 19 -22.4mm (M) | | | 26.5 -31.5mm (L) | | |
|---|---|---|---|---|---|---|---|---|---|
| Energy targeted (kWh/t) | 0.25 | 1 | 2.5 | 0.25 | 1 | 2.5 | 0.25 | 1 | 2.5 |
| Calibrated RPM required | 1357 | 2641 | 4103 | 1357 | 2641 | 4103 | 1357 | 2641 | 4103 |
| RPM Used | 1357 | 2641 | 4103 | 1357 | 2641 | 4103 | 1357 | 2641 | 4103 |
| | | | | | | | | | |
| Sample total mass (g) | | 184.9 | 190.6 | | 493.5 | 656.1 | 2964.6 | | |
| No of particles | | 30 | 30 | | 30 | 30 | 30 | | |
| Average particle mass (g) | | 6.2 | 6.4 | | 16.5 | 21.9 | 98.8 | | |
| | | | | | | | | | |
| Actual impact energy (kWh/t) | | 1.03 | 2.49 | | 1.03 | 2.49 | 0.27 | | |

| Particle size distributions | 13.2 -16mm (S) | | | | | | | | |
|---|---|---|---|---|---|---|---|---|---|
| **ENERGY (kWh/t)** | 0.25 | | | 1 | | | 2.5 | | |
| Size (mm) | Wt above | %retained | Cumu %passing | Wt above | %retained | Cumu %passing | Wt above | %retained | Cumu %passing |
| 13.2 | | | | 0 | 0.0 | 100.0 | 0 | 0.0 | 100.0 |
| 9.5 | | | | 10.2 | 5.5 | 94.5 | 0 | 0.0 | 100.0 |
| 6.7 | | | | 17.7 | 9.6 | 84.8 | 5.3 | 2.8 | 97.2 |
| 4.75 | | | | 23.3 | 12.7 | 72.2 | 14.2 | 7.5 | 89.7 |
| 3.35 | | | | 22.1 | 12.0 | 60.2 | 15.1 | 8.0 | 81.7 |
| 2.36 | | | | 22.3 | 12.1 | 48.1 | 20.5 | 10.8 | 70.8 |
| 1.7 | | | | 15 | 8.1 | 39.9 | 15.8 | 8.4 | 62.5 |
| 1.18 | | | | 13.1 | 7.1 | 32.8 | 15.6 | 8.3 | 54.2 |
| 0.85 | | | | 7.8 | 4.2 | 28.6 | 11.9 | 6.3 | 47.9 |
| 0.6 | | | | 10.9 | 5.9 | 22.7 | 14.9 | 7.9 | 40.1 |
| 0.425 | | | | 7.6 | 4.1 | 18.5 | 11.2 | 5.9 | 34.1 |
| 0.3 | | | | 7.4 | 4.0 | 14.5 | 11.8 | 6.2 | 27.9 |
| 0.212 | | | | 5.9 | 3.2 | 11.3 | 10.3 | 5.4 | 22.4 |
| 0.15 | | | | 5.2 | 2.8 | 8.5 | 9.5 | 5.0 | 17.4 |
| 0.106 | | | | 3.6 | 2.0 | 6.5 | 7 | 3.7 | 13.7 |
| Pan | | | | 12 | 6.5 | 0.0 | 25.9 | 13.7 | 0.0 |
| Totals | | | | 184.1 | 100 | | 189 | 100 | |
| Mass discrepancy | | | | 0.8 | | | 1.6 | | |
| | | | | | | | | | |
| t2 | | | | | | 86.8 | | | 97.8 |
| t4 | | | | | | 62.6 | | | 83.3 |
| t5 | | | | | | 54.8 | | | 76.8 |
| t10 | | | | | | 36.5 | | | 58.6 |
| P80 size | | | | | | 5.95 | | | 3.20 |

| Particle size distributions | 19 -22.4mm (M) | | | | | | | | |
|---|---|---|---|---|---|---|---|---|---|
| **ENERGY (kWh/t)** | **0.25** | | | **1** | | | **2.5** | | |
| Size (mm) | Wt above | %retained | Cumu %passing | Wt above | %retained | Cumu %passing | Wt above | %retained | Cumu %passing |
| 19 | | | | 0 | 0.0 | 100.0 | 0 | 0.0 | 100.0 |
| 13.2 | | | | 17.2 | 3.5 | 96.5 | 3.4 | 0.5 | 99.5 |
| 9.5 | | | | 59.7 | 12.1 | 84.4 | 9.8 | 1.5 | 98.0 |
| 6.7 | | | | 52.6 | 10.7 | 73.7 | 29.9 | 4.6 | 93.4 |
| 4.75 | | | | 65.5 | 13.3 | 60.4 | 47.2 | 7.2 | 86.2 |
| 3.35 | | | | 51.5 | 10.4 | 50.0 | 56.8 | 8.7 | 77.5 |
| 2.36 | | | | 46.4 | 9.4 | 40.6 | 61.9 | 9.5 | 68.1 |
| 1.7 | | | | 32.4 | 6.6 | 34.0 | 49.5 | 7.6 | 60.5 |
| 1.18 | | | | 29.5 | 6.0 | 28.0 | 53.9 | 8.2 | 52.3 |
| 0.85 | | | | 21.3 | 4.3 | 23.7 | 40.7 | 6.2 | 46.1 |
| 0.6 | | | | 22.9 | 4.6 | 19.1 | 48.2 | 7.4 | 38.7 |
| 0.425 | | | | 16.7 | 3.4 | 15.7 | 36.8 | 5.6 | 33.1 |
| 0.3 | | | | 17.1 | 3.5 | 12.2 | 40 | 6.1 | 27.0 |
| 0.212 | | | | 14 | 2.8 | 9.4 | 35 | 5.3 | 21.6 |
| 0.15 | | | | 12.2 | 2.5 | 6.9 | 33.1 | 5.1 | 16.5 |
| Pan | | | | 33.9 | 6.9 | 0.0 | 108.3 | 16.5 | 0.0 |
| Totals | | | | 492.9 | 100 | | 654.5 | 100 | |
| Mass discrepancy | | | | 0.6 | | | 1.6 | | |
| | | | | | | | | | |
| t2 | | | | | | 87.1 | | | 98.3 |
| t4 | | | | | | 63.2 | | | 87.7 |
| t5 | | | | | | 55.8 | | | 82.3 |
| t10 | | | | | | 37.6 | | | 64.7 |
| P80 size | | | | | | 8.35 | | | 3.75 |

| Particle size distributions | 26.5 -31.5mm (L) | | |
|---|---|---|---|
| **ENERGY (kWh/t)** | **0.25** | | |
| Size (mm) | Wt above | %retained | Cumu %passing |
| 26.5 | 0 | 0.0 | 100.0 |
| 19 | 511.1 | 17.2 | 82.8 |
| 13.2 | 1043.9 | 35.2 | 47.5 |
| 9.5 | 454.5 | 15.3 | 32.2 |
| 6.7 | 371.5 | 12.5 | 19.6 |
| 4.75 | 166.2 | 5.6 | 14.0 |
| 3.35 | 94.9 | 3.2 | 10.8 |
| 2.36 | 71.4 | 2.4 | 8.4 |
| 1.7 | 46.2 | 1.6 | 6.9 |
| 1.18 | 40.6 | 1.4 | 5.5 |
| 0.85 | 28.4 | 1.0 | 4.5 |
| 0.6 | 25.7 | 0.9 | 3.7 |
| 0.425 | 20.5 | 0.7 | 3.0 |
| 0.3 | 19.5 | 0.7 | 2.3 |
| 0.212 | 16.2 | 0.5 | 1.8 |
| Pan | 52.4 | 1.8 | 0.0 |
| Totals | 2963 | 100.0 | |
| Mass discrepancy | 1.6 | | |
| | | | |
| t2 | | | 55.1 |
| t4 | | | 22.0 |
| t5 | | | 17.0 |
| t10 | | | 9.7 |
| P80 size | | | 17.80 |

**BS2-R: Rounded Blue Stone ore**
Energy calculations

| Size (mm) | 13.2 -16mm (S) | | | 19 -22.4mm (M) | | | 26.5 -31.5mm (L) | | |
|---|---|---|---|---|---|---|---|---|---|
| Energy targeted (kWh/t) | 0.25 | 1 | 2.5 | 0.25 | 1 | 2.5 | 0.25 | 1 | 2.5 |
| Calibrated RPM required | 1357 | 2641 | 4103 | 1357 | 2641 | 4103 | 1357 | 2641 | 4103 |
| RPM Used | 1357 | 2641 | 4103 | 1357 | 2641 | 4103 | 1357 | 2641 | 4103 |
| | | | | | | | | | |
| Sample total mass (g) | | 149.2 | 165.2 | | 880.9 | 929.6 | | 1203.9 | 1245.3 |
| No of particles | | 30 | 30 | | 30 | 30 | | 30 | 30 |
| Average particle mass (g) | | 5.0 | 5.5 | | 29.4 | 31.0 | | 40.1 | 41.5 |
| | | | | | | | | | |
| Actual impact energy (kWh/t) | | 1.03 | 2.49 | | 1.03 | 2.49 | | 1.03 | 2.49 |

| Particle size distributions | 13.2 -16mm (S) | | | | | | | | |
|---|---|---|---|---|---|---|---|---|---|
| **ENERGY (kWh/t)** | **0.25** | | | **1** | | | **2.5** | | |
| Size (mm) | Wt above | %retained | Cumu %passing | Wt above | | | Wt above | | |
| 13.2 | | | | 0 | 0.0 | 100.0 | 10.7 | 6.5 | 93.5 |
| 9.5 | | | | 14.3 | 9.7 | 90.3 | 3.2 | 1.9 | 91.6 |
| 6.7 | | | | 26.4 | 17.8 | 72.5 | 8.3 | 5.0 | 86.6 |
| 4.75 | | | | 20 | 13.5 | 59.0 | 18.2 | 11.0 | 75.6 |
| 3.35 | | | | 19.4 | 13.1 | 45.9 | 16.1 | 9.7 | 65.9 |
| 2.36 | | | | 17.9 | 12.1 | 33.8 | 17.7 | 10.7 | 55.2 |
| 1.7 | | | | 10.9 | 7.4 | 26.4 | 14.4 | 8.7 | 46.5 |
| 1.18 | | | | 9.4 | 6.4 | 20.1 | 13.5 | 8.2 | 38.3 |
| 0.85 | | | | 1.1 | 0.7 | 19.3 | 7.3 | 4.4 | 33.9 |
| 0.6 | | | | 6.5 | 4.4 | 14.9 | 8.9 | 5.4 | 28.5 |
| 0.425 | | | | 4.2 | 2.8 | 12.1 | 5.7 | 3.4 | 25.1 |
| 0.3 | | | | 3.8 | 2.6 | 9.5 | 5.6 | 3.4 | 21.7 |
| 0.212 | | | | 2.8 | 1.9 | 7.6 | 4.8 | 2.9 | 18.8 |
| 0.15 | | | | 2.4 | 1.6 | 6.0 | 4.8 | 2.9 | 15.9 |
| 0.106 | | | | 1.7 | 1.1 | 4.9 | 3.9 | 2.4 | 13.5 |
| Pan | | | | 7.2 | 4.9 | 0.0 | 22.4 | 13.5 | 0.0 |
| Totals | | | | 148 | 100 | | 165.5 | 100 | |
| Mass discrepancy | | | | 1.2 | | | -0.3 | | |
| | | | | | | | | | |
| t2 | | | | | | 76.1 | | | 87.6 |
| t4 | | | | | | 48.5 | | | 67.8 |
| t5 | | | | | | 40.5 | | | 61.1 |
| t10 | | | | | | 23.4 | | | 42.6 |
| P80 size | | | | | | 7.88 | | | 5.53 |

| Particle size distributions | 19 -22.4mm (M) | | | | | | | | |
|---|---|---|---|---|---|---|---|---|---|
| **ENERGY (kWh/t)** | 0.25 | | | 1 | | | 2.5 | | |
| Size (mm) | Wt above | %retained | Cumu %passing | Wt above | %retained | Cumu %passing | Wt above | %retained | Cumu %passing |
| 19 | | | | 0 | 0.0 | 100.0 | 0 | 0.0 | 100.0 |
| 13.2 | | | | 68.1 | 7.7 | 92.3 | 21.8 | 2.4 | 97.6 |
| 9.5 | | | | 141 | 16.0 | 76.2 | 34.9 | 3.8 | 93.9 |
| 6.7 | | | | 135.4 | 15.4 | 60.8 | 99.1 | 10.7 | 83.2 |
| 4.75 | | | | 125.8 | 14.3 | 46.5 | 111.7 | 12.0 | 71.2 |
| 3.35 | | | | 97.8 | 11.1 | 35.4 | 96.4 | 10.4 | 60.8 |
| 2.36 | | | | 78.9 | 9.0 | 26.4 | 101.4 | 10.9 | 49.8 |
| 1.7 | | | | 52.3 | 5.9 | 20.5 | 76.9 | 8.3 | 41.5 |
| 1.18 | | | | 43.5 | 4.9 | 15.5 | 74 | 8.0 | 33.6 |
| 0.85 | | | | 25.4 | 2.9 | 12.6 | 51 | 5.5 | 28.1 |
| 0.6 | | | | 25 | 2.8 | 9.8 | 51 | 5.5 | 22.6 |
| 0.425 | | | | 15 | 1.7 | 8.1 | 33.1 | 3.6 | 19.0 |
| 0.3 | | | | 13.9 | 1.6 | 6.5 | 32.3 | 3.5 | 15.5 |
| 0.212 | | | | 10.4 | 1.2 | 5.3 | 24.6 | 2.7 | 12.9 |
| 0.15 | | | | 9.1 | 1.0 | 4.3 | 23 | 2.5 | 10.4 |
| Pan | | | | 37.5 | 4.3 | 0.0 | 96.2 | 10.4 | 0.0 |
| Totals | | | | 879.1 | 100 | | 927.4 | 100 | |
| Mass discrepancy | | | | 1.8 | | | 2.2 | | |
| t2 | | | | | | 79.7 | | | 94.7 |
| t4 | | | | | | 49.5 | | | 73.7 |
| t5 | | | | | | 41.5 | | | 66.5 |
| t10 | | | | | | 23.7 | | | 46.1 |
| P80 size | | | | | | 10.37 | | | 6.18 |

| Particle size distributions | 26.5 -31.5mm (L) | | | | | | | | |
|---|---|---|---|---|---|---|---|---|---|
| ENERGY (kWh/t) | 0.25 | | | 1 | | | 2.5 | | |
| Size (mm) | Wt above | %retained | Cumu %passing | Wt above | %retained | Cumu %passing | Wt above | %retained | Cumu %passing |
| 26.5 | | | | 0 | 0.0 | 100.0 | 0 | 0.0 | 100.0 |
| 19 | | | | 0 | 0.0 | 100.0 | 104 | 8.4 | 91.6 |
| 13.2 | | | | 22.7 | 1.9 | 98.1 | 163.9 | 13.2 | 78.5 |
| 9.5 | | | | 50.5 | 4.2 | 93.9 | 164.8 | 13.3 | 65.2 |
| 6.7 | | | | 130.3 | 10.8 | 83.1 | 180.7 | 14.5 | 50.7 |
| 4.75 | | | | 128.8 | 10.7 | 72.4 | 143.2 | 11.5 | 39.1 |
| 3.35 | | | | 131.4 | 10.9 | 61.4 | 110.6 | 8.9 | 30.3 |
| 2.36 | | | | 129.8 | 10.8 | 50.6 | 93.4 | 7.5 | 22.7 |
| 1.7 | | | | 102.8 | 8.5 | 42.1 | 59.7 | 4.8 | 17.9 |
| 1.18 | | | | 94 | 7.8 | 34.3 | 50.4 | 4.1 | 13.9 |
| 0.85 | | | | 60.1 | 5.0 | 29.3 | 29.8 | 2.4 | 11.5 |
| 0.6 | | | | 60.4 | 5.0 | 24.3 | 29.2 | 2.3 | 9.1 |
| 0.425 | | | | 38.8 | 3.2 | 21.0 | 18.1 | 1.5 | 7.7 |
| 0.3 | | | | 39 | 3.2 | 17.8 | 16.9 | 1.4 | 6.3 |
| 0.212 | | | | 31.7 | 2.6 | 15.2 | 13.3 | 1.1 | 5.3 |
| Pan | | | | 182.3 | 15.2 | 0.0 | 65.3 | 5.3 | 0.0 |
| Totals | | | | 1202.6 | 100 | | 1243.3 | 100 | |
| Mass discrepancy | | | | 1.3 | | | 2 | | |
| | | | | | | | | | |
| t2 | | | | | | 98.5 | | | 81.3 |
| t4 | | | | | | 85.1 | | | 53.4 |
| t5 | | | | | | 78.0 | | | 45.2 |
| t10 | | | | | | 56.4 | | | 26.8 |
| P80 size | | | | | | 6.14 | | | 13.88 |

## 6 Groups of 5 particles each -22.4+19mm

6 groups of 5 particles each

| | Group 1 | Group 2 | Group 3 | Group 4 | Group 5 | Group 6 |
|---|---|---|---|---|---|---|
| Sample Weight (g) | 122.2 | 133.7 | 122.9 | 146 | 126.2 | 143.2 |
| Screen Aperture (mm) | | | | | | |
| 19 | 0 | 0 | 0 | 0 | 0 | 0 |
| 13.2 | 27.8 | 14.4 | 17.6 | 23.2 | 13 | 24.1 |
| 9.5 | 10.8 | 15.6 | 7.5 | 11.6 | 27.9 | 32.8 |
| 6.7 | 19.4 | 23.5 | 24.5 | 26.9 | 15.8 | 20.6 |
| 4.75 | 17 | 18 | 16.1 | 19.6 | 9.3 | 15.3 |
| 3.35 | 10.7 | 15.2 | 12.5 | 19.8 | 16.9 | 13.9 |
| 2.36 | 9.4 | 11.3 | 10.1 | 12.4 | 9 | 8.4 |
| 1.7 | 5.4 | 6.8 | 6.9 | 7.5 | 7 | 5.6 |
| 1.18 | 4.7 | 5.9 | 5.7 | 6.3 | 6.3 | 5 |
| 0.85 | 2.8 | 3.5 | 2.7 | 3.9 | 3.8 | 2.9 |
| 0.6 | 2.9 | 3.7 | 4.4 | 3.1 | 3.2 | 2.4 |
| 0.425 | 1.8 | 2.2 | 2.7 | 2.2 | 2.2 | 1.7 |
| 0.3 | 1.6 | 2 | 2.4 | 2 | 2 | 1.6 |
| 0.212 | 1.3 | 1.6 | 1.8 | 1.7 | 1.6 | 1.3 |
| 0.15 | 1.2 | 1.6 | 1.4 | 1.1 | 1.2 | 1.1 |
| Pan | 4.9 | 7.6 | 5.7 | 4.6 | 6.1 | 5.6 |
| Total | 116.8 | 125.3 | 116.3 | 141.3 | 119.2 | 136.7 |

| % cumulative passing | Group 1 | Group 2 | Group 3 | Group 4 | Group 5 | Group 6 |
|---|---|---|---|---|---|---|
| 19 | 100.00 | 100.00 | 100.00 | 100.00 | 100.00 | 100.00 |
| 13.2 | 77.25 | 89.23 | 85.68 | 84.11 | 89.70 | 83.17 |
| 9.5 | 68.41 | 77.56 | 79.58 | 76.16 | 67.59 | 60.27 |
| 6.7 | 52.54 | 59.99 | 59.64 | 57.74 | 55.07 | 45.88 |
| 4.75 | 38.63 | 46.52 | 46.54 | 44.32 | 47.70 | 35.20 |
| 3.35 | 29.87 | 35.15 | 36.37 | 30.75 | 34.31 | 25.49 |
| 2.36 | 22.18 | 26.70 | 28.15 | 22.26 | 27.18 | 19.62 |
| 1.7 | 17.76 | 21.62 | 22.54 | 17.12 | 21.63 | 15.71 |
| 1.18 | 13.91 | 17.20 | 17.90 | 12.81 | 16.64 | 12.22 |
| 0.85 | 11.62 | 14.58 | 15.70 | 10.14 | 13.63 | 10.20 |
| 0.6 | 9.25 | 11.82 | 12.12 | 8.01 | 11.09 | 8.52 |
| 0.425 | 7.77 | 10.17 | 9.93 | 6.51 | 9.35 | 7.33 |
| 0.3 | 6.46 | 8.68 | 7.97 | 5.14 | 7.77 | 6.22 |
| 0.212 | 5.40 | 7.48 | 6.51 | 3.97 | 6.50 | 5.31 |
| 0.15 | 4.42 | 6.28 | 5.37 | 3.22 | 5.55 | 4.54 |

**BS1-A: Angular Blue Stone ore**
Energy calculations

| Size (mm) | 13.2 -16mm (S) | | | 19 -22.4mm (M) | | | 26.5 -31.5mm (L) | | |
|---|---|---|---|---|---|---|---|---|---|
| Energy targeted (kWh/t) | 0.25 | 1 | 2.5 | 0.25 | 1 | 2.5 | 0.25 | 1 | 2.5 |
| Calibrated RPM required | 1357 | 2641 | 4103 | 1357 | 2641 | 4103 | 1357 | 2641 | 4103 |
| RPM Used | 1357 | 2641 | 4103 | 1357 | 2641 | 4103 | 1357 | 2641 | 4103 |
| | | | | | | | | | |
| Sample total mass (g) | | | 166 | | 880.9 | 929.6 | | 1054.4 | 968.9 |
| No of particles | | | 30 | | 30 | 30 | | 30 | 30 |
| Average particle mass (g) | | | 5.5 | | 29.4 | 31.0 | | 35.1 | 32.3 |
| | | | | | | | | | |
| Actual impact energy (kWh/t) | | | 2.49 | | 1.03 | 2.49 | | 1.03 | 2.49 |

| Particle size distributions | 13.2 -16mm (S) | | | | | | |
|---|---|---|---|---|---|---|---|
| **ENERGY (kWh/t)** | 0.25 | | | 1 | 2.5 | | |
| Size (mm) | Wt above | %retained | Cumu %passing | Wt above | Wt above | | |
| 13.2 | | | | | 10.7 | 6.5 | 93.5 |
| 9.5 | | | | | 3.2 | 1.9 | 91.6 |
| 6.7 | | | | | 8.3 | 5.0 | 86.6 |
| 4.75 | | | | | 18.2 | 11.0 | 75.6 |
| 3.35 | | | | | 16.1 | 9.7 | 65.9 |
| 2.36 | | | | | 17.7 | 10.7 | 55.2 |
| 1.7 | | | | | 14.4 | 8.7 | 46.5 |
| 1.18 | | | | | 13.5 | 8.2 | 38.3 |
| 0.85 | | | | | 7.3 | 4.4 | 33.9 |
| 0.6 | | | | | 8.9 | 5.4 | 28.5 |
| 0.425 | | | | | 5.7 | 3.4 | 25.1 |
| 0.3 | | | | | 5.6 | 3.4 | 21.7 |
| 0.212 | | | | | 4.8 | 2.9 | 18.8 |
| 0.15 | | | | | 4.8 | 2.9 | 15.9 |
| 0.106 | | | | | 3.9 | 2.4 | 13.5 |
| Pan | | | | | 22.4 | 13.5 | 0.0 |
| Totals | | | | | 165.5 | 100 | |
| Mass discrepancy | | | | | 0.5 | | |
| | | | | | | | |
| t2 | | | | | | | 87.6 |
| t4 | | | | | | | 67.8 |
| t5 | | | | | | | 61.1 |
| t10 | | | | | | | 42.6 |
| P80 size | | | | | | | 4.66 |

| Particle size distributions | 19 -22.4mm (M) | | | | | | | | |
|---|---|---|---|---|---|---|---|---|---|
| ENERGY (kWh/t) | 0.25 | | | 1 | | | 2.5 | | |
| Size (mm) | Wt above | %retained | Cumu %passing | Wt above | | | Wt above | | |
| 19 | | | | 22.1 | 3.1 | 96.9 | 25.3 | 3.4 | 96.6 |
| 13.2 | | | | 121.5 | 17.1 | 79.8 | 26.5 | 3.5 | 93.1 |
| 9.5 | | | | 95.6 | 13.4 | 66.4 | 54.4 | 7.3 | 85.8 |
| 6.7 | | | | 118.3 | 16.6 | 49.8 | 77.8 | 10.4 | 75.4 |
| 4.75 | | | | 83 | 11.6 | 38.2 | 75.8 | 10.1 | 65.3 |
| 3.35 | | | | 65.9 | 9.2 | 28.9 | 80.6 | 10.8 | 54.5 |
| 2.36 | | | | 53.2 | 7.5 | 21.5 | 73.8 | 9.9 | 44.6 |
| 1.7 | | | | 34.9 | 4.9 | 16.6 | 60.3 | 8.1 | 36.5 |
| 1.18 | | | | 30.6 | 4.3 | 12.3 | 53 | 7.1 | 29.5 |
| 0.85 | | | | 19 | 2.7 | 9.6 | 37.6 | 5.0 | 24.4 |
| 0.6 | | | | 15.1 | 2.1 | 7.5 | 32.7 | 4.4 | 20.1 |
| 0.425 | | | | 10.8 | 1.5 | 6.0 | 25.2 | 3.4 | 16.7 |
| 0.3 | | | | 9.2 | 1.3 | 4.7 | 23 | 3.1 | 13.6 |
| 0.212 | | | | 7.2 | 1.0 | 3.7 | 19.7 | 2.6 | 11.0 |
| 0.15 | | | | 5.4 | 0.8 | 2.9 | 15.1 | 2.0 | 9.0 |
| Pan | | | | 20.7 | 2.9 | 0.0 | 67 | 9.0 | 0.0 |
| Totals | | | | 712.5 | 100 | | 747.8 | 100 | |
| Mass discrepancy | | | | 168.4 | | | 181.8 | | |
| | | | | | | | | | |
| t2 | | | | | | 69.4 | | | 87.4 |
| t4 | | | | | | 40.6 | | | 67.4 |
| t5 | | | | | | 34.1 | | | 60.5 |
| t10 | | | | | | 19.3 | | | 41.0 |
| P80 size | | | | | | 11.79 | | | 7.59 |

| Particle size distributions | 26.5 -31.5mm (L) | | | | | | | | |
|---|---|---|---|---|---|---|---|---|---|
| **ENERGY (kWh/t)** | 0.25 | | | 1 | | | 2.5 | | |
| Size (mm) | Wt above | %retained | Cumu %passing | Wt above | | | Wt above | | |
| 26.5 | | | | 0 | 0.0 | 100.0 | 0 | 0.0 | 100.0 |
| 19 | | | | 74.1 | 7.0 | 93.0 | 12.3 | 1.3 | 98.7 |
| 13.2 | | | | 141.6 | 13.4 | 79.5 | 45.8 | 4.7 | 94.0 |
| 9.5 | | | | 139.9 | 13.3 | 66.3 | 79.3 | 8.2 | 85.8 |
| 6.7 | | | | 163 | 15.5 | 50.8 | 115.4 | 11.9 | 73.9 |
| 4.75 | | | | 108.3 | 10.3 | 40.5 | 99.3 | 10.3 | 63.6 |
| 3.35 | | | | 102.7 | 9.7 | 30.8 | 100.1 | 10.3 | 53.3 |
| 2.36 | | | | 79.9 | 7.6 | 23.2 | 92 | 9.5 | 43.7 |
| 1.7 | | | | 54.7 | 5.2 | 18.0 | 68.7 | 7.1 | 36.6 |
| 1.18 | | | | 45.9 | 4.4 | 13.7 | 68.1 | 7.0 | 29.6 |
| 0.85 | | | | 29 | 2.8 | 10.9 | 48.9 | 5.1 | 24.5 |
| 0.6 | | | | 23.1 | 2.2 | 8.7 | 42.8 | 4.4 | 20.1 |
| 0.425 | | | | 16.7 | 1.6 | 7.1 | 33.4 | 3.5 | 16.7 |
| 0.3 | | | | 14.5 | 1.4 | 5.7 | 30.1 | 3.1 | 13.6 |
| 0.212 | | | | 12.1 | 1.1 | 4.6 | 25.3 | 2.6 | 10.9 |
| Pan | | | | 48.5 | 4.6 | 0.0 | 105.8 | 10.9 | 0.0 |
| Totals | | | | 1054 | 100 | | 967.3 | 100 | |
| Mass discrepancy | | | | 0.4 | | | 1.6 | | |
| | | | | | | | | | |
| t2 | | | | | | 82.4 | | | 95.0 |
| t4 | | | | | | 53.7 | | | 76.1 |
| t5 | | | | | | 45.9 | | | 69.0 |
| t10 | | | | | | 27.2 | | | 48.8 |
| P80 size | | | | | | 13.33 | | | 7.87 |

6 groups of 5 particles each

| | Group 1 | Group 2 | Group 3 | Group 4 | Group 5 | Group 6 |
|---|---|---|---|---|---|---|
| Sample Weight (g) | 119.8 | 110.4 | 110.6 | 107.7 | 113 | 106.3 |
| Screen Aperture (mm) | | | | | | |
| 19 | 9.9 | 0 | 0 | 0 | 23.3 | 24.4 |
| 13.2 | 8.6 | 29 | 3.5 | 24.2 | 6.4 | 12.4 |
| 9.5 | 26.9 | 18 | 17.3 | 18 | 11 | 13.4 |
| 6.7 | 12.5 | 16.7 | 21.3 | 21 | 12.8 | 11.7 |
| 4.75 | 12.1 | 10.1 | 15 | 8.3 | 13.8 | 9.1 |
| 3.35 | 9.9 | 10.2 | 16.8 | 11 | 12 | 9.3 |
| 2.36 | 8 | 6.5 | 9.2 | 6 | 9 | 6.9 |
| 1.7 | 5.1 | 4.4 | 6.9 | 4.5 | 6.2 | 4 |
| 1.18 | 4.6 | 3.7 | 5.9 | 3.9 | 4.8 | 3.5 |
| 0.85 | 3.2 | 2.1 | 3.7 | 2.3 | 2.7 | 2.4 |
| 0.6 | 2.6 | 1.8 | 2.9 | 1.9 | 2.4 | 1.8 |
| 0.425 | 2 | 1.2 | 1.9 | 1.3 | 1.6 | 1.3 |
| 0.3 | 2 | 1.3 | 1.6 | 1.2 | 1.4 | 1.1 |
| 0.212 | 1.9 | 1 | 1.1 | 1 | 1.1 | 0.9 |
| 0.15 | 1.5 | 0.7 | 0.7 | 0.6 | 0.8 | 0.7 |
| Pan | 8.5 | 3.2 | 2.6 | 2.4 | 3.4 | 3 |
| Total | 100.9 | 106.7 | 107.8 | 105.2 | 86 | 78.5 |

| % cumulative passing | Group 1 | Group 2 | Group 3 | Group 4 | Group 5 | Group 6 |
|---|---|---|---|---|---|---|
| 19 | 100.00 | 100.00 | 100.00 | 100.00 | 100.00 | 100.00 |
| 13.2 | 92.82 | 73.73 | 96.84 | 77.53 | 94.34 | 88.33 |
| 9.5 | 70.37 | 57.43 | 81.19 | 60.82 | 84.60 | 75.73 |
| 6.7 | 59.93 | 42.30 | 61.93 | 41.32 | 73.27 | 64.72 |
| 4.75 | 49.83 | 33.15 | 48.37 | 33.61 | 61.06 | 56.16 |
| 3.35 | 41.57 | 23.91 | 33.18 | 23.40 | 50.44 | 47.41 |
| 2.36 | 34.89 | 18.03 | 24.86 | 17.83 | 42.48 | 40.92 |
| 1.7 | 30.63 | 14.04 | 18.63 | 13.65 | 36.99 | 37.16 |
| 1.18 | 26.79 | 10.69 | 13.29 | 10.03 | 32.74 | 33.87 |
| 0.85 | 24.12 | 8.79 | 9.95 | 7.89 | 30.35 | 31.61 |
| 0.6 | 21.95 | 7.16 | 7.32 | 6.13 | 28.23 | 29.92 |
| 0.425 | 20.28 | 6.07 | 5.61 | 4.92 | 26.81 | 28.69 |
| 0.3 | 18.61 | 4.89 | 4.16 | 3.81 | 25.58 | 27.66 |
| 0.212 | 17.03 | 3.99 | 3.16 | 2.88 | 24.60 | 26.81 |
| 0.15 | 15.78 | 3.35 | 2.53 | 2.32 | 23.89 | 26.15 |

# RBT INCREMENTAL BREAKAGE DATA

## BS2-R: Blue stone ore

Repeatability experiments

| | | | | | | | | | | | | | | | | |
|---|---|---|---|---|---|---|---|---|---|---|---|---|---|---|---|---|
| **ENERGY (kWh/t)** | 0.167 | | | | | | | | | | | | | | | |
| **RBT Rotor speed** | 1062 | | | | | | | | | | | | | | | |
| **Particle size distributions** | **26.5 -31.5mm (L)** | | | | | | | | | | | | | | | |
| | **Repeatability test 1** | | | **Repeatability test 2** | | | **Repeatability test 3** | | | **Repeatability test 4** | | | **Repeatability test 5** | | | |
| **Intial mass** | **3968** | | | **3858** | | | **3925** | | | **3842** | | | **3756** | | | |
| **No of particles** | **100** | | | **100** | | | **100** | | | **100** | | | **100** | | | |
| **Average particle mass** | **39.68** | | | **38.58** | | | **39.25** | | | **38.42** | | | **37.56** | | | |
| Size (mm) | Wt above | %retained | Cumu %pa | Wt above | %retained | Cumu %pa | Wt above | %retained | Cumu %pa | Wt above | %retained | Cumu %pa | Wt above | %retained | Cumu %pa | |
| 26.5 | 672 | 17.0 | 83.0 | 451 | 11.7 | 88.3 | 492 | 12.6 | 87.4 | 441 | 11.5 | 88.5 | 480 | 12.8 | 87.2 | |
| 22.4 | 795 | 20.1 | 62.9 | 718 | 18.7 | 69.6 | 438 | 11.3 | 76.1 | 631 | 16.5 | 72.0 | 861 | 22.9 | 64.3 | |
| 19 | 640.6 | 16.2 | 46.7 | 485.8 | 12.6 | 57.0 | 587.6 | 15.1 | 61.0 | 613.6 | 16.0 | 55.9 | 498.1 | 13.3 | 51.0 | |
| 13.2 | 805.9 | 20.4 | 26.4 | 989.3 | 25.7 | 31.3 | 1039.9 | 26.7 | 34.3 | 973.1 | 25.5 | 30.5 | 805.5 | 21.4 | 29.6 | |
| 9.5 | 348.9 | 8.8 | 17.5 | 454 | 11.8 | 19.5 | 523.2 | 13.4 | 20.9 | 426.5 | 11.2 | 19.3 | 389.5 | 10.4 | 19.2 | |
| 6.7 | 270 | 6.8 | 10.7 | 290 | 7.5 | 11.9 | 319.6 | 8.2 | 12.6 | 292.6 | 7.7 | 11.7 | 289.1 | 7.7 | 11.5 | |
| 4.75 | 142 | 3.6 | 7.1 | 154.9 | 4.0 | 7.9 | 170.7 | 4.4 | 8.3 | 157.4 | 4.1 | 7.5 | 145.1 | 3.9 | 7.6 | |
| 3.35 | 83.6 | 2.1 | 5.0 | 105 | 2.7 | 5.2 | 101.6 | 2.6 | 5.7 | 95.7 | 2.5 | 5.0 | 94.1 | 2.5 | 5.1 | |
| 2.36 | 57.7 | 1.5 | 3.6 | 56.2 | 1.5 | 3.7 | 70.7 | 1.8 | 3.8 | 61.4 | 1.6 | 3.4 | 54.2 | 1.4 | 3.7 | |
| 1.7 | 34.2 | 0.9 | 2.7 | 34.2 | 0.9 | 2.8 | 38.5 | 1.0 | 2.8 | 34.3 | 0.9 | 2.5 | 33.9 | 0.9 | 2.8 | |
| 1.18 | 27.2 | 0.7 | 2.0 | 27.7 | 0.7 | 2.1 | 28.9 | 0.7 | 2.1 | 26.9 | 0.7 | 1.8 | 26.7 | 0.7 | 2.1 | |
| 0.85 | 16.5 | 0.4 | 1.6 | 16.5 | 0.4 | 1.7 | 17.4 | 0.4 | 1.7 | 15.8 | 0.4 | 1.4 | 16.1 | 0.4 | 1.7 | |
| 0.6 | 13 | 0.3 | 1.3 | 13 | 0.3 | 1.3 | 13.5 | 0.3 | 1.3 | 12.4 | 0.3 | 1.1 | 12.6 | 0.3 | 1.3 | |
| 0.425 | 9.1 | 0.2 | 1.0 | 9.1 | 0.2 | 1.1 | 9.4 | 0.2 | 1.1 | 8.8 | 0.2 | 0.9 | 8.9 | 0.2 | 1.1 | |
| 0.3 | 8 | 0.2 | 0.8 | 8 | 0.2 | 0.9 | 8.3 | 0.2 | 0.9 | 7.5 | 0.2 | 0.7 | 7.7 | 0.2 | 0.9 | |
| 0.212 | 6.8 | 0.2 | 0.7 | 6.8 | 0.2 | 0.7 | 6.8 | 0.2 | 0.7 | 6.1 | 0.2 | 0.5 | 6.7 | 0.2 | 0.7 | |
| Pan | 25.9 | 0.7 | 0.0 | 26.8 | 0.7 | 0.0 | 26.6 | 0.7 | 0.0 | 19.3 | 0.5 | 0.0 | 26.2 | 0.7 | 0.0 | |
| Totals | 3956.4 | 100.0 | | 3846.3 | 100 | | 3892.7 | 100 | | 3823.4 | 100 | | 3755.4 | 100 | | |
| Mass discrepancy | 11.6 | | | 11.7 | | | 32.3 | | | 18.6 | | | 0.6 | | | |
| Percentage broken/probability | 62.74 | | | 69.40 | | | 75.48 | | | 71.61 | | | 64.28 | | | |
| Probability of particle breakage on impact | 62.74 | | | 69.40 | | | 75.48 | | | 71.61 | | | 64.28 | | | |
| t10 size | 2.89 | | | 2.89 | | | 2.89 | | | 2.89 | | | 2.89 | | | |
| t10 | 4.34 | | | 4.48 | | | 4.81 | | | 4.29 | | | 4.47 | | | |
| P80 | 25.88 | | | 24.68 | | | 23.82 | | | 24.40 | | | 25.21 | | | |

| ENERGY (kWh/t) | 0.091 E3 |
|---|---|
| RBT Rotor speed (rpm) | 785 |
| Hit number | Hit 1 |
| **Particle size distributions** | |
| **Intial mass** | **3908** |
| **No of particles** | **100** |
| **Average particle mass** | **39.08** |

| Size (mm) | Wt above | %retained | Cumu %pa |
|---|---|---|---|
| 26.5 | 875 | 22.4 | 77.6 |
| 22.4 | 932 | 23.9 | 53.7 |
| 19 | 514.7 | 13.2 | 40.5 |
| 13.2 | 713.6 | 18.3 | 22.3 |
| 9.5 | 343.7 | 8.8 | 13.4 |
| 6.7 | 226.7 | 5.8 | 7.6 |
| 4.75 | 112.5 | 2.9 | 4.8 |
| 3.35 | 59.3 | 1.5 | 3.2 |
| 2.36 | 37 | 0.9 | 2.3 |
| 1.7 | 23.4 | 0.6 | 1.7 |
| 1.18 | 16.8 | 0.4 | 1.3 |
| 0.85 | 10.1 | 0.3 | 1.0 |
| 0.6 | 7.9 | 0.2 | 0.8 |
| 0.425 | 5.6 | 0.1 | 0.7 |
| 0.3 | 4.9 | 0.1 | 0.5 |
| 0.212 | 4.2 | 0.1 | 0.4 |
| Pan | 16.7 | 0.4 | 0.0 |
| Totals | 3904.1 | 100 | |
| Mass discrepancy | 3.9 | | |
| Percentage broken/probability | 53.66 | | |
| Probability of particle breakage on impact | 53.66 | | |
| t10 size | 2.89 | | |
| t10 | 2.80 | | |
| P80 | 26.91 | | |

| ENERGY (kWh/t) | 0.167 E4 |
|---|---|
| RBT Rotor speed (rpm) | 1062 |
| Hit number | Hit 1 |
| **Particle size distributions** | |
| **Intial mass** | **3968** |
| **No of particles** | **100** |
| **Average particle mass** | **39.68** |

| Size (mm) | Wt above | %retained | Cumu %pa |
|---|---|---|---|
| 26.5 | 672 | 17.0 | 83.0 |
| 22.4 | 795 | 20.1 | 62.9 |
| 19 | 640.6 | 16.2 | 46.7 |
| 13.2 | 805.9 | 20.4 | 26.4 |
| 9.5 | 348.9 | 8.8 | 17.5 |
| 6.7 | 270 | 6.8 | 10.7 |
| 4.75 | 142 | 3.6 | 7.1 |
| 3.35 | 83.6 | 2.1 | 5.0 |
| 2.36 | 57.7 | 1.5 | 3.6 |
| 1.7 | 34.2 | 0.9 | 2.7 |
| 1.18 | 27.2 | 0.7 | 2.0 |
| 0.85 | 16.5 | 0.4 | 1.6 |
| 0.6 | 13 | 0.3 | 1.3 |
| 0.425 | 9.1 | 0.2 | 1.0 |
| 0.3 | 8 | 0.2 | 0.8 |
| 0.212 | 6.8 | 0.2 | 0.7 |
| Pan | 25.9 | 0.7 | 0.0 |
| Totals | 3956.4 | 100 | |
| Mass discrepancy | 11.6 | | |
| Percentage broken/probability | 62.74 | | |
| Probability of particle breakage on impact | 62.74 | | |
| t10 size | 2.89 | | |
| t10 | 4.34 | | |
| P80 | 25.88 | | |

| | | | | |
|---|---|---|---|---|
| **ENERGY (kWh/t)** | | 0.273 E5 | | |
| **RBT Rotor speed (rpm)** | | 1357 | | |
| Hit number | | Hit 1 | | |
| **Particle size distributions** | | | | |
| **Intial mass** | | **3571** | | |
| **No of particles** | | **100** | | |
| **Average particle mass** | | **35.71** | | |
| Size (mm) | | Wt above | %retained | Cumu %pa |
| | 26.5 | 108 | 3.0 | 97.0 |
| | 22.4 | 423 | 11.9 | 85.0 |
| | 19 | 375.6 | 10.6 | 74.4 |
| | 13.2 | 940.4 | 26.6 | 47.9 |
| | 9.5 | 537.9 | 15.2 | 32.7 |
| | 6.7 | 411.1 | 11.6 | 21.1 |
| | 4.75 | 238.5 | 6.7 | 14.3 |
| | 3.35 | 154.4 | 4.4 | 10.0 |
| | 2.36 | 96.7 | 2.7 | 7.2 |
| | 1.7 | 61.7 | 1.7 | 5.5 |
| | 1.18 | 47.1 | 1.3 | 4.2 |
| | 0.85 | 28 | 0.8 | 3.4 |
| | 0.6 | 21.7 | 0.6 | 2.8 |
| | 0.425 | 15.2 | 0.4 | 2.3 |
| | 0.3 | 13.2 | 0.4 | 2.0 |
| | 0.212 | 11.2 | 0.3 | 1.6 |
| Pan | | 58.2 | 1.6 | 0.0 |
| **Totals** | | 3541.9 | 100 | |
| Mass discrepancy | | 29.1 | | |
| Percentage broken/probability | | 84.32 | | |
| Probability of particle breakage on impact | | 84.32 | | |
| t10 size | | 2.89 | | |
| t10 | | 8.70 | | |
| P80 | | 20.68 | | |

## AG2-R: Rounded Gold ore

| | | | | | | | | | | | | | | | | |
|---|---|---|---|---|---|---|---|---|---|---|---|---|---|---|---|---|
| **ENERGY (kWh/t)** | 0.013 E1 | | | | | | | | | | | | | | | |
| **RBT Rotor speed (rpm)** | 300 | | | | | | | | | | | | | | | |
| Hit number | Hit 1 | | | Hit 2 | | | Hit 3 | | | Hit 4 | | | Hit 5 | | | |
| **Particle size distributions** | | | | | | | | | | | | | | | | |
| **Intial mass** | **4313.4** | | | **4086** | | | **3890** | | | **3268** | | | **3145** | | | |
| **No of particles** | **100** | | | - | | | - | | | - | | | - | | | |
| **Average particle mass** | **43.134** | | | | | | | | | | | | | | | |
| Size (mm) | Wt above | %retained | Cumu %pa | Wt above | %retained | Cumu %pa | Wt above | %retained | Cumu %pa | Wt above | %retained | Cumu %pa | Wt above | %retained | Cumu %pa | |
| 26.5 | 3763 | 87.4 | 12.6 | 3345 | 82.1 | 17.9 | 2519 | 65.0 | 35.0 | 2355 | 72.0 | 28.0 | 2081 | 66.4 | 33.6 | |
| 22.4 | 323 | 7.5 | 5.1 | 545 | 13.4 | 4.6 | 749 | 19.3 | 15.7 | 790 | 24.2 | 3.8 | 838 | 26.8 | 6.8 | |
| 19 | 95.8 | 2.2 | 2.9 | 79.7 | 2.0 | 2.6 | 152.9 | 3.9 | 11.7 | 52.7 | 1.6 | 2.2 | 112 | 3.6 | 3.2 | |
| 13.2 | 62 | 1.4 | 1.5 | 57.8 | 1.4 | 1.2 | 308.3 | 8.0 | 3.8 | 35.6 | 1.1 | 1.1 | 50 | 1.6 | 1.6 | |
| 9.5 | 30.8 | 0.7 | 0.7 | 17.4 | 0.4 | 0.8 | 49 | 1.3 | 2.5 | 12.9 | 0.4 | 0.7 | 19.3 | 0.6 | 1.0 | |
| 6.7 | 10.4 | 0.2 | 0.5 | 11.4 | 0.3 | 0.5 | 38.8 | 1.0 | 1.5 | 7 | 0.2 | 0.5 | 13.7 | 0.4 | 0.6 | |
| 4.75 | 5.8 | 0.1 | 0.4 | 4 | 0.1 | 0.4 | 14.5 | 0.4 | 1.2 | 5.9 | 0.2 | 0.3 | 4.2 | 0.1 | 0.5 | |
| 3.35 | 4 | 0.1 | 0.3 | 4.4 | 0.1 | 0.3 | 12.8 | 0.3 | 0.8 | 1.9 | 0.1 | 0.3 | 2.4 | 0.1 | 0.4 | |
| 2.36 | 2.3 | 0.1 | 0.2 | 2.1 | 0.1 | 0.2 | 7.2 | 0.2 | 0.6 | 1.7 | 0.1 | 0.2 | 2.2 | 0.1 | 0.3 | |
| 1.7 | 1.6 | 0.0 | 0.2 | 1.5 | 0.0 | 0.2 | 4.5 | 0.1 | 0.5 | 0.9 | 0.0 | 0.2 | 1.8 | 0.1 | 0.2 | |
| 1.18 | 1.6 | 0.0 | 0.1 | 1.5 | 0.0 | 0.2 | 4 | 0.1 | 0.4 | 0.9 | 0.0 | 0.1 | 1.2 | 0.0 | 0.2 | |
| 0.85 | 1.1 | 0.0 | 0.1 | 1 | 0.0 | 0.1 | 2.6 | 0.1 | 0.4 | 0.7 | 0.0 | 0.1 | 1 | 0.0 | 0.2 | |
| 0.6 | 1 | 0.0 | 0.1 | 1 | 0.0 | 0.1 | 2.6 | 0.1 | 0.3 | 0.7 | 0.0 | 0.1 | 1 | 0.0 | 0.1 | |
| 0.425 | 0.8 | 0.0 | 0.1 | 0.7 | 0.0 | 0.1 | 2 | 0.1 | 0.2 | 0.6 | 0.0 | 0.1 | 0.8 | 0.0 | 0.1 | |
| 0.3 | 0.8 | 0.0 | 0.1 | 0.8 | 0.0 | 0.1 | 2 | 0.1 | 0.2 | 0.6 | 0.0 | 0.1 | 0.9 | 0.0 | 0.1 | |
| 0.212 | 0.7 | 0.0 | 0.0 | 0.7 | 0.0 | 0.1 | 1.7 | 0.0 | 0.1 | 0.6 | 0.0 | 0.0 | 0.7 | 0.0 | 0.1 | |
| Pan | 2 | 0.0 | 0.0 | 2.3 | 0.1 | 0.0 | 5.4 | 0.1 | 0.0 | 1.6 | 0.0 | 0.0 | 2.2 | 0.1 | 0.0 | |
| Totals | 4306.7 | 100 | | 4076.3 | 100 | | 3876.3 | 100 | | 3269.3 | 100 | | 3132.4 | 100 | | |
| Mass discrepancy | 6.7 | | | 9.7 | | | 13.7 | | | -1.3 | | | 12.6 | | | |
| Total Percentage broken/probability | 5.12 | | | 9.44 | | | 23.54 | | | 26.42 | | | 33.11 | | | |
| Probability of particle breakage on impact | 5.12 | | | 4.56 | | | 15.64 | | | 3.80 | | | 6.79 | | | |
| t10 size | 2.89 | | | 2.89 | | | 2.89 | | | 2.89 | | | 2.89 | | | |
| t10 | 0.25 | | | 0.26 | | | 0.74 | | | 0.23 | | | 0.34 | | | |

| | | | | | | | | | | | | | |
|---|---|---|---|---|---|---|---|---|---|---|---|---|---|
| **ENERGY (kWh/t)** | 0.047 E2 | | | | | | | | | | | | |
| **RBT Rotor speed (rpm)** | 562 | | | | | | | | | | | | |
| Hit number | Hit 1 | | | Hit 2 | | | Hit 3 | | | Hit 4 | | | |
| **Particle size distributions** | | | | | | | | | | | | | |
| **Intial mass** | **4207.4** | | | **2703** | | | **1606** | | | **1213** | | | |
| **No of particles** | **100** | | | - | | | - | | | - | | | |
| **Average particle mass** | **42.074** | | | | | | | | | | | | |
| Size (mm) | Wt above | %retained | Cumu %pa | Wt above | %retained | Cumu %pa | Wt above | %retained | Cumu %pa | Wt above | %retained | Cumu %pa | |
| 26.5 | 1730 | 41.3 | 58.7 | 872 | 32.5 | 67.5 | 684 | 42.6 | 57.4 | 351 | 28.9 | 71.1 | |
| 22.4 | 973 | 23.2 | 35.5 | 734 | 27.3 | 40.2 | 529 | 32.9 | 24.5 | 513 | 42.2 | 28.9 | |
| 19 | 427.5 | 10.2 | 25.3 | 474.9 | 17.7 | 22.5 | 157.9 | 9.8 | 14.6 | 150.3 | 12.4 | 16.5 | |
| 13.2 | 514 | 12.3 | 13.0 | 328 | 12.2 | 10.3 | 125.9 | 7.8 | 6.8 | 88.2 | 7.3 | 9.2 | |
| 9.5 | 225 | 5.4 | 7.7 | 99.9 | 3.7 | 6.5 | 45.9 | 2.9 | 3.9 | 47.5 | 3.9 | 5.3 | |
| 6.7 | 130 | 3.1 | 4.6 | 71.2 | 2.7 | 3.9 | 21.1 | 1.3 | 2.6 | 18 | 1.5 | 3.8 | |
| 4.75 | 50.7 | 1.2 | 3.4 | 33 | 1.2 | 2.7 | 8.7 | 0.5 | 2.1 | 18 | 1.5 | 2.4 | |
| 3.35 | 36.9 | 0.9 | 2.5 | 21 | 0.8 | 1.9 | 8.9 | 0.6 | 1.5 | 7.2 | 0.6 | 1.8 | |
| 2.36 | 21.5 | 0.5 | 2.0 | 11.4 | 0.4 | 1.4 | 5.5 | 0.3 | 1.2 | 5.7 | 0.5 | 1.3 | |
| 1.7 | 15.8 | 0.4 | 1.6 | 7.2 | 0.3 | 1.2 | 3.6 | 0.2 | 1.0 | 3.9 | 0.3 | 1.0 | |
| 1.18 | 14.3 | 0.3 | 1.2 | 6.6 | 0.2 | 0.9 | 3.2 | 0.2 | 0.8 | 2.3 | 0.2 | 0.8 | |
| 0.85 | 9.6 | 0.2 | 1.0 | 4.5 | 0.2 | 0.8 | 2.2 | 0.1 | 0.6 | 1.9 | 0.2 | 0.6 | |
| 0.6 | 8.8 | 0.2 | 0.8 | 4.1 | 0.2 | 0.6 | 2 | 0.1 | 0.5 | 1.5 | 0.1 | 0.5 | |
| 0.425 | 6.8 | 0.2 | 0.6 | 3.3 | 0.1 | 0.5 | 1.7 | 0.1 | 0.4 | 1.3 | 0.1 | 0.4 | |
| 0.3 | 6.3 | 0.2 | 0.5 | 3.1 | 0.1 | 0.4 | 1.5 | 0.1 | 0.3 | 1.1 | 0.1 | 0.3 | |
| 0.212 | 5.1 | 0.1 | 0.4 | 2.6 | 0.1 | 0.3 | 1.3 | 0.1 | 0.2 | 1.1 | 0.1 | 0.2 | |
| Pan | 15.3 | 0.4 | 0.0 | 7.5 | 0.3 | 0.0 | 3.7 | 0.2 | 0.0 | 2.7 | 0.2 | 0.0 | |
| Totals | 4190.6 | 100 | | 2684.3 | 100 | | 1606.1 | 100 | | 1214.7 | 100 | | |
| Mass discrepancy | 16.8 | | | 18.7 | | | -0.1 | | | -1.7 | | | |
| Total Percentage broken/probability | 35.36 | | | 60.99 | | | 70.33 | | | 78.66 | | | |
| Probability of particle breakage on impact | 35.36 | | | 39.89 | | | 24.48 | | | 28.91 | | | |
| t10 size | 2.89 | | | 2.89 | | | 2.89 | | | 2.89 | | | |
| t10 | 2.23 | | | 1.68 | | | 1.38 | | | 1.55 | | | |

| | | | | | | | |
|---|---|---|---|---|---|---|---|
| **ENERGY (kWh/t)** | 0.091 E3 | | | | | | |
| **RBT Rotor speed (rpm)** | 785 | | | | | | |
| Hit number | Hit 1 | | | Hit 2 | | | |
| **Particle size distributions** | | | | | | | |
| **Intial mass** | **4103.4** | | | **2004** | | | |
| **No of particles** | **100** | | | - | | | |
| **Average particle mass** | **41.034** | | | | | | |
| Size (mm) | Wt above | %retained | Cumu %pa | Wt above | %retained | Cumu %pa | |
| 26.5 | 1181 | 29.0 | 71.0 | 372 | 18.6 | 81.4 | |
| 22.4 | 823 | 20.2 | 50.8 | 490 | 24.5 | 56.9 | |
| 19 | 503.5 | 12.4 | 38.5 | 366.6 | 18.3 | 38.6 | |
| 13.2 | 707.4 | 17.4 | 21.1 | 350.7 | 17.5 | 21.1 | |
| 9.5 | 327.4 | 8.0 | 13.1 | 186.2 | 9.3 | 11.8 | |
| 6.7 | 206.7 | 5.1 | 8.0 | 90.2 | 4.5 | 7.2 | |
| 4.75 | 91.5 | 2.2 | 5.7 | 40 | 2.0 | 5.2 | |
| 3.35 | 57.5 | 1.4 | 4.3 | 24.6 | 1.2 | 4.0 | |
| 2.36 | 40.6 | 1.0 | 3.3 | 18.8 | 0.9 | 3.1 | |
| 1.7 | 26 | 0.6 | 2.7 | 11.8 | 0.6 | 2.5 | |
| 1.18 | 22.4 | 0.5 | 2.1 | 9.7 | 0.5 | 2.0 | |
| 0.85 | 15.6 | 0.4 | 1.8 | 7.1 | 0.4 | 1.6 | |
| 0.6 | 14.5 | 0.4 | 1.4 | 6.4 | 0.3 | 1.3 | |
| 0.425 | 11.4 | 0.3 | 1.1 | 5 | 0.2 | 1.1 | |
| 0.3 | 10.8 | 0.3 | 0.9 | 4.7 | 0.2 | 0.8 | |
| 0.212 | 8.9 | 0.2 | 0.6 | 4 | 0.2 | 0.6 | |
| Pan | 26.2 | 0.6 | 0.0 | 12.9 | 0.6 | 0.0 | |
| Totals | 4074.4 | 100 | | 2000.7 | 100 | | |
| Mass discrepancy | 29 | | | 3.3 | | | |
| Total Percentage broken/probability | 50.46 | | | 78.21 | | | |
| Probability of particle breakage on impact | 50.46 | | | 56.82 | | | |
| t10 size | 2.89 | | | 2.89 | | | |
| t10 | 3.87 | | | 3.58 | | | |

| | | | | |
|---|---|---|---|---|
| **ENERGY (kWh/t)** | | 0.167 E4 | | |
| **RBT Rotor speed (rpm)** | | 1062 | | |
| Hit number | | Hit 1 | | |
| **Particle size distributions** | | | | |
| **Intial mass** | | **4054.1** | | |
| **No of particles** | | **100** | | |
| **Average particle mass** | | **40.541** | | |
| Size (mm) | | Wt above | %retained | Cumu %pa |
| | 26.5 | 452 | 11.2 | 88.8 |
| | 22.4 | 637 | 15.7 | 73.1 |
| | 19 | 511.1 | 12.6 | 60.5 |
| | 13.2 | 1043.9 | 25.8 | 34.7 |
| | 9.5 | 454.5 | 11.2 | 23.5 |
| | 6.7 | 371.5 | 9.2 | 14.4 |
| | 4.75 | 166.2 | 4.1 | 10.3 |
| | 3.35 | 94.9 | 2.3 | 7.9 |
| | 2.36 | 71.4 | 1.8 | 6.2 |
| | 1.7 | 46.2 | 1.1 | 5.0 |
| | 1.18 | 40.6 | 1.0 | 4.0 |
| | 0.85 | 28.4 | 0.7 | 3.3 |
| | 0.6 | 25.7 | 0.6 | 2.7 |
| | 0.425 | 20.5 | 0.5 | 2.2 |
| | 0.3 | 19.5 | 0.5 | 1.7 |
| | 0.212 | 16.2 | 0.4 | 1.3 |
| Pan | | 52.4 | 1.3 | 0.0 |
| Totals | | 4052 | 100.0 | |
| Mass discrepancy | | 2.1 | | |
| Percentage broken/probability | | 73.09 | | |
| Probability of particle breakage on impact | | 73.09 | | |
| t10 size | | 2.89 | | |
| t10 | | 7.10 | | |